Interplay of Weak Interactions in Layered Structures of Ionic Complexes of Divalent Cobalt, Nickel, Copper, Zinc and Trivalent Lanthanum

A Dissertation submitted to the
Indian Institute of Technology Guwahati as
partial fulfillment for the Degree of
Doctor of Philosophy in Chemistry

Submitted by

Krapa Shankar

Department of Chemistry

Indian Institute of Technology Guwahati

February 2017

Dedicated to My Father…

…who taught me the value of education.

Statement

I hereby declare that this thesis entitled "**Interplay of Weak Interactions in Layered Structures of Ionic Complexes of Divalent Cobalt, Nickel, Copper, Zinc and Trivalent Lanthanum**" is the outcome of research work carried out by me under the supervision of Prof. Jubaraj B. Baruah, at the Department of Chemistry, Indian Institute of Technology Guwahati, India.

In keeping with the general practice of reporting scientific observations, due acknowledgement has been made whenever work described here has been based on the findings of other investigators.

IIT Guwahati
February 2017

Krapa Shankar

Certificate

This is to certify that Krapa Shankar has been working under my supervision since July, 2012 as a regular registered Ph. D. student. I am forwarding his thesis entitled "**Interplay of Weak Interactions in Layered Structures of Ionic Complexes of Divalent Cobalt, Nickel, Copper, Zinc and Trivalent Lanthanum**" being submitted for the Ph. D. (Science) Degree of this Institute.

I certify that he has fulfilled all the requirements according to the rules of this institute regarding the investigations embodied in his thesis and this work has not been submitted elsewhere for a degree.

IIT Guwahati
February 2017

Prof. Jubaraj B. Baruah

Acknowledgements

The enlightening experience of doing science under the guidance of Prof. Jubaraj B. Baruah can hardly be described in words. The numerous discussions and interactions I had with him expanded my horizons to hitherto unknown frontiers of science and knowledge. I am in debt to this wonderful person for all that he has given me and above all for motivating me towards scientific research.

I would like to acknowledge my sincere gratitude to all my doctoral committee members, Dr. V. Manivannan, Dr. s. S. Bag and Dr. K. sahu for their insightful advices and valuable suggestions. I am also grateful to the entire faculty and staff in the Department of Chemistry, Indian Institute of Technology Guwahati for providing a wonderful work atmosphere throughout this period.

I would like to thank my group members Dr. Babulal Das, Dr. Bhaskar Nath, Dr. Bigyan R. Jali, Dr. Prithiviraj khakhlary, Dr. Jayant K. nath, Dr. Nithi Phukan, Arup, Munendra, whome I had an opportunity to work with and other group member Dr. Prashant Ray, Dr. Barun K. Dutta,Dr. somnath Ghosh, Dr. sameer ghorai, Debu, Karuna, Sayan, Kuldeep, somen, Soham, Wajid, Akhtar, Sahnawaz, Vijay, Vinod for their timely help, support and for the wonderful time we shared during this period. No words can express my thankfulness for giving me their time and companionship, which made the time spent in the laboratory pleasant and memorable. I would also like to thank some amazing people Rahul, Prahlad, Sachin, Ajeet, Sanket, Purushottam, who make my life easy and happy at IIT Guwahati. I would like to give my special thanks to my lab seniors Dr. Babulal Das with whom I had an opportunity to work.

I would like to thank Indian Institute of Technology for the research fellowship.

This Thesis wouldn't have seen the light of this day without the care, encouragement and help of some wonderful person like Dr.Chandra Shekhar Kashyap, Dr. Pankaj Kumar, Mr. Akbar khan, Mr. Shabir khan, Mr. Mukul Raizada, Lokesh, Ram Naresh. I would like to furnish my sincere gratitude to these wonderful people in my life for their constant motivation which made me reach this point.

I would like to acknowledge my teachers Dr. Mohd. Shahid, Mr.Suresh Kumar Baghel, Mr.Suresh Chand Sharma and my all teachers of AMU and Adarsh Meena Inter Collage (Dalelgarhi) for their excellent teaching, motivation, love and blessing.

Finally, my Ph. D. endeavor could not be completed without the endless love, unending support, tolerance and blessings from my family. I wish to express my sincere gratitude to my parents (Late Preetam singh and Mrs. Pushpa Devi), my wife Priyanka Kashyap, my younger brothers(Munesh, Jitendra), uncle (Mangal Sain, Harkesh, Vinod, Arvind, Mukesh, Beenesh), aunty (Omwati, Beervati, Kamlesh, Bimlesh). They are the main soul and inspiration for each and every step that I achieve in my life.

Preview

Varieties of self-assemblies are formed by interactions of discrete molecules or sub-assemblies within an assembly through van der Waals interactions, and various other weak non-covalent interactions such as hydrogen bond, π-π, cation-π, anion-π, C-H···π interactions. Directional properties and hierarchical strengths of weak interactions make avenues to generate different assemblies with novel properties. Inspired by nature emerging concepts of supramolecular building blocks with biological species such as DNA and proteins have been studied. Orderly arranged molecular assemblies guided by directional properties of hydrogen bond helps in function of several natural processes. Intense interest is generated on supramolecular aspects of inorganic complexes to use in bottom-up synthesis procedure to construct assemblies with new material properties. Molecular level understanding of self-assemblies of simple metal complexes requires identifications of sub-assemblies within an assembly to think of new constructions. This is basically important in inorganic chemistry due to presence of relatively strong dative bonds and strong ionic interactions in comparisons to other weak interactions in supramolecular chemistry. These can be utilized to generate supramolecular assembly with ionic compounds as host molecules. A recent literature suggests that conjugate acid base pairs acts as host and have interesting host-guest chemistry. On the other hand, bottom up constructions of coordination polymers, self-assemblies and metal-organic frameworks contribute significantly in design of robust structures in predicted ways. Various factors such as the conformation, stacking, packing solvation, coordination numbers and oxidation state of central metal atoms plays key role in architectures of self-assemblies. With such a background the present thesis comprising of five chapters deals with self-assembling of anionic and cationic complexes and coordination polymer to understand guest recognition and modulation of optical properties.

Accordingly first chapter of the thesis introduces general aspects of weak interactions, coordination polymers to define the research problem. The discussion includes coordination polymers of selected examples of carboxylate complexes.

Examples are brought from coordination behavior of different isomers of pyridinedicarboxylic acids to illustrate self-assemblies, coordination polymers and inclusion properties of such complexes. The aim of the thesis is described at this section to evaluate and analyse self-assembling properties of cationic and anionic metal complexes with π-decorated ligands.

In the **chapter 2** self-assemblies of copper(II) 2,3-pyridinedicarboxylate (**Cu23pdc**) and 2,5-pyridinedicarboxylate (**Cu25pdc**) having different organo-cations are presented. For this purpose the chapter is divided into two parts.

First part of this chapter organo-cation containing copper(II) 2,3-pyridinedicarboxylate mononuclear complexes, dinuclear complexes and coordination polymers are discussed. Two types of coordination polymers, one type of dinuclear complexes and several types of mononuclear complexes were formed which are illustrated in **scheme 1**.

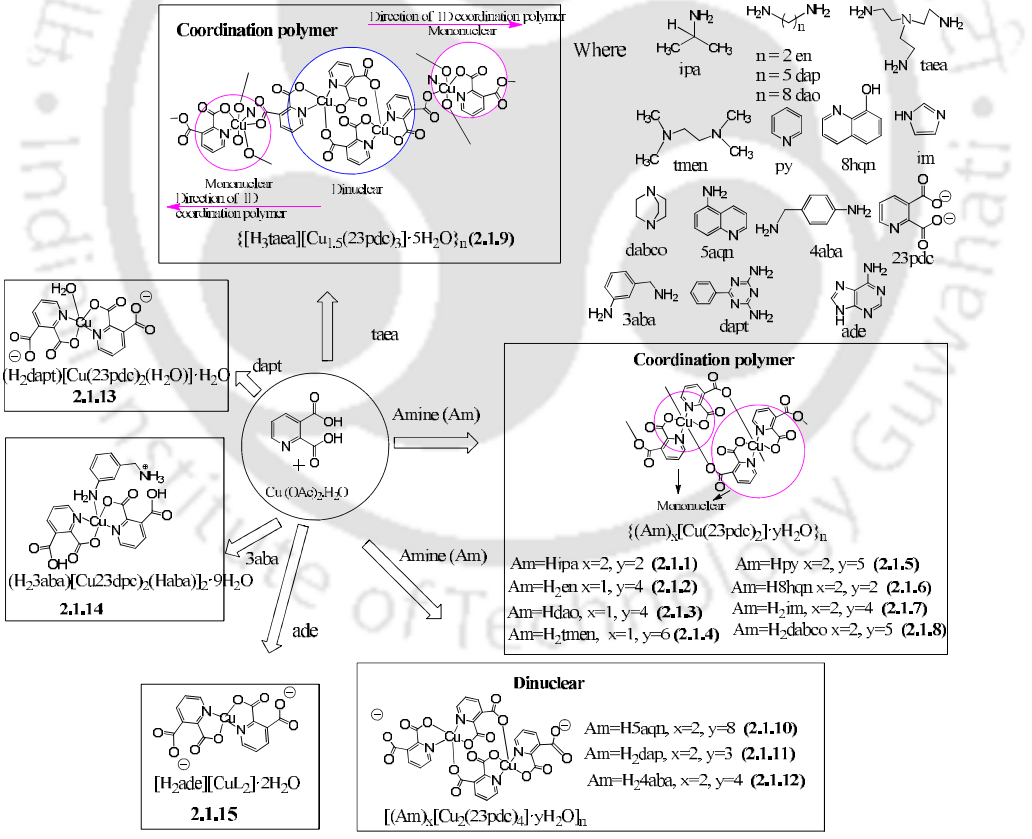

Scheme 1: Three different types of copper(II) 2,3-pyridinedicarboxylate complexes depending on organocations.

The complexes **2.1.1-2.1.8** are coordination polymers having mono-nuclear repeat anion which is shown in scheme 1. Each repeat unit of these coordination polymers is formed by chelation of pyridine nitrogen atom along with an oxygen atom of carboxylic acid at 2-position. Each carboxylic acid group present at 3-position of the ligand bridges neighboring copper ion. This resulted in formation of polymeric chain of the anionic part. These coordination polymers have similar structural features a representative example with the hydrogen bonds with cation is shown in Figure 1(a). This type of coordination polymer are commonly observed in copper(II)2,3-pyridinedicarboxylate complexes.

An exceptional coordination polymer was formed when tri cation of tris-2-aminoethylamine is the counter cation. This coordination polymer has combination of dinuclear and mononuclear repeat units as illustrated in Figure 1(b).

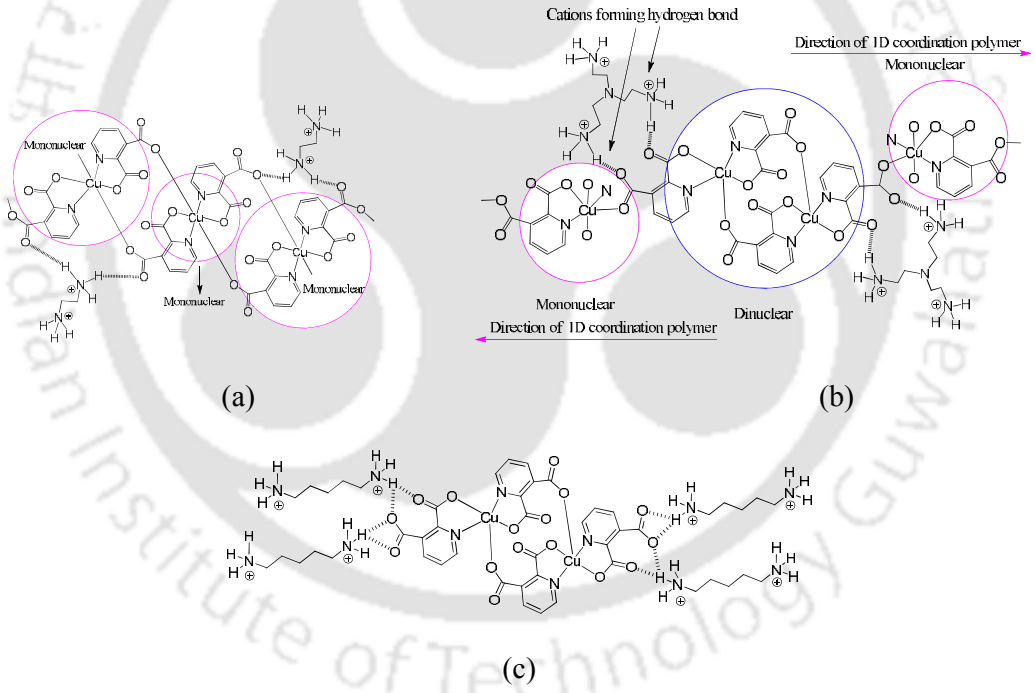

Figure 1: Ionic type hydrogen bonds in (a) coordination polymer **2.1.2**, (b) coordination polymer **2.1.9**, (c) Dinuclear complex **2.1.11**.

Each penta-coordinated mononuclear unit is followed by two hexa-coordinated dinuclear unit. The coordination polymer is guided by strong hydrogen bonds of three ammonium sites. Thus to accommodate such complementing interaction this exceptional structure was formed.

Copper(II)2,3-pyridinedicarboxylate complexes possessing cations of 5-aminoquinoline, 4-aminobenzylamine or 1,5-diaminopentane were dinuclear complexes. In these cases dinuclear complexes having penta-coordinated square-pyramidal copper complexes are obtained. These three complexes have similar self-assemblies which have the similarity, show strong hydrogen bonds of cations with uncoordinated carboxylate groups.

In addition to these another three other types of mononuclear complexes were obtained, For example, Complex having cations of 2,4-diamino-6-phenyl-1,3,5-triazine is a mono nuclear complex **2.1.13**. It is a penta-coordinated complex having square pyramidal geometry. It has two bis chelated **23pdc** and water molecule. On the other hand, the 3-aminobenzylamine forms hexa-coordinated copper(II)2,3-pyridinedicarboxylate complex **2.1.14** by coordinating through the amino group directly attached to the ring and other side being protonated. Such amines occupies the axial postions and equatorial position of octahedral geometry are occupied by chelating 2,3-pyridinedicarboxylate. Adeninium cation containing complex **2.1.15** is mononuclear have a distorted square planar geometry.

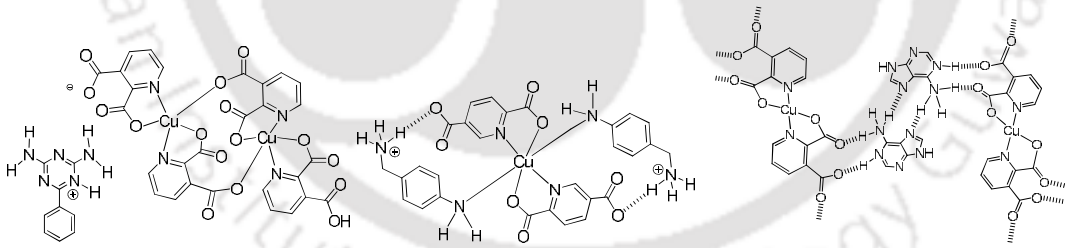

(a) (b) (c)

Figure 2: Hydrogen bonds between anionic part with cationic part in mononuclear complexes (a) **2.1.13**, (b) **2.1.14**, (c) **2.1.15**.

The self-assembly of each complex is analyzed and found out that the assemblies are guided by strong ionic type hydrogen bonds and complementing effect to form self-assemblies.

Significant difference in the type of complex formed by the ammonium cations of **4aba** and **3aba** are clear indication that the complementary intramolecular hydrogen bonded structures in the later case such effect helps to coordinate the amino group to the copper ion. It is seen that, the coordination of the acid group to the metal ion and as well as form salts are the two factors that decided the formation of various types of structures. Further to these the complexes were characterized by various spectroscopic techniques and by studying their thermal degradations.

All these complexes showed layered structures of anions where cations are intercalated. The distances of separations between anionic layers are 8.50Å-13.50Å. Thermal degradation of each coordination polymer were studied and found to show that majority of the coordination polymer formed copper oxide in the ranges of 500°C-600°C. Thermal decomposition of complex **2.1.4** at 600°C formed of nano dimensional copper oxide having average particle sizes 17.6nm.

Second part of this chapter deals with a similar study but with another positional isomer 2,5-pyridinedicarboxylic acid. In this case a series of coordination polymers, a trinuclear complex and several types of mononuclear complexes of Cu(II)2,5-pyridinedicarboxylate having organo-cations were obtained.

2,5-pyridinedicarboxylate complexes having dications of 1,5-diaminopentane, 1,4-Diazabicyclo[2.2.2]octane, N,N,N',N'-tetramethylenediamine were mononuclear complexes. In these complexes each complex has two **25pdc** and a water ligand coordinating to a copper ion to form penta coordinated square pyramidal geometry. In each case the free carboxylate group strongly hydrogen bonded to cations, which prevents formation of higher nuclearity complexes. The $-NH_3^+$ and coordinated water molecule groups hydrogen bonds with carboxylate group (Figure 3a) as a result blocks carboxylate group to further polymerize.

It may be mentioned that in the case of **23pdc**, 1,5-diaminopentane dication containing complex was dinuclear. A close analysis showed that in these two cases due to orientation of the two free carboxylate groups force hydrogen bonds to be from different geometry in each case, thereby making a large difference in the nuclearity. This indicates that the organic cation play key role to decide the nature of assembly in these crystal lattices.

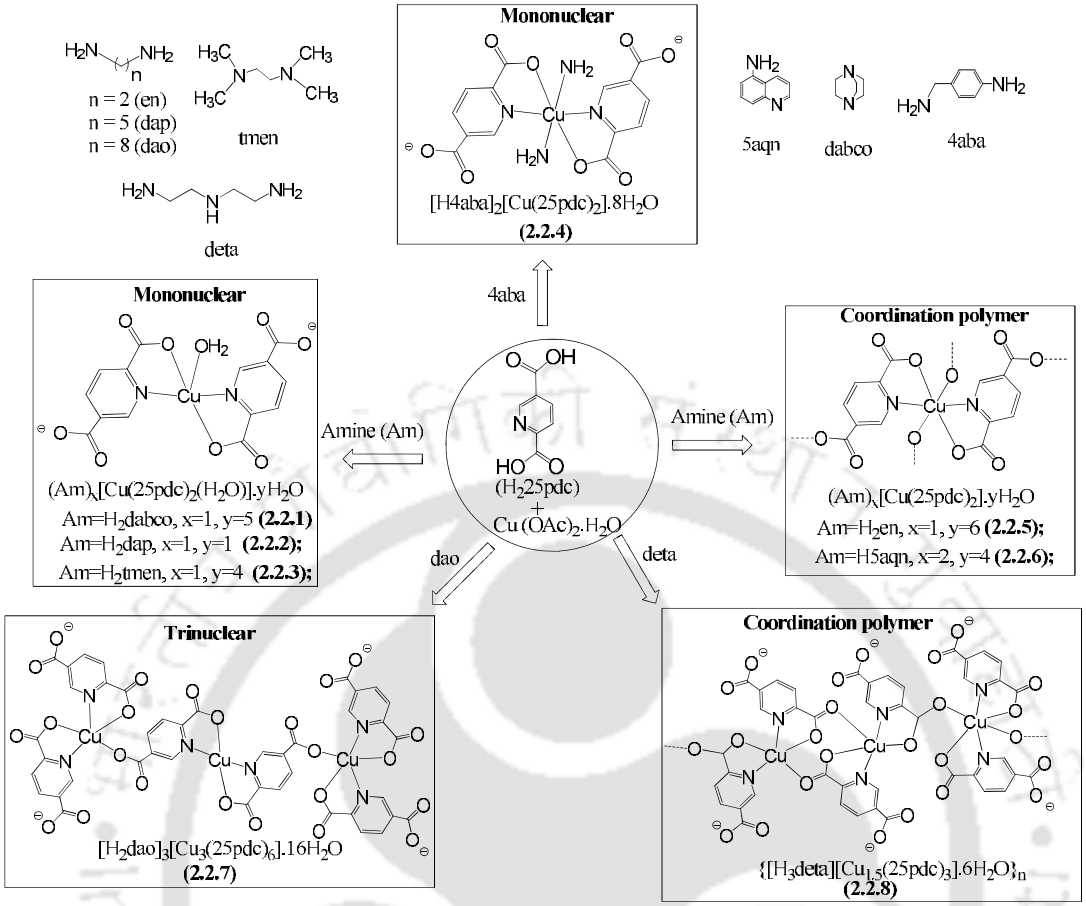

Scheme 2: Synthesis of copper(II) 2,5-pyridinedicarboxylate complexes.

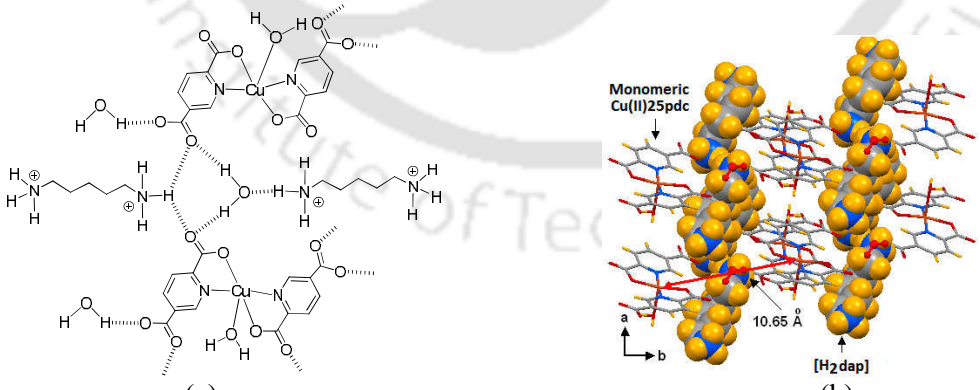

(a) (b)

Figure 3: (a) Hydrogen bonds of cation with anion in **2.2.2**, (b) Packing diagram of **2.2.2** showing layered structure.

Dication of protonated 1,8-diaminooctane containing **25pdc** complex was a trinuclear complex. The structure of the complex **2.2.7** consists of the anionic skeleton (Figure 4a). Complex anion $[Cu_3(25pdc)_6]^{6-}$ has two different copper(II) environments. Two copper at terminal ends are having square pyramidal and one in between square planar.

This unique trinuclear $[Cu_3(25pdc)_6]^{6-}$ complex anion form layers with cations and anions in the ratio 1:1 (Figure 4b). The hydrogen bond in layers is formed such that the end of each trinuclear unit is terminated by ionic hydrogen bond.

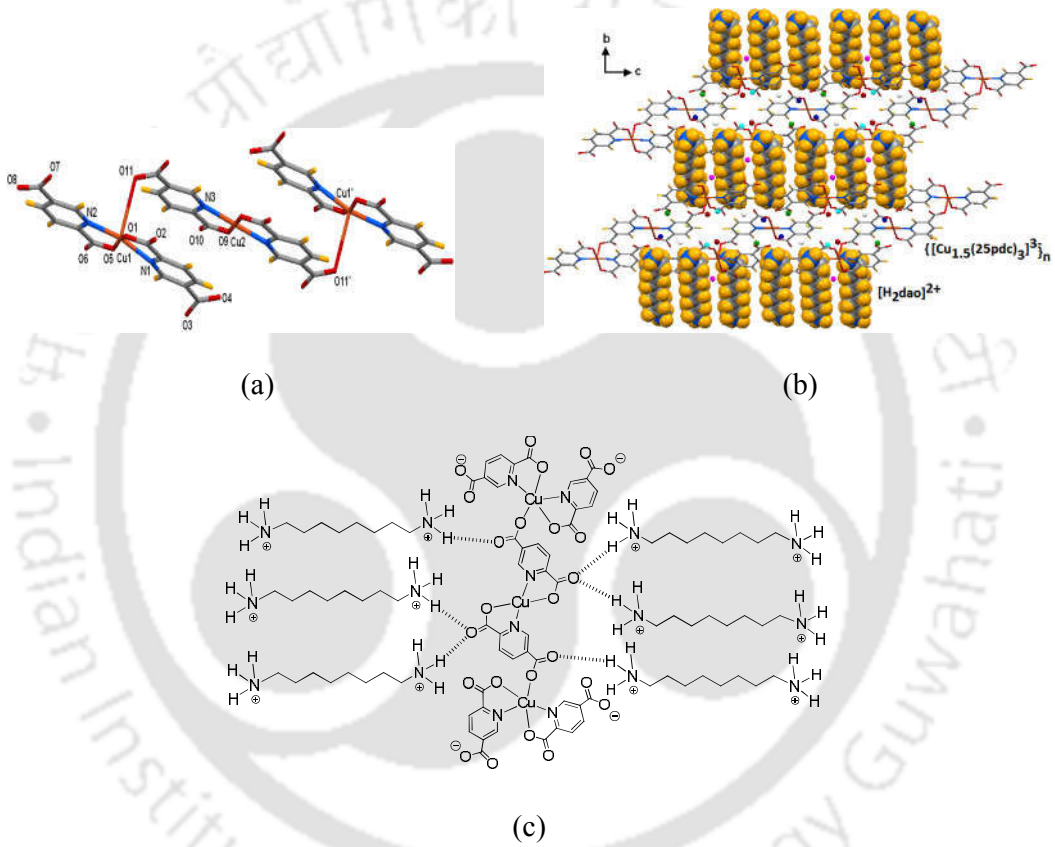

Figure 4 (a) Anionic part of trinuclear complex **2.2.7**, (b) Packing diagram of **2.2.7**, (c) Hydrogen bonds between cations and anionic part in complex **2.2.7.**

When ethylenediamine was used to provide the cationic part, a coordination polymer was obtained. It consists of dication $[H_2en]^{2+}$, polymeric $\{[Cu(25pdc)_2]^{2-}\}_n$ complex anion, and six lattice water molecules. The anionic part of the polymer is comprise of dinuclear repeat units where each copper has two five member chelate of 2,5-pyridinedicarboxylate ligand. The chelates are interconnected by free carboxy oxygens.

The **25pdc** complex having trication of diethyltriamine is an unique coordination polymer **2.2.8**. The polymeric complex anion of this is constituted by copper ions at two different environment, namely in distorted square pyramidal and octahedral environment (Figure 5b).

In this polymer the side arm carbonyl of dinuclear unit coordinates to copper ions leaving aside the carboxylic acids free. Each carboxylate is involved in strong hydrogen bonds with cations.

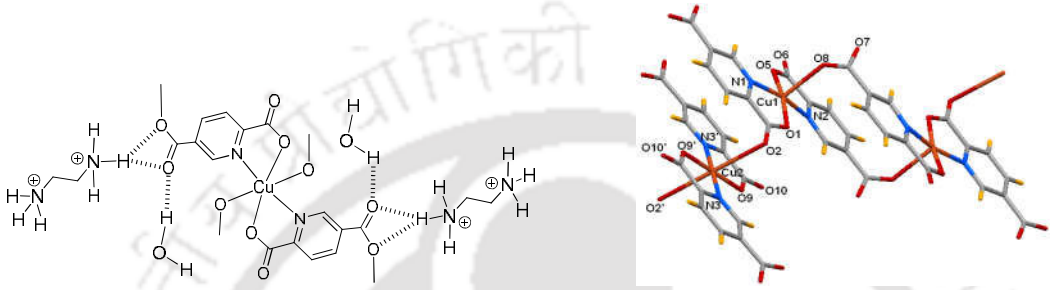

(a) (b)

Figure 5: (a) Hydrogen bond of cation with repeat unit of coordination polymer **2.2.5**; (b) Repeat anionic inorganic part of coordination polymer **2.2.8.**

Distinctions among the coordination environment of copper(II) ions with d^9-electronic configuration are reflected in their respective ESR spectra. ESR of the linear coordination polymer **2.2.5**, mononuclear complex **2.2.3** and the zigzag coordination polymer **2.2.8** are distinguishable.

Thus, in this chapter it is shown that analogous to **23pdc** complexes of copper, the copper **25pdc** complexes also adopt various structures guided by complementary effect of strong hydrogen bond of organocations.

Third chapter of the thesis is on utility of copper(II) 2,3pyridinedicarboxylates in bottom up synthesis and in cation exchange. First part of this chapter describes utility of complex **2.1.13** in construction of multinuclear heterometallic coordination polymer.

Complex **2.1.13** with zinc(II) acetate or gadolinium(III) acetate along with pyridine, resulted in formation of corresponding coordination polymer heterometallic **3.1.2** or 3D **3.1.3** (Scheme 3). Thermal decomposition of **3.1.2** and **3.1.3** yielded nano-dimensional mixed metal oxides. The complex **2.1.13** on treatment with pyridine formed dinuclear complex **3.1.1.** Structural analysis of each of these complexes is discussed.

Formation of the dinuclear complex **3.1.1** is due to the adjustment of pH by pyridine making less number of strong ionic type hydrogen bonds by partly neutralizing the di-cation to mono-cation.

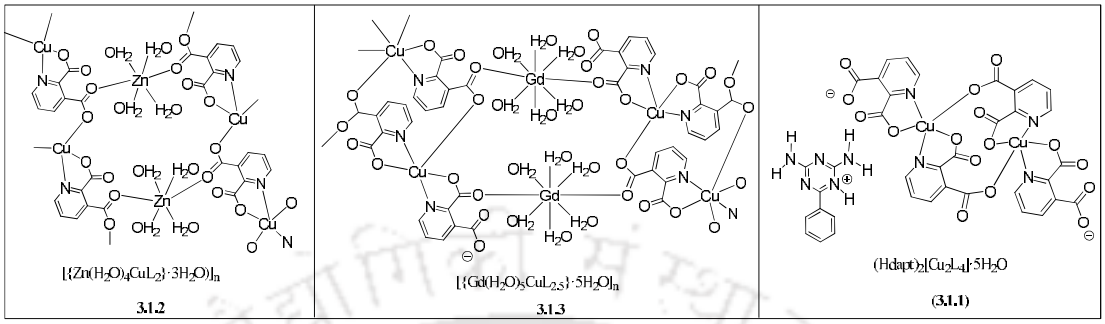

Scheme 3. Synthesis of heterometallic 2D **(3.1.2)** and 3D **(3.1.3)** and dinuclear complex **3.1.1**.

In the second part synthesis, characterisation of Copper(II)2,3-pyridinedicarboxylate complexes with protonated cytosine and cytidine are discussed.

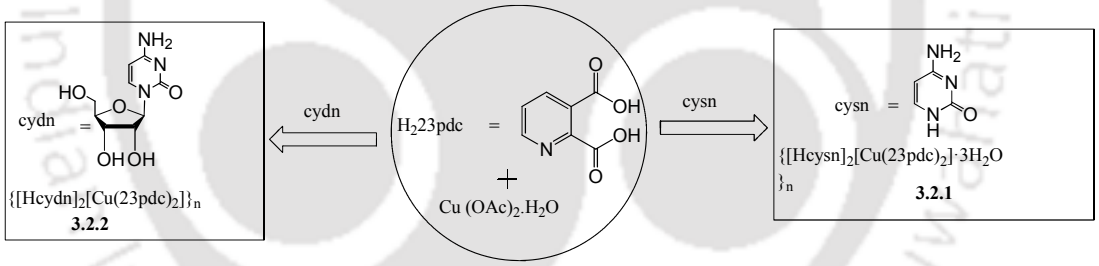

Scheme 4: Copper(II) 2,3-pyridinine dicarboxylate possessing cations of nucleobases.

The **23pdc** copper complex with cytosinium is a coordination polymer with six coordinate copper ions. Cytidine is a nucleoside with cytosine attached to a ribose ring through a β-N1-glycosidic bond. A similar coordination polymer is obtained when cation of cytidine in place of cation of cytosine was used.

Having a ribose unit in complex **3.2.2** this complex has wide separation between layers of anions (15.9Å) (Figure 6b). This compound is utilised to exchange of cations and used to make several other layered structures having inorganic and organic cations.

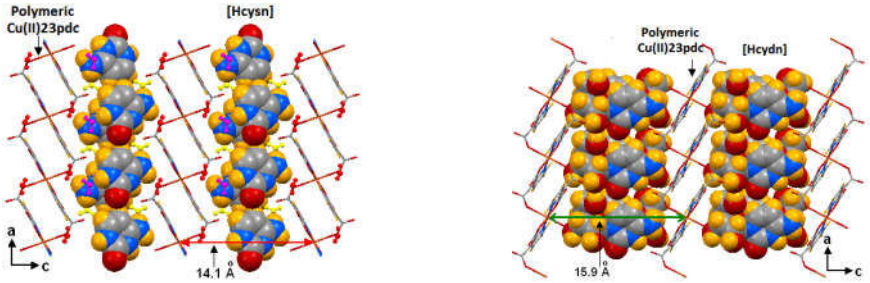

(a) (b)

Figure 6: Closed packed structures showing layered arrangements of cations and anions in complexes (a) **3.2.1**, (b) **3.2.2.**

The chapter 4 is divided into four parts, each part depicting self-assemblies and host-guest binding of the complex cations and anions depicted in figure 7.

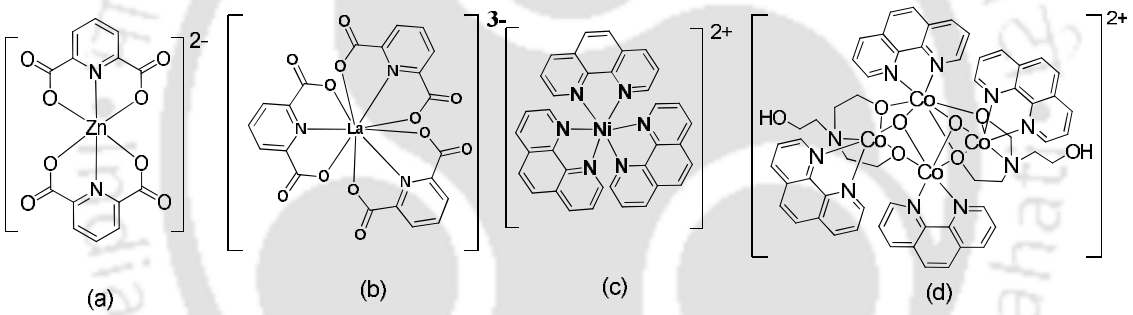

(a) (b) (c) (d)

Figure 7: Different metal templates used for study of self-assemblies for guest inclusions.

In part 1 of this chapter Zn(II)2,6-pyridinedicarboxylate $[H_2tmbpy][Zn(26pdc)_2]\cdot 5H_2O$ **(4.1.1)** $[H_2bpy][Zn(26pdc)_2]\cdot 6H_2O$ **(4.1.2)** were synthesized and characterized. Host-guest complexes with 2,6-dihydroxynaphthalene, 2,7-dihydroxynaphthalene and pyrogallol with the parent complexes shown in figure 8 were studied.

The structural study revealed that guest organic molecules accommodated in the layers of zinc 2,6-pyridinedicarboxylate anions. The complex **4.1.1** and **4.1.2** have differences in packing pattern as shown in figure 8.

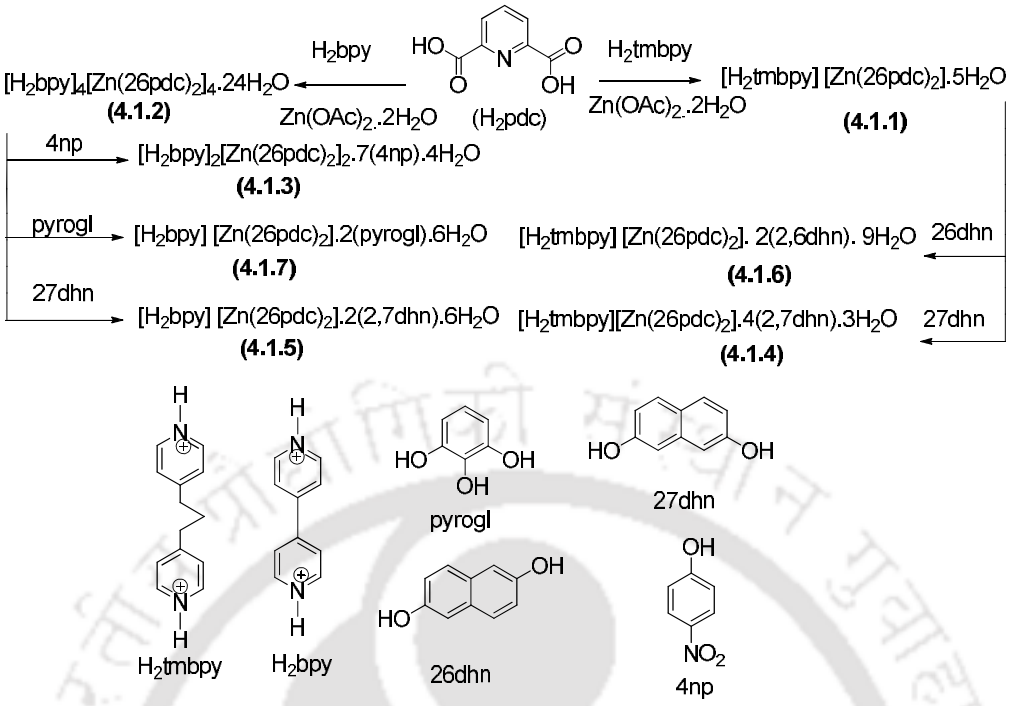

Scheme 5: Synthesis of various guest included complexes of **4.1.1** and **4.1.2**.

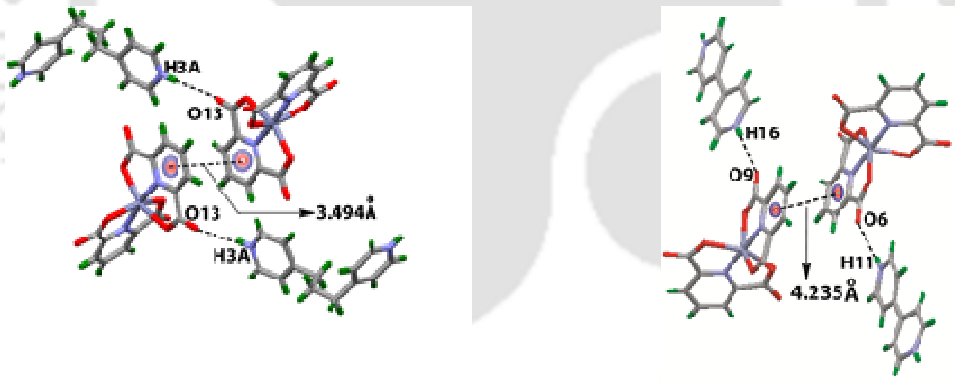

(a) (b)

Figure 8: Self-assemblies of complex **(4.1.1)** and (b) **(4.1.2)**.

Selective binding of 4-nitrophenol with complex **(4.1.2)** to form an adduct **(4.1.3)** 4-nitrophenol was observed. In solution, addition of an aqueous solution of 4-nitrophenol to an aqueous solution of complex **(4.1.2)** leads to a steady growth of an absorption peak at 432nm in the UV-vis spectrum. On the other hand, there is no interaction between 4-nitrophenol in a similar experiment with complex **(4.1.1)**, as no shift in absorption on titration with **(4.1.1)** was detected.

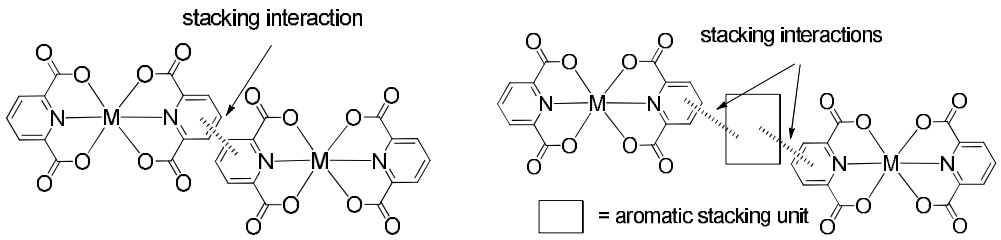

Figure 9: Two different ways of π-stacking arrangements to form layered structures in metal 2,6-pyridinedicarboxylate complexes.

In these it is found that the flexible and rigid cation changes the π-stacking patterns of Zn(II)2,6-pyridinedicarboxylate in different manner and thereby helps to recognize guest aromatic molecules. The host guest complexes and parent compounds have the either of the assemblies formed by the stacking effect as illustrated in figure 9. Preferential formation of such staking helps the molecular recognition process.

In the second part of this chapter inclusion complexes of nona-coordinated $(H_2bpy)_3[La(26pdc)_3]_2.15H_2O$ (**4.2.1**) with different aromatic diols are studied. The complex **4.2.1** was prepared by reacting lanthanum nitrate with **$H_2$26pdc** in presence of 4,4'-bipyridine. This complex formed various inclusion complexes with dihydroxyaromatic compounds as illustrated in scheme 6. The host guest complexes are characterised by determining single crystal structure by X-ray diffraction. The guest inclusion with coordination polymer of lanthanide and with 4,4'-bipyridine were studied showed that the absence of 4,4'-bipyridine no inclusion took place. This indicated that the cationic part of the complex controls the self-assembly and proves electron rich planar dihydroxy aromatics to get accommodated as guests.

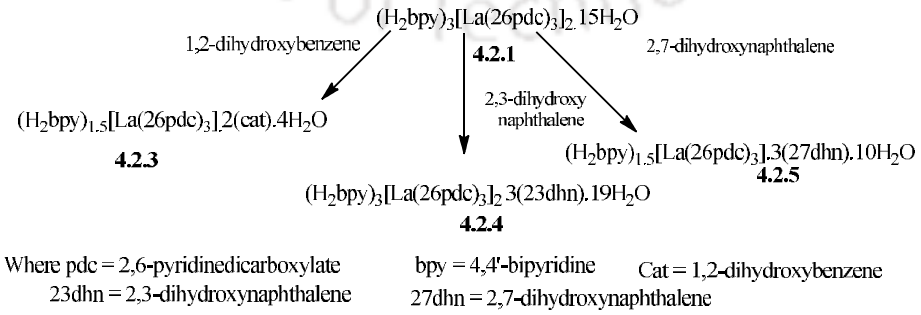

Scheme 6: Host guest complexes of complex **4.2.1**

Third part of this chapter is on mixed anionic complex tris-(phn)nickel(II) nitrate **(4.3.1)** (where phn= 1,10-phenanthroline). $[Ni(phn)_3]^{2+}$ is highly stable and widely studied complex cation is capable to stack in packing. Nitro aromatic compounds such as 4-nitrophenol, 2,4-dinitrophenol and 3-nitrobenzoic acid form inclusion complex with this complex. Accordingly a series of complexes, namely, $[Ni(phn)_3](NO_3)_2(Hnp)_2H_2O$ **(4.3.2)**, $[Ni(phn)_3]_2(dnp)_3(NO_3).11H_2O$ **(4.3.3)**, $[Ni(phn)_3](nba)\ (NO_3)_3.11H_2O$ **(4.3.4)** as shown in scheme 7 were prepared and characterized by various spectroscopic tools and finally determining structures.

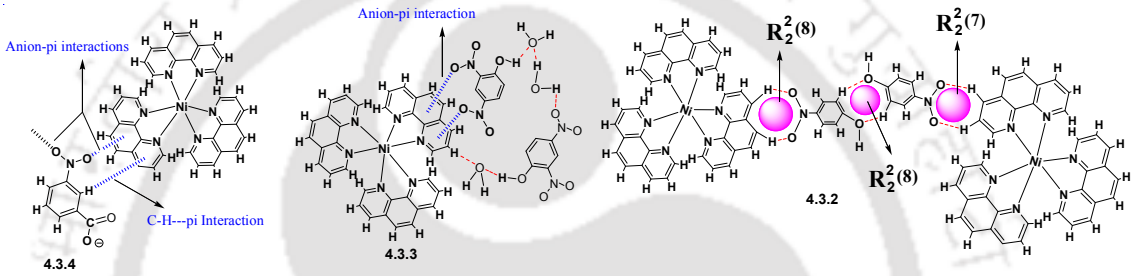

Scheme 7: Different weak interactions in host guest complexes **4.3.1-4.3.4**.

Complex **4.3.1** is fluorescent in methanol, it emits at 378nm on excitation at 340nm. As expected the anion-π interactions quenches the fluorescence in complex **4.3.3** and **4.3.4**, these two complexes are very weakly fluorescent upon excitation at 340nm. Complex **4.3.2** on the other hand do not show anion-π interaction, thus the fluorescence emission changes are less in this case.

The fourth part of the chapter deals with the synthesis of cationic mixed valent tetranuclear cobalt clusters derived from 1,10-phenanthroline or 2,2′-bipyridine with triethanolamine using cobalt(II) chloride.

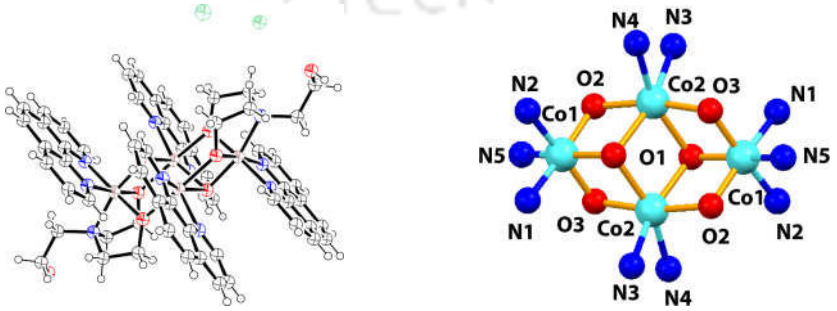

(a) (b)

Figure 10: Structure of the (a) complex **4.4.1** and (b) Tetranuclear core in each complex.

Mixed-valent complex having cobalt at +2, +3 oxidation states, namely $[(\mu_2\text{-Htea})_2(phen)_2Co_2(\mu_3\text{-O})_2Co_2(phen)_2]Cl_2.5H_2O$ **(4.4.1)** was formed from reaction of cobalt chloride with 1,10-phenanthroline (**phen**) and triethanolamine (**H_3tea**). When reaction was performed 2,2'-bipyridine in place of 1,10-phenanthroline, a double salt $[(\mu_2\text{-Htea})_2(bpy)_2Co_2(\mu_3\text{-O})_2Co_2(bpy)_2]Cl_2.[Co(H_2O)_6]Cl_2.5H_2O$ **(4.4.2)** was formed. Thus there were wide differences in products depending on heterocyclic aromatic ligands used in these reactions. Complex **(4.4.1)** and **(4.4.2)** had a defect dicubane tetranuclear cobalt complex cation (Figure 4.4.1b). In each case four cobalt sites were chelated by 1,10-phenanthroline or 2,2´-bipyridine ligands. Each $Htea^{2-}$ ion bridged three cobalt ions through two oxygen atoms. Thus, two arms among three flexible arms of $Htea^{2-}$ were used in coordination, leaving one ethyl hydroxy group free. Host-guest complexes with nitro phenols such as 4-nitrophenol, 2,4-dinitrophenol, 3-aminobenzoic acid were prepared and characterized. In solution, complex **(4.4.1)** as well as complex **(4.4.2)** were weakly fluorescent, both emitted at 309nm ($\lambda_{ex,}$270nm).

Addition of nitro phenols consistently decreased fluorescence emission of solutions of complex **(4.4.1)** and **(4.4.2)**. 2-Nitrophenol caused least fluorescence quenching of both the complexes; whereas 3 or 4-nitrophenol did not show uniform trend in decrease in fluorescence intensities. 3-Nitrophenol was found to be a good quencher for both complexes. Thus recognition of 3-nitrophenol over the other two positional isomers were obtained. The recognition is attributing to the least delocalization of electrons over the aromatic ring in this particular case.

Last chapter is description of a series of copper(II) ethylenediamine complexes as with various carboxylic acids such as benzoic acid, 4-hydroxy benzoic acid, cinnamic acid, pyrazole- 3, 5-dicarboxylic acid, 2,2'-biquinoline-4,4'-dicarboxylic acid. In all complexes shown in scheme 8, the anions are intercalated in the layers of cations held by self-complimentary hydrogen bonds between the cations and the anions. Analysis of different structures have shown that anions guide the interlayer separation between cations.

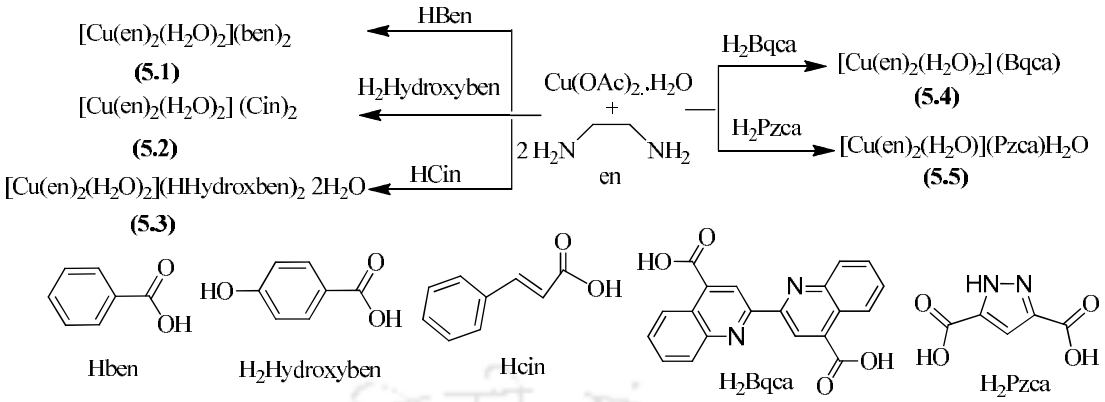

Scheme 8: Synthesis of various copper(II) ethylenediamine carboxylate complexes.

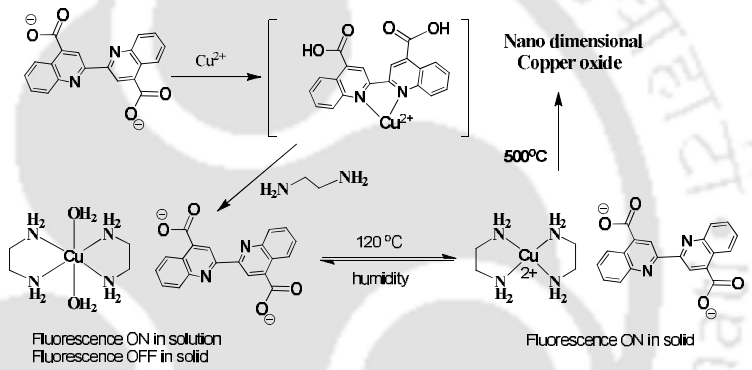

Scheme 9: Modulation of fluorescence emission

Modulation of fluorescence of H_2bqca by the interplay of supramolecular effects and complexation with copper(II) ions is shown in this chapter. Compound **H_2bqca** has several characteristic features: (a) Anion of this compound is big, hence a non-covalent assembly constructed by such anions may be easily dismantled; (b) A big anion will be reluctant to coordinate to a metal ion;

(c) **H_2bqca** being a flexible molecule it has possibility to adopt different orientations by rotation around C_{ipso}-C_{ipso} bond, (d) there is existing literature on coordination ability of the 2,2'-biquinoline-4,4'-dicarboxylic acid for chelation and to form coordination polymers, and (e) finally this acid is likely to π-stack as a characteristic feature associated with quinoline based compounds. Based on these effect fluorescence ON-OFF sequence are generated as illustrated in scheme 9. In solid state hydrated and anhydrous form behaves differently, which is attributed to conformational adjustments in the self-assembly of a copper(II) complex **(5.4)**.

A conclusion on the finding of the thesis is compiled at the end of the thesis. Relevant literatures and experimental sections of each chapter is compiled after summary in each chapter. The crystallographic parameters are given as an appendix and corresponding crystallographic information files are provided as soft copy attached to the thesis.

Contents

List of Abbreviations

Ade	Adenine	**Hbn**	Hydroxybenzene
3aba	3-aminobenzylamine	**8hqn**	8-hydroxyquinoline
4aba	4-aminobenzylamine	**Im**	Imidazole
5aqn	5-aminoquinoline	**Ipa**	Isopropylamine
Ben	Benzene	**Nba**	Nitrobenzoic acid
Bpy	4,4′-bipyridinium	**4np**	4-nitrophenol
Bqca	2,2′-biquinoline-4,4′-dicarboxylate	**23pdc**	2,3-pyridinedicarboxylate
Cat	1,2-dihydroxybenzene	**24pdc**	2,4-pyridinedicarboxylate
Cydn	Cytidine	**25pdc**	2,5-pyridinedicarboxylate
Cysn	Cytosine	**26pdc**	2,6-pyridinedicarboxylate
Dao	1,8-diaminooctane	**Phn**	1,10-phenanthroline
Dap	1,5-diaminopentane	**Py**	Pyridine
Dapt	3,5-diamino-phenyl-1,2,4-triazine	**Pzca**	Pyrazole-3,5-dicarboxylate
Dabco	1,4 diazabicyclo[2.2.2]octane	**Taea**	Tris(2-aminoethyl)amine
Deta	Diethylenetriamine	**Tea**	Triethanolamine
23dhn	2,3-dihydroxynaphthalene	**Tmbpy**	1,3-bis(4-pyridine)propane
26dhn	2,6-dihydroxynaphthalene	**Tmen**	N,N,N′,N′tetramethylethylenediamine
27dhn	2,7-dihydroxynaphthalene	**DMF**	Dimethylformamide
Dnp	Dinitrophenol	**DMSO**	Dimethyl sulfoxide
En	Ethylenediamine		

Chapter 1

Introduction

1.1 Background

Supramolecular chemistry deals with consequences of weak interactions in different types of assemblies.[1] In this branch of chemistry, interactions of discrete molecules through van der waal interactions,[2] and various other weak non-covalent interactions such as hydrogen bond[3], π-π interactions[4], cation-π interactions[5], anion-π interactions[6], C-H···π interactions[7], etc. to generate new supramolecular architecture are dealt.[8] The field of supramolecular chemistry has grown considerably and numbers of areas have evolved. Some areas such as host-guest chemistry[9], self-assembly[10], molecular recognition[11] and supramolecular complexes[12], template-directed synthesis and molecular machines etc. are now well developed.[13] Inspired by nature emerging concepts of supramolecular building blocks with biological species such as DNA[14] and proteins have been studied.[15] Orderly arranged molecular assemblies guided by directional properties of hydrogen bond[16] helps in function of several natural processes.[17]

In comparison of a covalent bonds supramolecular interactions are weak.[18] For example C-H bond energy is 430 KJ/mole and C-O bond energy is 340 KJ/mol. Whereas C-H···O interactions is less than 20 KJ/mol. Comparison of some covalent and non-covalent bonds (supramolecular interactions) are listed in table 1.1. It clearly suggests that a supramolecular assembly will be easily dismantled in comparision to covalently linked system.

Table 1.1 Strength of different supramolecular interactions and covalent bonds

Non-covalent bonds		**Covalent bonds**	
Hydrogen bond	~120 kJ / mol	C-C bond	360 kJ / mol
Electrostatic interaction	~20 kJ / mol	C-H bond	430kJ / mol
van der Waals interaction	~0.4-4kJ / mol	C=C bond	600 kJ / mol
π- π interaction	0-50 kJ / mol	C=O bond	690 kJ / mol
Cation- π interaction	5-80 kJ / mol		

Hydrogen bond is the most common primary weak interaction associated with various supramolecular assemblies.[19] Hydrogen bonds provide directional properties to self-assemblies and for such purpose distances and angles are used as shown in Figure 1.1 as descriptors of hydrogen bond parameters of a bond on focus. In the Figure 1.1 hydrogen atom attached to a relatively electronegative atom represented by D-H is attracted toward electronegative atom A to form a hydrogen bond.[20]

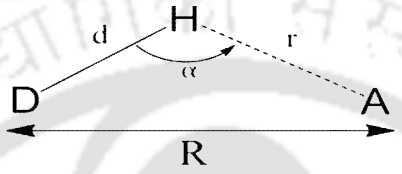

Figure 1.1: Schematic representation of a hydrogen bond.

A hydrogen bond is usually written as D-H···A, where D is called the hydrogen bond donor atom while A is called the hydrogen bond acceptor. The distance of separation between the D and A is the donor-acceptor separation distance which is represented by R. Whereas the H···A distance is represented by r. The angle <DHA is an important factor deciding the strength of a hydrogen bond. Hydrogen bonds are classified into three types based on their strength; namely, strong, moderate and weak hydrogen bonds. Characteristic hydrogen bond-parameters used to classify them into different categories are listed in table 1.1.

Table 1.2 Donor -acceptor distances and angles in different type hydrogen bonds.

Parameters	Strong	Moderate	Weak
Bond energy ($kJmol^{-1}$)	60-120	16-60	>12
Interactions type	Mostly covalent	Mostly electrostatic	Electrostatic
H···A (Å)	1.2-1.5	1.5-2.2	2.2-3.2
D···A (Å)	2.2-2.5	2.5-3.2	3.2-4.0
<D-H···A (Å)	175-180	130-180	90-150

Based on the structures the hydrogen bonds are also classified as discrete, infinite chain, intramolecular and cyclic type hydrogen bonds.[21]

On the other hand, depending on numbers of hydrogen bond donors involved with a particular electronegative atom to form hydrogen bonds result in formation of bifurcated, trifurcated hydrogen bonds[22] shown in Figure 1.2.

Such bonds are very useful in construction of hydrogen bonded bridged structures. In general hydrogen bond consist of a donor group X-H and an acceptor A, and it is denoted as X-H···A. Hydrogen bond interactions are wide range interactions, hence there may be possibility for a donor group to hydrogen bond with more than one acceptor site at a time.[23] If donor group hydrogen bonded with two acceptor atoms, it is termed as bifurcated hydrogen bond.[23] When a donor atom hydrogen bonds with three acceptor atoms at a time, it is called as trifurcated[24] hydrogen bond (right side of Figure 1.2).

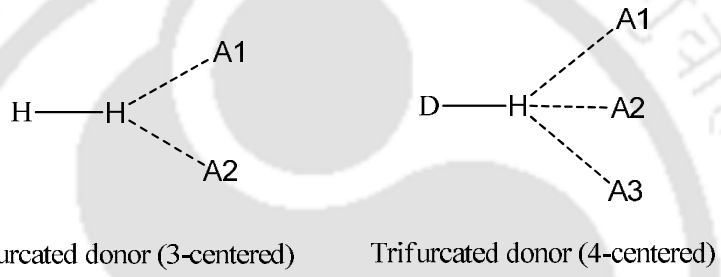

Figure 1.2: Bifurcated and trifurcated hydrogen bonds.

Graph set notations are conventionally used notations to describe different types of hydrogen bonds in assemblies. In this notation the morphology of hydrogen-bonded network in three dimensional solids are described. Graph set notation is developed based upon graph-theory was introduced by Etter, Bernstein and co-workers.[25] A general graph set descriptor is shown below.

$$G_d^a(n)$$

Where G = Graph set designator C/R/D/S

d = Number of donor atoms

a = Number of acceptor atoms

n = Total number of atoms present in hydrogen-bonded motifs

To assign a graph set notation, in first step is identification of different types of hydrogen bond present in the structure, as defined by the nature of donors and acceptors present in the structure of interest. Depending on the type of hydrogen bond smallest building blocks one of four designators, R (ring), D (dimer), C (chain) and S (self or intermolecular hydrogen bond) are assigned.

The number of donors and acceptors present in the in each motif are designated as subscript and superscript respectively and total number of atoms used in the repeat unit is denoted in brackets, Some examples of designating hydrogen bonded assemblies are given in Figure 1.3. Thus, using graph set notation focus on the hydrogen-bonded pattern present in an assembly can be ascertained.

Another way put forward by Desiraju to designate supramolecular assemblies in solid state assemblies is by synthons.[26] This concept in supramolecular assembly is an extension of original description of synthons in covalent compounds, where synthon defines as the smallest intermolecular contact. The non covalent interaction between two molecules in supramolecular assemblies can be termed as supramolecular synthon.[27] Synthons can be key descriptors for supramolecule and isosteric synthons present within in a series of self-assemblies provides means for predesign non-covalent synthesis.[28] Some examples of cyclic hydrogen bonded synthons with corresponding graph-set notation are depicted in Figure 1.3.

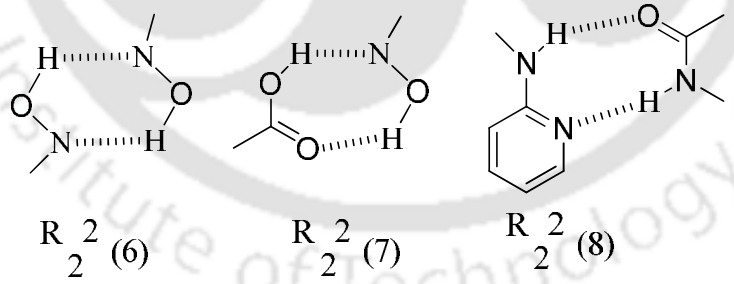

Figure 1.3: Examples of hydrogen bonded cyclic heteromeric synthons with graph-set notations

As far as organic functional groups are concerned, hydrogen bonds between same functional group within a self-assembly may occur in different ways, for example a carboxylic acid functional group can be form cyclic dimer, carboxyl dimer (which can be carbonyl type or hydroxyl type) [29]

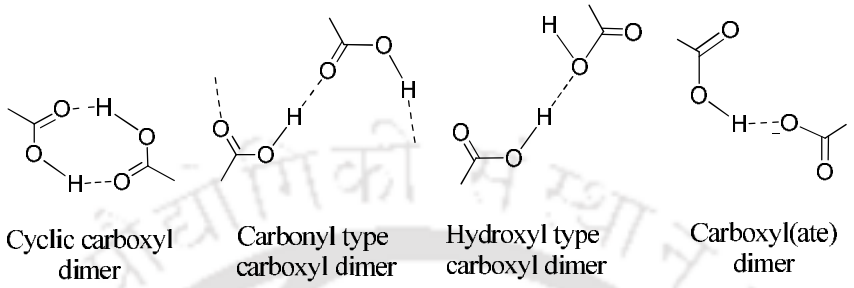

Figure 1.4: Different assemblies of carboxylic acids.

Similarly amide functional group can form different types of assemblies (Figure 1.5) based on primary and secondary amide.[30]

Figure 1.5: Hydrogen bond motifs from amide-amide and acid-amide.

The above assemblies are formed between similar functional groups and different combinations are possible, but in many self-assemblies the homodimeric sub-assemblies are the repeat units. Similarly, interactions between two functional groups[31] such as acid and amide provide scope to form linear combination or cyclic units such as homodimer shown in Figure 1.6.

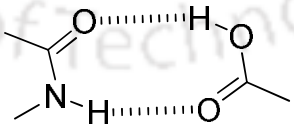

Figure 1.6: Hydrogen bonded hetero-dimer formed between an acid and an amide.

Complementary hydrogen bonds between molecules with same functional group or different functional groups generates different patterns in solid state structures.[32]

Though hydrogen bonds are from between many types of groups, amide and carboxylic acid group are most studied, because both of them can act as hydrogen bond donor as well as acceptor.[33]

Besides the strong and weak hydrogen bond interaction there are also weak C-H···X interactions which significantly contribute to supramolecular self-assemblies.[34]

Generally N and O atoms are participates in hydrogen bonding. Whereas in recent years it has been established that C-H group also participate in hydrogen bonding and it can serve as hydrogen bond donor. The carbon atom is not electronegative, however there is some evidence to formation of C-H···X interactions, considered as C-H···X (X: O, N, π) hydrogen bonds are weak in nature and first detected in crystal structure of organic compound. These non-classical hydrogen bonds play significant roles in biological macromolecules and specially stabilize nucleic acids and protein structures.[35]

Study of supramolecular chemistry provides a basis to the realm of host-guest chemistry and multi-components crystals.[36] Such subject areas find applications in drugs,[37]applied materials,[38] separation technology and molecular recognition,[39] molecular imprinting etc. A supramolecular host may be considered as a template to accommodate one or more molecule/s or ionic or radical species by supramolecular interactions. Such templates may be comprised of a molecule having energetically favourable geometry, binding sites to accommodate a guest molecule. Accordingly, a simple molecule having sites for weak interactions may bind to another molecule to form a host-guest complex. Alternatively, it may be an assembly of molecules having pre-organised geometry or can reorganise to adopt a suitable geometry for holding a guest molecule.

As a simple elucidation of host-guest system, a host can be constructed through chemical reactions between two molecules having definite shape through covalent bond and subsequently accommodate a guest molecule (step A of scheme shown in Figure 1.7).

A host can be assembly formed in an alternative way by interactions between two non-covalently liked molecules and which can accommodate a guest molecule as illustrated in step A' of Figure 1.7. In the later case, the assembly formed will be considered as multi-components assembly.

Foregoing discussion has showed the importance of hydrogen bonds in different self-assemblies. However, even in a highly hydrogen bonded self-assemblies there exists different other weak interactions.

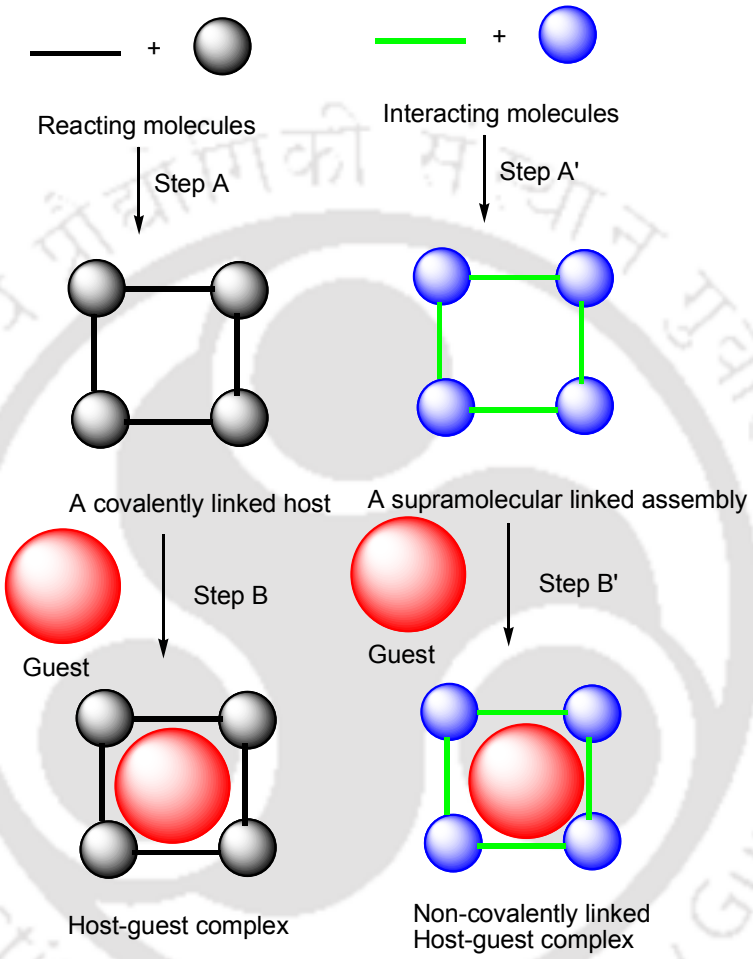

Figure 1.7: Covalently linked host and supramolecular host to form host-guest complex.

A self-assembly may also be formed without hydrogen bonds with the aid of other weak interactions. Interactions arising from π-systems such as arene-arene, anion-π, cation-π and C-H···π interactions are commonly encountered in supramolecular chemistry.[40]

Among π-interactions arene–arene interactions are significant to have stacking of π-electron cloud of one aromatic ring over π-electron cloud.

It is unfavourable to have parallel stacking in a sandwiching manner shown in Figure 1.8, primarily due to repulsion of quadrupoles, however such repulsive effect is counter-balanced by forming a lattice. Some of such parallel interactions can become favourable as in the case of two rings having electron rich and electron defiant rings or between to dipolar rings. On the other hand, there can be stacking of aromatic rings to adopt T-shaped or parallel-offset manner which are energetically favourable.

The latter type of interactions arise due to attraction between the rings having different electronic environment properties.[41] No direct face to face stacking interaction is reported in literature but offset face to face interactions are seen in assemblies where one of the aromatic ring is slightly slipped relative to the second ring.[42]

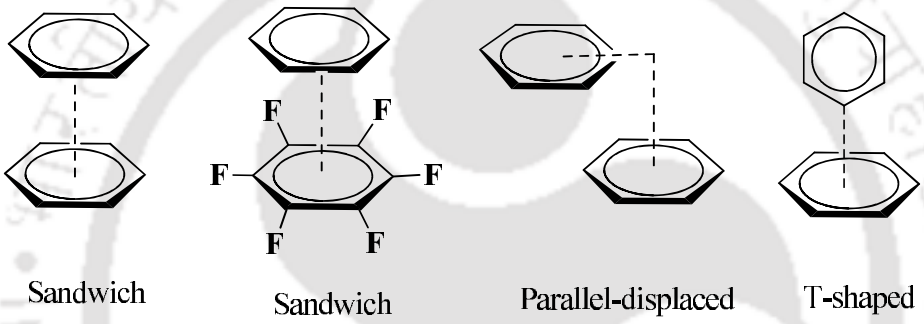

Figure 1.8: Different types of π-stacking interactions of aromatic rings.

A cation placed near a face of a π-system at a favourable distance with appropriate geometry may interact with the π-system.[43] Such situations is observed with organo-cation pointed towards a π-system to show cation π-interaction.[44]

For example, cationic unit of lysine $-NH_3^+$ and guanidinium group of arginine communicate with aromatic protein side chains by cation-π interactions.[45] On the other hand, tryptophan is most a common π-system found in protein which show cation-π interactions, while arginine is the most common cation in biology to show such interactions.[46] Cation-π interaction is generally a relatively strong interactions, in gas phase it has binding energies up to ~40 kJ/mol.

Smaller cations with high charge density form stronger cation-π interactions than lager cations. Electron donating group on present on a ring strengthen cation-π interactions while electron withdrawing group weaken interactions.[47] The cation-π interactions play a major role in stabilizing the protein structure.[48]

There can be interactions between an anion and π-system which can be explained as favourable non-covalent interaction between an electron deficient aromatic system and an anion. Such interactions may occur through (i) support of a host; (ii) anion and cation placed at alternate positions, (iii) anions sandwiched by cations as illustrated in Figure 1.10.

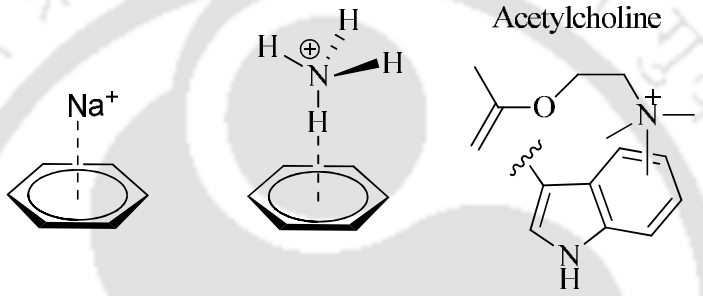

Figure 1.9: Cation-π interactions between some aromatic rings and cations.

Higher polarising power of small anions generates strong anion-π interactions. Most researchers believed that these interactions between anions and π-aromatic system would repulsive while innovative idea and theoretical study revealed that these interactions are energetically favourable (~20–50 kJmol^{-1}). Anion-π interactions are used to design of highly selective anion receptors and channels useful in chemical and biological processes.[50]

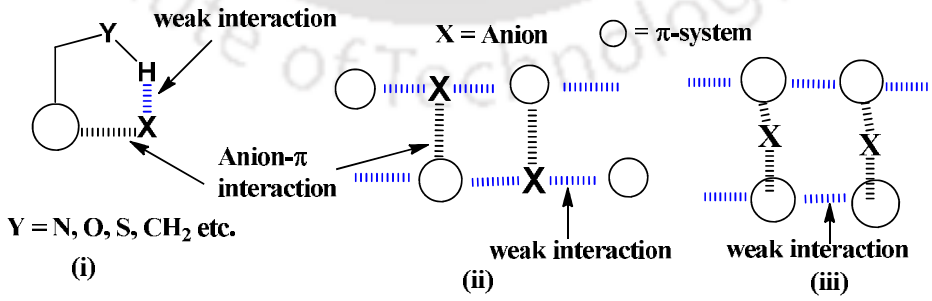

Figure 1.10: Representation of positioning of anions to have anion-π interactions.

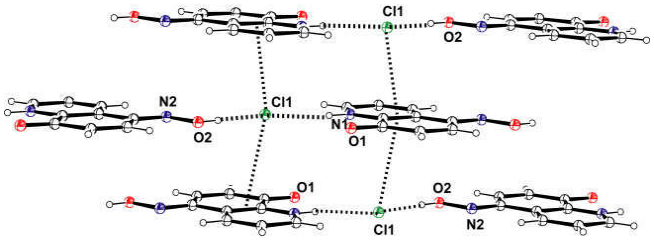

Figure 1.11: Anion-π interactions.

Another important weak interaction in the design of supramolecular assemblies that has attracted interest is the halogen-halogen interaction.[51] Halogen bond may occur between two covalently linked C-X bonds. For instance, to form a halogen bond between C-C···Cl, the chlorine-chlorine contact must have favourable geometries. Such geometries are generally explained as type I ($\theta_1 = \theta_2$) or type II ($\theta_1 = 180$, $\theta_2 = 90$) where θ_1 and θ_2 are the C-Cl···Cl angles as shown in Figure 1.12. Such geometries are found in supramolecular assemblies due to (i) presence of specific attractive forces in certain direction or (ii) nonspherical shapes. When supramolecular assembly possess type (I) arrangement, the halogen-halogen contacts are attractive, while close packing of non-spherical atomic moieties of molecules provides type (II) arrangement.

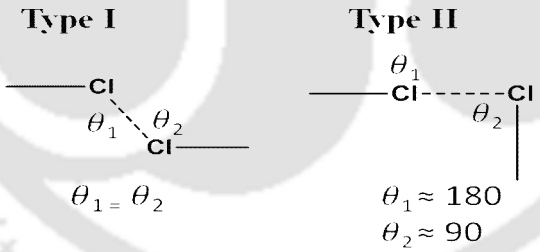

Figure 1.12: Two types of Cl···Cl contacts.

Analogously, halogen-oxygen bonds can be defined as interactions C-X···O-Y, where C-X is carbon bonded chlorine, bromine or iodine and O-Y is hydroxyl, carbonyl, charged carboxylate or phosphate group In which the distance between X···O lesser than or equal to van der Waals radii 3.27Å for Cl···O, 3.37Å for Br···O, and 3.50Å for I···O.

In such type of interactions, there is always a directional preference to adopt relative positions of the contacting groups.

Origin of halogen bonds are explained by σ-hole interaction. A σ-hole interaction as a result of electron deficiency on the outer lobe of a half filled p orbital of halogen atom of a covalent bond.[52] As a result of electron deficiency a region of positive electrostatic potential is developed which interacts with electron-rich acceptors. The interactions of σ-hole may be with negative and neutral covalently linked oxygen, sulfur and nitrogen atom located at the interacting partner. σ-Hole interactions are directional and occur along the extension of a covalent bond. Such interactions are established experimentally and computationally in covalently bonded atoms of group V-VII. There is also another type of similar interactions called π-hole interaction. This interaction occurs due to a region of positive electrostatic potential which is perpendicular to a portion of a molecular framework. The σ-holes and π-holes are more positive in heavier atoms.[53]

Interactions between C-H group and π electron cloud of an aromatic ring is often termed as polar–π interaction, plays an important role in physical, chemical, and biological proesses.[54] The gas-phase energies of such interactions ranges from 8-20kJ/mol and their distances between the hydrogen atom and centroid of the ring ranges 2.4Å-3.2Å.

These interactions are commonly found in proteins. The van der waals interactions are main cause of formation of C-H···π interactions. In some cases contribution of electrostatic interaction is also observed, for example C-H···π interaction with very weak acidic C-H bond such as acetylene or chloroform has some electrostatic contribution. Due to weak nature of C-H···π interactions such interactions are subsidiary interactions when hydrogen bonds are also present to guide the directionality of a self-assembly.[55ab]

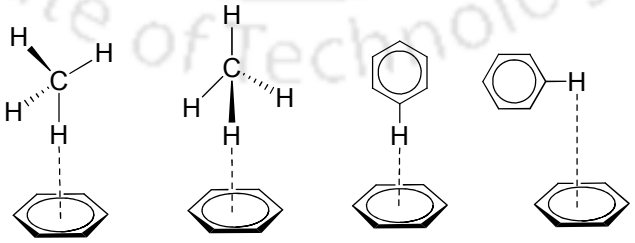

Figure 1.13: Some ways for C-H···π interactions.

On the other hand, a flexible component having possibility to change conformation, are able to adopt various conformations depending on the solvent, crystallisation process or external stimuli. Thus, conformational requirement in self-assembling process is immense. The self-assemblies guided by conformation have generated considerable interest in molecular recognition, properties and in polymorphic materials.[55c]

1.2 Self assemblies of inorganic complexes

Similar to self assemblies of organic compounds, self-assemblies of inorganic compounds have immense importance in biology and material sciences. Such self-assemblies may be between inorganic complexes or inorganic complexes interacting with organic molecules, or between or within inorganic macromolecules such as in coordination polymers and metal-organic frameworks. Common feature of the inorganic complexes is to have coordinate bonds contributing to form discrete or polymeric networks. Supramolecular features associated with such frames inorganic molecules either on the ligand or metal ion or both may contribute to provide architectures of different shape, sizes and dimensions.[56]

Thus, self-assembly of inorganic compounds are dealt with perspectives of coordinate bonds and other weak interactions associated with them. The metal ions in a complex caries charges and provides scope for electrostatic interactions and the inorganic assemblies are more rigid than conventional self-assemblies of organic compounds.

Supramolecular assemblies may be constructed from cationic, anionic and neutral metal complexes.

1.2.1 Coordination polymer

Besides the self-assemblies of discrete mononuclear or polynuclear metal complexes "coordination polymer"[57] are inorganic polymers formed through non-covalent forces in which structural units formed by a repeated unit of coordination complexes.

In inorganic chemistry coordination polymers composed of infinite 1D, 2D and 3D coordination compounds built up with metal ions and ligands as primary building units linked through coordinate bond and other weak forces.[58] A schematic representation of coordination polymer formed between a spacer S and metal ion M is shown in Figure 1.14. This example illustrates an one dimensional coordination polymer but it can be formed in other dimensions depending on the coordination ability of the metal ions and the ligands.

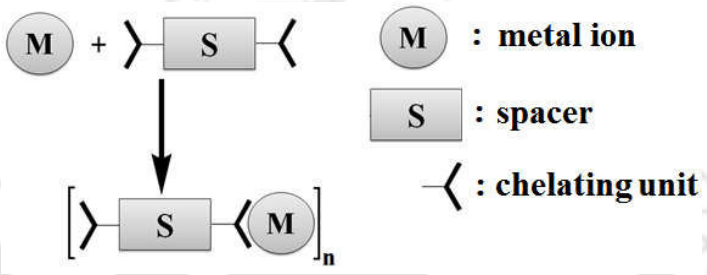

Figure 1.14: Schematic representation of a coordination polymer.

The coordination polymers are of great interest in solid state chemistry depending on structures they are also classified as metal-organic network or framework.[59]

Coordination polymers have advantages over covalently linked polymers[51] such as regular, crystalline structures due to the greater reversibility of the coordination bond compared to the covalent bond and incorporation of metals which leads to properties such as catalysis, luminescence and magnetism.

Coordination polymers shows highly directional structures the common problem arises in dealing with large scale from toxicity of some metal ions.[60] Similar to the organic self-assemblies formed by hydrogen bonds, the presence of hydrogen bonded functional groups in coordination polymers or presence of hydrogen bonding solvent molecules as ligand or solvent of crystallisation can dictate the properties associated with a coordination polymer. Coordination polymers formation process is generally determined by the strength of the coordination bond between the metal ion and supramolecular ligand.[61]

Solvent play an important role in construction of high molar mass coordination polymers. During synthesis solvent compete with ligand to react with metal ion and can control intermediate product, and in fact some cases stable intermediate mono or polynuclear metal complexes can be isolated.

1.2.2 Role of ligands in Coordination polymers

Generally, ligands contribute to coordination polymers to provide bridges between metals thus they are act as linkers and the metal centers are act as connect or node. A ligand can be a part of a coordination polymer as subsidiary ligand with or without providing avenues for supramolecular interactions.

Some common ligands that bridges metal ions are such as halides, hydroxide, oxide, water, amide, thiocynate, isocyanate, cyanide, carboxylate, phosphate, sulphate, nitrate etc. On the other hand, polydentate ligands are good linkers to prepare coordination polymers upon reactions with metal ions. Overall structural features and topology of a coordination polymer or framework structures are influenced by ligands. For example, flexible aliphatic linker generally form a non-porous structure while rigid conjugated linkers lead to open and porous framework.[63] Shape and length of organic linker influence fundamental properties, topology, crystallinity, porosity and surface area.[64] Moreover, number of donor groups on a ligand such as bidentate, tridentate and polydentate nature influences topology.[65] Carboxylate ligands are widely used as a bridiging ligand to genarate porous material.[66]

The varieties of coordination polymers are constructed from the polycarboxylate ligands due to the number of carboxylate groups, spatial orientation of carboxylate group and the coordination mode of carboxylic group, so the depending on these factors, coordination polymer may adopt different architectures.[67]

Due to versatility of carboxylic acid as well as the content of the thesis in preceding chapters we discuss here different aspects of metal carboxylate coordination polymers. Carboxylic acids are widespread in nature and are typically weak acids.

Conjugate base of carboxylic acids, is called carboxylate, which is stabilized by inductive or resonance effects and can have various ways to bind to metals shown in Figure 1.15. Carboxylate functional group widely use for construction of varieties of coordination polymer due to the following reason. (i) The special orientation of carboxylate group, (ii) Versatile coordination modes of carboxylate group, (ii) The number of carboxylate group. (iv) Anciallary ligand in the coordination sphere of the metal ions, (v) Ability to generate metal-oxygen chains to form thermally stable compounds.

Among different mode such as monodentate[57], bridging bidentate[68], symmetric chelating[69], bidentate chelate bridging[70] has its own characteristic feature in conferring a geometrical pattern to coordination polymers. Carboxylate complexes may be also be a part of aggregates comprising of M-O-M bonds as part of polynuclear units, which are referred to as secondary building blocks.

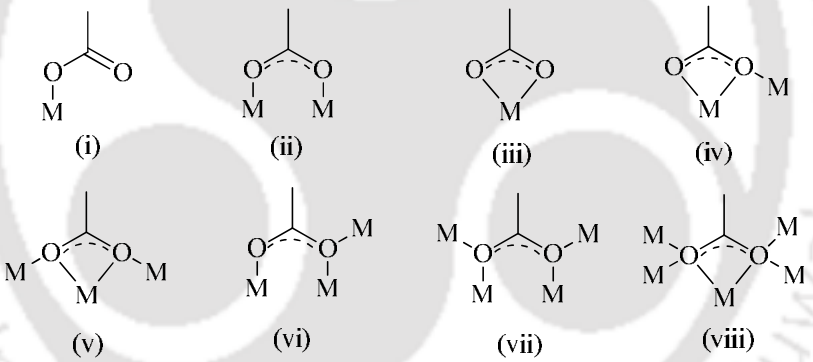

Figure 1.15: Different binding modes of carboxylate anion.

Such secondary building blocks are used to construct metal organic frameworks with defined orientations. On the other hand polycarboxylic acid groups attached to aromatic units become deciding factors in making different types of structures of coordination polymer. In these cases, rigidity of aromatic ring and position of ring where the carboxylic acid group is attached decides their structures. Some commonly used polycarboxylic aromatic ligands are shown in Figure 1.16.

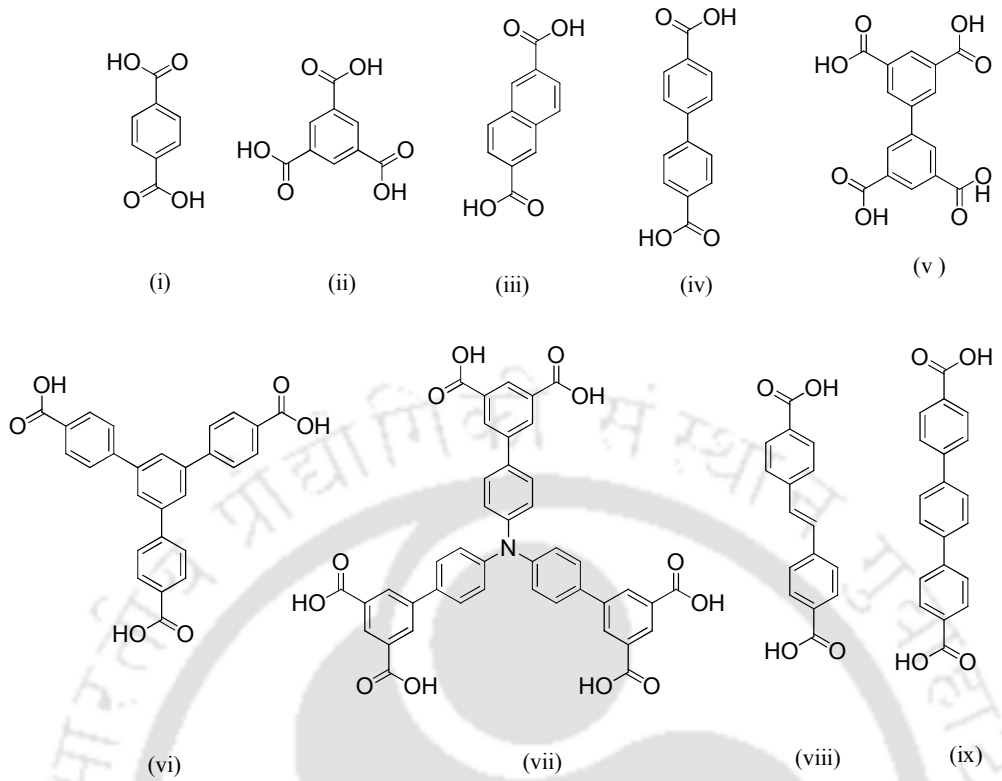

Figure 1.16: Examples of polycarboxylic acids used in construction of coordination polymers.

Generally, a coordination polymer contains other sets of ligands to act as subsidiary ligand or as also contributing as connect along with a carboxylate ligand. For such purposes bis-chelating polyaromatic ligands such as bipyridines, phenanthrolines are widely used together with a carboxylic acid.[71] These ligands control aggregation due to their chelating behaviour around the metal centre.

The use of nitrogen containing heterocycles such as pyridine have the metal coordinating sites, which has become a popular methodology to generate more stable coordination polymers.[72] On the other hand, there are many polydentate heteroaromatic ligands that are useful to construct mixed ligand coordination polymers, some such examples are listed in Figure 1.17.

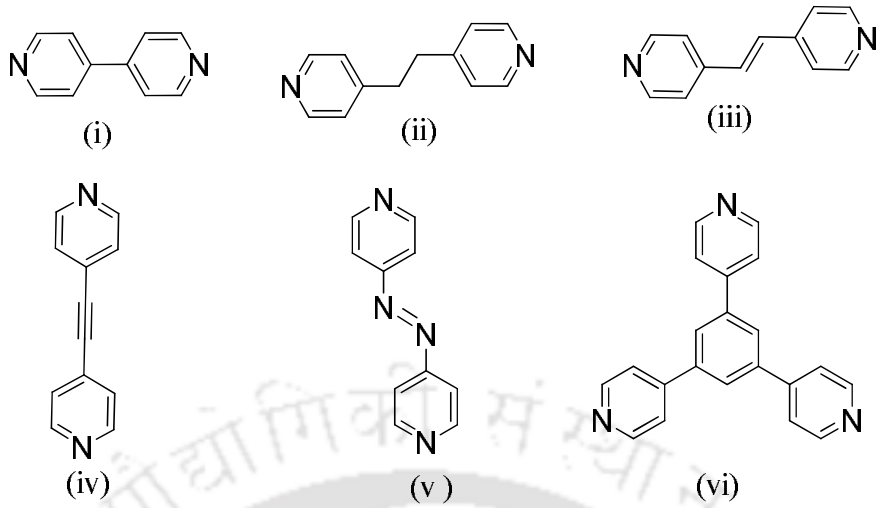

Figure 1.17: Some common ligands with pyridyl donor group.

Due to strong affinity of nitrogen atoms towards most transition metal ions, these linkers impart additional stability to carboxylate coordination polymers by forming thermodynamically stable architectures.[73]

1.2.3 Directional effect of metal ions in Coordination polymers:

Metal ion has its own characteristic coordination numbers, binding strength, exchange rate and stability. Thus, different geometries such as linear, T-shaped, trigonal-planar, tetrahedral, square-planar, square-pyramidal, octahedral, trigonal-prismatic, pentagonal bipyramidal to trigonal-bipyramidal geometry around the metal ions are formed depending on the metal ion under consideration.

For example, lanthanide ions have larger atomic radius and higher coordination number varying from 6-10 are useful for diverse supramolecular architecture.[74]

On the other hand counter ions have important role in construction of supramolecular assemblies. Counter ions present in the vicinity of a metal ion also affects the morphology of metallo-supramolecular architecture,[75] especially in solid state.

Utility of metal ions as connect depends on the affinity of metal towards a particular ligand and on coordination behaviour of metal ion. For example, a linear linker is used in construction of square architecture, if the metal ion has propensity to for a square planar geometry. One such molecular square[76] is shown in Figure 1.18.

These types of inorganic complexes can be easily extended in different dimensions to prepare coordination polymers.

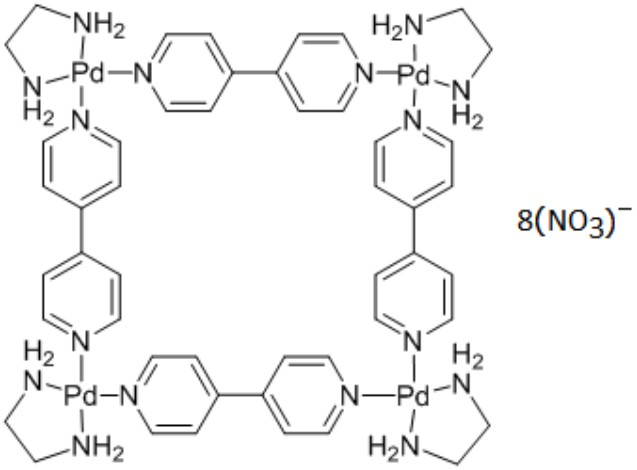

Figure 1.18: A palladium complex with architecture of molecular square **(1.1).**

Rigid ligands generally yield symmetric assemblies, while structural varieties are achieved by using flexible ligands due to different conformations. Presence of groups like methylene, ethylene and propylene as component of a linker provide flexibilities to structures of coordination polymers. An example of helical structure observed in silver complex of a flexible tris(bipyridine) ligand[77] is shown in Figure 1.19.

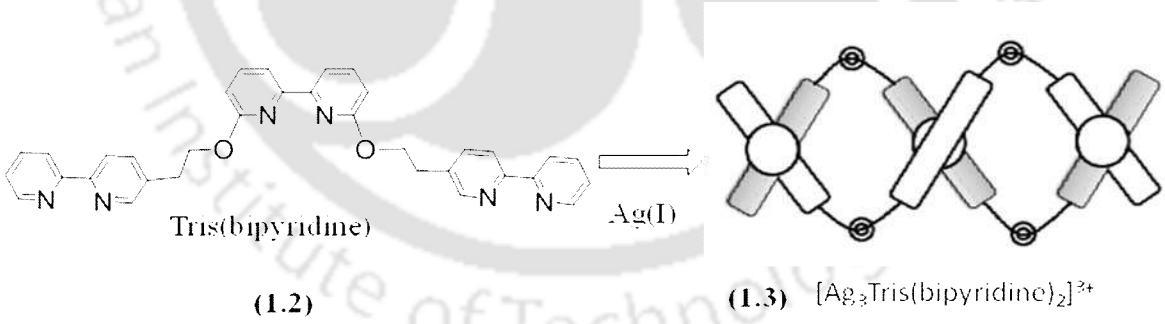

Figure 1.19: A schematic representation of helical complex from a semi-flexible ligand.

Self-assembly of Cu^{2+} complex of oligo-2,2'-bipyridine[78] adopts a helical structure as shown in Figure 1.20. Copper(II) ion prefers tetrahedral geometry which guides the formation of a double-strand helix upon coordination with oligo-bipyridine.

Similar complexes with Ni^{2+} ions posses octahedral geometry around nickel ions. Due to this three chains get coordinated to nickel ions to make triple-stranded helical structure.

This clearly shows the selective formation of a helical structure is guided by the metal ion under consideration and makes avenue for molecular recognition.

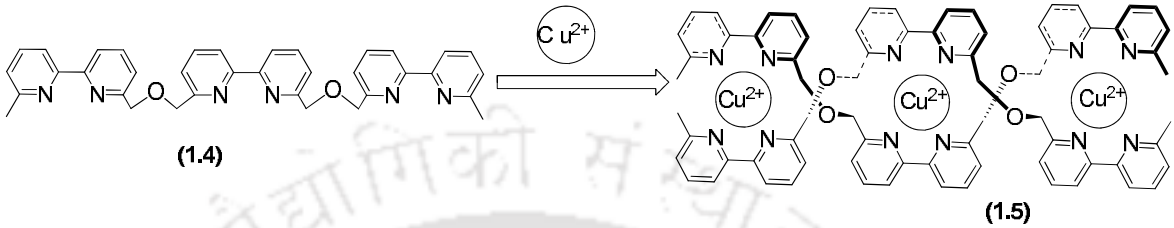

Figure 1.20: Formation of double helical structure.

Ruthenium(II) based polynuclear coordination polymers are useful in information storage and conversion of light into chemical energy.[79] A useful terpyridine-based coordination polymer is which can play a role in catalysing splitting of water is shown in Figure 1.21.[78]

Silver(I) coordination polymer with rigid pyridine derivative[80] leading to grid-type architectural pattern is shown in Figure 1.22. In this coordination polymer, the bipyridine ligands are present at two different orientations perpendicular to each other. The silver ions distorted tetrahedral geometry by forming four Ag-N bonds per silver ion.

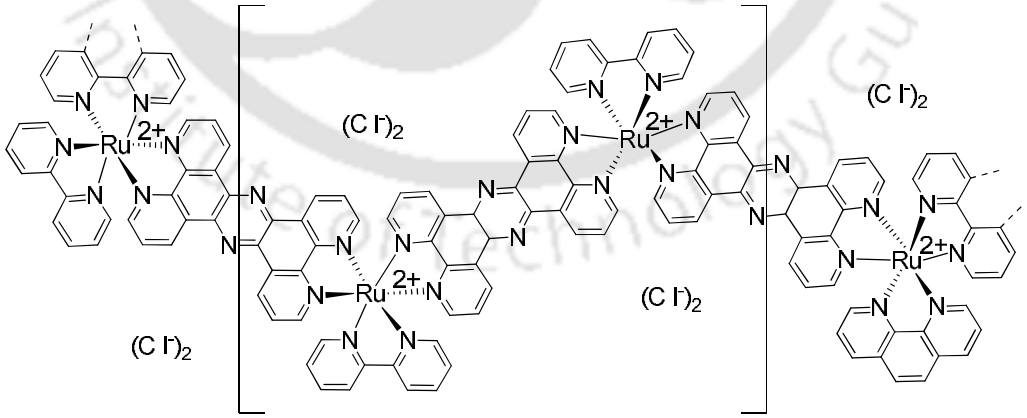

Figure 1.21: A terpyridine based Ruthenium coordination polymer **(1.6).**

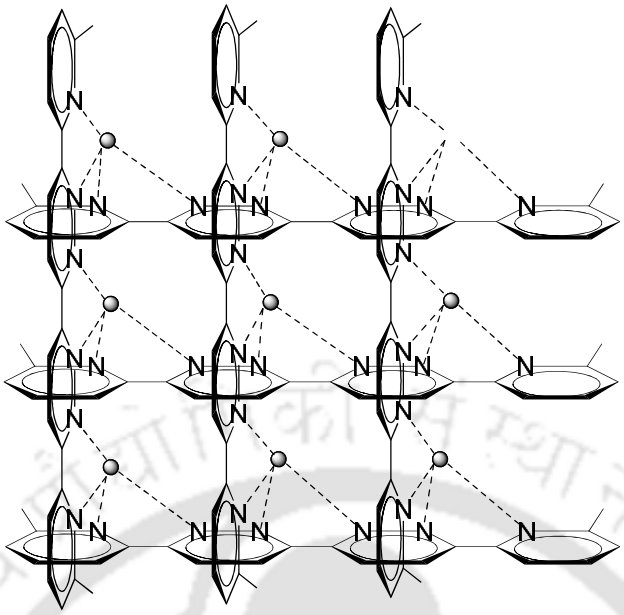

Figure 1.22: Cationic part of a grid-type structure of a silver coordination complex **(1.7).**

1.2.4 Dimensionality of coordination polymers

Dimensionality of coordination polymers are usually determined by connects/nodes. An one dimensional coordination polymer has metal ions coordinated generally to two ligands in such a way that metal ions and ligands arranged alternately to form infinite chain. Different types of structural patterns are generated in coordination polymers and some architectures are illustrated in Figures1.23-1.25.

Two-dimensional coordination polymers are formed by combination of three or four ligands coordinating to the metal ion and primary pattern expand in two directions whereas a three-dimensional coordination polymer expands along three directions. Metal ions higher coordination numbers facilitates formation of three dimensional coordination polymers and large numbers of examples are associated with polymers having tetrahedral or octahedral nodes.

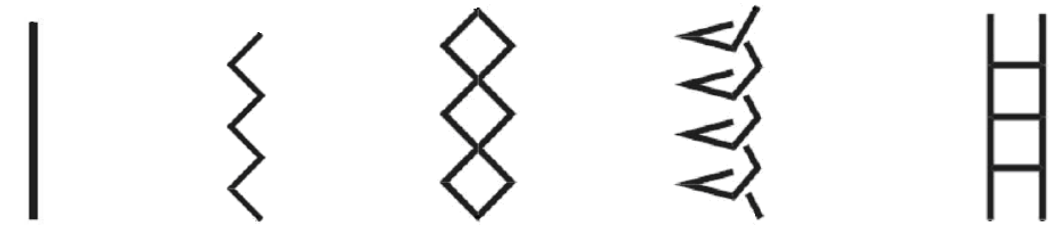

Linear chain Zigzag chain Double chain Helix Ladder

Figure 1.23: One dimensional architectures of coordination polymers **(1.8).**

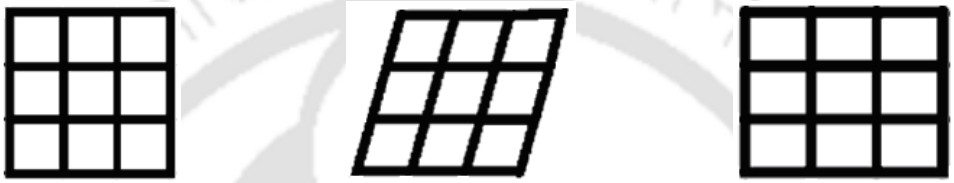

Square grid Rhombic grid Rectangular grid

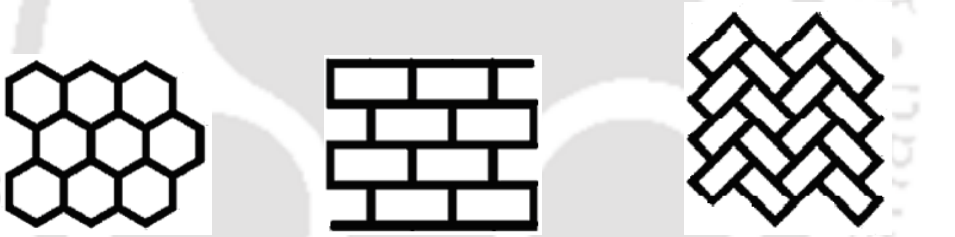

Honeycomb grid Brick wall Herringbone

Figure 1.24: Two dimensional architectures of coordination polymers **(1.9).**

Diamondoid net octahedral net

Figure 1.25: Three dimensional architectures of coordination polymers **(1.10).**

Control on the orientation and stereochemistry of the building blocks are essential to obtain a desired molecular topology.[81] Metal organic framework (MOF) may also be formed by combination of coordination bond and other weak interactions.

1.3 One dimensional coordination polymers

1.3.1 Single chain

Chains are representation of simple one dimensional coordination polymers. For example, linear chain coordination polymer $[Cu_2(4,4'\text{-bipyridine})_2(\text{thiopheneacetate})_4]_n$ **(1.11)** has copper(II) ions bonded with 4,4'-bipyridine and acetate. In this coordination polymer copper ions have distorted square planar geometry.[82]

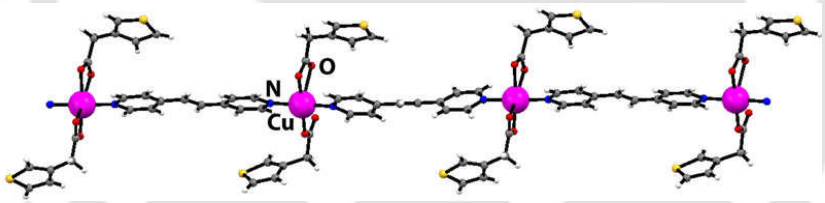

Figure 1.26: Complex **(1.11)** as an example of 1-D coordination polymer.

One-dimensional coordination polymers may adopt zig-zag structure, for example complex $[Cu\ (1,10\text{-phenanthroline})(\text{terephthalate})]_n$ **(1.12)** has a zig-zag polymeric chain as shown in Figure 1.27.[83]

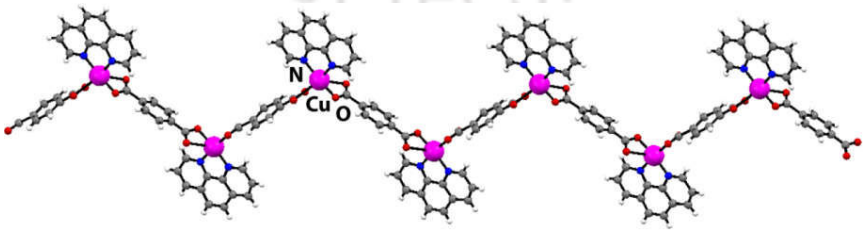

Figure 1.27: Coordination polymer **(1.12)** as an example of zig-zag structure.

Copper (II) ions adopt distorted square planar geometry and each is coordinated to two nitrogen atoms from phenanthroline, two carboxylate-oxygen atoms from two different terephthalate and one oxygen atom from coordinated water molecule.

1.3.2 Double chain

As name suggests these are combinations of two chains grown in two independent dimensions. $\{[In_2(2,2'\text{-bipyridine})_2(1,3,5\text{-benzenetricarboxylate})_2].4H_2O\}_n$ **(1.13)** is an example of 2D net coordination polymer. It has indium ions binding to five oxygen atoms of carboxylates and two nitrogen atom of 2,2'-bipyridine forming distorted pentagonal bipyramidal coordination geometry around each indium ion as illustrated in Figure 1.28.[85]

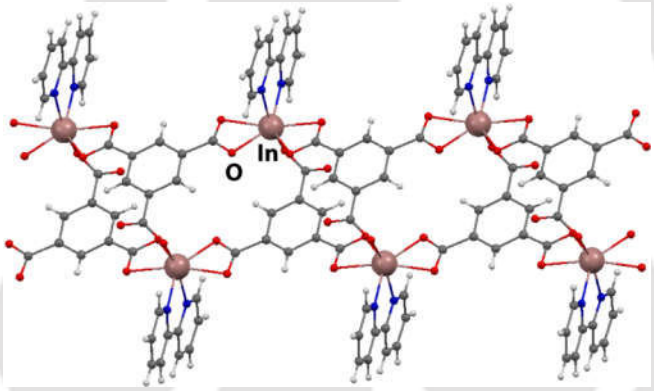

Figure 1.28: Double chain Structure of Complex **(1.13).**

1.3.3 Ladder

Ladder type coordination polymers are of great interest for construction of rational solid material with interesting properties. One example is $\{[Cu(4,4'\text{-bipyridine})(acetate)_2]\}_n$ **(1.14)** ,which consists of symmetric copper(II) acetate dimer linked to 4,4'-bipyridine, and each copper has a monodentate acetate.[86] Resulting complex has square pyramidal geometry around metal centers.

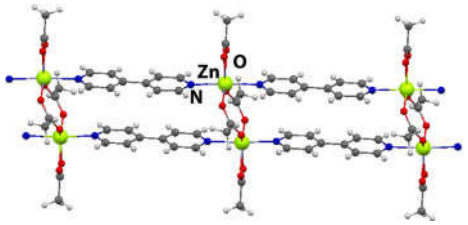

Figure 1.29: Ladder-like structure in $\{[Cu(4,4'\text{-bipyridine})(acetate)_2]\}_n$ **(1.14).**

1.3.4 Helix

Reaction of cobalt(II) ions with 2,2'-bipyridyl-3,3'-dicarboxylic acid generates helical one dimensional coordination polymer **(1.15)**.[86] Cobalt(II) ions adopt distorted octahedral geometry by coordination with three water oxygen atoms; one oxygen atom of the carboxylate of a 2,2'-bipyridyl-3,3'-dicarboxylic acid coordinate to the a metal ion and two nitrogen atoms from another 2,2'-bipyridyl-3,3'-dicarboxylic acid. It gives rise to 1D helical coordination polymer. The helical chains are linked by hydrogen bonds between oxygen atoms of carboxylate and a water molecule of an adjacent helical chain, which leads to 2D networks.

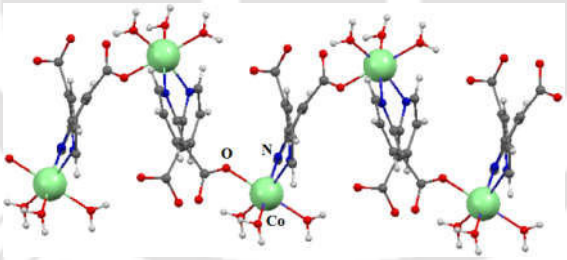

Figure 1.30: Structure of a 1D helical coordination polymer **(1.15).**

1.4 Two dimensional coordination polymers

1.4.1 Square grid

Square grids are commonly observed architecture among different two dimensional coordination polymers.

The structure of $[Zn(nicotinate)_2]_n$ **(1.16)** consists of distorted tetrahedral zinc metal ions.[87] There are two nitrogen atoms of pyridyl group and two oxygen atoms of carboxylate group of nicotinate ligand binds with zinc ions as shown in Figure 1.30.

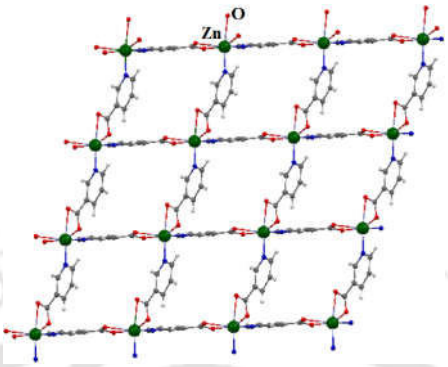

Figure 1.31: Two dimensional square grid structure of complex **(1.16)**.

1.4.2 Rhomboid grid

Rhombic grid-like structure is observed in structure of $[Ni(pyridine)_2(4\text{-sulfanylmethyl-}4'\text{-phenylcarboxylate}]_n$ **(1.17)**. Rhombus grid has dimensions 11.72Å × 11.09Å. Each ligand acts as bridge linking two nickel ions through pyridine nitrogen atom and oxygen atoms of carboxylate to form an infinite two-dimensional structure.[88]

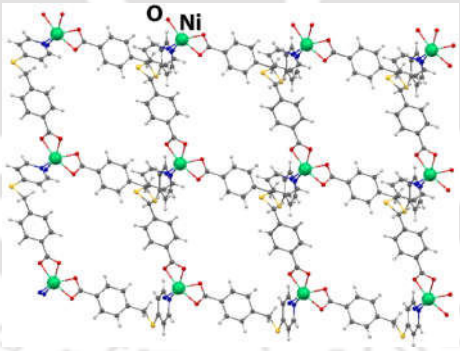

Figure 1.32: Rhombic grid in $[Ni(pyridine)_2(4\text{-sulfanylmethyl-}4'\text{-phenylcarboxylate}]_n$ **(1.17)**.

1.4.3 Rectangular Grid

An example of two dimensional rectangular grid type coordination polymer is $[Co(H_2O)_6][Co(8,9\text{-dimethylthio-2,3-dicarboxylatetetrathiafulvalene})_2(DMF)_2]$ **(1.18)** is shown in Figure 1.33.

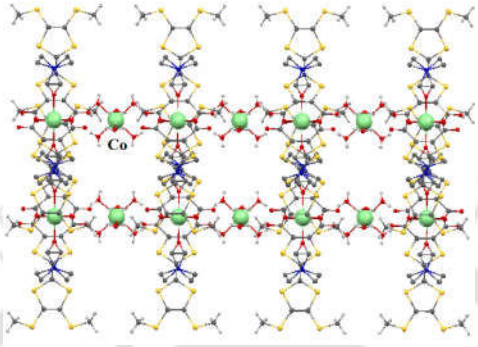

Figure 1.33: Structure of complex $[Co(H_2O)_6][Co(8,9\text{-dimethylthio-2,3-dicarboxylate tetrathiafulvalene})_2(DMF)_2]$ showing rectangular grids **(1.18).**

An example of two dimensional rectangular grid type coordination polymer is $[Co(H_2O)_6][Co(8,9\text{-dimethylthio-2,3-dicarboxylatetetrathiafulvalene})_2(DMF)_2]$ **(1.18)** is shown in Figure 1.33. Structure comprises of cobalt ions, each is coordinated by four oxygen atoms of carboxylate in the equatorial plane and there are two oxygen atoms of DMF molecules occupying apical positions.[89]

1.4.4 Honeycomb

It is unique architecture among two dimensional coordination polymers which can be prepared by reactions of multifunctional ligands with metal ions. For instance, two-dimensional complex of iron(II), $\{[Fe_2(2,2'\text{-bipyrimidine})(oxalate)_2].5H_2O\}_n$ **(1.19)** has a honeycomb structure.[90] Structure of the complex has oxalato-bridged iron(II) chains cross-linked by *bis*-chelating bipyrimidine affording a honeycomb type lattice. Honeycomb like architecture (Figure1.34) have uniform distribution of high-density active sites which enhances the mass transport of gas and electrolyte.

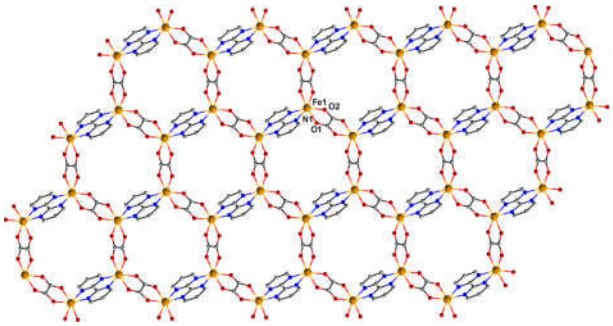

Figure 1.34: Honeycomb like structure in coodination polymer $\{[Fe_2(2,2'\text{-bipyrimidine})(oxalate)_2].5H_2O\}_n$.

1.4.5 Herringbone

In Herringbone type structure three ligands coordinate to metal ion forming "T-shape" around a node. These repeat units are connected with other sets to form layers. Two dimensional coordination polymer, $\{[Ni\ (4,4'\text{-dipyridylamine})(phthalate)]\ 1.33H_2O\}_n$ **(1.20)** has a herringbone type architecture.[91]

The structure is constructed from a 4,4'-dipyridylamine and a phthalate ligands as illustrated in Figure 1.35. Large asymmetric unit of the complex consists of three crystallographically unique nickel atoms along with phthalate dianions and 4,4'-dipyridylamine ligands. There also four water molecules of crystallization. All the nickel ions adopt distorted octahedral geometry.

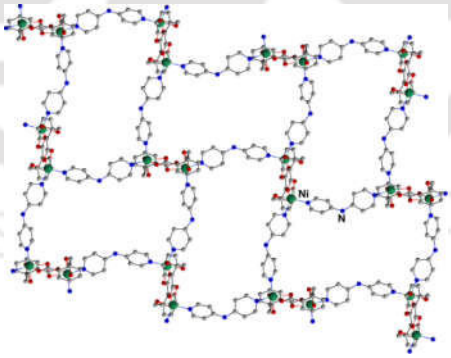

Figure 1.35: Herringbone structure of $\{[Ni(4,4'\text{-dipyridylamine})(phthalate)].1.33H_2O\}_n$ **(1.20)**

1.4.6 Brick wall

Reaction of 1,3,5-benzenetricarboxylate anion with nickel macrocyclic complex shown in Figure **1.21(a)** gives a coordination polymer **1.22(b)**. This coordination polymer has brickwall structure illustrated in Figure 1.36(b).

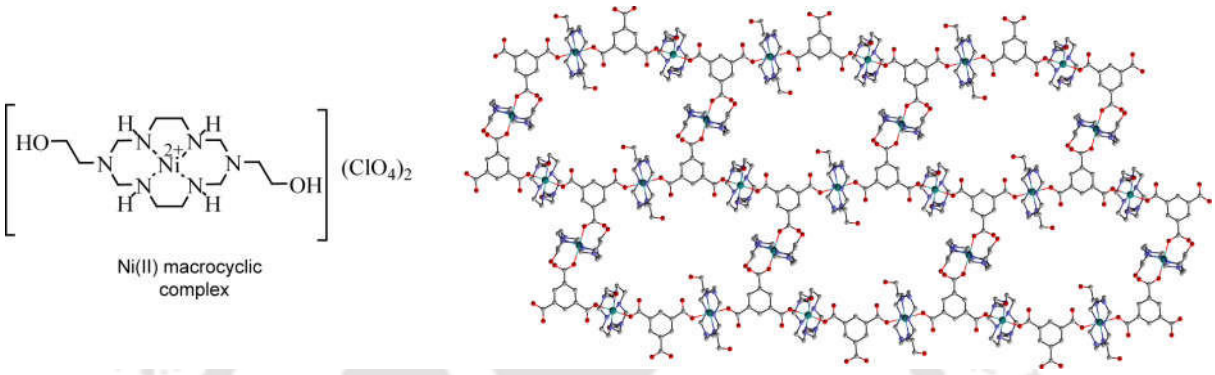

Figure 1.36: (a) Structure of nickel(II) macrocyclic complex, (b) Brickwall type structure of complex **1.22** constructed by nickel macrocycle and 1,3,5-benzenetricarboxylate

Tetragonally distorted octahedron geometry is observed around nickel ions. The effective cavity size of the two dimensional complex is 6.7Å x 13Å. The cavities are filled with guest molecules. The structure of the coordination polymer is greatly affected by change of the guest molecules. In the presence of pyridine the structures of complex change to honeycomb from brickwall motif.[92]

1.5 Three dimensional coordination polymers

There is wide range of structural variations are observed in three dimensional coordination polymers. Thus some commonly observed structures are discussed under different subheadings.

1.5.1 Diamondoid net

Hydrothermal reaction of manganous sulphate with 2-(4-carboxyphenyl)imidazo(4,5)(1,10-phenanthroline) yields diamond type network **(1.23)** as shown in Figure1.37(b).

In which each manganese (II) ion is coordinated by four nitrogen atom of phenanthroline molecule and two oxygen from carboxylate group adopt distorted octahedral environment around metal ions.[93]

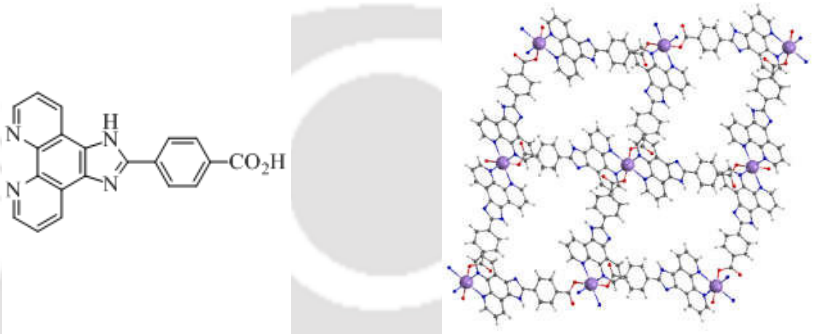

(a) (b)

Figure 1.37: (a) Structure of 2-(4-carboxyphenyl)imidazol(4,5)(1,10-phenanthroline), (b) Structure of 3D diamond-like network constructed by **(1.23)**.

1.5.2 Octahedral net

Octahedral nets are based on the extension of the framework in the three directions from octahedral nodes.

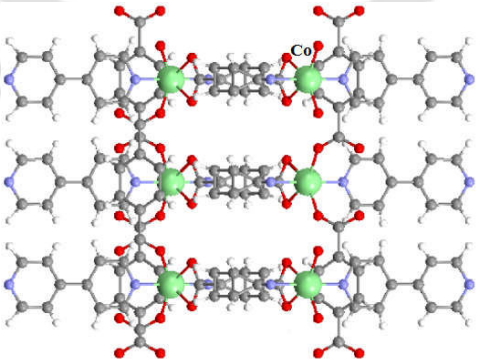

Figure 1.38: Octahedral net of cobalt with terephthalic acid and 4,4'-bipyridine **(1.24).**

Octahedral net of cobalt with terephthalic acid and 4,4'-bipyridine are formed where apical positions of the octahedral metal ions are occupied by water molecules, other solvent molecules or counter anions, and results in network of low dimensionality. Reaction of cobalt (II) nitrate hexahydrate with terephthalic acid and 4,4'-bipyridine gives [Co(4,4'-bipyridine) (terephthalate)]$_n$ **(1.24)** shown in Figure 1.37.[94]

Bipyridine molecules are linked to cobalt(II) cations through apical positions and structure expands to third direction. The dimension of 2D rectangular sheets of metal and terephthalate is 10.30Å × 11.37Å. Polycaboxylate ligands have attracted attention in the field of crystal engineering due to its versatile coordination modes and ability to generate supramolecular architecture by connection with the metal centers.

1.6 Coordination Polymers and Self-assemblies of Pyridinedicarboxylates

It is evident that coordinating hetero-atoms of a bridging ligand influence structure of coordination polymer. Pyridinedicarboxylic acid is a simple system to understand combine effect of two carboxylate with a pyridine in coordination to metal ions.

Pyridinedicarboxylic acid has different positional isomers which are shown in Figure 1.39. Each isomer has characteristic ways to coordinate to metal to generated different scaffolds in coordination polymers. Due to directional nature of the ligating sites in these isomers diverse structural variations can be brought about. In this section, some coordination polymers and self-assemblies[95] of different positional isomers of pyridinedicarboxylate[96] are discussed.

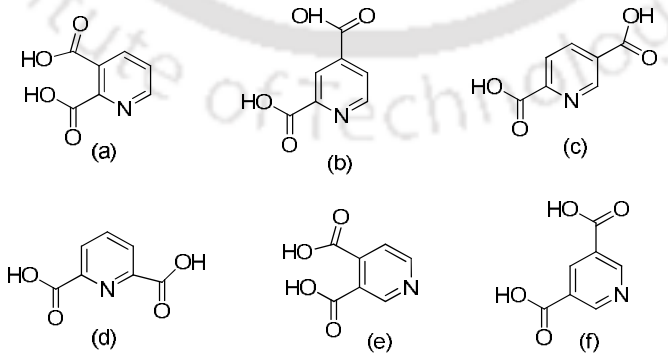

Figure 1.39: Different positional isomers of pyridinedicarboxylic acids **(1.25).**

Bioinorganic chemistry associated with this class of compounds has increased their attention.[97] Coordination complex formed by each isomer is different, hence coordination chemistry of individual isomers is discussed under separate sub-headings.

1.6.1 2,3-Pyridinedicarboxylate (23pdc) complexes

2,3-Pyridinedicarboxylic acid is a good ligand for formation of mononuclear and poly-nuclear metal complexes. In mononuclear complex it binds to metal forming chelate leaving one carboxylic acid free. It also forms dinuclear complexes where one carboxylic acid group acts as bridge between two metal ions. Such complexes form self-assemblies utilising free carboxylic acid group.

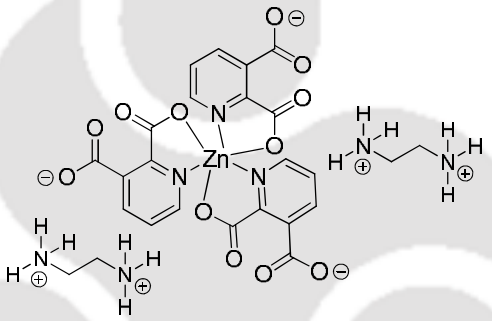

Figure 1.40: Bis-ethylenenediammonium zinc(II) tris2,3-pyrdinedicarboxylate complex **(1.26).**

Numbers of 2,3-pyridinedicarboxylate coordination polymers are much larger than mononuclear complexes. Depending upon the reaction procedure and organic cations mononuclear complex can be formed. The reaction of 2,3-pyridinedicarboxylic acid, ethylenediamine with zinc acetate dehydrate gives a mononuclear complex (ethylenediamineH_2)$_2$[Zn(23pdc)$_3$]·2H_2O. In this complex has (II) ion coordinated with three molecules of **23pdc** ligand through N atom of pyridine ring and O atom of carboxylate group in where zinc ion adopt octahedral environment.[98]

Copper(II) 2,3pyridinedicarboxylate with 2-ethyl-4-methyl-imidazole as ancillary ligands has is a dinuclear complex having a structure shown in Figure 1.41.

Dinuclear complexes such as copper(II) 2,3-pyridinecarboxylate complexes containing 4,4'-dipyridyl-N,N'-dioxide and 1,3-bis(4-pyridyl)propane are reported in literature.[129] The structural analysis revealed these complexes have dinuclear copper pyridinedicarboxylate units linked by 4,4'-dipyridyl-N,N'-dioxide or 1,3-bis(4-pyridyl)propane to form two dimensional supramolecular architecture.[99]

Large structural differences between copper(II) and cadmium(II) 2,3-pyridinedicarboxylate arises in the coordination numbers of the metal ions. Copper coordination polymer having 1,3-bis(4-pyridyl)propane[134] has five coordinated copper(II) ions.

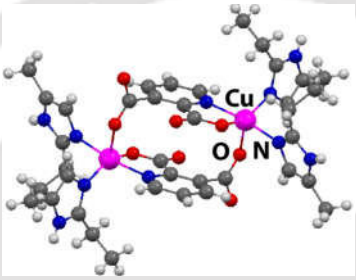

Figure 1.41: Dinuclear $[Cu_2(23pdc)_2(2\text{-ethyl 4-methylimidazole})_4]$ **(1.27).**

Whereas, similar cadmium(II) coordination polymer has six coordinated cadmium ions as illustrated in Figure 1.42. Cadmium(II) ions are coordinated to one **23pdc**, one 1,3-bis(4-pyridyl)propane, one coordinated water molecule to adopt octahedral geometry.[100]

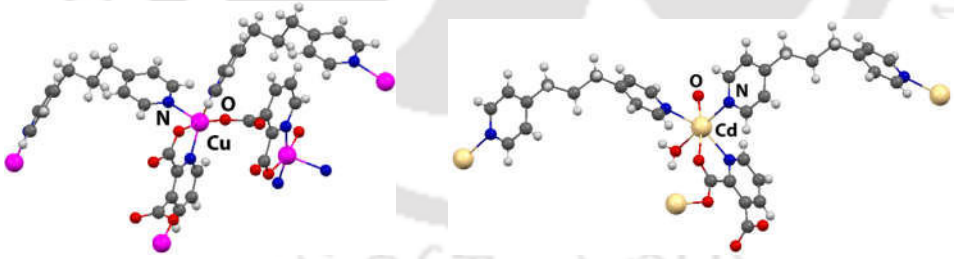

(a) (b)

Figure 1.42: (a) Copper(II) and (b) Cadmium(II) coordination polymers with **23pdc** and 1,3-bis(4-pyridyl)propane**.**

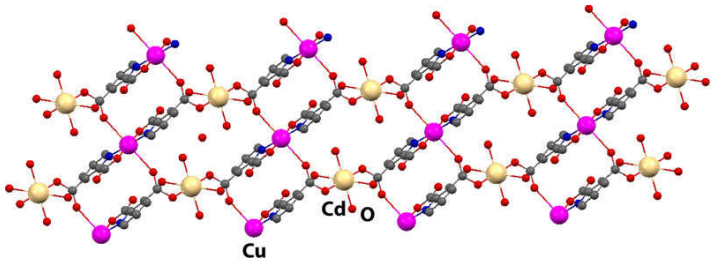

Figure 1.43: Two dimension coordination polymer of copper(II) 2,3-pyridinedicarboxylate with Cd(II) ion **(1.29).**

Heterometallic coordination polymer of cadmium and copper such as $\{[Cd(H_2O)_4Cu(\mu\text{-}23pdc)_2].2H_2O\}_n$ **(1.29)** has two dimensional architecture. It comprises of complex cation $[Cd(H_2O)_4]^{2+}$ which act as interlink between two dinuclear copper pyridinedicarboxylates, leading to two dimensional arrangement. Copper(II) ion coordinate with N and O atoms of from 2,3-pyridinedicarboxylate ligand and cadmium(II) ion coordinate to four water molecules and two O atom of carboxylate group at *meta* position of 2,3-pyridinedicarboxylate ligands. Both metal ions adopt distorted octahedral geometry. Thus, depending on metal ions and ancillary ligands, nuclearity of 2,3-pyridinedicarboxylate metal complexes varies.

1.6.2 2,4-Pyridinedicarboxylate (24pdc) complexes

2,4-Pyridinedicarboxylic acid form chelate complexes by coordinating through the nitrogen atom and carboxylic acid at 2-position of the pyridine ring. In such a chelate one carboxylate when remain free, it forms mononuclear complex,[101] and when this caboxylate group coordinates to another metal ion it forms coordination polymer or higher nuclearity complex. One representative example of mononuclear complex of 2,4-pyridinedicarboxylate is $[Cu(24\text{-}Hpdc)_2].2H_2O$ **(1.30).**

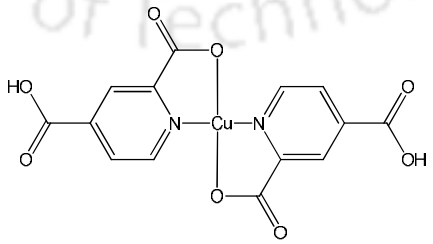

Figure 1.44: Mononuclear copper(II) 24pdc complex **(1.30).**

This complex is formed by hydrothermal reaction of copper(II) oxide with 2,4-pyridinedicarboxylic acid. Crystal structure analysis have revealed that copper(II) ion is coordinated by two N atom and two O atoms of carboxylate group.[102] Copper(II) ion is tetra coordinate having distorted planar geometry as shown in Figure 1.45.

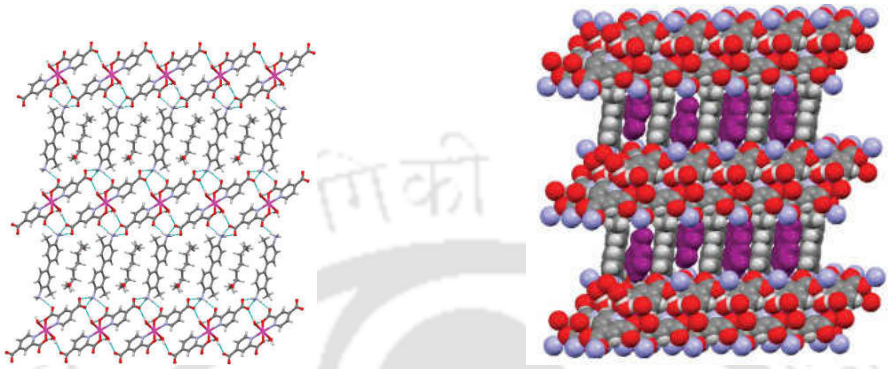

(a) (b)

Figure 1.45: (a) n-Hexanol inclusion in [(3,3'- dimethylbenzidinium)] $[Zn(24pdc)_2(H_2O)_2]$, (b) Space-filled representation.

There are large numbers of coordination polymers constructed from the 2,4-pyridinedicarboxylate. A mononuclear Zn(II) complex $[Zn(24Hpdc)_2(H_2O)_2]$ reacted with 3,3'-dimethylbenzidine to form a $[(3,3'\text{-dimethylbenzidinium})][Zn(24pdc)_2(H_2O)_2]$ **(1.31)** pillared layered like structure in which diamine molecule serve as a pillar and pyridinedicarboxylates unit work as a metal containing layer. Strong hydrogen bonds between carboxylates with amines provide stability to the framework. Framework derived by combining of inorganic and organic components can be easily modified. This stable framework includes varieties of guest molecules. In the complex **(1.31)** four different guest molecules namely, p-xylene, nitrobenzene, hexanol and acetone were successfully incorporated in between the pillar layered structures without disturbing of layered framework. One such example of structure having n-hexanol as guest is shown in Figure 1.45. A similar reaction as that of complex **(1.31)**, the reaction of $[Cu(24\text{-}Hpdc)_2(H_2O)_2]$ with flexible amine 4-methylphenylethylamine in methanol leads to hydrogen bonded supramolecular architectures of $\{[Cu(24\text{-}Hpdc)_2(H_2O)_2](4\text{-methylphenylethylamine})_2\}$ (acetone) (Figure 1.46) **(1.32)**.[103] This coordination polymer has a lamellar structure which can hold various guest molecules.

(a) (b)

Figure 1.46: (a) Skeleton of $[copper(II)(24pdc)_2(H_2O)_2]^{2-}$, (b) Hydrogen-bonded layers holding acetone molecules as guests.

1.6.3 2,5-Pyridinedicarboxylate (25pdc) complexes

2,5-Pyridinedicarboxylate complexes have close structural similarities to the corresponding analogous complexes that of **23pdc** isomer. Due to change in position and the bite angle in these cases, there are examples of formation of tetranuclear complexes **(1.33)** of **25pdc** ligand.[104]

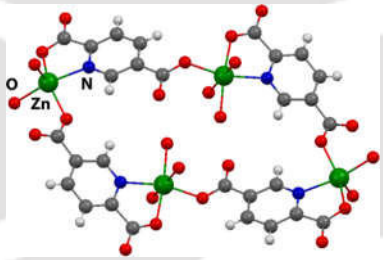

Figure 1.47: Tetranuclear complex $\{[Zn(25pdc)(H_2O)_2][Zn(25pdc)(H_2O)_3]\}_2$ **(1.33)**.

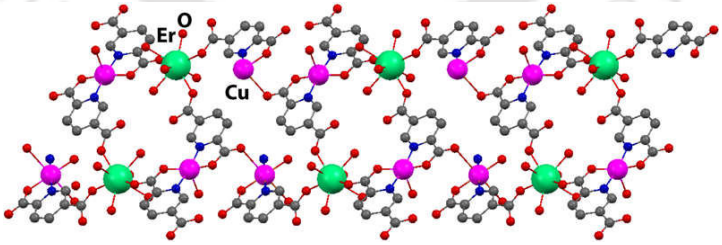

Figure 1.48: Structure of coordination polymer $[\{Er_2Cu_3(25pdc)_6(H_2O)_{12}\}.4H_2O]_n$ **(1.34)**.

$\{[Zn(25pdc)(H_2O)_2][Zn(25pdc)(H_2O)_3]\}_2$ is such an example of a tetranuclear metallacycle.[105] It comprises of two dinuclear $\{[Zn(25pdc)(H_2O)_2][Zn(25pdc)(H_2O)_3]\}$ sub units connected together by bridging carboxylates. Two zinc ions are at two different coordination environments. One zinc ion is six coordinated has two **25pdc** ligands and three water molecules, whereas other zinc metal ion is in a trigonal bipyramidal coordination environment and coordinated by **25pdc** ligand and two water molecules. Further to this macrocycles are connected together to form three dimensional supramolecular framework through hydrogen bonds and π-stacking. There are examples of coordination polymers such as mixed cationic **25pdc** coordination polymers of erbium and copper namely $[\{Er_2Cu_3(25pdc)_6(H_2O)12\}.4H_2O]_n$ **(1.34)**.

The polymeric chain of this coordination polymer is a combination of two building blocks comprising of $[Er_2Cu_2\ (25pdc)_4(H_2O)_{12}]$ and $[Cu(25pdc)_2]$(Figure 1.48). These building blocks are linked to each other by pyridinedicarboxylate ligands through Er-O bond. Coordination environments around two copper ions in the structure of the coordination polymer are different. At one site $[Cu(25pdc)_2]$ is chelated by two **25pdc** ligand to provide a square planar geometry. Copper atoms of $[Er_2Cu_2(25pdc)_4(H_2O)_{12}]$ is coordinated through two **25pdc** and a water molecule and it adopts distorted square pyramidal geometry.

1.6.4 2,6-Pyridinedicarboxylate (26pdc) complexes

2,6-Pyridinedicarboxylic acid binds to a metal by different types of binding modes such as monodentate, bidentate or tridentate. It forms supramolecular coordination polymers. Metal complexes of **26pdc** provide template to stack while forming host-guest complexes with planar guest molecules. Further advantage of dealing with coordination complexes **26pdc** is that they are soluble in common protic solvent such as water, methanol and ethanol. Mononuclear vanadium and cobalt 2,6-pyridinedicarboxylate complexes exhibit insulin mimic properties.

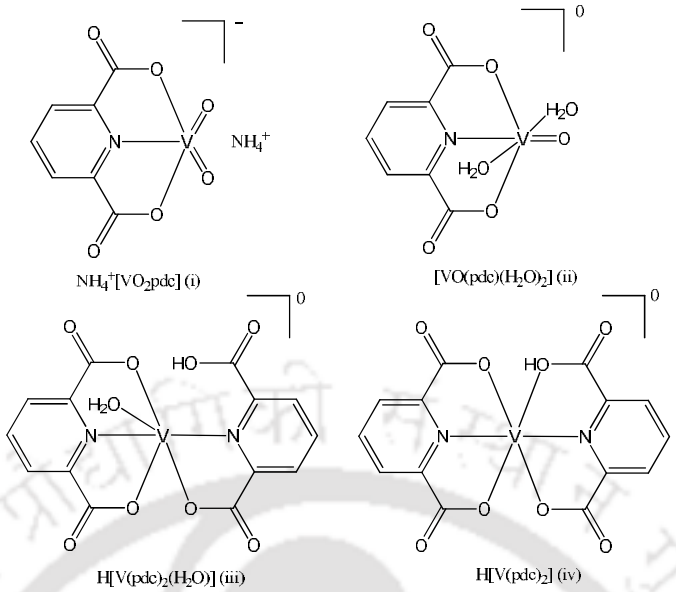

Figure 1.49: Examples of some vanadium complexes possessing 2,6-pyridinedicarboxylic acid.

Oral administration of {$H[V^{III}(26pdc)_2H_2O].3H_2O$, $[V^{IV}O(26pdc)(H_2O)_2].2H_2O$, and $NH_4[V^{V}O_2(26pdc)]$} lower the hyperglycemia and hyperlipidemia of diabetes.[106] Examples of 2,6-pyridinedicarboxylate vanadium complexes formed under different reaction conditions are listed in Figure 1.49.

In addition to neutral and anionic **26pdc** complexes, there are acidic **26pdc** complexes. For example $[H_2Cu(26pdc)_2]\cdot H_2O$ is like a neutral acid coordinating to copper. The examples of iron complex illustrated in Figure 1.50 is a neutral complex containing only one **pdc**, whereas a copper complex contains one **26pdc** and one **26-H_2pdc** ligand.[107]

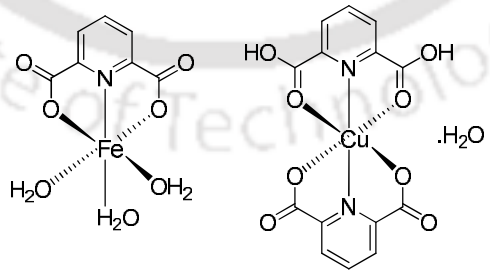

Figure 1.50: Mononuclear 2,6-pyridinedicarboxylate iron(II) and copper(II) complexes.

2,6-Pyridinedicarboxylate complexes derived from divalent and trivalent metal ions generate layered structures guided by π-stacking interactions.

Among these dicarboxylate ligands 2,6-pyridinedicarboxylate shows extra-ordinary ability to form layered like structure.[108] π-Sacking interactions of these derivatives can be applied for stabilization of supramolecular architectures and can be utilize for molecular recognition.[109]

Lanthanide pyridinedicarboxylates generally contains three tridentate **26pdc** ligands, form nona-coordinated complex such as $[Eu(pdc)_3]^{3-}$ **(1.37)** shown in Figure 1.51.[110]

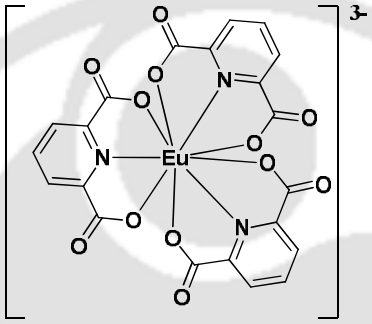

Figure 1.51: Tris-(26pdc) europium trianion **(1.37)**.

There are examples of dinuclear complexes such as $[Mn_2(26pdc)_2(H_2O)_6]$ **(1.38)**. In this complex, each manganese ion possesses dipicolinate ligand which acts as chelate and bridging ligand. Manganese ions are coordinated by three water molecules each. The two halves of dimeric unit are linked through two Mn-O-Mn bridges. Packing pattern of the complex has hydrogen bonds between coordinated water molecules and pyridinedicarboxylates.[111]

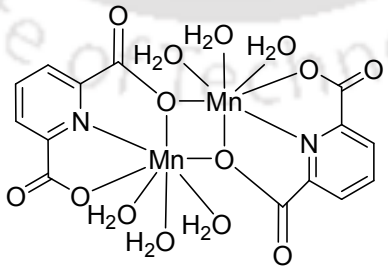

Figure 1.52: Dinuclear manganese **26pdc** complex **(1.38)**.

Copper(II) also forms **26pdc** dinuclear complexes having dipyridyl or dipyridinedioxide as spacers. One such example is $[Cu_2(26pdc)_2(4,4'\text{-dipyridyl-N,N'-dioxide})(H_2O)_2]_n$.

It has square planar geometry around copper ions. **26pdc** and water molecules along with the difunctional spacer forms linear dinuclear complex.

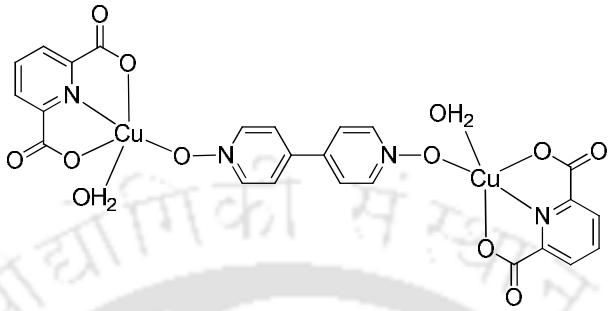

Figure 1.53: Copper(II)26pdc dinuclear complex having 4,4'-dipyridyl-N,N'-dioxide.

There are also examples of trinuclear **26pdc** complexes. $[(26pdc)_2(26pdcH)_2Fe^{II}_3(H_2O)_4]$ **(1.40a)**[113] is such an example which is made up of two $[(26pdc)(26pdcH)Fe^{II}]$ subunits sharing oxygen atom with a $[Fe^{II}(H_2O)_4O_2]$ subunit as shown in Figure 1.54. Another trinuclear complex is $[Mn_3(26pdc)_3(bpy)_3(H_2O)_2]$ **(1.40b)**.[114] In this complex the manganous ions are seven coordinated and have distorted pentagonal-bipyramidal geometries. Both bipyridine and **26pdc** ligands in the complex are chelated to manganese ions through bi and tridentate modes. Whereas, a water molecule coordinate to each manganese ion to provide similar coordination environment to all the metal centers in the complex.

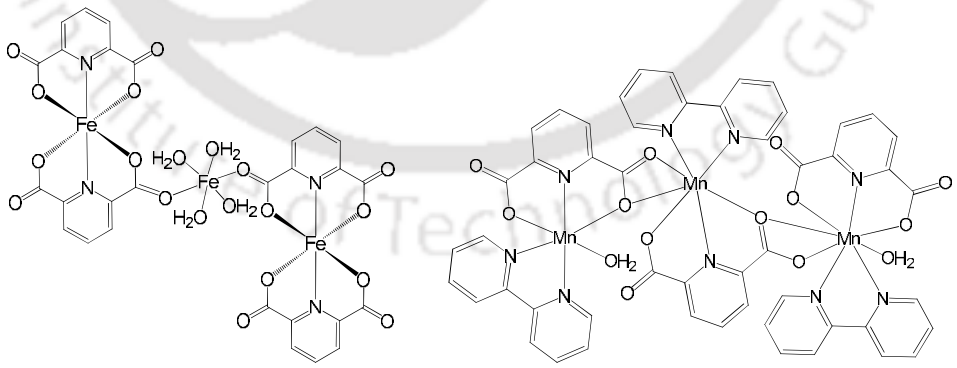

Figure 1.54: Trinuclear (a) Iron(II) complex **(1.40a)** (b) Manganese(II) complex **(1.40b).**

Protonated nucleobases such as adenine (ade) and cytosine (cysn) ribbons are stabilised by hydrogen bonds present in their respective *bis* **26pdc** metal (metal = manganese, copper, zinc at +2 oxidation state) complexes. Protonated assemblies of adenine are found as infinite chain embedded in the self-assemblies of such complex.

1D zigzag ribbons comprised of alternate adeninium cations are trapped in such assemblies. On the other hand, assembly of protonated cytosinium cation with neutral cytosine to form pairs and assemble to form tetrameric units of length 33.45Å (Figure 1.54), which are stabilised in self-assembly of manganese **26pdc** complex. This particular manganese complex has seven coordination geometry.[115]

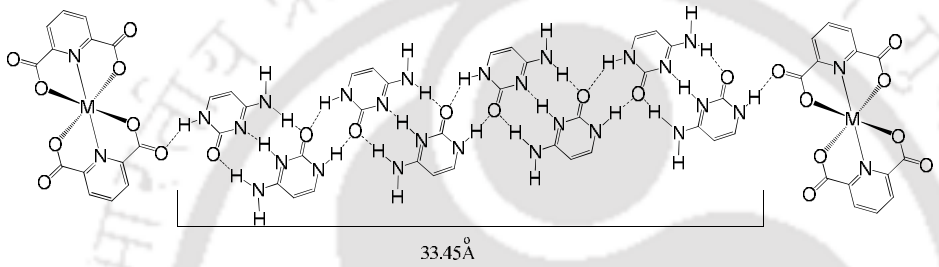

Figure 1.55: End capped assemblies of cytosine and cytosinium cations by copper(II) 26pdc complex anions.

Tetranuclear mixed-valent complex $[Mn^{II}_2Mn^{III}_2(26pdc)_6(H_2O)_4]\cdot 2CH_3OH\cdot 4H_2O$ **(1.42)** complex[116] having two manganese(II) and two manganese(III) ions bridged by four **26pdc** ligands is reported in literature. This tetranuclear complex forms a chain having two manganese(II) 26pdc complex and two manganese(III) ions.

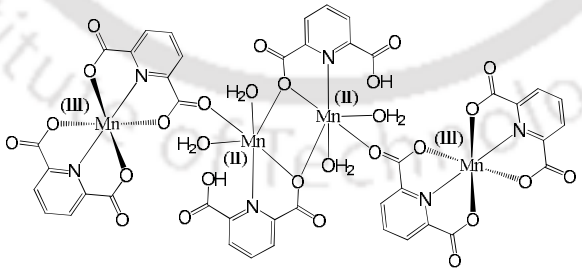

Figure 1.56: Mixed valent complex $[Mn^{II}_2Mn^{III}_2(26pdc)_6(H_2O)_4]\cdot 2CH_3OH.4H_2O$(**1.42)**

(solvent molecules are omitted for clarity).

Three dimensional wave like polymeric structure are found in $[\{Sm_4Cu_2(pdc)_8(H_2O)_{12}\}\cdot 4H_2O]_n$.[117] The basic unit of this complex is $[\{Sm_4Cu_2(pdc)_8(H_2O)_{12}\}]$ **(1.43)** which is linked in a head to tail manner to form infinite zigzag chains through Sm-O bonds. Each repeat unit in the chain is linked together to produce a two dimensionl architecture.

These two-dimensional polymeric chains are connected to each other by **26pdc** to generate three dimensional architecture as shown in Figure 1.57.

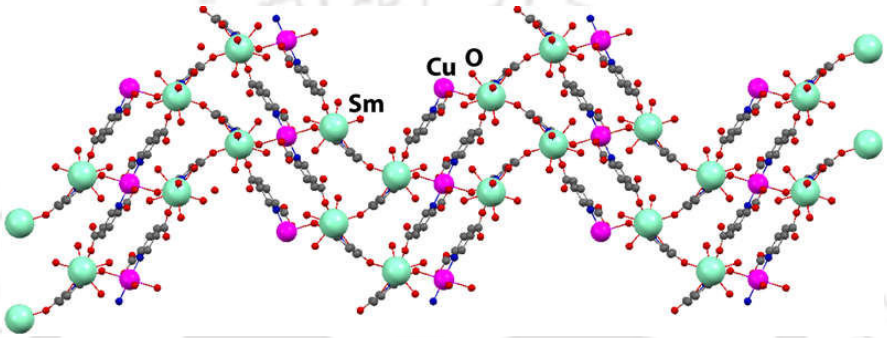

Figure 1.57: Corrugated 2D sheet of complex (**1.43).**

Heterometallic coordination polymer $\{[Eu(26pdc)_3Mn_{1.5}(H_2O)_3]\ 3.25H_2O\}_n$ **(1.44)** consists of two independent building blocks, namely $Ln(26pdc)_3$ and $MnO_4(H_2O)_2$ is a luminescent polymer. In this polymer, the manganese ions adopt octahedral geometry. In this complex, each **26pdc** ligand is chelated to europium ion.

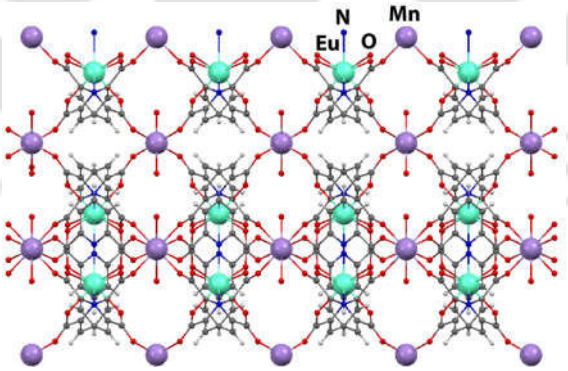

Figure 1.58: Channels in backbone of complex (**1.44**).

Each europium ion combined to two manganese ions by bridging oxygen atom of carboxylate. It has a three dimensional architecture,[119] This coordination polymer has one dimensional channel of around 1.8 nm diameter as shown in Figure 1.58.

Nano-dimensional tubular metal organic framework structures are obtained in coordination polymers such as $[La(26pdc)(H_2O)_4]Cl$ (**1.45a)** or $[La(26pic)(H_2O)_4]NO_3$ (**1.45b).** Structures of these coordination polymers have six lanthanide ions to construct circular geometry. Such arrangements are built by bridging carboxylate as shown in Figure 1.59. Counter anions and water molecules occupy the tubular spaces and the stability of nano tubes are decided by anions. For example, chloride or nitrate ions stabilises tube-like structure. Whereas, BF_4^- ions break tubular structure but stabilises three-dimensional metal-organic framework structure.

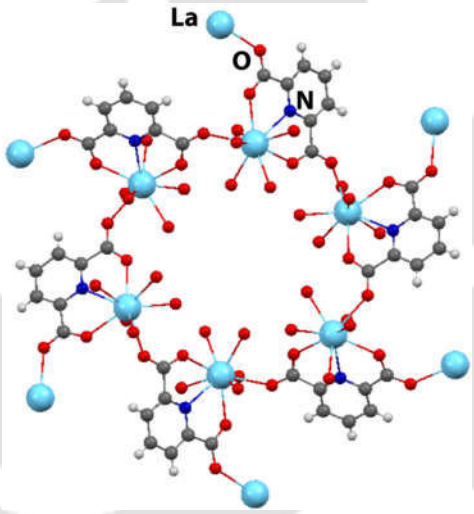

Figure 1.59: Circular cavity formed in complex **1.45a (**anions are omitted for clarity).

Praseodymium(III) forms 2 or 3-dimensional 2,6-pyridinedicarboxylate coordination polymers. $\{[Pr_3(26pdc)_4(26pdcH)(H_2O)_8.8H_2O\}_n$ is a three dimension coordination polymer which has nano-sized square sub-units as a building block. These sub-units are constructed by eight praseodymium(III) ions, that further assembles into a highly ordered two-dimensional grids.[120]

On the other hand, repeat unit found in decanuclear praseodymium metal-based complex $\{[Pr_2(26pdc)_3(H_2O)_3]\cdot H_2O\}_n$, participates in formation of novel three-dimensional coordination polymer.

On the other hand, $\{[Pr(26pdc)(H_2O)_4]\cdot ClO_4\}_n$ is a three dimensional coordination polymer which has hexanuclear praseodymium units as a building blocks. In this coordination polymer perchlorate anions are trapped in the cavity formed within the structure. Similarly, in $\{[Pr_2\ (26pdc)_2(H_2O)_5SO_4]\cdot 2H_2O\}_n$, forms two dimensional grid-like structure with the help of six praseodymium ions, two sulphate ions, and **26pdc**. Sulphate ions show unusual bridging coordination mode by chelating two metal ions at two sides.

The above examples have clearly showed that there lots of variations in structures can be brought about by using any of the isomer of pyridinedicarboxylate in coordination polymers or polynuclear metal complexes. The supramolecular assembly formation in these complexes and coordination polymers are very common leading to interesting architecture for porous frames or for molecular recognitions. Moreover, many of these structures are sensitive to cations and anions, hence leaves scopes to modify them as per requirement.

1.7 Scope of the present work

With progress of crystal engineering supramolecular architecture of carboxylate complexes have been greatly developed. Among smaller building blocks used from self-assembling purposes the inorganic complexes with π-stacks have a special status. In many such metal-organic networks π-stacking along with other interplaying weak interactions have helped to develop new self-assemblies.[121] Among them pyridinedicarboxylate complexes alone or in conjunction with multifunctional ligands provides anionic templates are widely studied to construct different architectures.[122] Various metal complexes derived from the pyridinedicarboxylate and planar aromatic delocalized π-systems ligands have shown applications in material sciences or advanced material[123], biology[124], catalysis.[125] Metal-organic framework derived from the pyridinedicarboxylate ligands are used as storage material[126], sensors, molecular recognition[127] and molecular magnetic material.[128]

The pyridinedicarboxylic acid itself shows interesting selectivity to recognise guest molecules. One example is the selective crystallisation of theophylline from a mixture having caffeine by 2,6-pyridinedicarboxylic acid (**1.46)**.

It is due to water assisted assemblies of 2,6-pyridinedicarboxylic acid forming cocrystal with theophylline (Figure 1.60).[129]

Thermal decomposition of metal pyridinedicarboxylate coordination polymers provides an easy way to prepare nano-dimensional metal oxides.[130] Such methodology may provide avenues to prepare metal oxides of definite sizes and shapes using inorganic precursors which may be of interest due to need of preparing low cost metal oxide catalyst and nanostructures with shapes.[131]

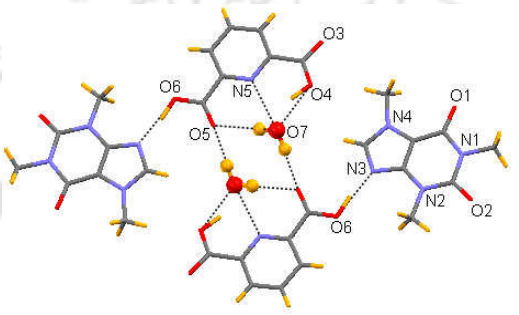

Figure 1.60: Water bridged assembly of picoline dicarboxylic acid as template for binding to theophylline (**1.46).**

Nanometer sized metal oxides are receiving considerable interest because of their important functionalities and technologically constructive structural, electronic,[132] photophysical and magnetic properties.[133]

On the other hand, layered double hydroxides are well studied and have attracted increasing attention because of their potential application in the field of storage material, molecular recognition, trapping of pollutant, exchange of guest molecules, selective catalysis, polymer hybrids and nano composites and biomaterials for drug or DNA delivery.[134] Hybrid materials based on layered double hydroxides (LDHs) are the examples of cationic layers containing metal part and these materials are most interesting layered structure made up of metal oxides and organic matter.[135] It is necessary to prepare both anionic and cationic layered structures with controlled separation between layers as functional materials.

Among inorganic complexes layered structures of 2,6-pyridinedicarboxylate have shown promise to control the interlayer separation which needs attention. For example, divalent nickel, cobalt and zinc complexes with **26pdc** having cations of primary amines have layered structures. The interlayer separations are dependent on cations for a series of ligands shown in table 1.3 are in the range of 10.4Å-13.4Å. Since the most of these complexes are isostructural, change in metal ion does not make a significant structural change. The metal ion act as interchangeable component and the organic cation is responsible for change in dimension of the organic layer. In such complexes anions with the aid of lattice water molecules makes interesting self-assemblies.[136] Two packing diagrams of illustrative examples are shown in Figure 1.61.

Table 1.3: Interlayer separation in copper and nickel-2,6-pyridinedicarboxylate complexes.

Complex	Cation(abbreviation)	Interlayer separation (Å)
$[enH_2][Ni(26pdc)_2]\cdot 3H_2O$	Ethylenediamine (en)	8.1
$[pnH_2][Cu(26pdc)_2]\cdot xH_2O$	1,3-diaminopropane (pn)	10.4
$[penH_2][Cu(26pdc)_2]\cdot 5H_2O$	1,5-diaminopentane (pen)	11.2
$[bamH]_2[Cu(26pdc)_2]\cdot 5H_2O$	4-aminobenzylamine (bam)	13.4

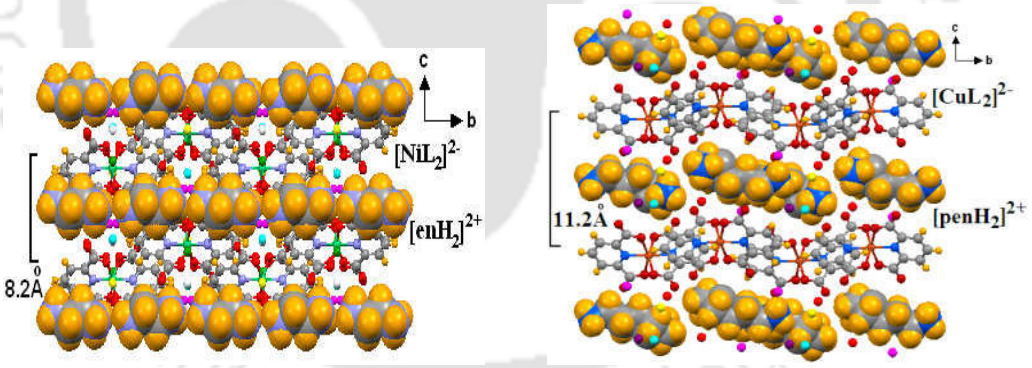

(a) (b)

Figure 1.61: (a) Diagram showing interlayer separations in complexes $[enH_2][Ni(26pdc)_2]\cdot 3H_2O$, (b) $[dapH_2][Cu(26pdc)_2]\cdot 5H_2O$

The basic building blocks for layer structures can also be from cations. For example guanidinium (G) cations and disulfonate (S) anions form pillared-layer like structures[137] through charge-assisted hydrogen bonds between the protons of guanidinium cations and oxygen atoms of sulfonate anions (**1.48a)** as shown in Figure 1.62.

The organic components of the disulfonates act as pillars, whereas spaces between the pillars are occupied by the guest mole Complex cation such as $[Co(NH_3)_6]^{3+}$ and 4,4′-biphenyldisulfonate anion form hydrogen-bonded pillared layer like structures (**1.48b)**[138] as shown in Figure 1.62.

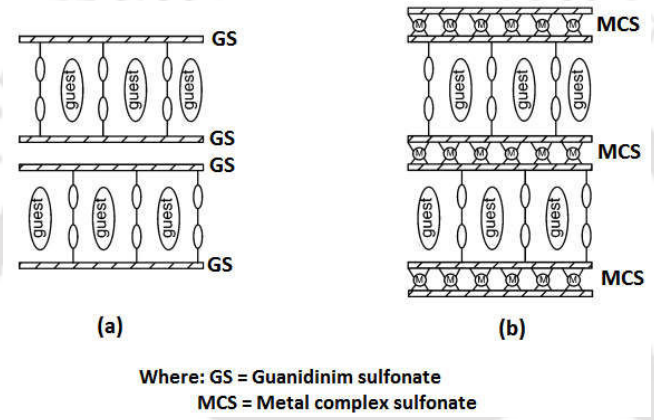

Figure 1.62: Schematic diagram depicting (a) Layered structure formed guanidinium cations with the aid of disulfonate anions (**1.48a)** and (b) in a hexa-ammino metal disulfonate (**1.48b)**.

Isostructural **26pdc** complexes $[imidazolium]_2[M(26pdc)_2]\cdot 3H_2O$ (**1.50)** (where M = Mn, Co, Ni, Cu, or Zn) can exchange metal ions at different proportions to provide different colours to crystals shown in figure 1.63.[139]

Figure 1.63: Different crystal morphologies of single crystals of $[imidazolium]_2$-$[M(26pdc)_2]\cdot 3H_2O$ having different proportion of metal ions.

3-Dimensional porous structures observed in metal-organic frame works $[Ln_2(25\text{-}pdc)_3(DMF)_2]_\infty$ (Ln = europium or ytterbium) show interesting properties.[140] Solvated forms of these metal-organic frameworks undergo transformation of one form of crystal to another form of crystal by reversible exchange of the solvent under thermal conditions. The porous forms are capable of absorbing H_2, N_2 gas and benzene.

From the above discussion, it is clear that there is definite scope to understand layered structures of metal complexes and distributions of ions and guest binding abilities in the layers. These layered structures will not only have provisions for control of interlayer separations but also for could be chosen such that they may be easily decomposed to less harmful wastes. With such background in this in the work presented this thesis is based on layered structures in metal-pdc, metal-ethylenediamine, and tetranuclear metal clusters for understanding their propeies related to ion exchange and molecular recognition properties and thermal stabilities.

References:

1 M. W. Hosseini, *Chem. Commun*., 2005, 5825-5829.

2 (a) J. P. Sauvage, *Acc. Chem. Res*., 1998**, 31**, 611; (b) M. Fujita, *Acc. Chem. Res*., 1999, **32**, 53-61; (c) D. L. Caulder, K. N. Raymond, *Acc. Chem. Res*., 1999, **32**, 975-982; (d) P. J. Stang, *Chem. Rev*., 2000,**100***,* 853-908.

3 (a) J. M. Lehn, *Pure Appl. Chem.,* 1978, **50**, 871-892; (b) J. M. Lehn, *Acc. Chem. Res*.,1978, **11**, 49-57.

4. S. K. Burley, G. A. Petsko, *Science*, 1985, **229**, 23-28.

5 (a) J. C. Ma, D. A. Dougherty, *Chem. Rev*., 1997, **97**, 1303-1324; (b) P. B. Crowley, A. Golovin, *Proteins Struct. Funct. Bioinf*., 2005, **59**, 231-239.

6 (a) D. Quinonero, C. Garau, C. Rotger, A. Frontera, P. Ballester, A. Costa, P. M. Deya, *Angew. Chem. Int. Ed. Eng*., 2002, **41**, 3389-3392; (b) C. Garau, A. Frontera, D. Quinonero, P. Ballester, A. Costa, P. M. Deya, *ChemPhysChem*., 2003,**4**,1344-1348;

(c) D. Quinonero, A. Frontera, C. Garau, P.Ballester, A. Costa, P. M. Deya,*ChemPhysChem*.,2006, **7**, 2487-2491.

7 A. Gil, V. Branchadell, M. J. Calhorda, *RSC Adv*., 2016, **6**, 85891-85902.

8 S. Bracco, A. Comotti, L. Ferretti, P. Sozzani, *J. Am. Chem. Soc*., 2011, **133**, 8982-8994.

9 S. Roche, C. Haslam, H. Adams, S. L. Heath, J. A. Thomas, *Chem. Commun*., 1998, **65**, 1681-1682.

10 (a) M. Chiper, M. A. R. Meier, D. Wouters, S. Hoeppener, C. A. Fustin, J. F. Gohy, U. S. Schubert, *Macromolecules*, 2008, **41**, 2771-2777; (b) S. J. Rowan, J. B. Beck, *Faraday Discuss*., 2005, **128**, 43-53.

11 A. Harada, K. Kobyashi, Y. Takashima, A. Hashidzume, H. Yamaguchi, *Nature Chem.*, 2011, **3**, 34-37.

12 F. Diederich, Symposium on Molecular Architecture Volume 67 Number 10 October 1990. 813.

13 B. H. Northrop, F. Africo, N. Tangchiavang, J. D. Badjic, J. F. Stoddart, *Org. Lett.*, 2006, **8**, 3899-3902.

14 S. Sivakova, S. J. Rowan, *Chem. Soc. Rev*., 2005, **34**, 9-21.

15 F. Zeng, S. C. Zimmerman, *Chem. Rev*., 1997, **97**, 1681-1712.

16 A. C. Lego, D. J. Mille, *Acc. Chem. Res*., 1987, **20**, 39-46.

17 Thomas Steiner, *Angew. Chem. Int. Ed*., 2002, **41**, 48-76.

18. G. R. Desiraju, *Acc. Chem. Res*., 1991, **24**, 290-296.

19 (a) G. R. Desiraju, *Acc. Chem. Res*., 2002, **35**, 565-573; (b) G. R. Desiraju, *Angew. Chem. Int. Ed.Eng*., 2011, **50**, 52-59.

20 G. R. Desiraju, *Acc. Chem. Res*., 1996, **29**, 441-449.

21 (a) V. R. Thalladi, H. C. Weiss, D. Blaser, R. Boese, A. Nangia, G. R. Desiraju, *J. Am. Chem. Soc*., 1998, **120**, 8702-8710; (b) H. C. Weiss, R. Boese, H. L. Smith, M. M. Haley, *Chem. Commun*., 1997, 2403-2404.

22 I. Rozas, I. Alkorta, J. Elguero, *J. Phys. Chem. A.,* 1998, **102**, 9925-9932.

23 G. R. Desiraju, T. Steiner, The weak hydrogen bond in structural chemistry and biology. 1999, Oxford: Oxford University Press.

24 I. Rozas, I. Alkorta, J. Elguero, *J. Phys. Chem.A*, 1998, **102**, 9925-9932.

25 M. C. Etter, J. C. MacDonald, J. Bernstein, *Acta. Crystallogr.,* 1990**, B46**, 256-262.

26 (a) G. R. Desiraju, *Angew. Chem. Int. Ed. Eng.,*1995, **34**, 2311-2327; (b) G. R. Desiraju, *Chem. Commun*., 1997, 1475-1482.

27 E. Peresypkina, A. Virovets, M. Scheer, *Cryst.Growth Des*., 2016, **16**, 2335-2341.

28 J. N.Moorthy, R. Natarajan, P. Venugopalan, *J. Mol. Struct*., 2005, 741, 107–114.

29 K. Shankar, J. B. Baruah. *J. Chem. Sci*., 2016, **128**, 771-778.

30 M. Seo, J. Park, S. Y. Kim, *Org. Biomol. Chem*., 2012, **10**, 5332-5342.

31 I. D. Tzeli, G. Petsalakis, J. R. Theodorakopoulos, *J. Struct. Chem*., 2015, **26**, 1585-1601.

32 J. C. MacDonald, G. M. Whiteside, *Chem. Rev*., 1994, **94**, 2383-2420.

33 P. L. Wash, E. Maverick, J. Chiefari, D. A. Lightner, *J. Am. Chem. Soc*., 1997, **119**, 3803-3804.

34 Y. M. Gutfreund, H. Margalit1, R. L. Jernigan, V. B. Zhurkin, *J. Mol. Biol*., 1998, **277**, 1129-1140.

35 S. Horowitz, R. C. Trievel, *J. Biol Chem*., 2012, **287**, 41576-41582.

36 J. N. Moorthy, P. Natarajan, *Chem. Eur. J*., 2010, **16**, 7796-7802.

37 L. Zhao,Y. Cheng, J. Hu,Q. Wu, T. Xu, *J. Phys. Chem. B*, 2009, **113**, 14168-14173.

38 C. B. Rodell, J. E. Mealy, J. A. Burdick, *Bioconjugate Chem.*, 2015, **26**, 2279-2289.

39 G. Yu, K. Jie, F. Huang, *Chem. Rev.*, 2015, **115**, 7240-7303.

40 G. Resnati, E. Boldyreva, P. Bombiczd, M. Kawano, *IUCrJ*., 2015, **2**, 675-690.

41 A. Sygula, F. R. Fronczek, R. Sygula, P. W. Rabideau, M. M. Olmstead, *J. Am. Chem. Soc*., 2007, **129**, 3842-3843.

42 C. R. Martinez, B. L. Iverson, *Chem. Sci.*, 2012, **3**, 2191-2201.

43 G. W. Gokel, *Chem. Commun*.**,** 2003, 2847-2852.

44 F. Hof, *Chem. Commun.*, 2016, **52**, 10093-10108.

45 C. Trujillo, A. A. R. Sanz, I. Rozas, *Molecules*., 2015, **20**, 9214-9228.

46 C. T. Armstrong, P. E. Mason, J. L. R. Anderson, C. E. Dempsey, *Sci. Reports*, 2016, 21746-21759.

47 K. K. Bania, A. K. Guha, P. K. Bhattacharyya, S. Sinha, *Dalton Trans.,* 2014, **43** ,1769-1784.

48 M. M. Gromiha, C. Santhosh, S. Ahmad, *Int. J. Biol. Macromol*., 2004, **34**, 203-211.

49 D. X. Wang, M. X. Wang, *J.Am. Chem.Soc*., 2013, **135**, 892-897.

50 P. Gamez, *Inorg. Chem. Front*., 2014, **1**, 35-43.

51 P. Politzer, J. S. Murray. T. Clark, *Phys. Chem. Chem. Phys*., 2013, **15**, 11178-11189.

52 A. Mukherjee, S. Tothadi, G. R. Desiraju, *Acc. Chem. Res*., 2014, **47**, 2514-2524.

53 A. Bauza, A. Frontera, T. J. Mooibroek*, Cryst, Growth Des*., 2016, **16**, 5520-5524.

54 (a) M. J. Plevin, D. L. Bryce, J. Boisbouvier, *Nature Chem.,* 2010, **2**, 466-471; (b) E. J. Moreno, G. J. Oses, A. M. Gomez , A. G. Santana , F. Corzana, A. Bastida, J. J. Barbero, J. L. Asensio, *Chem. Sci*., 2015, **6**, 6076-6085.

55 A. Frontera, C. Garau, D. Quinonero, P. Ballester, A. Costa, P. M. Deya, *Org. Lett*., 2003, **5**, 1133-1136; (b) B. Nepal, S. Scheiner, *J. Phys.Chem*., *A*, 2014, **118**, 9575-9587; (c) A. J. C. Cabeza, G. M. Day, W. Jones, *Chem. Eur. J*., 2009, **15**, 13033-13040.

56 H. E. Bakkali, A. Castineiras, I. G. Santos, J. M. G. Perez, J. N. Gutierrez, *Cryst. Growth Des.*, 2014, **14**, 249-260.

57 (a) K. L. Gurunatha, T. K. Maji, *Inorg. Chim. Acta.,* 2009, **362**, 1541-1545; (b) A. E. Tapper, J. R. Long, R. J. Staples, P. Stavropoulos, *Angew. Chem. Int. Ed. Eng*., 2000, **39**, 2339-2343; (c) S. B. Marr, R. O. Carvel, D. T. Richens, H. J. Lee, M. Lane, P. Stavropoulos, *Inorg. Chem*., 2000, **39**, 4630-4638.

58 (a) C. Janiak, *J. Chem. Soc. Dalton Trans.*, 2003, 2781-2804; (b) R. Robson, B. F. Abrahams, S. R. Batten, R. W. Gable, B. F. Hoskins, J. P. Liu, *ACS Symp. Ser*., 1992, **499**, 256-273.

59 (a) N. L. Rosi, J. Eckert, M. Eddaoudi, D. T. Vodak, J. Kim, M. OKeeffe, O. M. Yaghi, *Science*, 2003, **300**, 1127-1129; (b) J. L. C. Rowsell, O. M. Yaghi, *Angew. Chem. Int. Ed*., 2005, **44**, 4670-4679.

60 (a) C. R. Bondy, P. A. Gale, S. J. Loeb, *J. Am. Chem. Soc*., 2004, **126**, 5030-5031; (b) P. A. Gale*, Chem. Commun*., 2011*,* **47***,* 82-86.

61 T. R. Cook, Y. R. Zheng, P.J. Stang, *Chem Rev*., 2013, **113**, 734-777.

62 A. D. Burrows, K. Cassar, R. M. W. Friend, M. F. Mahon, S. P. Rigby, J. E. Warren, *CrystEngComm*., 2005, **7**, 548-550.

63 L. M. Duan, J. Q. Xu, F.T. Xie, Y. B. Liu, H. Ding, *Inorg. Chem. Commun*., 2004, 7, 216-217.

64 W. Lu, H. Wei, Z. Y. Gu, T. F. Liu, J. Park, J. Park, J. Tian, M. Zhang, A. Q. Zhang, T. Gentle, M. B. H. C. Zhou, *Chem.Soc.Rev*., 2014, **43** ,5561-5593.

65 E. V. Alexandrov, A. V. Virovets, V. A. Blatov, E. V. Peresypkina, *Chem. Rev*., 2015, **115**, 12286-12319.

66 H. H. Wang, L. N. Jia, W. J. Shi, L. Hou, Z. Zhu, Y. Y. Wang, *Inorg. Chem*., 2015, **54**, 1841-1846.

67 C. C. Wang, G. B. Sheu, S. Y. Ke, C. Y. Shin, Y. J. Cheng, Y. T. Chen, C. H. Cho, M. L. Ho, W. T. Chen, R. H. Liao, G. H. Lee, H. S. Sheu, *CrystEngComm*., 2015,**17**,1264-1272.

68 R. L. Rardin, P. Poganiuch, A. Bino, D. P. Goldberg, W. B. Tolman, S. Liu, S. J. Lippard, *J. Am. Chem. Soc*., 1992, **114**, 5240-5249.

69 F. A. Cotton, C. Lin, C. A. Murillo, *Acc. Chem. Res*., 2001, **34**, 759-771.

70 R. Murugavel, M. G. Walawalkar, M. Dan, H. W. Roesky, C. N. R. Rao, *Acc.Chem. Res*., 2004, **37**, 763-774.

71 C. Kaes, A. Katz, M .W. Hosseini. *Chem. Rev*., 2000, **100**, 3553-3590.

72 K. Manna, T. Zhang, F. X. Greene, W. Lin, *J. Am. Chem. Soc.*, 2015, **137**, 2665-2673.

73 R. Wang, X. Liu, D. Qi, Y. Xu, L. Zhang, X. Liu, J. Jiang, F. Dai, X. Xiao, D. Sun, *Inorg.Chem*., 2015, **54**, 10587-10592.

74 (a) D. Braga, F. Grepioni, G. R. Desiraju, *Chem. Rev*., 1998, **98**, 1375-1406; (b) B. H. Ye, M. L. Tong, X. M. Chen, *Coord.Chem. Rev*., 2005, **249**, 545-565.

75 D. G. Kurth, *Sci. Technol. Adv. Mater*., 2008, **9**, 19-25.

76 M. Fujita, J. Yazaki, K. Ogura, *J. Am. Chem. Soc.*,1990, **112**, 5645-5647.

77 T. M. Garret, U. Koert, J. M. Lehn, A. Rigault, D. Meyer, J. Fishcher, *J. Chem. Soc. Chem. Commun*., 1990, 557-558.

78 (a) J. M. Lehn, A. Rigault, J. Siegel, J. Harrowfield, B. Chevrier, D. Moras, *Proc. Nat.*
Acad. Sci., 1987, **84**, 2565-2569; (b) A. Pfeil, J. M. Lehn, *J. Chem. Soc. Chem. Commun*., 1992, 838-840; (c) K. Kramer, J. M. Lehn, R. A. Marquis, *Proc. Natl. Acad. Sci.,* 1993, **90**, 5394-5398.

79 (a) R. Knapp, A. Schott, M. Rehahn, *Macromolecules,* 1996, **29**, 478-480; (b) S. Kelch, M. Rehahn, *Macromolecules,* 1997, **30**, 6185-6193; (c) S. Kelch, M. Rehahn, *Macromolecules*, 1998, **31**, 4102-4106.

80 P.N.W. Baxter, J. M. Lehn, J. Fischer, M.T. Youinou, *Angew. Chem. Int. Ed. Eng*., 1994, **33**, 2284-2287.

81 S. Kitagawa, S. Noro, *Comp. Coord. Chem*., 2004, **7**, 23-247.

82 L. F. Marques, M. V. Marinho, C. C. Correa, N. L. Speziali, R. Diniza, F. C. Machado, *Inorg. Chim. Acta*., 2011, **368**, 242-246.

83 D. Sun, R. Cao, Y. Liang, Q. Shi, W. Su, M. Hong, *J. Chem. Soc*. *Dalton Trans*., 2001, 2335-2340.

84 Z. Lin, L. Chen, F. Jiang, M. Hong, *Inorg. Chem. Commun*., 2005, **8**, 199-201.

85 B. Conerney, P. Jensen, P. E. Kruger, B. Moubaraki, K. S. Murray, *Cryst. Eng. Comm*., 2003, **5**, 454-458.

86 O. K. Kwak, K. S. Min, B. G. Kim, *Inorg. Chim. Acta*, 2007, **360**, 1670-1678.

87 J Y. Lu, E. E. Kohler, *Inorg. Chem. Commun*., 2002, **5**, 600-601.

88 Y. Zhao, M. Hong, D. Sun, R. Cao, *J. Chem. Soc. Dalton Trans*., 2002, 1354-1357.

89 J. Gu, Q. Y. Zhu, Y. Zhang, W. Lu, G. Y. Niu, J. Dai, *Inorg. Chem. Commun*., 2008, **11**, 175-178.

90 J. Y. Zhang,Y. Ma, A. L. Cheng, Q. Yue, Q. Sun, E. Q. Gao, *Dalton Trans*., 2008, 206-2066.

91 M. A. Braverman, R. J. Staples, R. M. Supkowski, R. L. LaDuca, *Polyhedron*, 2008, **27**, 2291-2296.

92 H. J. Choi, M. P. Suh, *J. Am. Chem. Soc*., 1998, **120**, 10622-10628.

93 Y. Wei, Y. Yu, K. Wu, *Cryst. Growth Des*., 2007, **7**, 2262-2264.

94 J. Tao, M. L. Tong, X. M. Chen, *J. Chem. Soc*. *Dalton Trans*., 2000, 3669-3674.

95 A. D. Gonzalez, H. Hopfl, F. Medrano, A. K. Yatsimirsky, *J. Org. Chem.,* 2010,**75**, 2259-2273.

96 G. Beobide, O. Castillo, A. Luque, U. G. Couceiro, J. P. G. Tern, P. Roman, *Inorg. Chem*., 2006, **45**, 5367-5382.

97 (a) Y. Hamada, H. Ohta, N. Miyamoto, R. Yamaguchi, A. Yamani, K. Hidaka, T. Kimura, K. Saito, Y. Hayashi, S. Ishiura, Y. Kiso, *Bioorg. Med. Chem. Lett*., 2008, **18**, 1654-1657; (b) B. Schmidt, J. Jiricek, A. Titz, G. Ye, K. Parang, *Bioorg. Med. Chem. Lett*., 2004, **14**, 4201-4203.

98 W. M. Singh, B. R. Jali, B. Das, J. B. Baruah, *Inorg. Chim. Acta*, 2011, **372**, 37–41.

99 F. Semerci, O. Z. Yesilel, S. Keskin, C. Darcan, M. Tas, H. Dal, *CrystEngComm*., 2013, **15**, 1244-1256.

100 G. H. Wang, Z. G. Li, H. Q. Jia, N. H. Hu, J. W. Xu, *CrystEngComm*., 2009, **11**, 292-297.

101 Y. Liang, M. Hong, R. Cao, Q. Shi, *Acta. Crystallogr*., 2001, **E57**, 380-381.

102 A. M. Beatty, B. A. Helfrich, G. A. Hogan, B. A. Reed. *Cryst. Growth Des*., 2006, **6**, 122-126.

103 C. L. Chen, A. M. Beatty, *J. Am. Chem. Soc*., *2008,* **130**, 17222-17223.

104 Y. Wei, H. Hou, L. Li, Y. Fan, Y. Zhu, *Cryst. Growth Des*., 2005, **5**,1405-1414.

105 (a) Y. Zhou, M. Hong, X. Wu, *Chem. Commun*., 2006, 135-143; (b) A. A. Holder, L.C. L. Alleyne, D. V. Derveer, Dipicolinic acid, its Analogues and Derivatives: Aspects of their Coordination Chemistry; Nova Science Publishers Inc: NY, USA, 2011.

106 P. Buglyo, D. C. Crans, E. M. Nagy, R. L. Lindo, L. Yang, J. J. Smee, W. Jin, L. H. Chi, M. E. Godzala, G. R. Willsky, *Inorg. Chem*., 2005, **44**, 5416-5427.

107 (a) P. Laine, A. Gourdon, J. P .Launay, *Inorg. Chem*., 1995, **34**, 5129-5137; (b) N. Okabe, N. Oya*, Acta Crystallogr*., 2000, **C56**, 305-307.

108 (a) T. D. Keene, I. Zimmermann, A. Neels, O. Sereda, J. Hauser, S. X. Liu, S. Decurtins, *Cryst. Growth Des*., 2010, **10**, 1854-1859;

(b) J. C. MacDonald, P. C. Dorrestein, M. M. Pilley, M. M. Foote, J. L. Lundburg, R. W. Henning, A. J. Schutlz, J. L. Manson, *J. Am. Chem. Soc*., 2000, **122**, 11692-11694.

(c) C. L. Chen, A. M. Beatty, *J. Am. Chem. Soc*., 2008, **130**, 17222-17223.

109 M. P. B. Blanco, D. C. Lazarte, A. D. Martín, A. M. Hernandez , J. M. G. Perez, A. Castineiras, J. N. Gutierrez, *J. Inorg. Biochem*., 2013, **127,** 211-219.

110 C. B. Cabarrecq, J. D. Ghys, A. Fernandes, J. Jaud, J. C. Trombe, *Inorg. Chim. Acta,* 2008, **361**, 2909-2917.

111 M. M. Najafpoura, V. M. Kee, *Catal. Commun*., 2010, **1**, 1032-1035.

112 S. C. Manna, E. Zangrando, N. R. Chaudhuri, *J. Mol. Struct*., 2008, **877**, 145-151.

113 P. Lain, A. Gourdon, J. P. Launay. *Inorg. Chem.*, 1995, **34**, 5138-5149.

114 C. Ma, C. Chen, Q. Liu, D. Liao, L. Li, *Eur. J. Inorg. Chem*., 2003, 1227-1231.

115 B. Das, A. K. Boudalis, J. B. Baruah, *Inorg. Chem. Commun*., 2010, **13**,1244-1248.

116 R. Uhrecky, J. Moncol, M. Koman, J. Titisb, R. Boca, *Dalton Trans*., 2013, **42**, 9490-9494.

117 Y. Liang, M. Hong, W. Su, R. Cao, W. Zhang, *Inorg. Chem*., 2001, **40**, 4574-4582.

118 B. Zhao, X. Y. Chen, P. Cheng, D. Z. Liao, S. P. Yan, Z. H. Jiang, *J. Am. Chem. Soc*., 2004, **126**, 15394-15395.

119 Y. Zhou, M. Hong, X. Wu., *Chem. Commun*., 2006, 135-143.

120 B. Zhao, L. Yi, Y. Dai, X. Yan Chen, P. Cheng, D. Z. Liao, S. P. Yan, Z. H. Jiang, *Inorg. Chem*., 2005, **44**, 911-920.

121 (a) S. B. Yu, S. J. Lippard, I. Shweky, A. Bino, *Inorg. Chem*., 1992, **31**, 3502-3504; (b) U. Turpeinen, R. Hamalainen, J. Reedijk, *Polyhedron*, 1987, **6**, 1603-1610; (c) K. Geetha, M. Nethaji, A. R. Chakravarty, N. Y. Vasanthacharya, *Inorg. Chem*., 1996, **35**, 7666-7670;
(d) F. A. Mautner, R. Vicente, F. R.Y. Louka, S. S. Massoud, *Inorg. Chim. Acta*, 2008, **361**, 1339-1348.

122 J. Xu, W. Su, M. Hong, *Cryst. Growth Des*., 2011, **11**, 337-343

123 (a)Y. B. Xie, Q. Gao, C. Y. Zhang, J. H. Sun, *J. Solid State Chem*., 2009, **182**, 1761-1766; (b) C. Wibowo , M. D. Smith, J. Yeon, P. S. Halasyamani, H. C. Loye, *J. Solid State Chem*., 2012, **195**, 94-100.

124 (a)T. Jakusch, W. Jin, L. Yang, T. Kiss, D. C. Crans, *J. Inorg. Biochem.,* 2003, **95**, 1-13; (b) D. C. Crans, M. M. Tahir, M. D. Johnson, P. C. Wilkins, L. Yanga, K. Robbinsa, A. Johnsonb, J. A. Alfanod, M. E. Godzala, L. T. Austind, G. R. Willsky, *Inorg. Chim. Acta*, 2003, **356**, 365-378.

125 (a) J. An, L. Duan, L. Sun, *Farad. Discuss*., 2012, **155**, 267-275; (b) F. J. Arnaiz, R. Aguado, M. R. Pedrosa, A. De Cian, J. Fischer, *Polyhedron*, 2000, **19**, 2141- 2147; (c) P. Mahata, G. Madras, S. Natarajan, *Catal. Lett*., 2007, **115**, 1-7.

126 (a) F. Semerci, O. Z. Yesilel, M. S. Soylu, S. Keskin, O. Buyukgungor, Polyhedron, 2013 **50**, 314-320; (b) A. C. Wibowo, M. D. Smith, H. C. Loye, *Solid State Sci*., 2011, **13**, 607-615; (c) P. Teo, T.S. A. Hor, *Coord. Chem. Rev*., 2011, **255**, 273-289; (d) S. Roy, A. Chakraborty, T. K. Maji*, Coord. Chem. Rev*., 2014, 273-274.

127 (a) B. Das, A. K. Boudalis , J. B. Baruah*, Inorg. Chem. Commun*., 2010,**13**, 1244-1248; (b) P. A. Gale, S. E. G. Garrido, J. Garric, *Chem. Soc. Rev*., 2008, **37**, 151-190.

128 (a) M. L. Han, X. Q. Wu, G. W. Xu, G. X. Wen, D. S. Li, L. F. Ma, *Inorg. Chem.Commun*., 2016, **69**, 31-34; (b) S. Cui, Y. Zhao, J. Zhang, Q. Liu, Y. Zhan, *Cryst. Growth Des*., 2008, **8**, 3803-3809.

129 B. Das, J. B. Baruah, *Cryst. Growth Des*., 2011, **11**, 278-286.

130 (a) A. C. Wibowo, M. D. Smith, H. C. Loye, *Cryst. Growth Des*., 2011, **11**, 4449-4457; (b) M. Ranjbar, M. Yousefi*, J. Inorg. Organomet. Polymer*, 2014, **24**, 652-655.

131 (a) K. Liu, Z. R. Shen, Y. Li, S. D. Han, T. L. Hu, D. S. Zhang, X. H. Bu, W. J. Ruan, *Sci. Reports*, 2014, **4**, 1-7; (b) A. Tahmasian, A. Morsali, S. W. Joo, *Ultrason. Sonochem.,* 2013, **20** 1254-1260

132 (a) A. Carne, C. Carbonell, I. Imaz, D. Maspoch, *Chem. Soc. Rev*., 2011, **40**, 291-305; (b) H. Saravani, M. T. Ghahfarokhi, M. R. Esmaeilzaei, *J. Inorg. Organomet. Polym*., 2016 , **26**, 660-666.

133 Q. F. Li, D. Yue, W. Lu, X. Zhang, C. Li, Z. Wang, *Sci. Reports*, 2015, **5***:* 8385.

134 (a) C. Sanchez, B. Julian, P. Belleville and M. Popall, *J. Mater. Chem.*, 2005, **15**, 3559-3592; (b) M. Gonzalez, A. A. L. Santana, J. R. Hernandez, M. Knobel, E. Reguera, *J. Solid State Chem*., 2012, **197**, 317-322; (c) R. Hailili, L. X. Chang, L. Wang, Y. N. Huang, W. Qian, M. H. Zeng, Z. Abulizi*, Inorg. Chem. Commun.*, 2013, **35**, 113-116; (d) G. Lakshminarayana, M. Nogami, *Electrochim. Acta*, 2009, **54**, 473-4740.

135 (a) Z. Gu, J. J. Athertonab, Z. P. Xu, *Chem. Commun*., 2015, **51**, 3024-3036; (b). Q. Wang. D. O. Hare, *Chem. Commun*., 2013, **49**, 6301-6303.

136 B. Das, J. B. Baruah, *Inorg. Chim. Acta*, 2010, **363**, 1479-1487.

137 (a)V. A. Russell, M. D. Ward, *J. Mater. Chem*., 1997, **7**, 1123-1133; (b) V. A. Russel, M. C. Etter, M. D. Ward, *Chem. Mater*., 1994, **6**, 1206-1217; (c) V. A. Russel, M. C. Etter, M. D. Ward, *J. Am. Chem. Soc*., 1994, **116**, 1941-1952.

138 X. Y. Wang, R. Justice, S. C. Sevov, *Inorg. Chem*., 2007, **46**, 4626-4631.

139 J. C. MacDonald, P. C. Dorrestein, M. M. Pilley, M. M. Foote, J. L. Lundburg, R. W. Henning, A. J. Schultz, J. L. Manson, *J. Am. Chem. Soc*., 2000, **122**, 11692-11702.

140 J. Jia, X. Lin, A. J. Blake, N. R. Champness, P. Hubberstey, L. Shao, G. Walker, C. Wilson, M. Schroder, *Inorg. Chem*., 2006, **45**, 8838-8840.

Chapter 2

Self-assemblies of copper(II) pyridinedicarboxylates and intercalation of organic ammonium cations

2.1 Background

Organic ammonium cations intercalated in various organic and inorganic host-systems are of general interest to theoretical and experimental chemists.[1] From application point of view organic ammonium cations play important role in synthesis of meso-porous zeolites[2] and in layered structures such as that of clays.[3] These structures are rigid due to rigid host systems formed through covalent or dative bonds, thus there is need to search for similar structures generated through non-covalently linked but with good stability. A non-covalently linked assembly would provide flexibility and would be easily reorganize to adopt a shape that is decided by the partner molecules. From such a point of view, organic ammonium cations associated with anionic frameworks would provide stability through ionic hydrogen bonds and would be dismantled easily. Various layered materials incorporating organic ammonium cations are intercalated in layers formed by anionic metal-organic frameworks. These complexes are projected as new functional materials in the field of catalysis[3], optics[4], sensors[5], luminescent and fluorescent materials[6], electronics[7], magnetic materials[8], medicines[9] etc. Among such metal-organic frameworks, metal carboxylates find special attention due to their additional ability to provide sites for peripheral hydrogen bonds or to accommodate functionality suitable for peripheral hydrogen bonds.[10] Several metal carboxylates appeared recently based on transitions metal dicarboxylates such as oxalates[11], malonates[12],1,4-benzenedicarboxylate, different isomers of pyridinedicarboxylate[13],3,5-pyrazoledicarboxylates etc[13] sandwiching organic ammonium cations.[14] These complexes are relevant to porous and modular materials[15] and as clay mimics.[16] Such layered structures are investigated with objectives to increase the metrics of channel and/or pore sizes by using organic cations.[17] A large porous size may suite for gas storage, selective adsorption and ion exchange process.[18] Though, lamellar structures of certain pyridinedicarboxylate have been studied,[19a] systematic study on effects of cations to generation of different nuclearity of coordination complexes, interlayer spacing and self-assembling aspects have scope to study.

We have set our study to examine self-assemblies and stability of various organic ammonium cation containing pyridinedicarboxylate complexes of copper are reported in this chapter. In this chapter the copper complexes possessing 2,3- or 2,5-pyridinedicarboxylate (Figure 2.1.1) are described. The chapter has two parts where first part deals with copper complexes with 2,3-pyridinedicarboxylate whereas second part is on 2,5-pyridinedicarboxylate complexes.

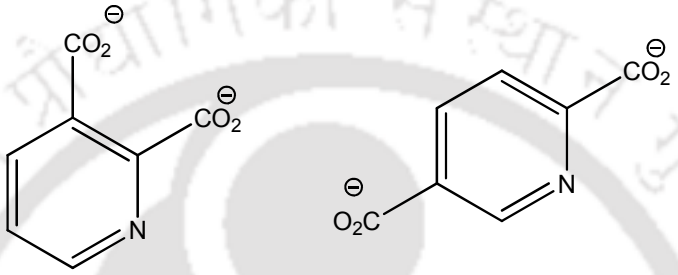

2,3-pyridinedicarboxylate ion 2,5-pyridinedicarboxylate ion

Figure 2.1: Two ligands derived from positional isomers.

Part A

Self-assemblies of copper(II) 2,3-pyridinedicarboxylate complexes

2.1.1 Synthesis of complexes

Copper(II)acetate was used as a common reactant to prepare a series of copper(II)2,3pyridinedicarboxylate complexes with a wide range of organic ammonium cations. Nitrogen containing compounds were chosen to generate cations in situ by reactions of copper(II)acetate, 2,3-pyridinecarboxylic acid followed by reaction with respective amine. Nitrogen containing aromatic compounds was varied from mono, di, and tri-aliphatic amine, diamine having combination of aliphatic and aromatic amine, different nitrogen containing heterocycles and nucleobases listed in top-right side of Scheme 2.1.1. The reactions were found to be amine specific and different nuclearity complexes varying from mono-, di- and poly-nuclear copper complexes are observed. In each case the reaction products were isolated by crystallization and characterized by recoding IR, UV-visible, elemental analysis. The thermal stability in each case was determined by therogravimetric analysis. In none of the case amine were inside the coordination sphere except in the case of complex derived from complex 3-aminobenzylamine. Observation on having the organo-cationic part originating from amine outside the coordination sphere is inherently due to the reaction conditions in which products were formed. In the case of a reverse addition of amine to copper acetate followed by treatment with carboxylic acid are well known to form amine complexes leaving the carboxylates as counter anions. But our perspectives being to understand role of self-assembly, getting crystalline complex was primary requirement. From reverse addition we did not get crystalline copper(II) ammine complexes with pyridinedicarboxylate outside coordination sphere hence this aspect was not pursued, but we did dealt with similar situations by isolating copper-ethylenediamine complexes having carboxylates outside coordination sphere which are described independently in chapter 5. 2,3-Pyridinecarboxylates having two carboxylic acid groups and a pyridine nitrogen atoms to bind to metal ions, they can have several ways to bind to the metal ions making the variation in the structures.

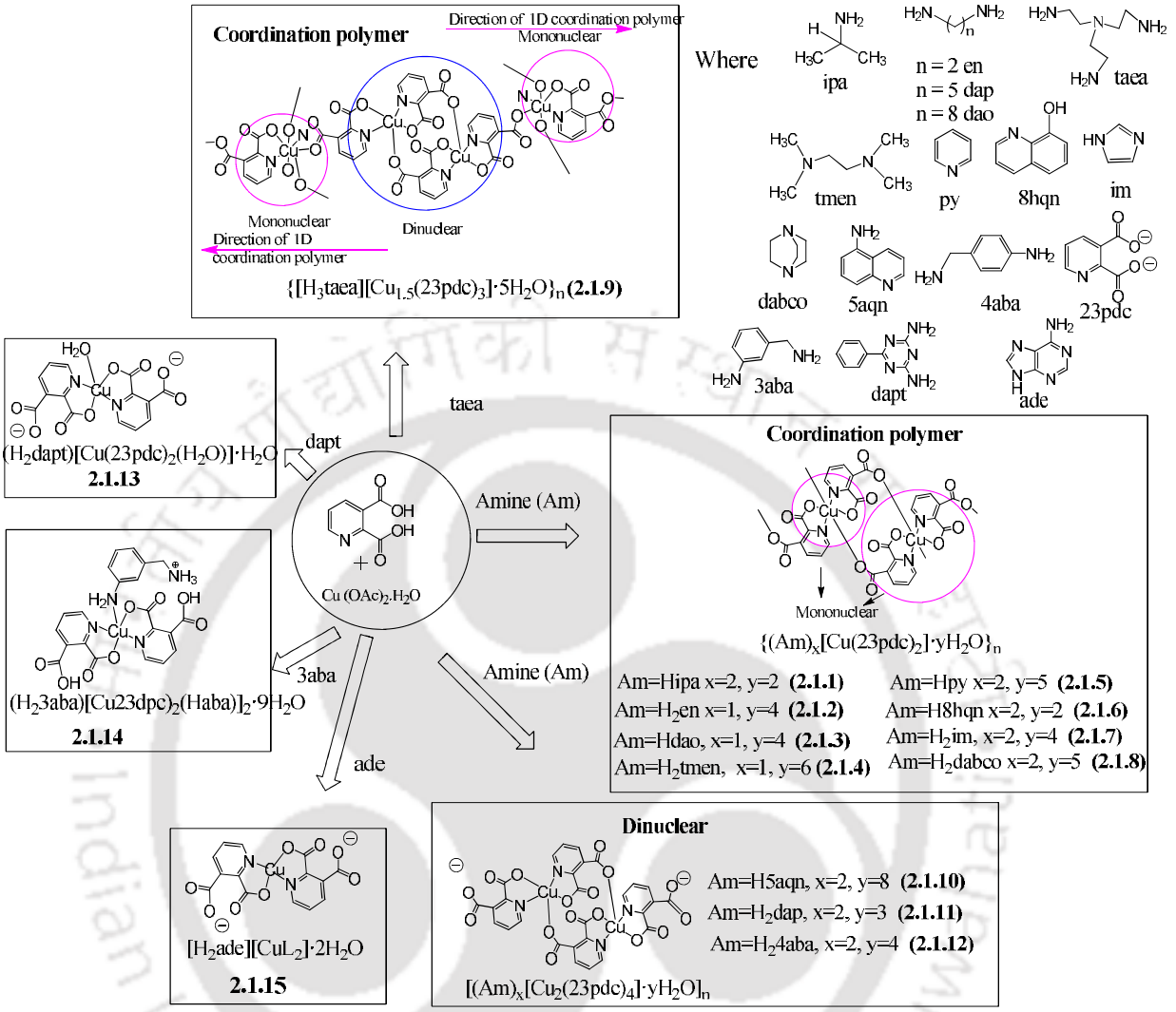

Scheme 2.1.1: Formation of mononuclear, dinuclear and coordination polymer of Cu(II)2,3-pyridinedicarboxylates.

To get information on the possible role of cations to guide structures, crystal structures of each complex were determined by single crystal diffraction technique. From crystallographic study a wide spectrum of structural variations as illustrated in Scheme 2.1.1 were established, hence self-assembling aspects are discussed by categorizing the structures based on nuclearity of the anionic metal complex parts.

Prior to crystal structure determination complex of the pyridinedicarboxylate were ascertained from preliminarily comparisons of IR spectra of the complexes with IR of the parent organic counterparts. Ligand 2,3-pyridinecarboxylic acid has IR absorptions at 1700cm^{-1} due to carbonyl, upon complex formation it appears at 1656cm^{-1}-1615cm^{-1}, 1596cm^{-1}-1582 cm^{-1}. In the literature[19b] it is suggested that the different modes of carboxylic acids have characteristic IR frequencies. For example, a mono-dentate carboxylate appear at 1653cm^{-1}, bidentate at 1588cm^{-1} and bridging at 154cm^{-1}. Presence of ammonium cations shows $^{+}$N-H stretching in the region 3304cm^{-1}-2637cm^{-1}, whereas the parent amines N-H stretch appear at 3355cm^{-1}-3150cm^{-1}. The complexes in each case were green in color and have characteristic d-d transition in the ranges 610nm-734nm which are of d^{9}-system copper ions at +2 oxidation state. In the discussion followed in this chapter, complexes of copper(II) pyridinedicarboxylates are described in a sequence followed as coordination polymers, diuclear complexes and mono-nuclear complexes as the coordination polymers of the 2,3-pyridinedicarboxylates are conventional and are routinely observed.

2.1.2 Coordination polymers of copper(II) 2,3-pyridinedicarboxylate

Copper(II)2,3-pyridinedicarboxylate coordination polymers were obtained when the cations were derived from amines namely isopropylamine, ethylenediamine, 1,8-diaminooctane, N,N,N′,N′-tetramethylethylenediamine, pyridine, 8-hydroxyquinoline, imidazole and 1,4 diazabicyclo[2.2.2]octane. These coordination polymers have identical backbone of anionic portion, which is comprised of mono-nuclear repeat anionic unit illustrated in Figure 2.1.1.

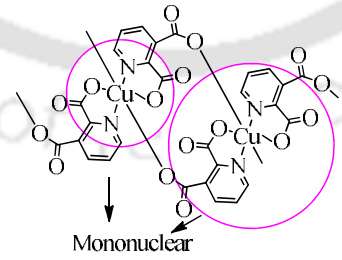

Figure 2.1.1: Mononuclear repeat unit in coordination polymer of complexes **2.1.1-2.1.8**.

Each anionic repeat unit present these coordination polymers is formed by chelation of pyridine nitrogen atom along with an oxygen atom of carboxylic acid at 2-position. Carboxylic acid group present at 3-position of the ligand bridges neighboring copper ion results in the formation of polymeric chain of the anionic part. This type of coordination polymer are commonly observed in copper(II) 2,3-pyridinedicarboxylate.[20]

Asymmetric unit of unit cells in single crystal structure of polymeric complex **2.1.1** consists of an anionic unit $0.5[Cu(23pdc)_2]^{2-}$ unit, one isopropyl ammonium cation and a water molecule held together *via* electrostatic interactions and hydrogen bonds. Since the coordination polymers **2.1.1** to **2.1.8** are guided by ionic hydrogen bonds having electrostatic character, Such type of hydrogen bonds are listed in table 2.1.1. The hydrogen bonds are shown in Figure 2.1.2b. The strong hydrogen bonds are realized from short N-H···O distance lying in the range 2.78Å-2.91Å. The perspective view of anionic polymeric $[Cu(23pdc)_2]^{2-}$unit with atom numbering is shown in Figure 2.1.3a. Similar anionic polymeric units were reported earlier in copper complexes having cations derived from nucleobases and with alkali metal ions.[21] On the other hand isopropyl ammonium cations is a substrate that has been extensively studied as cations in layer-like self-assemblies of various discrete dianions such as in $[CuCl_4]$, $[MoS_4]$ or $[WS_4]$ by weak N-H···Cl and N-H···S interactions is available in literature.[22] From comparison it is advantageous to have form an unidirectional polymeric anionic chain with the aid of this particular cation, which has varieties to form layered structures holding discrete complex anions of metal-haildes or metal sulphides.

Table 2.1.1: Selected hydrogen bond parameters for the complex **2.1.1**.

Bond (symmetry)	dD-H(Å)	dH···A(Å)	dD···A(Å)	<D-H···A(°)
N(2)-H(2A)···O(3) [x,-1+y,z]	0.89	1.90	2.787(7)	174
N(2) -H(2B)···O(4) [1-x,-3/2+y,1/2-z]	0.89	2.02	2.914(7)	177
N(2)-H(2C)···O(3) [1-x,-1/2+y,1/2-z]	0.89	11.98	2.853(6)	166

Coordination polymer **2.1.1** has distorted octahedron coordination copper(II) polyhedrons. The coordination sphere of each copper ion is completed by four O atoms and two N atoms of **23pdc** ligand having μ-(κ^3N,O^2:O^3) coordination mode. That is, oxygen atom of a carboxylate at 2-position of the ring and pyridine N atom chelate one copper atom and O atom of carboxylate at 3-position binds to another metal ion.

The equatorial Cu-O and Cu-N bond lengths are 1.937Å(3) and 1.971Å(3), whereas the axial distance is 2.679Å(3), which are comparable to bond lengths observed in similar complex.[23] The polymeric anion $[Cu(23pdc)_2]^{2-}$ build a two-dimensional layer along crystallographic *a* and *b* axis. The isopropyl ammonium cation interacts with the two adjacent layers of complex anion *via* $-NH_3^+$-COO^- hydrogen bond, the selected hydrogen bond parameters are given in table 2.1.1.

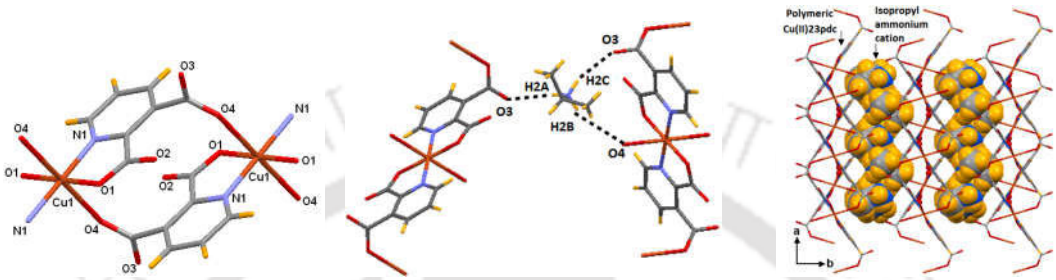

(a) (b) (c)

Figure 2.1.2: (a) Anionic unit of coordination polymer **2.1.1**, (b) Prominent hydrogen bonds in self-assemblies coordination polymer **2.1.1**, (c) Layer-like structure of the coordination polymer **2.1.1**.

This results in layered motif between the polymeric complex anion and the organic cation in A-B-A manner, where A is the organic cation and B represents the complex anionic layer. The interlayer separation (based on adjacent Cu(II)-Cu(II) distance) between the rows of isopropyl ammonium cations layer is 11.40Å.

Structure of **2.1.2** consists of a centro-symmetric polymeric complex anion $\{[Cu(23pdc)_2]\}_n^{2-}$, ethylenediammonium ion (protonated at both the terminal N atom) along with lattice water molecule. In complex **2.1.2**, polymeric complex anionic layers are hydrogen bonded to the cations and also lattice water molecule forms two separate inorganic and organic layers that propagate along the *a* and *b* axes (Figure 2.1.3a). From crystal engineering point of view, the interlayer separation is 11.0Å along *b* axes. In this case the cations are found as segregated into different cavities of formed by anioninc layers, thus the cations present are as arrays. It is to be mentioned that ethylenediammonium intercalated vanadyl phosphate complex was synthesized in hydrothermal conditions.[24]

In that complex, $[enH_2]^{2+}$cations occupy cavities in between the layers made up of VO_5 square pyramids and PO_4 tetrahedra.

We have also studied the effect of cations by increasing the chain length of the intervening flexible part by taking 1,8-diaminooctane as a source of cation. It has been noticed that being symmetrical in nature 1,8-diaminooctane can easily interact with polymeric complex anion through $-NH_3^+-COO^-$ unit in the form of complex **2.1.3**. It forms layered structures in the crystal lattice similar to that of complex **2.1.2**.

The flexible dications of diaminooctane fill the voids created by the bulky anionic complex units, and interlayer separation is 10.00Å. Beatty and coworkers showed that metal complexes with positional isomeric dicarboxylic acid namely nickel(II) and cobalt(II) 2,4-pyridinedicarboxylate complexes possessing octylammonium cations resulted in the layered structures with larger interlayer separation.[25] But in such cases data with complexes having cations of 1,8-diamino octane is not available for direct comparison. Analogous organic systems containing 3,5-pyrazoledicarboxylic acid and octylammonium cation also generate lamellar structures with large interlayer separation.[26] These suggest that there is a difference in interlayer separation caused by octyl-1,8-diammonium cation over the 1-octylammonium cation to anionic environment. To compare directly the distance of separations of such a complex with reported cases similar reaction of 1-octylamine with copper(II) acetate and 2,3-pyridinedicarboxylic acid but single crystals suitable for X-ray diffraction could not be obtained. Hence based on the shrinkage observed in interlayer separation in **2.1.3** than the coordination polymer possessing ethylenediammonium cation **2.1.2** is notable. With such information we moved to analyze inter-anion layer separation we prepared coordination polymer **2.1.4**, having N,N,N',N'-tetramethylethylenediammonium cation. The structure determined by single crystal X-ray diffraction data showed a layer-like inorganic-organic hybrid structure of **2.1.4** that resembles the structure that of **2.1.2**. But in this case **2.1.4** there is a larger interlayer separation than ethylenediammonium containing complex. Complex **2.1.4** exhibits two dimensional layer-like arrangements, but in this case cations are arranged as distinct layers which are continuous (Figure 2.1.3c), this was not the case in ethylenediammnium cation containing coordination polymer. Such interlayer separation along *b* axis is 13.50Å. These results shows that though 1,8-diaminooctane has larger chain length with respect to ethylenediamine it is not being able to increase interlayer separation.

But ethylenediamine and tetramethylethylenediamine have similar distance between the two nitrogen atoms, but in latter case a cation resulted in much higher separation inter-anionic layer separation clearly suggesting role of packing arrangements and change of directional weak hydrogen bond scheme contributing to interlayer separation within the structures of individual coordination polymers. Another interesting observation of the complex **2.1.4** is that, it has six water molecules in the crystal lattice, that are involved in formation of one-dimensional infinite chain-like structure of water clusters.

Chain-like arrangements are formed by alternative cyclic tetrameric and hexameric clusters (Figure 2.1.3d).

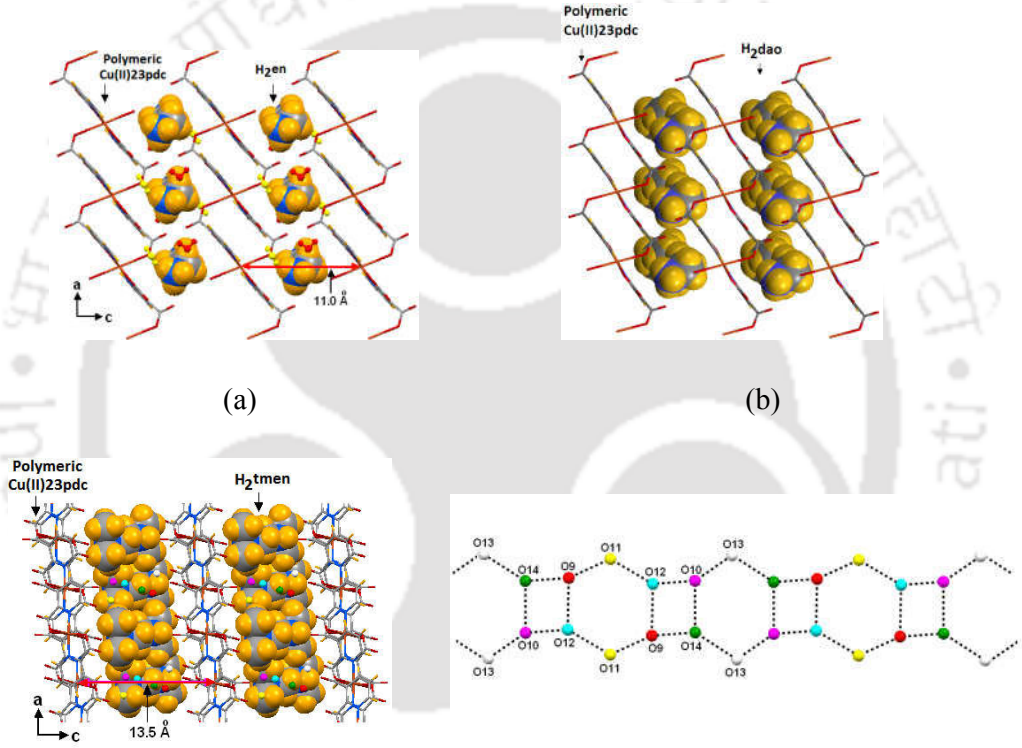

Figure 2.1.3: (a) Layered structure of the coordination polymer **2.1.2**, (b) Layered structure of the coordination polymer **2.1.3**, (c) Layered structure of the coordination polymer **2.1.4**, (d) One-dimensional infinite chain comprising of tetrameric and hexameric water clusters in **2.1.4**.

Linear or branched chain like arrangements of water clusters are reported in literature,[27] this type infinite chain-like arrangements of water clusters were not reported earlier.

Infinite chain-like arrangements of water molecules are held by hydrogen bonds with -COO- units of polymeric complex anions.

From the foregoing study it is clear that skeleton aliphatic organic amines can control inter-anionic separations. Similar aspects on control of interlayer separations are observed in the coordination polymers having cations derived from heterocyclic organic base or amines. The coordination polymer with pyridininium cation **2.1.5**, has two-dimensional layers of polymeric complex anions where protonated pyridine molecules are trapped.

The packing pattern is dominated by charge assisted $-N^{+}-H-COO^{-}$ hydrogen bonds interactions. Pyridinium cations interact with the complex anions via $-N^{+}-H\cdots COO^{-}$ interactions. In the lattice, pyridinium cations are sandwiched between the polymeric complex anion in A-B-A manner (Figure 2.1.4a). The distance between copper ions of complex anions that sandwiches the organic layers along *c* axis is 12.1Å. Pyridinium ions are observed as arrays of molecules separated by a set of water molecules along crystallographic *a* axis. There are also lattice water molecules occupying the interstitial spaces between the anionic complexes. Hydrogen bonds between water molecules and oxygen atoms of pyridinedicarboxylate as well as with pyridinium cations occur.

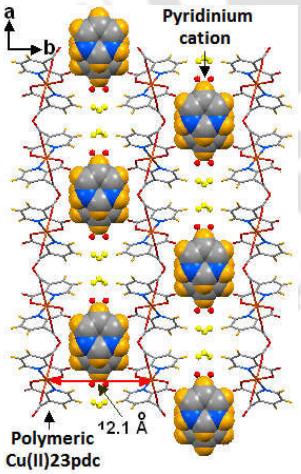

(a)

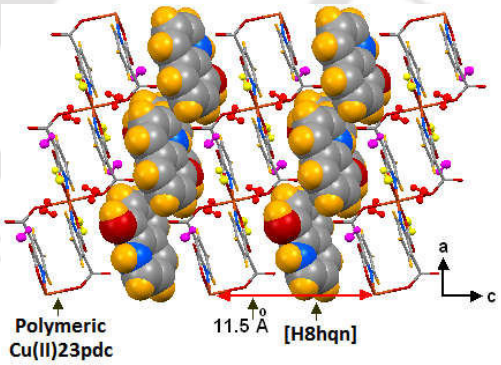

(c)

(b) (d)

Figure 2.1.4: (a) Layered structure of the coordination polymer **2.1.5**, (b) Coordination polymer **2.1.6**, (c) Layers in coordination polymer **2.1.6**, (d) Hexameric and tetrameric water cluster in complex **2.1.6**.

Literature suggests that vanadium 2,6-pyrdinedicarboxylate with protonated pyridine forms channel-like structures.[28] Coordination polymer **2.1.6** that has 8-hydroxyquinolinium cation stabilized in layers of polymeric complex anions. Hydroxyquinolinium cation is generated by protonation at quinoline nitrogen atom and protonated -NH and -OH, being on one side, easily interacts with the 2- and 3-carboxylate group of $\{[Cu(23pdc)_2]^{2-}\}_n$ through hydrogen bonds resulting the symmetrical polymeric complex anion (Figure 2.1.5b). As a result of these interactions, the partially slipped 8-hydroxyquinolinium cations form a well-defined infinite layer sandwiched between the polymeric complex anion (Figure 2.1.5c). Rings of cationic parts are partially stacked over each other and propagate along *a*-crystallographic direction in a continuous manner. Another interesting observation about **2.1.6** is the three water molecules form an infinite water cluster based on hexameric and tetrameric clusters. Water clusters are stabilized between the two adjacent polymeric complex anions (Figure 2.1.4d) through hydrogen bonds. Coordination polymer **2.1.7** has mono protonated imidazole is also consists of similar polymeric complex anions. Here also complex is stabilized by charge assisted hydrogen bonds between protonated nitrogen atom and carboxylate group $-N^{+}$-H-COO^{-}. Imidazolium cations are held zigzag in between the layers formed by anions which have separation 11.90Å as shown in Figure 2.1.5a. Crystalline inorganic-organic hybrid materials imidazolium cations intercalated in layers of first row transition metal 2,6-pyridinedicarboxylates through stacking effect of anions to for supramolecular assembly.[29]

In those structures, the organic cation serves as structural component, which governed the packing arrangement and the metal served as an interchangeable component.

In present case the anionic part itself is polymeric thus have more structural rigidity and property associated would be expected to have directional contribution.

Crystal structure of coordination polymer **2.1.8** has similar basic primary building unit, $\{[Cu(23pdc)_2]^{2-}\}_n$ as of the complex described above, but it has dication of 1,4-diazabicyclo[2.2.2]octane (**dabco**) and four water molecules. These are held together *via* electrostatic and hydrogen bond interactions. The dication is observed as crystallographically disordered unit. Disorder is attributed to the symmetric nature to adopt a shape through exchange of equivalent positions. Protonated dabco and the complex anions are separated into two distinct rows running in the *a* and *b* axis via N3-H3N···O4 interactions ($d_{D\ldots H}$, 1.79Å, $d_{D\cdots A}$, 2.78Å; < D-H···A, 173º). Stacking is further facilitated by hydrogen bonding interactions of the lattice water molecules. Interlayer distance between anionic layers is 12.3Å along crystallographic b axis (Figure 2.1.5b). This separation is longer than the one created by ethylenediammonium cation and shorter than the one caused by tetramethyl ethylenediammonium cation.

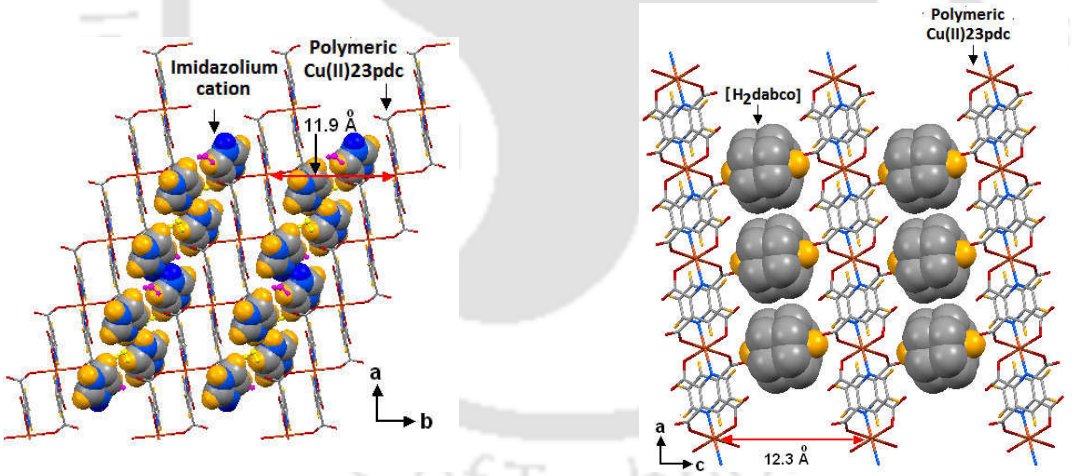

(a) (b)

Figure 2.1.5 : (a) Layered structure of coordination polymer **2.1.7**, (b) Layered structure of the coordination polymer of complex **2.1.8**.

An exceptional coordination polymer was formed when tri cation of tris-2-aminoethylamine is used as counter cation of copper(II) 2,3-pyridinedicarboxylate. This coordination polymer has combination of dinuclear and mononuclear repeat units.

The dinuclear and mononuclear components are encircled in Figure 2.1.6. The mononuclear units are comprised of hexa-coordinated copper complexes, whereas the dincuclear unit has both the copper ions in pentacoordinate environments. In the polymeric chain, each hexa-coordinated mononuclear unit is followed by a penta-coordinated dinuclear unit. The coordination polymer is guided by strong hydrogen bonds of three ammonium sites. Thus to accommodate such the tri-cation with such interactions this exceptional structure was formed.

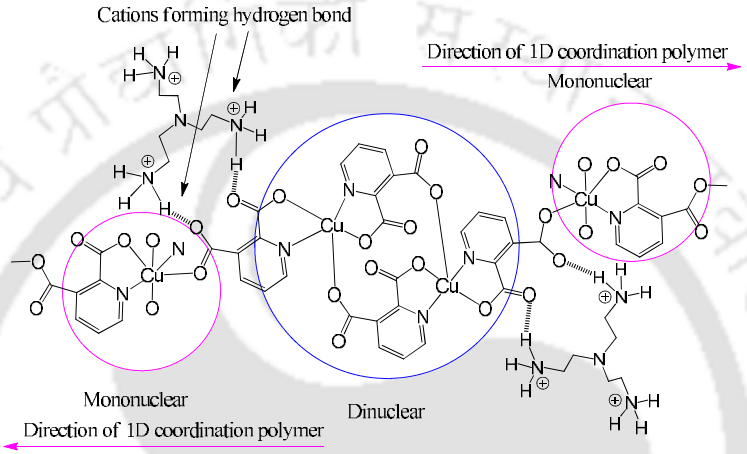

Figure 2.1.6: Mononuclear and dinuclear repeat unit in coordination polymer of complex **2.1.9**.

In the complex, a trication formed by protonation at all the amine groups of the tripodal amine. Due to +3 charge on the cation, polymeric anionic part is distributed in two parts, $[Cu(23pdc)_2]^{2-}$ and $0.5[Cu(23pdc)_2]^{2-}$ resulting in overall -3 charge per repeat unit of polymeric anion to form a neutral complex (Figure 2.1.7a).Two different copper(II) sites in the polymeric chain exhibits an altogether different structures than the obtained with other ammonium cations. This has been observed as an isolated where the complex anion exhibits multiple charges depending on the charge of cation. The **taea** trication is encapsulated (Figure 2.1.7b) between the polymeric complex anion through charge assisted ammonium-carboxylate and ammonium-water interactions.

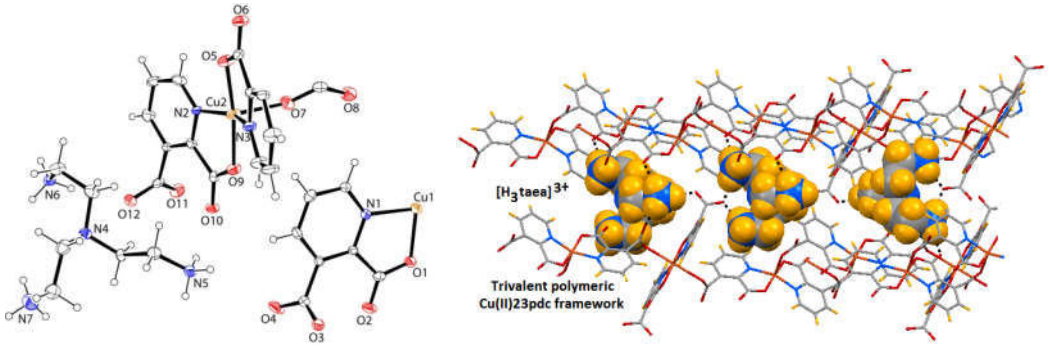

(a) (b)

Figure 2.1.7: (a) Asymmetric unit of complex **2.1.9**, (b) Encapsulation of **taea** by complex anion of **2.1.9**.

With these interactions, protonated amine is encapsulated in such a way that the complex does not form well-defined layered structure as obtained in earlier cases. Complexation of protonated tripodal amine with small inorganic anions such as NO_3^-, SO_4^{2-}, TsO^-, PO_4^{3-}, $P_2O_7^{4-}$ also takes place *via* electrostatic forces, hydrogen bonding interactions and solvation.[30]

Generally electron paramagnetic resonance spectra of copper complexes are used for ascertaining geometry around the copper ions.[31] Distinction between the two types of coordination polymers are reflected in the electron paramagnetic resonance spectra. The coordination polymers of solid samples of coordination polymers **2.1.1-2.1.8** have conventional spectra of copper(II) square pyramidal geometry, they have broad single signal at 2.071G. The coordination polymer **2.1.9** has two copper environments of which two copper centers are five coordinated and one is octahedral. Accordingly two different environments are reflected showing multiple numbers of signals illustrated in Figure 2.1.8. Thus the two types of coordination polymers could be distinguished.

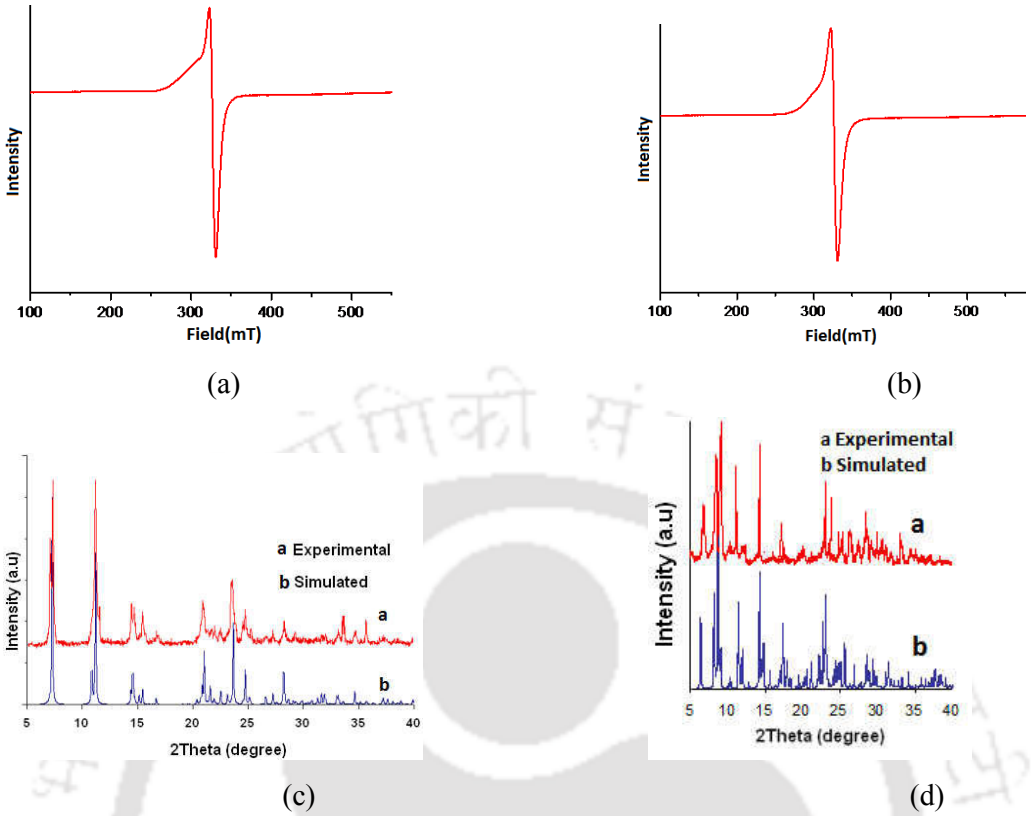

Figure 2.1.8: EPR spectra (band, room temperature solid sample) of coordination polymer (a) **2.1.4**, (b) **2.1.9.** Powder XRD pattern of complex (c) **2.1.4**, (d) **2.1.9**.

Further, the coordination polymers were characterized by powder XRD to ascertain their phase purity, there is excellent agreement between the experimental data and the powder patterns simulated from the CIF files with the Mercury program.

As an illustrative example, the indexed powder XRD pattern of **2.1.4** and **2.19** are shown in Figure 2.1.8c and 2.1.8d, agreement between experimentally found and simulated shows that each coordination polymer is comprised of single phase.

2.1.3 Dinuclear copper(II)2,3-pyridinedicarboxylate complexes

When cations derived from 5-aminoquinoline, 4-aminobenzylamine or 1,5-diaminopentane were generated in situ as counter ions for copper(II)2,3-pyrdinedicarboxylate than dinuclear copper complexes were obtained. In all the cases same dinuclear complex anion illustrated in Figure 2.1.9 was obtained. The dinuclear anion has penta-coordinated square-pyramidal copper ions.

Self-assemblies of these complexes **2.1.10-2.1.12** have similarity in showing strong hydrogen bonds between N-H bonds of cations with uncoordinated carboxylate groups. The principle hydrogen bonds guiding assemblies of complex **2.1.10** are listed in table 2.1.2.

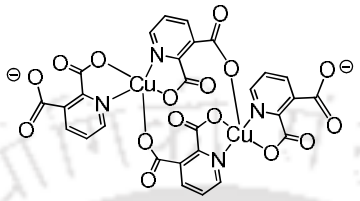

Figure 2.1.9: Dinuclear anionic unit in complex **2.1.10-2.1.12**.

Table 2.1.2: Bond parameters of prominent hydrogen bonds of complex **2.1.10**.

Bond (symmetry)	dD-H(Å)	dH···A(Å)	dD···A(Å)	<D-H···A(°)
O(6)-H(6B)···O(7) [x,y,z]	0.81(3)	2.03	2.838(5)	173
O(7)-H(7B)···O(8) [-1+x, y, z]	0.78(4)	2.00	2.754(4)	162
O(5)-H(5A)···O(3) [1+x,y,z]	0.82	1.74	2.557(2)	172
O(8)-H(8A)···O(6) [x,y,z]	0.82(5)	1.98	2.791(5)	170
O(8)-H(8B)···O(2) [1+x,y,z]	0.77(4)	2.07	2.813(4)	166
O(7)-H(7A)···O(1) [x,y,z]	0.81(3)	2.02	2.829(4)	174

Complex **2.1.10** possessing 5-aminoquinolinium cation consists of dinuclear anionic unit and protonated 5-aminoquinoline. 5-Aminoquinoline is protonated at quinoline nitrogen atom and amine nitrogen atom. In the cation the protonated nitrogen of quinoline and the amine projects in opposite with respect to the central fused ring. Further due to π-stacking (centroid to centroid distance ~3.71Å) with the adjacent crystallographically independent unit (Figure 2.1.10a), it requires relatively large number hydrogen bonding acceptor sites to complete the donor acceptor functionality. In such a situation a dimeric anionic part formed provides large number of hydrogen bonding acceptor sites for the cation to stabilize the crystal lattice. In packing, the **H5aqn** cations does not form well-defined infinite layer, rather involves in formation of tetrameric assembly via π-stacking in layers of copper dinuclear anionic polyhedral (Figure 2.1.10b and c).

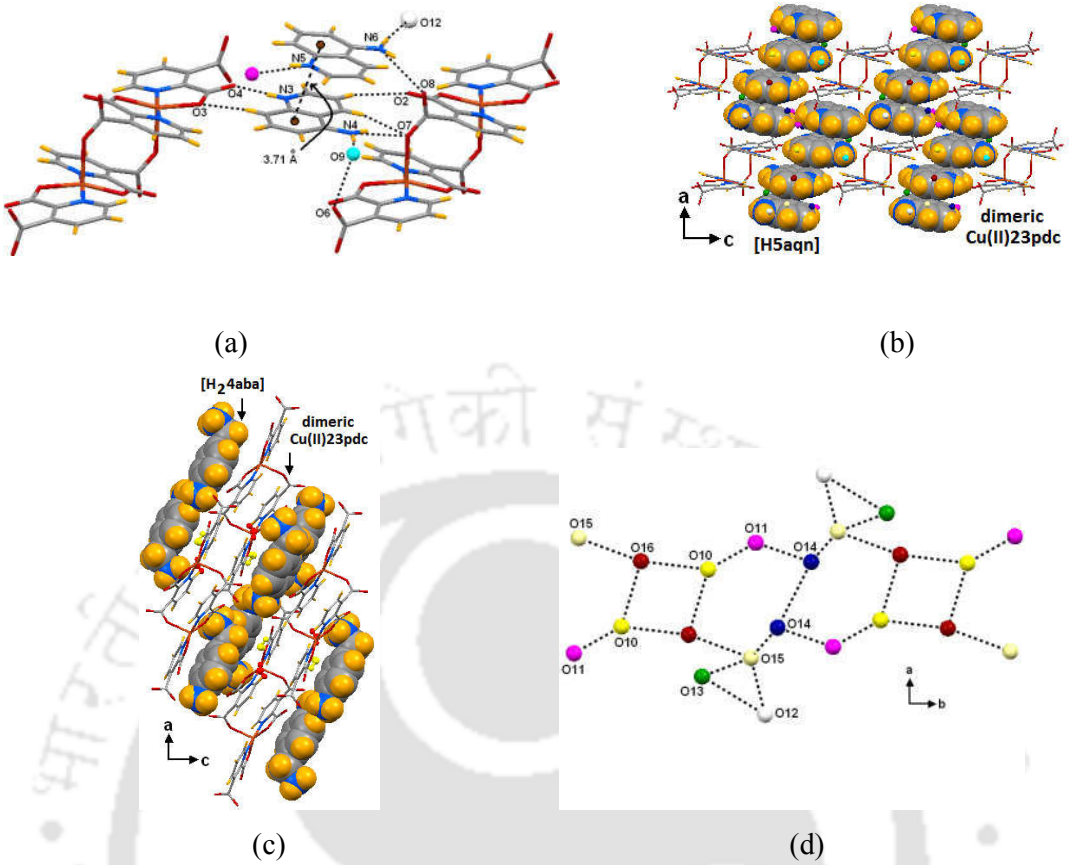

Figure 2.1.10: (a) Weak interactions in complex **2.1.10**, (b) Layered structure of dinuclear complex of **2.1.10**, (c) Layered structure of dinuclear complex of **2.1.10**, (d) Tetrameric and hexameric water cluster in the crystal lattice of complex **2.1.10**.

Further, the eight lattice water molecules available due to complete the hydrogen bonding functionality of the carboxylate groups of dinuclear complex anion, involves in formation of infinite water cluster. The hydrogen bonded water cluster consists of cyclic trinuclear, tetranuclear and hexanuclear core in the chain (Figure 2.1.10d). Despite of dinuclear anionic unit in **2.1.10**, the layered like structure of metal anionic and protonated **5aqn** is formed. π-Stacking of 5-aminoquinolonium ions with copper 2,6-pyridinedicarboxylates were observed which disfavor formation of layer-like structure.[30] Hence, self-interacting behavior of cations form homodimers that competes while forming self-assemblies of these complexes.

Complex **2.1.11** has isostructural anionic unit to complex **2.1.10**, whereas the cationic part is 1,5-diaminopentane (**dap**). The anionic unit of complex **2.1.11** is a dinuclear anion, whereas the dication of **dap** exhibits different conformer than the parent amine.

The cation derived from amine **dap** has two terminal $-NH_3^+$ group, that behave differently, therefore requires more numbers of hydrogen bonding acceptor sites to complete the packing pattern (Figure 2.1.11a). This may also be a complimentary criterion for the formation of dinuclear anionic unit present as anion of the complex. Alternatively, one may say that this process to be a cation directed assembly formation in the lattice. It also forms layered structures in the crystal lattice.

Complex **2.1.12** possessing 4-aminobenzylamonium cation is isostructural with **2.1.11**. Amine is protonated at both the ends, namely benzylic site and the amine group directly attached to phenyl unit (Figure 2.1.11b). There is a difference between the complex derived from positional isomer copper(II) 2,6-pyridinedicarboxylate possessing same cation. In such a situation a mono cation of 4-aminobenzylamine acted as the cationic counterpart.[32] Formation of dinuclear copper(II)2,3-pyridinedicarboxylate complex in case of **2.1.12** is attributed to the presence of two symmetrically different ammonium groups available in the aromatic dication to form complementary hydrogen bonds. Dications are encapsulated by the dinuclear complex anions via $-NH_3^+$-COO^- charge assisted hydrogen bonds. In the packing pattern cations are not interdigitated, rather shows π-π interactions between aromatic rings of complex anions. Such π-π interactions (centroid to centroid distance) is measured as 3.57Å (Figure 2.1.11c). In lattice, the complex anion and the aromatic dication form closely packed layered structures along crystallographic *b* axis.

The interlayer separation is ~8.84Å. Literature suggests that complexes derived from copper(II)malonates with benzylammonium cations give relatively larger interlayer separations.[33] Interlayer separations for these complexes were found to be in the range of 11.4Å-11.9Å. Thus, depending on cations interlayer separation in 2,3-pyridinedicarboxylate copper complexes varies.

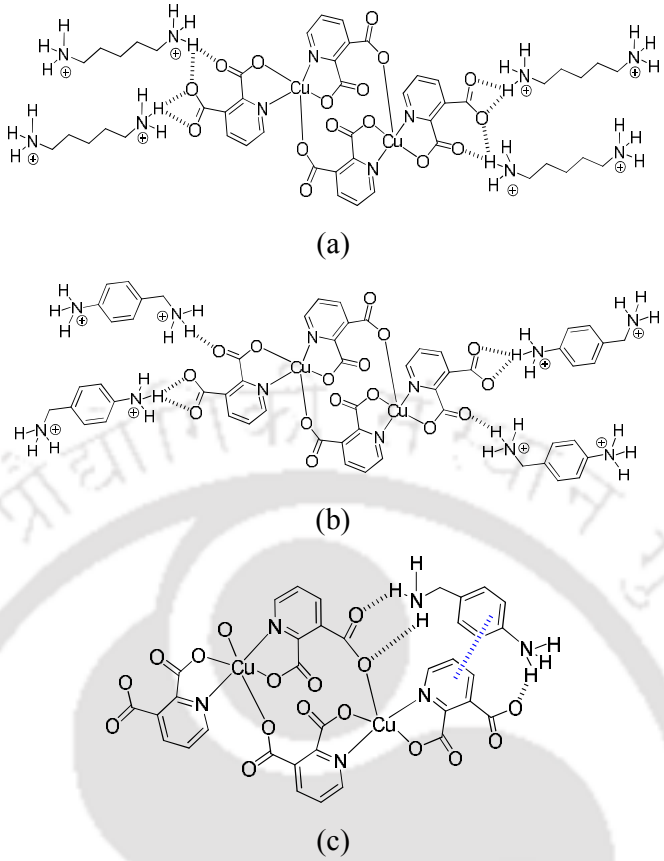

Figure 2.1.11: Surrounding anionic part of complex (a) **2.1.11**, (b) **2.1.12** showing hydrogen bond of cations with anion, (c) π-stacking observed in complex **2.1.12**.

2.1.4 Mono-nuclear copper(II) 2,3-pyridinedicarboxylate complexes

Mononuclear complexes of three distinct categories were observed depending on cation. For example, copper 2,3-dipyridinecarboxylate complex possessing cations of 3,5-diamino-phenyl-1,2,4-triazine is a penta-coordinate mono nuclear complex (Figure 2.1.12a). It has a square pyramidal geometry. It has two *bis*-chelated 2,3-pyridinedicarboxylate and a water molecule coordinating to copper ion.

On the other hand, complex having 3-aminobenzylammonium cation forms penta-coordinated copper complex by coordinating through amino group of benzylamine to copper ion and other site of the amine is protonated (Figure 2.1.12b). Such amines occupy the axial positions and equatorial position of octahedral structure is occupied by chelating 2,3-pyridinedicarboxylates.

There are strong hydrogen bonds between the free carboxylate anion and ammonium cation. Finally the complex having adeninium cation is also a mononuclear complex, it has a distorted square planar geometry (Figure 1.2.12c).

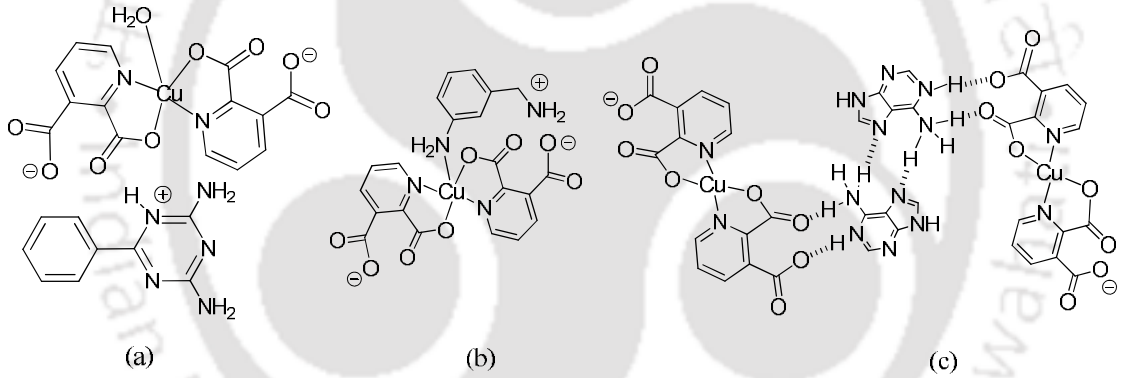

Figure 2.1.12: Mono-nuclear complex (a) **2.1.13**, (b) **2.1.14**. (c) Self-assembly of complex **2.1.15**.

Mononuclear complexes **2.1.13** and **2.1.14** comprise five-coordinate copper(II) centers and a main difference between these compounds consists in the number of cations per mononuclear anion. Distinction also arises in having distinct types of ligands occupying the respective square pyramid coordination sites. Complex **2.1.13** posseses a water molecule as a ligand at the axial position, whereas a protonated **3aba** moiety is present in the axial site in **2.1.14**. Complex **2.1.14** generates further structural interest as it has two symmetry independent molecules in its crystallographic unit cell.

The two symmetry independent molecules in unit cell are in fact two independent conformational state, one having cation derived from **3aba**, ammonium group project inward so that it can form an intramolecular hydrogen bond with a non-coordinating carboxylate group of the same molecule. The other counterpart has a benzylammonium part with the amine group projecting outwards, (Figure 2.1.13) thus not form intramolecular hydrogen bond but involves in intermolecular hydrogen bonds with carboxylate group of a neighboring molecule. Such process results in the self-assembly of two symmetry independent molecules.

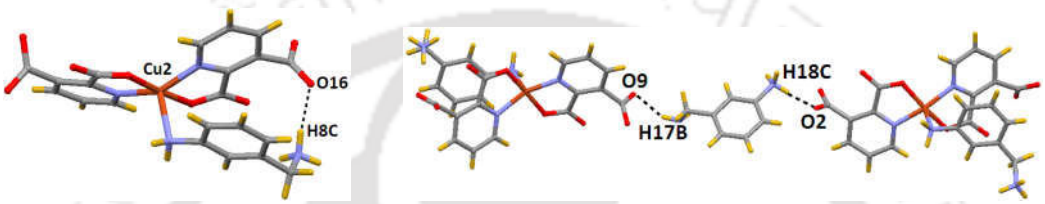

Figure 2.1.13: Hydrogen bonded self-assemblies of two independent conformers found as complex **2.1.13.**

Comparision of this complex **2.1.14** with complex **2.1.11** both posseses cations of positional isomers, large difference in structure and compositions are observed as later is a dinuclear complex. Thus, it is clear that the requirement for forming reoraganised templates for complementing hydrogen bond patterns of copper 2,3-pyridinedicarboxylate complexes of the positional isomers of the aminobenzylamine causes wide structural variations in terms of composition and binding. In other words, isomeric aminobenzylamines are recognised in different ways by the same anionic complex. On the other hand, copper 2,6-pyridinedicarboxylate complex having dications of **4aba** is mononuclear, and in this case the cation also does not participate in coordination.[32]

Further the mononuclear complex was formed with adeninium cation, $[H_2ade][Cu(23pdc)_2]\cdot 2H_2O$ (**2.1.15**) shows stabilization of adeninium cation in layers by forming dimeric self-assemblies of cations (Figure 2.1.14a).

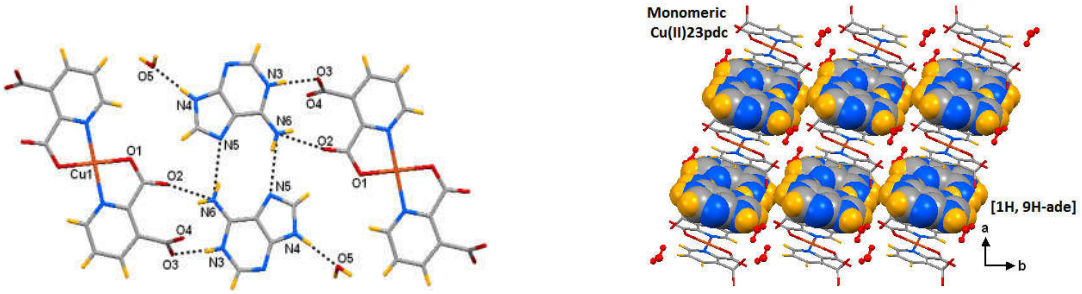

(a) (b)

Figure 2.1.14: (a) Hydrogen bonds in complex **2.1.15**, (b) Layer-like structure of complex **2.1.15**.

The coordination polyhedra of complex anions, exhibits square planar geometry, where the metal ion is coordinated with the pyridine nitrogen atom and one oxygen atom of deprotonated 2-carboxyl group of **23pdc** ligands. Adenine is protonated at the N1 and N9 position, which is known as the most stable tautomeric form of adeninium cation.[34] Planar adeninium cations form a dimer through $R_2^2(8)$ hydrogen bond motif (Figure 2.1.14a). Homo dimers of cations are formed *via* Hoogsteen face, i.e., through the -NH_2 group of pyrimidine ring and the unprotonated nitrogen atom of imidazole ring of adeninium cation. The homodimeric cations are further stabilized by hydrogen bonds with complex anions and lattice water molecules. The planar hydrogen bonded adeninium dimers are held between the parallel layers of mononuclear $[Cu(23pdc)_2]^{2-}$ complex anions. Interlayer separation between the anionic layers formed by self-assemblies of anions is 10.19Å (Figure 2.1.14b). Adenenium cations are trapped easily in different inorganic motifs. It is to be noted that density functional theory calculations shows that 1H,9H-adeninium cation is the most stable form followed by 3H,7H-adeninium cation by an energy difference of 0.46 kcal/mol. Recently, stabilizations of 1H,9H-adeninium cation has been observed in Cu(II) oxalate complexes with adenine, $(1H,9H\text{-ade})_2$ $[Cu(ox)_2(H_2O)]$ [where ox = oxalate]. The isostructural complexes with other metal ion such as Co(II) and Zn(II) showed formation of 3H,7H-adeninium cation in the complex. Both the 1H,9H-adeninium and 3H,7H-adeninium cation showed formation of 1D self-assemblies independently in layers of these metal oxalate complexes stabilized by hydrogen bond and π-π stacking interactions. Similarly, 1D assemblies of 1H,9H-adeninium cation in the form of cationic ribbon were established in Cu(II) malonate complexes by the same group of coworkers.

The other complexes with Co(II) or Ni(II) showed coordinated as well as adeninium cation outside the coordination sphere. Inter anionic layer separation in each case is presented in table 2.1.3. From the table it is suggested that nuclearity of the complex anions does not make large difference in the interlayer seapation. It is the cation that controls the interlayer separations.

Table 2.1.3: Distance between anionic layers in copper(II) 2,3-pyridinedicarboxylate.

Complex	Type of cation	Nature of anion	Distance between layers (Å)
$\{[Hipa)_2\{Cu(23pdc)_2]\ .2H_2O\}_n$	Monocation	Polymeric	11.40 (Å)
$\{(H_2en)\ [Cu(23pdc)_2]\ \cdot 2H_2O\}_n$	Dication	Polymeric	11.00 (Å)
$\{(H_2tmen)\ [Cu(23pdc)_2]\cdot 6H_2O\}_n$	Dication	Polymeric	13.50 (Å)
$\{(H_2dao)\ [Cu(23pdc)_2].4H_2O\}_n$	Dication	Polymeric	10.00 (Å)
$\{(H_3taea)\ [Cu_{1.5}(23pdc)_3]\cdot 5H_2O\}_n$	Trication	Polymeric	12.72 (Å)
$\{(H_2dabco)\ [Cu(23pdc)_2]\cdot 4H_2O\}_n$	Dication	Polymeric	12.30 (Å)
$\{(Him)_2\ [Cu(23pdc)_2]\cdot 4H_2O\}_n$	Monocation	Polymeric	11.90 (Å)
$\{(Hpy)_2\ [Cu(23pdc)_2]\cdot 5H_2O\}_n$	Monocation	Polymeric	12.10 (Å)
$\{(H8hqn)_2\ [Cu(23pdc)_2]\cdot 6H_2O\}_n$	Monocation	Polymeric	11.50 (Å)
$(Hdapt)[Cu(H23pdc)\ H_2O)]\ .H_2O$	Dication	Mononuclear	8.17 (Å)
$(H_23aba)[Cu(23pdc)_2(Haba)]_2.9H_2O$	Monocation	Mononuclear	8.65 (Å)
$(H_2dap)_2\ [Cu_2(23pdc)_4]\ \cdot 3H_2O$	Dication	Dinuclear	8.50 (Å)
$(H_24aba)_2\ [Cu_2(23pdc)_4]\cdot 4H_2O$	Dication	Dinuclear	8.84 (Å)
$(H5aqn)_2\ [Cu_2(23pdc)_4]\cdot\ 8H_2O$	Monocation	Dinuclear	11.82 (Å)
$(H_2ade)_2\ [Cu(23pdc)_2]\cdot 2H_2O$	Dication	Mononuclear	10.19 (Å)

2.1.5 Thermal stability and AC conductance

As mentioned in the introduction the non-covalently linked complexes have advantage of disassembling which is not the case with covalently linked compounds. Thus, the thermal stabilities of these complexes under consideration are important. Thermal decomposition study of the complexes in the ranges of temperature 30-600°C. Since the complexes are categorized by nuclearity, representative examples of thermogram from each class are discussed. Rest of the thermograms with weight loss sequences are given in appendix.

Thermal decomposition of coordination polymer **2.1.4** (Figure 2.1.15a) showed three sharp decomposition steps on heating a sample from room temperature to 600°C at rate of 1°C per minute. The first decomposition step spreads from 50°C-150°C involves loss of water molecules. Coordination polymer finally decomposes to form decomposition copper oxide.

Formation of copper oxide is confirmed by powder XRD (Figure 2.1.15b).

The powder XRD of the residue obtained after heating the coordination polymer at 600°C has powder patter that is super imposable with reported powder XRD pattern of copper oxide. Morphology of the residue was examined under transmission electron microscope. The residue is comprised of agglomeric particles of sizes varying from 12nm to 21nm (Figure 2.1.15c).

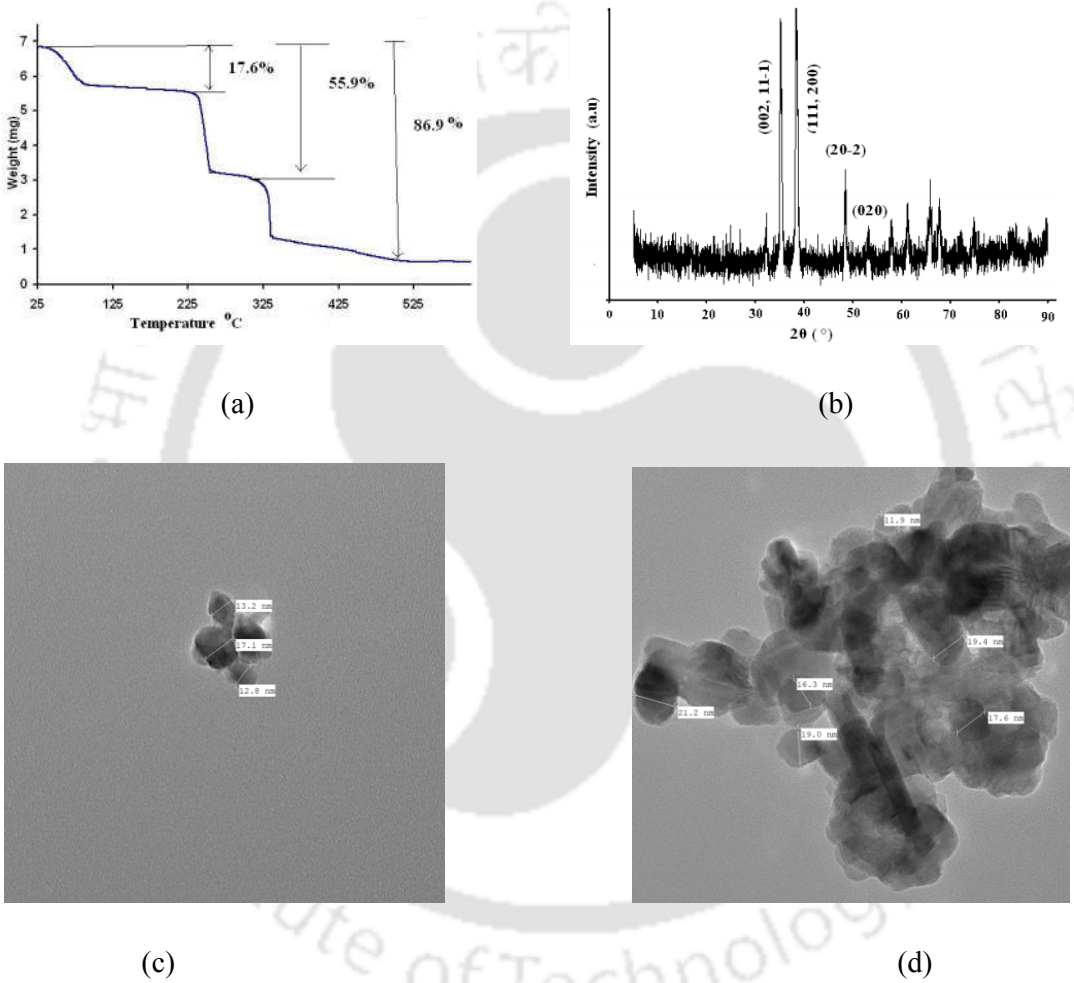

Figure 2.1.15: (a) Thermogram of complex **2.1.4** (heating rate 7°C/min), (b) Powder X-ray pattern of residue obtained from complex **2.1.4** after heating at 600°C, (c) and (d) Transmission electron micrograph of particles obtained from thermal decomposition of **2.1.4**.

This suggests definite control on the particle size to provide the decomposed oxide at nano-dimension to refer them as nano-particles. Similar decomposition of the coordination polymers are observed but the temperature for such decomposition varies. The particle size were analysed by TEM, showing that nano-dimensional oxides are formed.

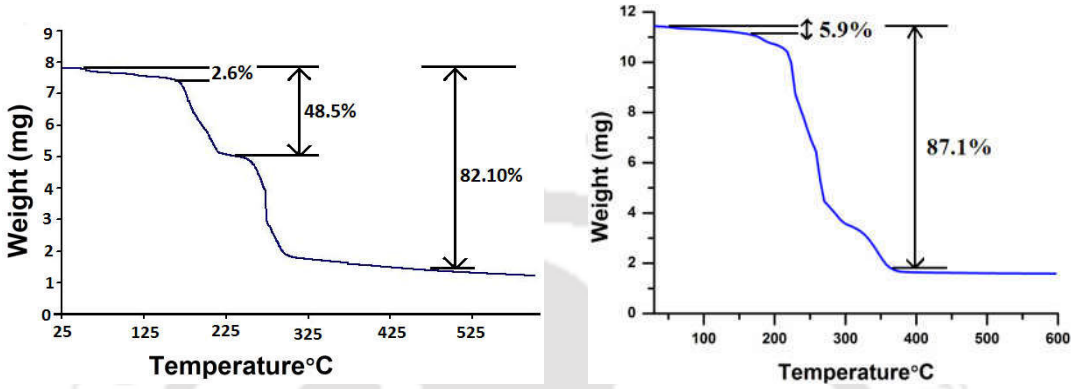

Figure 2.1.16: Thermogram of complex (a) **2.1.10**, (b) **2.1.13**.

The loss of water molecules in each case differ so as the decomposition temperature to form copper oxide. Among the complexes, **2.1.4** is most suitable for easy decomposion to form copper oxide. Copper oxide is prepared through thermal decomposition of different copper complexes or through calcination of **23pdc** complexes.[35]

Some metal-organic frameworks have shown promise for interesting applications of their proton conductivity properties.[36] Generally in molecular organic frameworks the band gaps[37] are reduced by multiple number of repeat units, but in a highly hydrogen bonded system proton conductance is prominent.[38] At room temperature, real part of conductance profile of the coordination polymers as well as mononuclear complexes changes with frequencies shows a curvature followed by increase of conductance (Figure 2.1.17). AC conductance shown by **2.1.3** is 1.1×10^{-4} S/cm, and that for **2.1.12** is 3.6×10^{-6} S/cm.

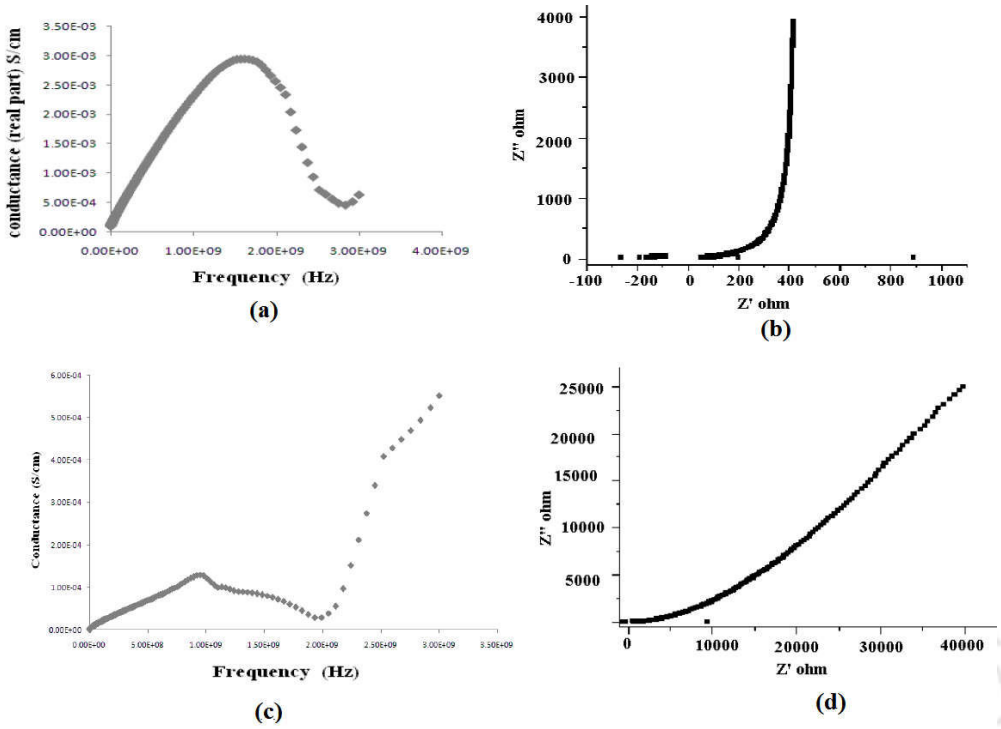

Figure 2.1.17:(a) Plot of solid state room temperature conductance vs frequency of complex **2.1.3**, (b) Cole-Cole plot of the complex **2.1.3**, (c)) Plot of solid state room temperature conductance vs frequency of complex **2.1.12**, (d) Cole-Cole plot of the complex**2.1.12**.

2.1.6 Summary

Nuclearity of copper(II) 2,3-pyrdinecarboxylate complexes are dependent on nature of organic ammonium cations. A new coordination polymer from combination of mono-nuclear and di-nuclear complex species is described. Other than di-nuclear complexes, the mononuclear complexes of copper(II) 2,3-pyrdinecarboxylate have generated interest due to varieties of structural features namely coordination number, coordination environment and self-assembling have opened up new avenues to examine them with care. The conformational isomers self-assembling in such complex is a unique feature. Besides the of anionic polyhedra are used as supramolecular building block that creates inorganic-organic layer-like structure to accommodate wide range of organic ammonium cations. Further, depending on the size and geometry of the cation, the inter anionic layer separation between the layers varies from 8.17Å to 13.50Å.

Part B

Self-assemblies of copper(II) 2,5-pyridinedicarboxylate and intercalation of organic ammonium cations.

2.2.1 Background

Different positional isomers of pyridinedicarboxylic acids such as 2,3- , 2,5- and 2,6-pyridinedicarboxylic acids form a variety of self-assembled supramolecular and metal-organic networks.[39] 2,6-pyridinedicarboxylate complexes of divalent metal ions generate layered structures guided by π-stacking interactions.[40] π-Stacking in 3,5-pyridinedicarboxylates or 2,6-pyridinedicarboxylates helps to generate lamellar structures.[41] A number of such 2,3-pyridinedicarboxylate systems have been described in section A of this chapter. Similar approach as that of part A of this chapter is discussed in part B section on findings with another positional isomer 2,5-pyridinedicarboxylic acid.

2.2.2 Synthesis and characterization of copper(II) 2,5-pyridinedicarboxylate complexes

Reaction of 2,5-pyridinedicarboxylic acid (**$H_2$25pdc**) with copper(II)acetate and various organic amines resulted in three different types of complexes namely mono-nuclear, tri-nuclear complexes or coordination polymers. Since one of the objectives of the present work has been to understand the effect of cations guiding nuclearity of pyridinedicarboxylate complexes, crystal structures of such complexes were determined. The complexes were characterized by recording their IR, UV, thermogravimetry, ESR and elemental analysis and by recording the powder XRD of each sample in bulk and comparing with the simulated powder XRD pattern from the crystallographic information file. IR spectra of 2,5-pyridinedicarboxylic acid has IR stretching at 1665cm^{-1} -1608 cm^{-1} and 1591cm^{-1} -1582 cm^{-1} due to for asymmetric (ν_{as}) and symmetric (ν_s) vibrations respectively. These characteristic stretching of carboxylate and the hydroxyl group changes, these are taken as preliminary study to confirm complexation of the carboxylate and abstraction of cations from the amine to form corresponding complex.

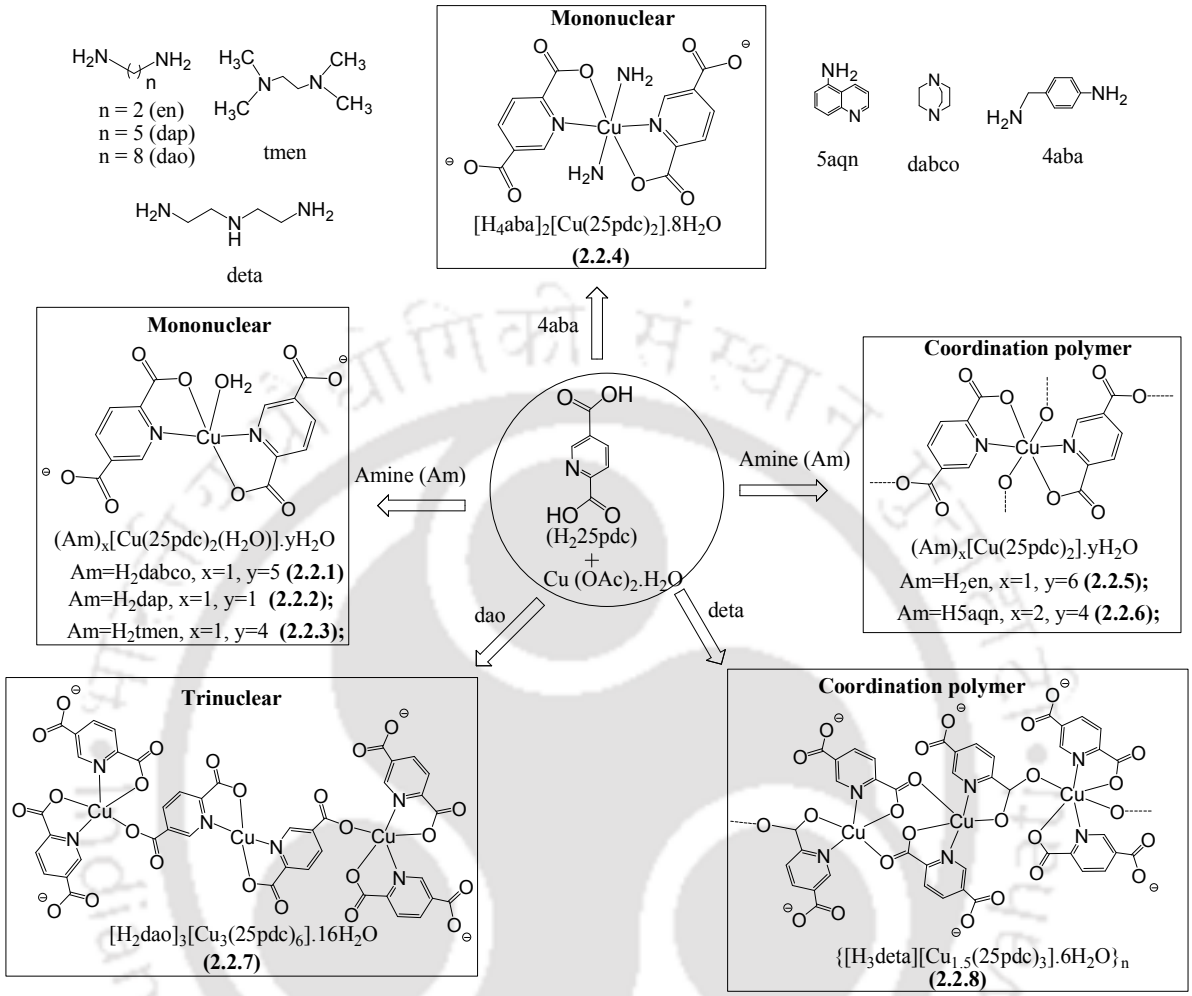

Scheme 2.2.1: Different copper(II) 2,5-pyridinedicarboxylate complexes.

Nuclearity of the complexes depend on the cation and different complexes prepared by using different types of amines are shown in scheme 2.2.1. Discussion on self assembly of complexes of individual series of complexes are described under independent sub-headings.

2.2.3 Mono-nuclear copper(II) 2,5-pyridinedicarboxylates

2.2.3.1: Five coordinated complexes

Copper 2,5-pyridinedicarboxylate complexes that posseses protonated 1,4-diazabicyclo[2.2.2]octane (**dabco**), 1,5-diaminopentane (**dap**), N,N,N',N'-tetramethyl ethylenediamine (**tmen**) cations are mono-nuclear complexes. In all these complexes 2.2.1-2.2.3 has common anionic part. Anionic part in case of is comprised of two chelating 2,5-pyridinedicarboxylate and a water coordinating to a copper ion. 2,5-Pyrydinedicraboxylate utilizes the nitrogen atom and the carboxy group at 2-position to form chelate with copper ions and occupy the basal plane of square-pyramidal structure. In the structure water molecules occupy axial position of penta coordinated copper to complete a square pyramidal geometry. Carboxylate group located at 5-position of the pyridine ring strongly hydrogen bonded to cations which prevents formation of higher nuclearity complex. In each case, free carboxylate group strongly hydrogen bonds to corresponding cation. These ionic hydrogen bonds are strong and stabilize mononuclear complexes.

Hydrogen bond environment in the complex **2.2.1** is shown in Figures 2.2.1(a). The -NH_3^+ and coordinated water molecule groups hydrogen bonds with carboxylate group forms the basis of self-assembly. As a result of the formation of hydrogen bonded sub-assemblies formed through complementing hydrogen bonds, mononuclear unit gets stabilsed and do not undergo further polymerization to form polynuclear complexes.

Packing pattern of the complex **2.2.1** in solid state has protonated **dabco** cations and the complex anions are arranged in parallel arrays like layers, such layers exists as independent layers running in the *a* and *b* axis [Figure 2.2.1(b)]. Hydrogen bond parameters of N3-H3N···O7 and N4-H4N···O3 ($d_{D\ldots H}$, 1.77Å, $d_{D\cdots A}$, 2.71Å; < D-H····A, 157º and $d_{D\ldots H}$, 1.61Å, $d_{D\cdots A}$, 2.56Å; < D-H····A, 171º) suggest them to be strong hydrogen bonds.[42] Complex **2.2.1** has **$[H_2dabco]^{2+}$** dication has highly crystallographically disordered structure, which was attributed to wiggle movement of the cation around one CH_2-CH_2 edge.[12]

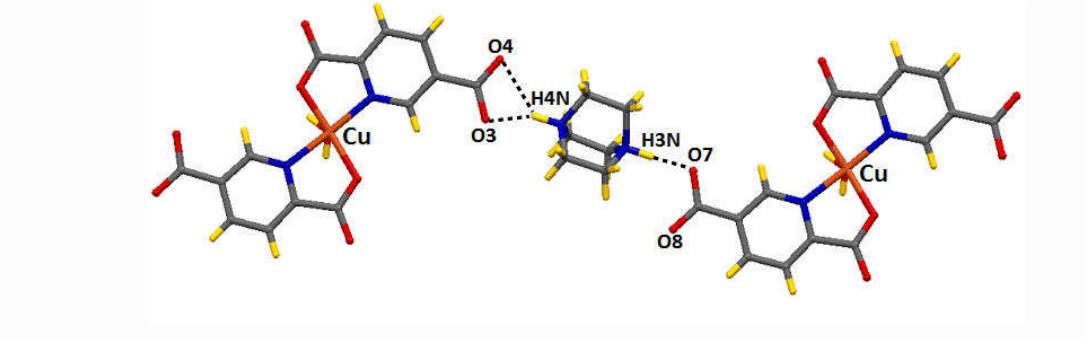

(a)

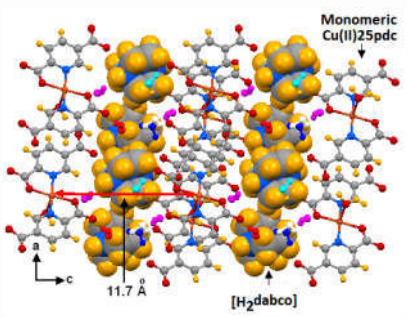

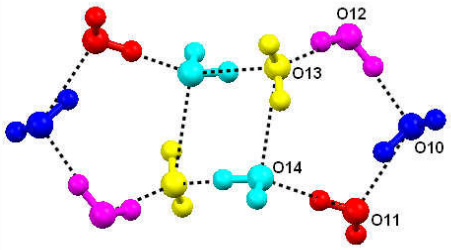

(b) (c)

Figure 2.2.1: (a) Hydrogen bonds between anions and cations in complex 2.2.1, (b) Packing diagram of complex **2.2.1** showing inter-layer separation, (c) Decameric water clusters in **2.2.1**.

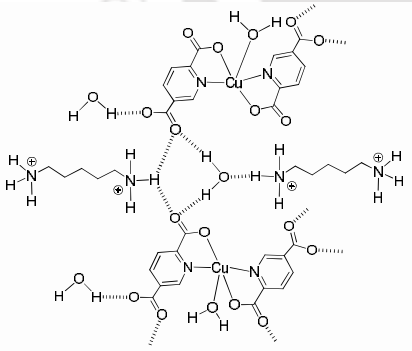

(a)

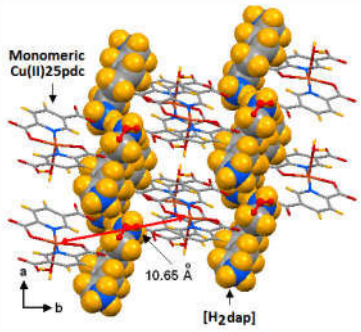

(b)

Figure 2.2.2: (a) Hydrogen bonds of cations with anions in complex **2.2.2**, (b) Packing pattern of complex **2.2.2** showing layer-like arrangements.

In the present example, structure determined at room temperature does not show such disorder. This could be related to the tight packed structure formed in a highly complementing hydrogen bonded environment.

Distance between copper ions located at parallel positions in two independent layers along crystallographic *b* axis is ~11.7Å (Figure 2.2.1b). There are five lattice water molecules in the complex, they form decameric clusters which are combination of tetrameric and pentameric cyclic units. Clusters exhibit intrinsic hydrogen bonds with the $-COO^-$ group of $[Cu(25pdc)_2(H_2O)]^{2-}$, contributes to form tight packed structure.

Complex **2.2.2** has anions embraced by actions through strong hydrogen bond shown in Figure 2.2.2a. Terminal ammonium groups of the cation hydrogen bond with coordinated water at one end and lattice water at another end (Figure 2.2.2a). The inorganic arrays of anions of this complex in its lattice is built up of $[Cu(25pdc)_2(H_2O)]^{2-}$. Whereas, organic layers are made up of protonated 1,5-diaminopentane form A-B-A pattern and propagates along crystallographic *a* and *c* axis. The metal-metal separation in the interlayers is ~10.65Å end (Figure 2.2.2b).

It may be mentioned that in the case positional isomeric 2,3-pyridinecarboxylate having, cations derived from 1,5-diaminopentane is a dinuclear complex. A comparison of the two structures have revealed that orientations of two free carboxylate groups force directional hydrogen bonds to differ in each case, thereby making difference in nuclearity. This provides direct evidence that the organic ammonium cation plays the key role to decide the nature of assembly in these complexes.

When cation N,N,N',N'-tetramethylenediamine was used, mononuclear complex **2.2.3** formed has protonated tetramethylethylenediammonium dication. Central copper(II) ion of this mononuclear complex has anion $[Cu(25pdc)_2(H_2O)]^{2-}$, has a distorted square pyramidal geometry (Figure 2.2.3a). Equatorial Cu(II)-O_{eq} and Cu(II)-N_{eq} distances are 1.946(2) and 1.994(2) Å respectively. Cu1-O_{aqua} bond distance is 2.319(3)Å. It may be mentioned that in an earlier report 3-methylaminopyridinium cobalt(II) 2,5-pyridinedicarboxylate complex has aqua ligandsin axial position.[43] But changing the ligand slightly, it was observed that isonicotinamide coordinates to cobalt(II). Beside these a dinuclear copper(II) 2,5-pyridinedicarboxylate complex 1,4-butanediammonium dication was reported.[44]

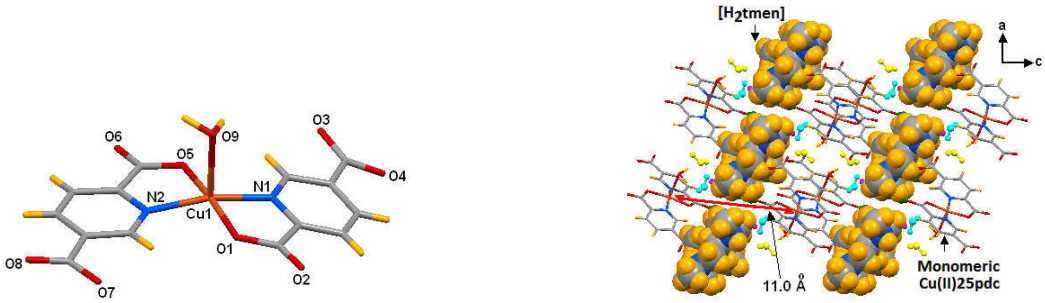

(a) (b)

Figure 2.2.3: (a) Structure of $[Cu(25pdc)_2(H_2O)]^{2-}$ in complex **2.2.3**, (b) Packing diagram of complex **2.2.3** showing arrays of cations.

As in the other two analogues, complex **2.2.3** has $[\mathbf{H_2tmen}]^{2+}$cations arranged in arrays like a layers held by another arrays formed by anions. In the layer, the arrays of dications and mononuclear dianions are alternatively positioned and have $-N^{+}-H\cdots COO^{-}$ hydrogen bonds with distance of separation between the anion layers is ~11.0Å (Figure 2.2.3b). Lattice water molecules are associated with formation of hydrogen bonds with the complex anions.

2.2.3.2: Hexacoordinated complex

A hexa coordinated Cu(II) 2,5-pyrdinedicarboxylate possessing octahedral geometry is observed when the cation was derived from monoprotonated 4-aminobenzylamine directly coordinated with the Cu(II) ion and protonation occur at relatively stronger benzylic amine. Cu-N_{ax} distance 2.636 (3)Å is much longer than the Cu-O_{eq} 1.958 (2)Å or Cu-N_{eq} 1.958 (2)Å, distance which is due to Jahn-Teller distortion or could be due to steric reasons to accomplish a stable solid state packing. In the lattice the aromatic rings of cation and anions are parallel and centroid-to-centroid distance between the aromatic rings of cations is ~3.56Å (Figure2.2.4a). This distance is suitable to have π-interaction.[45] Hence in the present case the observed distance is indicative of a strong charge transfer π-interactions. It may be mentioned that similar cation stabilizes dinuclear copper 2,3-pyridinedicarboxylate complex as described in earlier part of this chapter, hence the directed properties of hydrogen bonds and complementing directional weak interactions can be attributed to difference in nuclearity in each case.

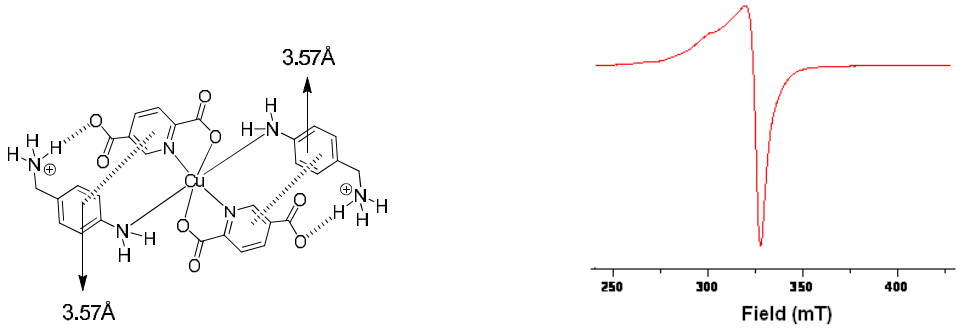

(a) (b)

Figure 2.2.4: (a) Intramolecular hydrogen bonds in complex of **2.2.4** with π-stacking, (b) ESR spectra of complex **2.2.4**.

Electron spin resonance (ESR) spectroscopy has been helpful to assign the geometry around the copper(II) ions.[46] The ESR spectrum complex was recorded. The solid-state EPR spectrum of the complex **2.2.4** (Figure 2.2.4b) is indicative of a six-coordinate complex with a distorted octahedral environment.

2.2.4 Trinuclear complex

Copper(II) pyridinedicarboxylate complex **2.2.7** possesing, 1,8- diammonium -octane is a tri-nuclear complex. The structure of the complex **2.2.7** consists of $[Cu_3(25pdc)_6]^{6-}$ anionic having a skeleton shown in Figure 2.2.5a. Complex anion $[Cu_3(25pdc)_6]^{6-}$ has two different copper(II) environments. Two copper at terminal ends are square pyramidal and one located in between is square planar. This unique trinuclear $[Cu_3(25pdc)_6]^{6-}$ complex anion form layers with cations and anions in the ratio 1:1 (Figure 2.2.5b). The hydrogen bonds in layers are such that the end of each tri-nuclear unit is terminated by ionic hydrogen bonds. Distinctions among the coordination environment of copper(II) ions with d^9-electronic configuration are reflected in their respective ESR spectra (Figure 2.2.5c).

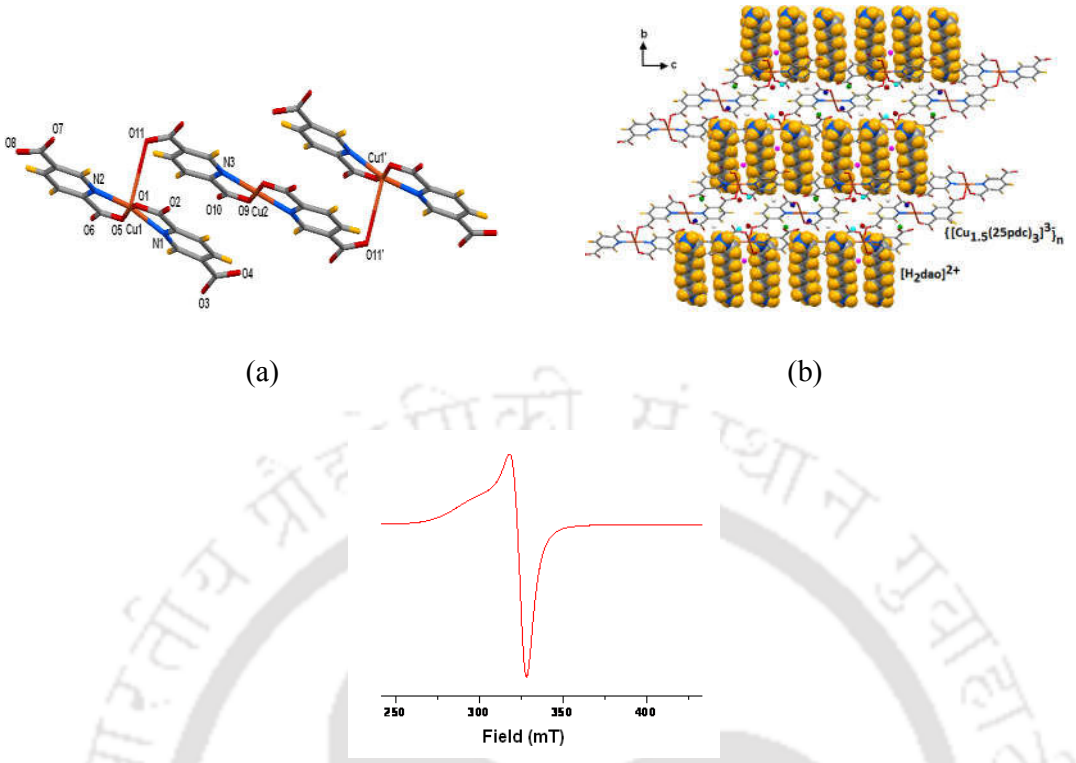

(a) (b)

(c)

Figure 2.2.5: (a) Anions of **2.2.7**, (b) Layered arrays of anions and cations in **2.2.7**, (c) ESR spectra of complex **2.2.7**.

2.2.5 Coordination polymers

When en and 5-amionoquinoline were used to generate the cations for copper(II)2,5-pyridinedicarboxylates, then coordination polymers was obtained in each case. Coordination polymers are composed of two mono-cations of 5-aminoquinoline or one dication of ethylenediamine, polymeric $\{[Cu(25pdc)_2]^{2-}\}_n$ complex anion, and lattice water molecules. The repeat units of the polymeric anions are dinuclear units having five member chelates formed by nitrogen atom and oxygen atoms of 2-carboxylate groups of **25pdc** ligand as shown in Figure 2.2.6. Axial positions of the coordination spheres of penta coordinated copper ions are occupied by oxygen atoms from 5-carboxylate groups of the **25pdc** ligand.

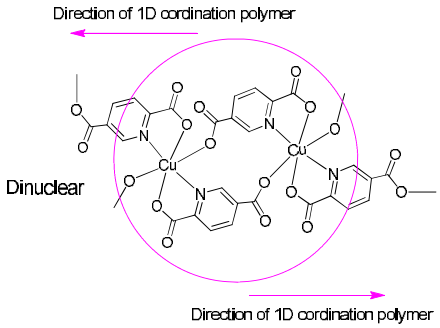

Figure 2.2.6: Polymeric unit of coordination polymer **2.2.5** or **2.2.6**.

Coordination polymer **2.2.5** possesing ethylenediammonium cation consists of dication $[H_2en]^{2+}$, polymeric $\{[Cu(25pdc)_2]^{2-}\}_n$ complex anion, and six lattice water molecules. In the polymeric anion equatorial Cu(II)-O_{eq} and Cu(II)-N_{eq} bond distances are 1.955Å and 1.969Å respectively. The axial Cu(II)-O_{aq} distance is 2.560Å, and the bond angles around the metal ion ranges from 83.29(2)-180.00(2)º which are of similar magnitudes to that of polymeric complexes reported with similar backbone but with different cations.[47] The cations are held between the polymeric chains and exhibits a bi-layer arrangement along crystallographic *a* and *b* axes. The $[H_2en]^{2+}$dication interacts with the complex anion $\{[Cu(25pdc)_2]^{2-}\}_n$ *via* $-NH_3^+$-COO^- hydrogen bonds. A layered packing arrangement of the complex **2.2.5** along *b* axis (Figure 2.2.7b). The inter-metal distance between the two adjacent polymeric layers is 11.6Å along *b* axis.

Water molecules in the lattice exhibit hydrogen bonds with both the carboxylates of complex anions and $-NH_3^+$ of dication leading to a tight packed structure in the lattice. There are examples of mono-nuclear metal complexes derived from 2, 3, or 2, 5-pyridinedicarboxylic acid[17] possessing ethylenediammonium cation. Packing patterns of such complexes have π-π interactions leading to layer-like arrangements. Further interesting features are observed in the structure of the complex **2.2.6**, derived from diprotonated 5aqn. It has polymeric anions forming layers similar to complex **2.2.5.** The separation between the metal centers of the interlayer is ~ 12.1Å (Figure 2.2.7c). In between such layers the cations of protonated **5aqn** form one dimensional chain like arrangement through π-stacking. The distances between the alternate planes of adjacent cations are 3.332Å and 3.337Å respectively (Figure 2.2.7d).

Aromatic inclusion compounds form dimer in many inclusion complexes[17], but in the present case has stacking between the π-cations to forms layers. The lattice water molecules are involved in hydrogen bonds to bridge adjacent polymeric complex anions.

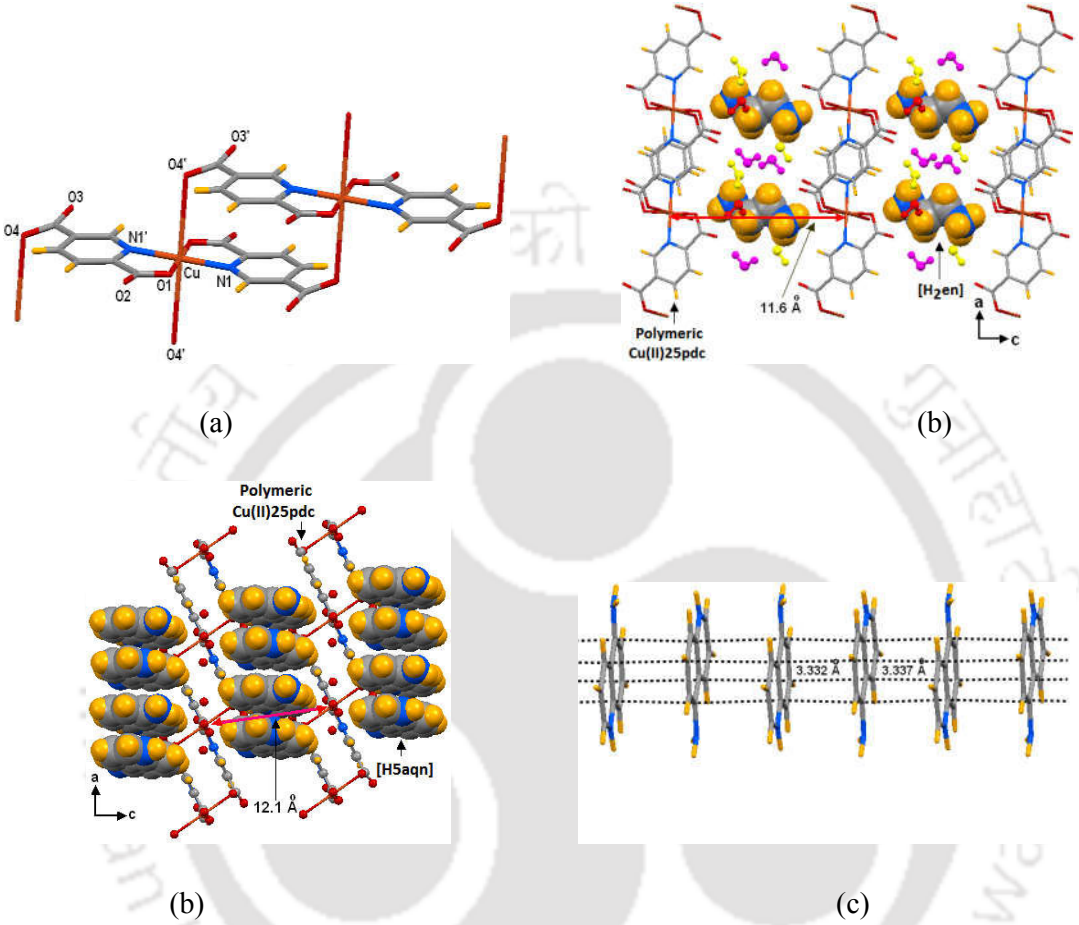

Figure 2.2.7: (a) Structure of $\{[Cu(25pdc)_2]^{2-}\}_n$ units of coordination polymer **2.2.5**, (b) Layered structure of the coordination polymer **2.2.5**, (c)Packing diagram of complex **2.2.6**, (d) The π- stacked protonated 5aqn cations held between the layers of $\{[Cu(25pdc)_2]^{2-}\}_n$ in **2.2.6**.

Trication of diethyltriamine with **25pdc** results in formation of unique coordination polymer.To neutralize the +3 charge of the trication on protonated diethylenetetramine, and to accommodate the cation in its lattice it forms self assemblies through coordination of the carbonyl group.

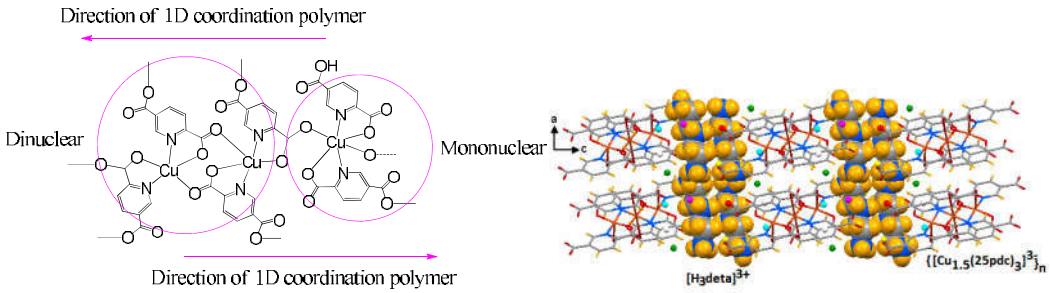

(a) (b)

Figure 2.2.8: Repeat units in coordination polymeric unit of coordination polymer **2.2.8**, (b) Packing diagram of complex **2.2.8**.

The polymeric complex anion is thus constituted by two different Cu(II) atoms having distorted square pyramidal and octahedral geometry in the polymeric chain(Figure 2.2.8a). In the asymmetric unit, the Cu(II) with distorted octahedral geometry possess 50% occupancy, thus resulting -3 charge of the polymeric complex and also exhibits a completely different polymeric structure. This indicates that the organic cation play key role to decide the nature of assembly in these crystal lattices. Thus, formation of the mono-nuclear and poly-nuclear species under similar condition in the present case have taken place due to variation of cations.

The thermogravimetry (TGA) of the pyridinedicarboxylate generally proceeds through complicated path. In a mononuclear and a trinuclear copper(II) complexes it was shown that at low temperature such complexes decomposes and mononuclear complex led to copper oxide at low temperature.[45] However, we have not observed formation of copper oxide at low temperature, except in one case. But thermogravimetry analysis is helpful in ascertaining the loss of the hydrated water in most of the cases and to show the tally of the crystallographically found out water molecules in bulk samples (Appendix Figure 2A2). In thermogravimetry the entire complexes show two major steps of weight loss. The weight loss for lattice water molecules occur in the range of 65ºC-145ºC. The 2nd weight loss occurs at temperature > 220ºC, this step is due to loss of the amines and 2,5-pyridinedicarboxylate depending on the complex. Details are given as a table 2.2.1. As an illustrative case the TGA of the complex **2.2.1** is shown in the Figure 2.2.9c.

In this case the first step there is loss of water of crystallization. This is followed by loss of **dabco** and pyridinedicarboxylic acid leading to a residue having composition of [CuO.Cu(25pdc)]. In order to understand the thermal decomposition, we have compared the IR spectra of the compound with parent compounds and the amine (in this case dabco) with the respective spectra obtained after heating at 75°C and at 275°C. The region where the O-H and N-H stretching appear namely 2700cm^{-1} - 4000cm^{-1} is shown separately from the fingerprint region of the IR (Figure 9a and 9b). As the samples loses water on heating at 75°C, the broad stretching frequency occurring for the presence of both N-H and O-H are shifted towards higher wavelength, suggesting loss of water. The heating also causes effect in the fingerprint region, there is clear change in intensity and width of the peak but due to overlapping of peaks the peak assignments are not done. While on heating at 275°C, the loss of amine molecules is suggested from the change in the IR signals arising from protonated dabco which are significantly diminished [refer figure 9a, 9b (iii) and (v)]. On the other hand, the sample has carbonyl frequencies showing that the pyridinedicarboxylate ligand remained attached to the copper ions at this temperature. Another example showing the effect of heating on IR spectra of sample of the complex **2.2.4** is shown in supporting information. In the case of complex **2.2.4**, at the temperature range 64°C-200°C the water of crystallization are lost and at temperature range 212°C-226°C, it losses one of the pyridinedicarboxylate and two 4-aminobenzylamine and results in the formation of $[Cu(25pdc)]_n$. In majority of the complexes, heating above the 220°C led to formation of $[Cu(25pdc)]_n$; from relatively higher thermal stability which presumably a coordination polymer. However, in the case of **2.2.3** we observe weight corresponding to formation of $[(en)Cu(25pdc)]_n$, on the other hand in the case of **2.2.2** we observe the weight loss corresponding to formation of CuO. In earlier study on thermal decomposition of copper(II) 2,4-pyridinedicarboxylate copper oxide was observed at relatively low temperature.[45] We have observed this only in one case below 600°C and we find varieties in thermally decomposed products on this class of complexes, which we are examining in details.

The X-ray powder diffraction patterns were recorded to check the bulk purity of these complexes. The measured PXRD patterns of the compounds have close resemblances to the simulated patterns from the respective single crystal data (Appendix Figure 2A1). This confirms the homogeneity of the bulk samples.

The PXRD of the complex **2.2.1** with the Miller indices of prominent peaks is shown an illustrative example in Figure 2.2.9d.

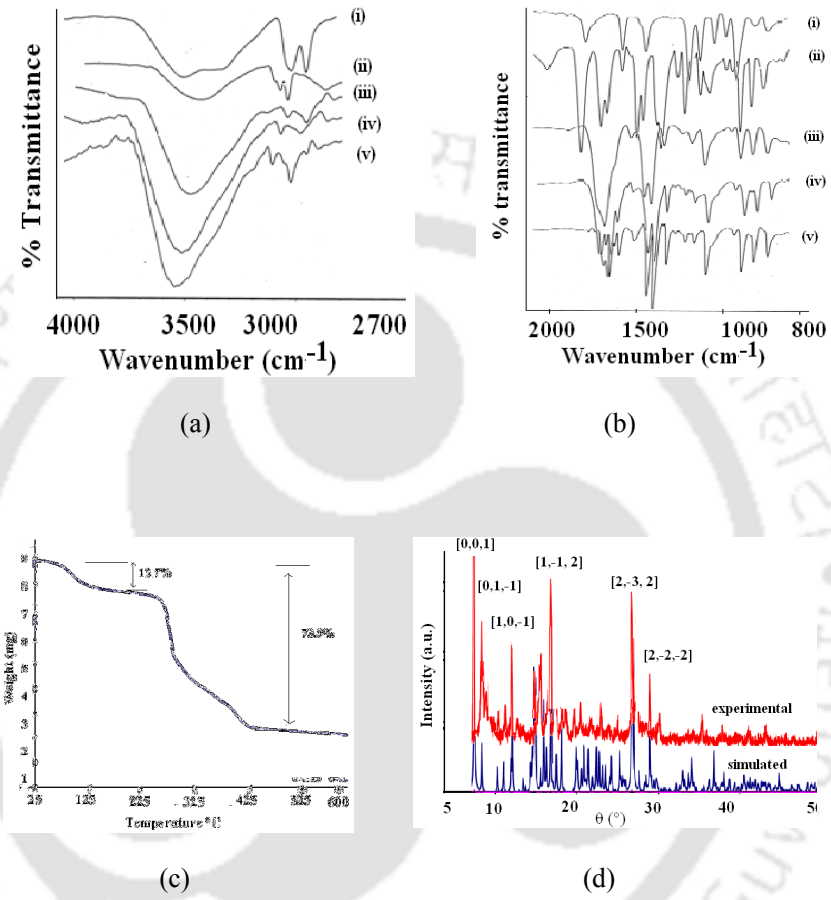

Figure 2.2.9: (a) and (b) are the IR spectra (KBr) of (i) **dabco**, (ii) $\{H_2[Cu(25pdc)_2]\}_n$, (iii) Complex **2.2.1** , (iv) Complex **2.2.1** after heating at 75°C for 30 min. (v) after heating the complex **2.2.1** at 275°C for 1hr. (c) Themogravimetry of the complex **2.2.1** recorded with a heating rate of 5°C per minute. (d) The experimentally determined and simulated (from CIF by Mercury program) powder XRD of the $[H_2dabco][Cu(25pdc)_2(H_2O)]\cdot 5H_2O$ (**2.2.1**).

Table 2.2.1: Temperature range for the loss of different components of the complexes **2.2.1-2.2.8**

Complex	Evaporation tem. Of lattice H_2O	Evaporation of organic cation	Evaporation range of complex cation
2.2.1	58-75	241-275	>510
2.2.2	68-137	201-258	>340
2.2.3	63-101	272-306	>512
2.2.4	64-92	212-241	>260
2.2.5	73-97	222-271	>420
2.2.6	121-142	228-262	>465
2.2.7	75-107	227-265	>450
2.2.8	64-144	224-258	>344

2.2.6 Summary

In conclusion, the nuclearity and coordination environment of $[Cu(25pdc)_2]^{2-}$ polyhedra are controlled by the type of organo-cations. Despite having different types of structural units in the complexes, each complex exhibits a lamellar structure; and the metal–metal separations between the interlayers are in the range of 10.6-12.1Å. Novel polymeric structures by combination of mononuclear and dinuclear units as building blocks in **2.2.8**, suggests that the $[Cu(25pdc)_2]^{2-}$ units are responsible for construction of such repeat units. So, this unit may be considered as a replica of the covalently linked polymeric structures formed from interaction of copper(II) ions with **25pdc** ligand. Comparision with two isomeric pyridinedicarboxylates have show that the directional hydrogen bonds and interplay of weak interactions make large differences in their respective complexes with same cation.

2.3 Experimental Section

Detailed synthetic methodologies are given below. Analytical data as well as spectroscopic data are also listed along with the each complex. Details of the instruments, crystallographic table are given in Appendix.

2.3.1: As all of the complexes were prepared by similar procedures, a typical experimental procedure is as follows: To a solution of 2,3-pyridinedicarboxylic acid and 2,5-pyridinedicarboxylic acid (0.167g, 1.0 mmol) and dissolved in methanol (20 ml), copper(II) acetate monohydrate (0.10g, 0.5 mmol) was added. The resulting blue solution led to the formation of a precipitate. The mixture was stirred and the corresponding nitrogenous base (0.5 mmol, dication) and (1mmol, monocation) were added in small portions. This led to a homogeneous solution, which was left overnight at room temperature. This resulted in the formation of blue precipitates, which were collected by filtration and dissolved in water or a water/pyridine mixture. Slow evaporation of the solution led to suitable X-ray quality crystals after 3-4 d.

2.3.2: $\{[Hipa]_2[Cu(23pdc)_2]\cdot 2H_2O\}_n$ **(2.1.1):** Isolated yield: ~65%. IR (KBr, cm^{-1}): 3422 (bs), 2979 (s), 2840 (w), 2734 (w), 2186 (w), 1646 (s), 1591 (s), 1569 (s), 1470(w), 1391 (s), 1346 (m), 1272 (m), 1117 (m), 877 (m), 835 (w), 729 (w). Elemental analysis calcd for $C_{20}H_{30}CuN_4O_{10}$, C, 43.63 H, 5.45; N, 10.18%; found C, 43.59, H, 5.51, N, 10.87. Vis. (solid state) λ_{max}: 616.0nm. ESR (solid state): g = 2.063.

2.3.3: $\{[H_2en][Cu(23pdc)_2]\cdot 4H_2O\}_n$ **(2.1.2):** Isolated yield: ~70%. IR (KBr, cm^{-1}): 3527 (bs), 3361 (w), 3179 (w), 1635 (m), 1610 (m), 1591 (m), 1566 (m), 1518 (w), 1475 (w), 1396 (s), 1364 (s), 1280 (w), 1161 (w), 1119 (m), 1071 (w), 876 (w). Elemental analysis calcd for$C_{16}H_{24}CuN_4O_{12}$, C, 36.40; H, 4.58, N, 10.61%; found C, 36.34, H, 4.51, N, 10.57. Vis. (solid state) λ_{max}: 610.0nm.

2.3.4: $\{(H_2dao)\ [CuL_2]\cdot 4H_2O\}_n$ **(2.1.3)**: Isolated yield: ~69%. IR (KBr, cm^{-1}): 3425 (bs), 2623 (m), 2586 (m), 2458 (s), 1635 (s), 1586 (s), 1435 (w), 1389 (m), 1352 (m), 1270 (m), 1235 (w), 1146 (w),1110 (s), 998 (w), 976 (w), 844 (w), 729 (w), 701 (w).Elemental analysis calcd for $C_{20}H_{22}CuN_4O_{14}$, C, 39.48, H, 3.62; N, 9.21%. Found C, 39.46, H, 3.62, N, 9.20%. Vis. (solid state) λ_{max}: 630.0nm. ESR (solid state): g = 2.039.

2.3.5: $\{(H_2tmen)\ [CuL_2]\cdot 6H_2O\}_n$ **(2.1.4):** Isolated yield: ~55%. IR (KBr, cm^{-1}): 3436 (bs), 3043 (w), 2926 (w), 1634 (s), 1584 (s), 1500 (w), 1436 (w), 1396 (m), 1358 (s), 1273 (m), 1237 (w), 1116 (s), 878 (m), 840 (m), 787 (w), 705 (w), 603 (w), 551 (w), 470 (w). Elemental analysis calcd for $C_{22}H_{36}CuN_4O_{12}$,C, 43.13; H, 5.88; N, 9.15%. Found C, 43.21; H, 5.75; N, 8.26%. Vis. (solid state) λ_{max}: 678.0nm. ESR (solid state): g = 2.069.

2.3.6: $\{(Hpy)_2\ [Cu(23pdc)_2]\cdot 5H_2O\}_n$ **(2.1.5):** Isolated yield: ~65%. IR (KBr, cm^{-1}): 3412 (m), 3110 (w), 3080 (w), 3000 (w), 2007 (w), 1701 (s), 1617 (s), 1592 (s), 1499 (m), 1449 (w), 1373 (s), 1336 (w), 1281 (w), 1222(m), 1152 (w), 1117 (m), 1065 (w), 812 (s), 679 (m) Vis. (solid state) λ_{max}: 505.0nm. ESR (solid state): g = 2.069.

2.3.7: $\{(H8hqn)_2\ [Cu(23pdc)_2]\cdot 6H_2O\}_n$ **(2.1.6):** Isolated yield: ~61%. IR (KBr, cm^{-1}): 3369 (bs), 3218 (s), 2683 (w), 1633 (m), 1586 (s), 1473 (m), 1434 (m), 1393 (w), 1365 (s), 1311 (w), 1271 (w), 1233 (w), 1111(m), 877 (w), 843 (w). Elemental analysis calcd for$C_{32}H_{34}CuN_4O_{16}$, C, 48.40, H, 4.32 N, 7.05%.Found C, 48.37, H, 4.31 N, 7.10Vis. (solid state) λ_{max}: 615.0nm. ESR (solid state): g = 2.070.

2.3.8: $\{(Him)_2\ [Cu(23pdc)_2]\cdot 4H_2O\}_n$ **(2.1.7):** Isolated yield: ~70%. IR (KBr, cm^{-1}): 3414 (s), 3075 (w), 2940 (w), 1740 (s), 1686 (s), 1637 (w), 1587 (m), 1382 (m), 1352 (m), 1272 (m), 1237 (w0, 1116 (s), 1088(m), 865 (w), 838 (m), 819 (m), 701 (m), 648 (w), 607 (w), 577 (w), 473 (w). Elemental analysis calcd for $C_{32}H_{34}CuN_8O_{18}$, C, 43.53; H, 3.85; N, 12.70%.Found C, 43.51; H, 3.79; N, 12.68%. Vis. (solid state) λ_{max}: 519.0nm. ESR (solid state): g = 2.072.

2.3.9: $\{(H_2dabco)\ [Cu(23pdc)_2]\cdot 4H_2O\}_n$ **(2.1.8):** Isolated yield: ~64%. IR (KBr, cm^{-1}): 3438 (bs), 1637 (bs), 1586 (s), 1479 (w), 1438 (w), 1394 (m), 1354 (s), 1267 (m), 1148 (w), 1115 (s), 1057 (w), 978 (w), 878 (m), 843 (m), 789 (w).Elemental analysis calcd for$C_{26}H_{24}CuN_4O_{12}$ C, 48.19; H, 3.73; N, 8.65% Found C, 48.18, H, 3.70, N, 8.64 Vis. (solid state) λ_{max}: 622.0nm. ESR (solid state): g = 2.061.

2.3.10: $\{(H_3taea)\ [Cu_{1.5}(23pdc)_3]\cdot 5H_2O\}_n$ **(2.1.9):** Isolated yield: ~60%. IR (KBr, cm^{-1}): 3421 (bs), 3098 (w), 2171 (w), 1621 (w), 1590 (s), 1433 (w), 1371 (s), 1274 (m), 1231 (w), 1146 (w), 1115 (m), 1037 (w), 879 (w), 841 (m).Elemental analysis calcd.for$C_{54}H_{60}Cu_3N_{14}O_{34}$, C, 38.58; H, 3.57; N, 11.67%. Found C, 39.01; H, 3.60; N, 11.92%.Vis. (solid state) λ_{max}: 684.0nm.

2.3.11: $(H5aqn)_2$ $[Cu_2(23pdc)_4]\cdot 8H_2O$ **(2.1.10):** Isolated yield: ~73%. IR (KBr, cm^{-1}): 3434 (w), 3357 (w), 3220 (w), 3057 (w), 2637 (w), 1682 (m), 1587 (bs), 1456 (w), 1434 (w), 1382 (m), 1335 (s), 1271 (m), 1232 (w), 1147 (w), 1113 (s), 879 (m), 845 (s), 785 (w), 730 (w), 706 (w), 557(m), 475 (s). Vis. (solid state) λ_{max}: 734.0nm. ESR (solid state): g = 2.066.

2.3.12: $(H_2dap)_2$ $[Cu_2(23pdc)_4]\cdot 3H_2O$ **(2.1.11)**: Isolated yield: ~72%. IR (KBr, cm^{-1}): 3462 (bs), 3060 (w), 2054 (w), 1587 (s), 1434 (w), 1399 (m), 1341 (s), 1275 (m), 1235 (w), 1114 (s), 879 (m), 844 (s), 789 (w), 732 (w), 708 (w), 691 (w), 471 (m). Vis. (solid state) λ_{max}: 710.0nm. ESR (solid state): g = 2.070.

2.3.13: $(H_24aba)_2$ $[Cu_2(23pdc)_4]\cdot 4H_2O$ **(2.1.12):** Isolated yield: ~73%. IR (KBr, cm^{-1}): 3434 (w), 3357 (w), 3220 (w), 3057 (w), 2637 (w), 1682 (m), 1587 (bs), 1456 (w), 1434 (w), 1382 (m), 1335 (s), 1271 (m), 1232 (w), 1147 (w), 1113 (s), 879 (m), 845 (s), 785 (w), 730 (w), 706 (w), 557(m), 475 (s). Vis. (solid state) λ_{max}: 734.0nm.

2.3.14: (Hdapt)$[Cu(23\text{-}Hpdc)(23pdc)(H_2O)]\cdot H_2O$ **(2.1.13):** Isolated yield: ~68%. IR (KBr, cm^{-1}): 3472 (bs), 3379 (bs), 2932 (w), 1628 (s), 1584 (s), 1433 (w), 1387 (w), 1366 (s), 1269 (m), 1152 (w), 1115 (m), 1022 (m), 879 (w), 832 (w), 698 (m), 605 (m). UV-Vis (solid state): λ_{max} = 636nm. ESR (solid state): g = 2.051. TGA: 50°C-200°C (–$5H_2O$ and - dapt; exptl. wt. loss 32.5%, calcd.30.0%), 225°C-380°C (formation of CuO; exptl. wt. loss 89.1%, calcd. 88.0%).

2.3.15: $(H_2aba)[Cu(23pdc)_2(Haba)]_2\cdot 9H_2O$ **(2.1.14):** Isolated yield: ~29%. IR (KBr, cm^{-1}): 3452 (br), 3329 (w), 3253 (w), 1644 (s), 1586 (s), 1473 (w), 1386 (s), 1349 (s), 1275 (m), 1234 (w), 1150 (w), 1112 (s), 915 (w), 877 (m), 840 (m), 787 (w), 7287 (w), 695 (s). UV-Vis (solid state): λ_{max}= 636nm. ESR (solid state): g = 2.075. TGA: 40°C-200°C (-$9H_2O$; exptl. wt. loss 10.9%, calcd. 12.4%), 220°C-380°C (formation of CuO; exptl. wt. loss 89.1%, calcd. 88.0%). ESR (solid state): g = 2.085.

2.3.16: $(H_2ade)_2$ $[Cu(23pdc)_2]\cdot 2H_2O$ **(2.1.15):** Isolated yield: ~67%. IR (KBr, cm^{-1}): 3304 (s), 3043 (w), 2917 (w), 1697 (m), 1664 (s), 1589 (m), 1400 (m), 1339 (s), 1279 (w), 1116 (m), 873 (w), 837 (w), 781 (w), 695 (w). Elemental analysis calcd for $C_{24}H_{22}CuN_{12}O_{10}$, C, 41.02; H, 2.01; N, 23.93%. Found C, 40.97, H, 1.99, N, 23.75%. Vis. (solid state) λ_{max}: 472.0nm. ESR (solid state): g = 2.055.

2.3.17: $[H_2dabco][Cu(25pdc)_2(H_2O)]\cdot 5H_2O$ **(2.2.1):** Isolated yield: ~64%. IR (KBr, cm^{-1}): 3440 (bs), 1639 (s), 1587 (s), 1468 (w), 1360 (s), 1268 (m), 1050 (w), 987 (w), 880 (m), 833 (m), 739 (w). Elemental anal.calcd for $C_{50}H_{74}Cu_3N_{12}O_{36}$; C, 37.27; N, 10.43; H, 4.59%, found; C, 37.37; N, 10.42; H, 4.57%. UV-visible spectroscopy (solid): 622.0nm. ESR (solid state): g = 2.061.

2.3.18: $[H_2dap]_2[Cu(25pdc)_2(H_2O)]\cdot H_2O$ **(2.2.2):** Isolated yield: ~69%. IR (KBr, cm^{-1}): 3397 (bs), 3208 (w), 3104 (w), 1665 (w), 1608 (s), 1390 (m), 1349 (s), 1278 (m), 1043 (m), 837 (m), 761 (m). Elemental anal.calcd for $C_{19}H_{26}CuN_4O_{10}$; C, 42.69; N, 10.48; H, 4.85%, found; C, 42.66; N, 10.45; H, 4.84%. UV-visible spectroscopy (solid): 623.0nm.

2.3.19: $[H_2tmen][Cu(25pdc)_2(H_2O)]\cdot 4H_2O$ **(2.2.3):** Isolated yield: ~70%. IR (KBr, cm^{-1}): 3371 (bs), 1615 (s), 1390 (s), 1350 (s), 1279 (m), 1038 (m), 835 (m), 763(m). Elemental anal. calcd for $C_{20}H_{34}Cu\ N_4O_{13}$; C, 39.86; N, 9.30; H, 5.64%, found; C, 39.86; N, 9.29; H, 5.61%. UV-visible spectroscopy (solid) lmax: 626.0nm.

2.3.20: $[H4aba]_2[Cu(25pdc)_2]\cdot 8H_2O$ **(2.2.4):** Isolated yield: ~60%. IR (KBr, cm^{-1}): 3371 (bs), 3049 (w), 2925 (w), 1711 (m), 1614 (s), 1396 (s), 1351 (m), 1292 (w), 1132 (m), 1046 (m), 756 (m). Elemental anal.calcd for $C_{28}H_{44}CuN_6O_{16}$; C, 42.84; N, 10.18; H, 5.61%, found; C, 42.80; N, 10.16; H, 5.60%. UV-visible spectroscopy (solid): 428.0nm.

2.3.21: $\{(H_2en)[Cu(23pdc)_2]\cdot 6H_2O\}_n$ **(2.2.5):** Isolated yield: ~65%. IR (KBr, cm^{-1}): 3522 (bs),3150 (w), 1635 (m), 1610 (m), 1591 (m), 1460 (w), 1380 (s), 1264 (w), 1157 (w), 840 (w), 732 (w). Elementalanal.calcd for $C_{16}H_{28}CuN_4\ O_{14}$; C, 34.04; N, 9.92; H, 4.96%, found; C, 34.00; N, 9.88; H, 4.94%. UV-visible spectroscopy (solid): 425.0nm.

2.3.22: $\{[H5aqn]_2[Cu(25pdc)_2]\cdot 4H_2O\}_n$ **(2.2.6):** Isolated yield: ~73%. IR (KBr, cm1): 3422 (bs), 3212 (bs), 3048 (w), 1657 (m), 1638 (w), 1612 (s), 1591 (s), 1563 (m), 1346 (s), 1312 (w), 1278 (w), 1045 (m), 828 (m), 790 (m), 767 (m) 689 (w). Elemental anal.calcd for $C_{32}H_{24}CuN_6O_{12}$; C, 51.32; N, 10.22; H, 3.20%, found; C, 51.30; N, 10.21; H, 3.18%. UV-visible spectroscopy (solid): 418.0nm.

2.3.23: $[H_2dao]_3[Cu_3(25pdc)_6]\cdot 6H_2O$ **(2.2.7):** Isolated yield 72%. IR (KBr, cm^{-1}): 3435 (bs),2933 (m), 2855 (w), 1614 (s), 1563 (w), 1388 (m), 1351 (s), 1276 (m), 1032 (m), 835 (m), 769 (m). Elemental anal.calcd for $C_{66}H_{84}Cu_3\ N_{12}O_{40}$; C, 42.21; N, 8.95; H, 4.47%, found; C, 42.20; N, 8.93; H, 4.50%. UV-visible spectroscopy (solid): 629.0nm.

2.3.24: $\{(H_3deta)\ [Cu_{1.5}(25pdc)_3]\cdot 6H_2O\}_n$ **(2.2.8):** Isolated yield: ~55%. IR (KBr, cm^{-1}): 3466 (bs), 3334 (w), 3069 (w), 1628 (w), 1560 (w), 1386 (m), 1347 (s), 1277(s), 1114 (m), 1038 (m), 831 (m), 759(m). Elemental anal.calcd for $C_{50}H_{74}Cu_3\ N_{12}O_{36}$; C, 37.29; N, 10.44; H, 4.59%, found; C, 37.26; N, 10.41; H, 4.58%. UV-visible spectroscopy (solid): 636.0nm.

References:

1 T. Yuge, M. Miyata, N. Tohnai, *Cryst. Growth Des*., 2006, **6**, 1271-1273.

2 H. Yin, S. X. Li, *J. Mole. Struc*., 2009, **918**, 165-173.

3 C. Li, *Catal. Rev.*, 2004, **46**, 419-492; (b) C. Li, H. Zhang, D. Jiang, Q. Yang, *Chem. Commun*., 2007, 547-558; (c) C. Balezao, H. Garcia, *Chem. Rev*., 2006, **106**, 3987-4043; (d) S. Bhattacharjee, J. A. Anderson, *Chem. Commun*., 2004, 554-555; (d) S. Bhattacharjee, T. J. Dines, J. A. Anderson, *J. Phys. Chem. C*, 2008, **112**, 14124-14130.

4 (a) T. E. Mallouk, J.A. Gavin, *Acc. Chem. Res*., 1998, **31,** 209-217; (b) T. Okada, Y. Ide, M. Ogawa, *Chem. Asian J*., 2012, **7**, 1980-1982.

5 (a) R. W. Grimshaw, *The Chemistry and Physics of Clays*, 4th ed.; Wiley: New York, 1971; (b) L. R. Nassimbeni, *Acc. Chem. Res*., 2003, **36**, 631-637; (c) S. R. Batten, K. S. Murray, *Coord. Chem. Rev*., 2003, **246**, 103-130; (d) K. Inoue, H. Imai, P. S. Ghalsasi, K. Kikuchi, M. Ohba, H. Okawa, J. V. Yakhmi, *Angew. Chem., Int. Ed. Engl.* 2001, **40**, 4242-4245.

6 R. Lyszczek, L. Mazur, *Polyhedron*, 2012, **41**, 7-19.

7 Y. Z. Tang, X. F. Huang, Y. M. Song, P. W. H. Chan, R. G. Xiong, *Inorg. Chem*., 2006, **45**, 4868-4870.

8 J. W. Zhang, X. M. Kan, X. L. Li, Y. Liu, B. Q. Liu. *Eur. J. Inorg. Chem*., 2016, 1060-1067

9 Y. Hamada, H. Ohta, N. Miyamoto, R. Yamaguchi, A. Yamani, K. Hidaka, T. Kimura, K. Saito, Y. Hayashi, S. Ishiura, Y. Kiso, Bioorg. *Med. Chem. Lett*., 2008, **18**, 1649-1654.

10 B. Ay, E. Yildiz, B. Kani, *J. Solid State Chem*., 2016, **233**, 44-51.

11 E. Cariati, R. Macchi, D. Roberto, R. Ugo, S.Galli, N. Casati, P. Macchi, A. Sironi, L. Bogani, A. Caneschi, D. Gatteschi. *J. Am. Chem. Soc*., 2007, **129**, 9410-9420.

12 M. Mitra, P. Manna, A. Das, S. K. Seth, M. Helliwell, A. Bauza, S. R. Choudhury, A. Frontera, S. Mukhopadhyay, *J. Phys. Chem. A*, 2013, **117**, 5802-5811.

13 T. D. Keene, I. Zimmermann, A. Neels, O. Sereda, J. Hauser, S. X. Liu, S. Decurtins, *Cryst. Growth Des*., 2010, **10**, 1854-1861.

14 P. King, R. Clerac, C. E. Anson,A. K. Powell, *Dalton Trans*., 2004, 852-86.

15 Z. H. Yan, W. Wang,L. Zhang, X. Zhang, L. Wang, R. Wang, D. Sun, *RSC Adv.*, 2015, **5**, 16190-16198.

16 (a) A. M. Beatty, C. M. Schneider, A. E. Simpson, J. L. Zaher, *CrystEngComm*., 2002, **4**, 282-287; (b) T. Yuge, M. Miyata, N. Tohnai, *Cryst. Growth Des*., 2006, **6**, 1271-1273.

17 A. M. Beatty, K. E. Granger, A. E. Simpson, *Chem. Eur. J*., 2002, **8**, 3254-3259.

18 (a) F. Sun, G. Zhu, *Inorg. Chem. Commun*., 2013, **38**, 115-118; (b) Y. T. Liu, Y. Q. Du, X. Wu, Z. P. Zheng, X. M. Lin, L. C. Zhu, Y. P. Cai, *CrystEngComm*., 2014, **16**, 6797-6802; (c) X. M. Lin, J. L. Niu, J. Lin, L. Hu, G. Zhang, Y. P. Cai, *Inorg. Chem.Commun*., 2016, **72**, 69-72.

19 (a) T. D. Keene, I. Zimmermann, A. Neels, O. Sereda, J. Hauser, S. X. Liu, S. Decurtins, *Cryst. Growth Des*., 2010, **10**, 1854-1859; (b) G.B. Deacon, R. J. Phillips, *Coord. Chem. Rev.,* 1980, **33**, 227-250.

20 D. R. Turner, S. R. Batten, *ActaCryst.*, 2007, **E63**, m452-m454.

21 (a) B. O. Patrick, C. L. Stevens, A. Storr , R. C. Thompson, *Polyhedron*, 2003, **22**, 3025-3035; (b) G. H. Wang, Z. G Li, H. Q Jia,N. H. Hu, J. W.Xu, *CrystEngComm*., 2009, **11**, 292-297; (c) P. Sengupta, S. Ghosh, T. C. W. Mark, *Polyhedron*, 2001, **20**, 855-975.

22 (a) Z. Biela, V.Siroklin, *Chem. Papers*,1988, **42**, 291-298; (b) B. R. Srinivasan, N. C Nather, A. R.W. Bensch, *ActaCryst*., 2008, **E64**, m66.

23 T. Suga, N. Okabe, *ActaCryst*., 1996, **52**, 1410-1412.

24 P. Ayyappan, M. Asnani, A. Ramanan, Y. Piffard. *Proc. Indian Acad. Sci. (Chem. Sci.)*., 2003, **115**, 33-40.

25 A. M. Beatty, K. E. Granger, A. E. Simpson, *Chem. Eur. J.* 2002, **8**, 3254-3259.

26 A. M Beatty, B. A. Helfrich, G. A. Hogan, B. A. Reed, *Cryst. Growth Des.*2006, **6**, 122-126.

27 L. E. Cheruzel, M. S. Pometun, M. R. Cecil, M. S. Mashuta, R. J. Wittebort, R. M. Buchanan, *Angew. Chem., Int. Ed.*, 2003, **42**, 5452-5455.

28 T. K. Dobravc, A. Meden, F. Perdih, *New J. Chem*., 2015, **39**, 4265-4277.

29 (a) J. C. MacDonald, P. C. Dorrestein, M. M. Pilley, M. M. Foote, J. L. Lundburg, R. W. Henning, A. J. Schutlz, J. L. Manson, *J. Am. Chem. Soc*., 2000, **122**, 11692-11702; (b) J. C. MacDonald, T. J. M. Luo, G. T. R. Palmore, *Cryst. Growth Des*., 2004, **4**, 1203-1209.

30 C. Bazzicalupi, A. Bencini, A. Bianchi, A. Danesi, C. Giorgi, B. Valtancoli, *Inorg. Chem.*, 2009, **48**, 2391-2398.

31 (a) A. Bencini, I. Bertini, D. Gatteschi, A. Scozzafava, *Inorg. Chem*., 1978, **17**, 3194-3197; (b) B. J. Hathaway, D. E. Billing ,*Coord. Chem. Rev*., 1970, **5**, 143-207.

32 B. Das, J. B. Baruah, *Inorg. Chim.Acta*, 2010, **363**, 1479-1487.

33 T. D. Keene, I. Zimmermann, A. Neels, O. Sereda, J. Hauser, S. X. Liu, S. Decurtins, *Cryst. Growth Des*., 2010, **10**, 185418-59.

34 C. Marian, D. Nolting, R. Weinkauf, *Phys. Chem.Chem.Phys.*, 2005, **7**, 3306-3316.

35 Y. Ma, Y. Ni, F. Guo, N. Xiang, *Cryst. Growth Des*., 2015, **15**, 2243-2252.

36 S. Sen, N. N. Nair, T. Yamada, H. Kitagawa, P. K. Bharadwaj, *J. Am. Chem. Soc.*, 2012, **134**, 19432-19437.

37 H. Q. Pham, T. Mai, N. N. P. Tran, *J. Phys. Chem. C*, 2014, **118**, 4567-4577.

38. A. Karmakar, R. Illathvalappil , B. Anothumakkool, A. Sen, P. Samanta, A . V. Desai, S. Kurungot, S. K, Ghosh, *Angew. Chem. Int. Ed*., 2016, **55**, 10667-10671.

39 H. Aghabozorga, F. Manteghi, S. Sheshmani, *J. Iran. Chem. Soc*., 2008, **5**, 184-227.

40 J. M. Harrowfield, N. Lugan, G. H. Shahverdizadeh, A. A. Soudi, P. Thuery, *Eur. J. Inorg. Chem*., 2006, 389-396.

41 X. Wang, Q. G. Zhai, S. N. Li, Y. C. Jiang, M. C. Hu, *Cryst. Growth Des*., 2014, **14**, 177-188.

42 A. H. Pakiari, K. Eskandari, *J. Mol. Stuct. THEOCHEM*, 2006, **759**, 51-60.

43 A. T. Colak, F. Colak, O. Z. Yesilel, D. Akduman, F. Yilmaz, M. Tumer, *Inorg. Chim. Acta*, 2010, **363**, 2149-2162.

44 A. T. Colak, O. Z. Yesilel, G. Pamuk, H. Gunay, O. Buyukgungor, *Polyhedron*, 2011, **30**, 1012-1022

45 R. Li, S. H. Wang, Z. F. Liu, X. X. Chen, Y. Xiao, F. K. Zheng, G. C. Guo, *Cryst. Growth Des*., 2016, **16**, 3969-3975.

46 G. Arena, R. P. Bonomo, A. Contino, C. Sgarlata, G. Spotoa, G. Tabbib, *Dalton Trans*., 2004, 3205-3211.

47 B. Das, D. C. Crans, J. B. Baruah, *Inorg. Chim. Acta*, 2013, **408**, 204-208.

Chapter 3

Bottom up synthesis and intercalation of nucleobases in self-assemblies of copper(II) 2,3-pyridinedicarboxylates

3.1 Background

Main challenge in coordination polymer is to develop methodology to control the architectures.[1] This is also true in the case of self-assembling of metal-complexes.[2] Bottom up construction of polymers or supramolecular assemblies is based on systematic building of repeat units in desired way.[3] For such a purpose suitable monomer identification provides the key sucess.[4] Identification of small molecular assemblies or building blocks also can be used as an artificial receptors for molecular recognition of various biologically related molecules such as amino acids[5] and nucleobases.[6] On the other hand, utility of coordination polymers lies on the fact that they will be useful if they can be degradable easily to products that are less hazardous. From this point of view the choice of ligands and the counter-ions in coordination polymers makes a difference. There are many examples where the coordination polymers are based on naturally occurring ligands and the coordination polymers carbohydrates,[7] amino acids,[8] nucleic acids which finds important place as environmentally benign polymers. In this chapter these two aspects are addressed with pyridinedicarboxylic acid based coordination polymers as pyridinedicarboxylic acid has analogy to amino acids, they are also easily degradable, and most importantly they form cationic complexes having organo-cations to provide wide scopes to introduce biologically benign organo-cations to such coordination polymers.

This chapter is divided in two parts, in the first part a bottom up synthetic approach using an anionic copper(II) 2,3pyridinedicarboxylates complex as a smaller building block for generation of heteromettalic coordination polymers or higher nuclearity of complexes is described. In the second part, utility of a cytidinium cation containing coordination polymer in exchange of cations is described.

Part A

Bottom up synthesis of homo-and heterometallic 2,3-pyridinedicarboxylate coordination complexes

3.1.1 Dinuclear Copper(II) complex from mononuclear complex

In last chapter the versatile reactions of 2,3-pyridinedicarboxylic acid with copper(II) acetate formed the basis to identify a suitable cation that would form an isolable mononuclear complex. Accordingly the complex **2.1.13** is chosen as a building block for construction of homo and heterometallic coordination compounds. Complex **2.1.13** has a cation derived from 2,4-Diamino-6-phenyl-1,3,5-triazine which has hydrogen bond donor sites in the ring and the amines of the periphery of heterocyclic rings act as hydrogen bond acceptors. Moreover any of these hydrogen bonding sites upon protonation would act in a reverse way as that of neutral counter-part. On the other hand the anion part having chelate ligand and free carboxylic acid provides the monomeric building block where the free carboxylic acid group and the coordination ability of the carbonyl oxygen would provide basis to form higher nuclear complexes under appropriate conditions.

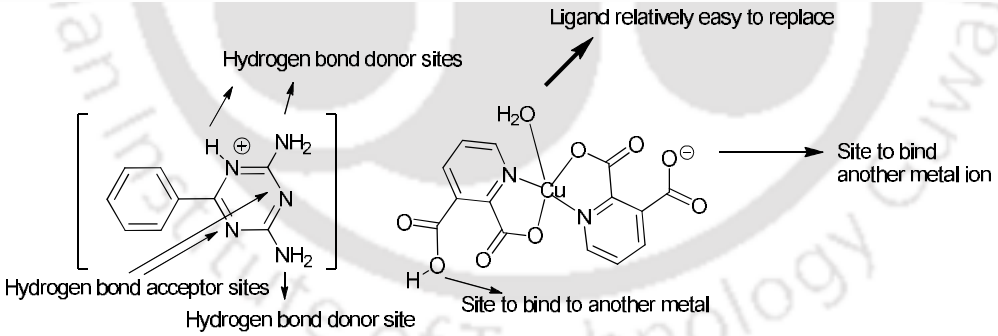

Figure 3.1.1: Binding sites in complex **2.1.13** making it suitable for bottom-up synthesis.

Complex **2.1.13** was obtained from reaction of a methanol solution of copper(II) acetate with under ambient condition and it has coordinated water molecule attached to copper site.

This complex was treated with pyridine with two objectives to replace the 2,4-Diamino-6-phenyl-1,3,5-triazine mono-cation by pyridine molecule as well as to replace the coordinated water molecule. Thus, the complex **2.1.13** was dissolved in methanol and reacted with pyridine. This reaction resulted in dehydration of the complex and yielded a dinuclearcopper(II) complex $(Hdapt)_2[Cu_2(H23pdc)_2(23pdc)_2]\cdot 5H_2O$ **(3.1.1)**. While neutral 4-Diamino-6-phenyl-1,3,5-triazine was also obtained from the reaction as side product. Thus the reaction occurs due to abstraction of proton from 4-Diamino-6-phenyl-1,3,5-triazine mono-cation and subsequent formation of the dinuclear complex by replacement of water molecules (Equation 3.1.1). It was found that the dinuclear complex **3.1.1** was formed when pH was adjusted to 8 which was also the pH of the medium to form the complex by adding pyridine as external source of base. Thus, pyridine acted as base to facilitate the dehydration reaction. Changing pH causes protonation of one of the pyridinedicarboxylate and thereby it results in the formation of a dinuclear complex which has two copper ions bound to two pyridinedicarboxylate which act as chelate and bridge whereas two mono anionic pyridinedicarboxylate acting as chelates and leaving one carboxylic acid free. This pair of mono anionic pyridinedicarboxylate is attached to two copper ions independently.

$2(Hdapt)[Cu(23pdc)(H23pdc)] + 2Py \rightarrow (Hdapt)_2[Cu_2(H23pdc)_2(23pdc)_2] + 2[(PyH)^+(OH)]$

Where Py = pyridine, dapt = from 4-Diamino-6-phenyl-1,3,5-triazine, 2,3-pdc = 2,3-pyridinedicarboxylate.

Equation 3.1.1: Dehydration of $(Hdapt)_2[Cu_2(H23pdc)_2(23pdc)_2]$

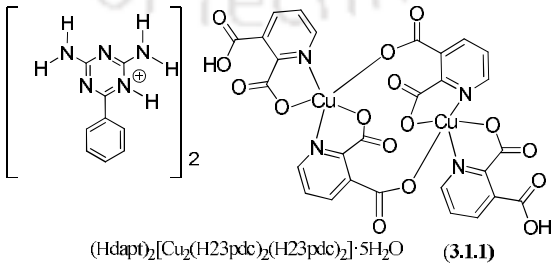

$(Hdapt)_2[Cu_2(H23pdc)_2(H23pdc)_2]\cdot 5H_2O$ **(3.1.1)**

Figure 3.1.2: Dinuclear copper(II) complex **3.1.1**

These two complexes namely complex **2.1.13** and complex **3.1.1** can be distinguished from their respective, powder XRD, IR and thermal decompositions. The complex **2.1.13** loses water molecules of crystallization and coordinated water molecules at 50-200°C whereas the complex **3.1.1** loses at 60-125°C. This obvious difference is due to the presence of tightly bound coordinated water molecule in the case of former case. Since the anionic part of both complexes have similar ligands the weight loss during decomposition of such ligands above 225°C are similar and both leads to formation of copper oxide after decomposing. In the former case the weight loss continued till 380°C to form copper oxide but in later case it is up to 365°C. Both the complexes show N-H and O-H IR stretching in the region of 3500-3200cm^{-1}. In complex **2.1.13** there are sharp absorptions at 3472cm^{-1}and at 3379cm^{-1} due to N-H and O-H but such peaks are 3320cm^{-1} and 3191cm^{-1} for complex **3.1.1**. The carbonyl peaks appear in case of complex **2.1.13** is at 1628cm^{-1}, 1584cm^{-1}, whereas for complex **3.1.1** they are at 1636cm^{-1}, 1542cm^{-1}. Thus, IR-spectra also make distinctions between the two complexes. Solid samples of the both complexes have very similar diffused UV-spectra complex **2.1.13** having absorption at 636 nm, whereas the complex **3.1.1** at 626 nm due d-d (^{2}E→ ^{2}T) transition of copper(II) ions with d^9 electronic configuration. Besides these the powder XRD patterns of the two complexes are clearly distinguishable and indexed powder spectra are shown in Figure 3.1.3.

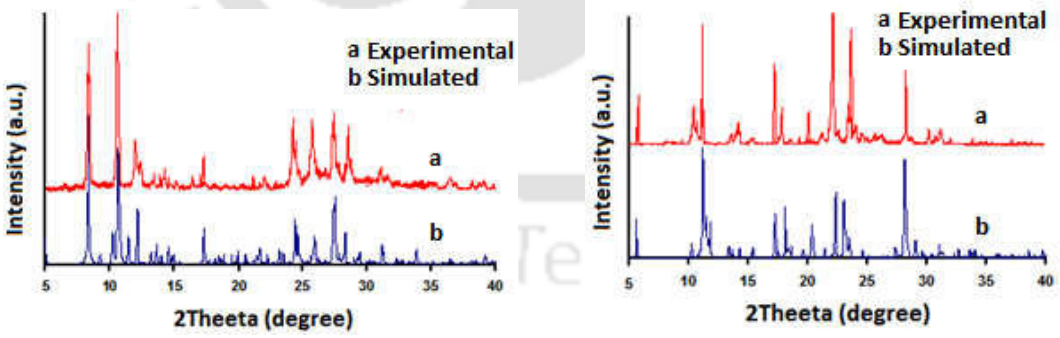

(a) (b)

Figure 3.1.3: Powder X-ray diffraction pattern for complex **3.1.1** and complex **2.1.13**.

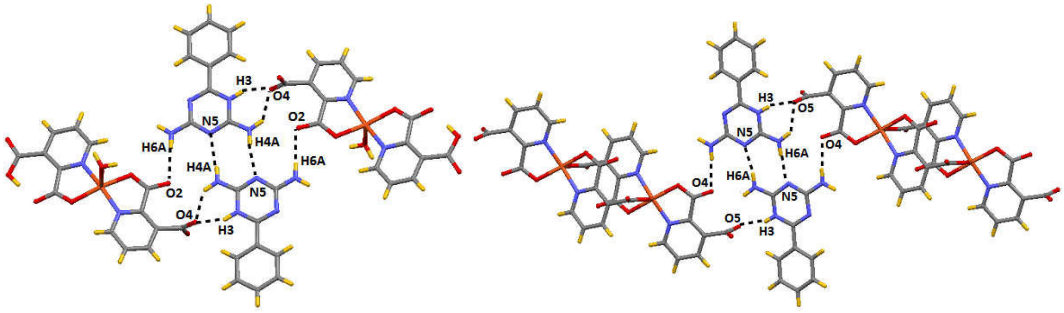

(a) (b)

Figure 3.1.4: Hydrogen bonded assemblies of complexes (a) **2.1.13** and (b) **3.1.1**.

The hydrogen bonded assemblies of the two complexes are illustrated in Figure 3.1.4 and the parameters for major hydrogen bonds are listed in Table 3.1.1.

Table 3.1.1: The major hydrogen bond parameters in complex **2.1.13** and **3.1.1.**

	Bond (symmetry)	$d_{D\text{-}H(Å)}$	$d_{H\cdots A(Å)}$	$d_{D\cdots A(Å)}$	<DH···A(°)
2.1.13	N(3)-H(3)···O(4) [x,1+y,z]	0.86	1.78	2.584(4)	155
	N(4)-H(4A)···N(5) [-x,2-y,1-z]	0.86	2.11	2.955(4)	169
	N(6)-H(6A)···O(2) [-x,1-y,1-z]	0.86	2.15	2.996(3)	167
	N(6)-H(6B)···O(10) [-x,1-y,1-z]	0.86	2.12	2.966(4)	167
	O(9)-H(9A)···O(8) [x,-1+y,z]	0.85	2.05	2.902(4)	174
	O(9)-H(9B)···O(10) [1-x,1-y,1-z]	0.85	2.12	2.963(4)	171
3.1.1	N(3)-H(3)···O(5) [1-x,1-y,-z]	0.73	1.99	2.702(4)	163
	N(6)-H(6A)···N(5) [-x,2-y,-z]	0.86	2.05	2.904(5)	169
	N(7)-H(7A)···O(4) [-1+x,1+y,z]	0.86	2.12	2.970(4)	171
	N(10)-H(10A)···O(7) [-1+x,y,z]	0.92	1.88	2.791(4)	169
	N(7)-H(7B)···O(10) [-x,-y,1-z]	0.86	2.25	3.086(5)	162
	N(12)-H(12B)···O(9) [-1+x,y,z]	0.86	2.02	2.859(6)	166

From the table it is found that N-H···O and O-H···O hydrogen bonds are nearly linear and have donor-acceptor bond distances are 2.584(4)Å and 2.902(4)Å. These show that these hydrogen-bonds are very strong and thus these self-assemblies are guided by electro-statistically controlled hydrogen bonds. Complex **3.1.1** consists of two mono-protonated ammonium cations per dinuclear unit. Dinuclear core of the complex being identical with the other dinuclear complexes of copper(II) 2,3-pyrdinedicarboxylates described in earlier chapter this is not discussed further. It was pointed out that strong ionic hydrogen bonds between protonated amine and carboxylate group in mononuclear penta-coordinate copper(II) complex **2.1.13** and propensity to form mononuclear complex arises from complementing hydrogen bonds with in its self-assembly.

Hence, to form a dinuclear complex having same sets of ligands and cations, the cation must have ability to form complementing hydrogen bonds to stabilise a dinuclear anionic species, as observed in the copper mononuclear complex. Since, mononuclear complex **2.1.13** with same sets of ligands transformed to a dinuclear complex with the help of pyridine, this complex was identified as building block for bottom up synthesis of heterometallic systems.

3.1.2 Heterometallic coordination polymers

As a follow up reactions the complex **2.1.13** was treated with zinc(II) acetate or gadolinium(III) acetate in presence of pyridine. These reactions independently resulted in formation of corresponding heterometallic coordination polymers namely $[\{Zn(H_2O)_4Cu(23pdc)_2\}\cdot 3H_2O)]_n$ **(3.1.2)** or $[\{Gd(H_2O)_5Cu(pdc)_{2.5}\}\cdot 5H_2O]_n$ **(3.1.3)** coordination polymers in good yield. The reactions are shown in Scheme 3.1.1.

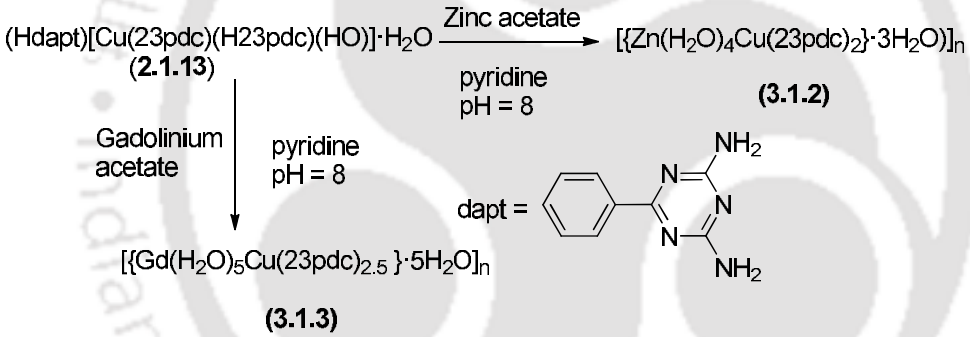

Scheme 3.1.1: Synthesis of heterometallic coordination polymers **3.1.2** and **3.1.3** from mononuclear building block **2.1.13**.

Coordination polymer $[\{Zn(H_2O)_4Cu(23pdc)_2\}\cdot 3H_2O)]_n$ (**3.1.2**) is comprises of chains formed by dinuclear copper 2,3-pyridinedicarboxylate units interlinked to each other through bridging carboxylate units.

Each copper ion chain has six-coordination environment as illustrated in Figure 3.1.5. $[Zn(H_2O)_4]^{2+}$ units interlink the one dimensional $[Cu_2(23pdc)_4]^{2-}$ chains, resulting in a two dimensional layer network (Figure3.1.5). In the network, each copper has hexa-coordinated geometry. Each copper ion has two chelating 2,3-pyridinedicarboxylates and each of these ligand also holds another set of copper ions by acting as oxygen donor ligand to occupy axial coordination positions.

Carboxylate group that do not chelate copper ion acts as bridging unit to zinc and copper ions of two-dimensional coordination polymer. Structural framework of complex **3.1.2** shown in Figure 3.1.5(b) may thus be considered as a building block to form the chain of the coordination polymer **3.1.2**. Such chains eventually are connected to tetra-aqua-zinc(II) cations forming two-dimensional structure. Process is a bottom up process starting with complex **2.1.13** forming dehydrated dinuclear complex (**3.1.1**) in situ, which self-assembles during cation exchange with tetra-aqua-zinc(II) cation forming coordination polymer **3.1.2**.

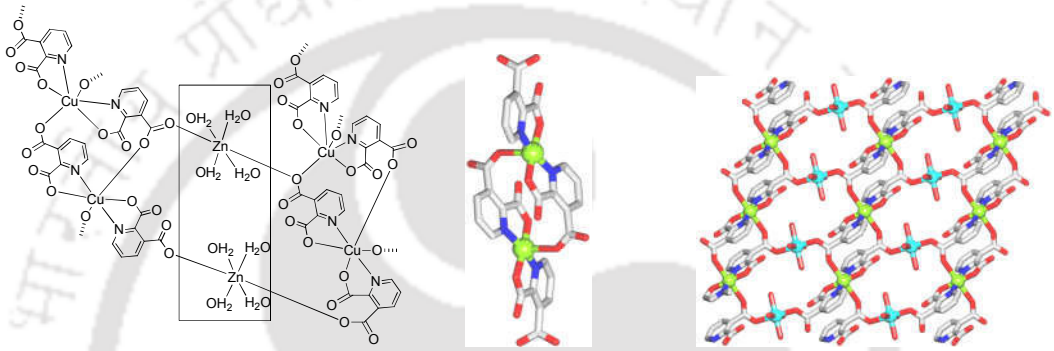

(a) (b) (c)

Figure 3.1.5: (a) Two-dimensional structure formed by connecting polymeric chain of dinuclear $[Cu_2(23pdc)_4]^{2-}$ anions bridged by $[Zn(H_2O)_4]^{2+}$ ions (bridging cationic part is shown within the square). Structural fragments **3.1.2** showing, (b) one $[Cu_2(23pdc)_4]^{4-}$ unit and (c) 2D metal-organic layer, H atoms and crystallization H_2O molecules are omitted for clarity, Color codes: Cu (green), Zn (cyan), O (red), N (blue), and C (gray).

When complex **2.1.13** was reacted with gadolinium acetate in presence of pyridine a copper-gadolinium mixed metal coordination polymer $[\{Gd(H_2O)_5Cu(23pdc)_{2.5}\}\cdot 5H_2O]_n$ (**3.1.3**) was formed (Figure 3.1.6a).

This coordination polymer is comprised of tricopper$[Cu_3(23pdc)_6]^{6-}$ secondary building blocks. These building blocks are interconnected to each other and also by six $[Gd(H_2O)_5]^{3+}$ units (Figure 3.1.6b), resulting in a very complex three-dimensional metal-organic framework structure (Figure 3.1.6c). All the copper atoms are six-coordinate and each adopt a distorted octahedral geometry.

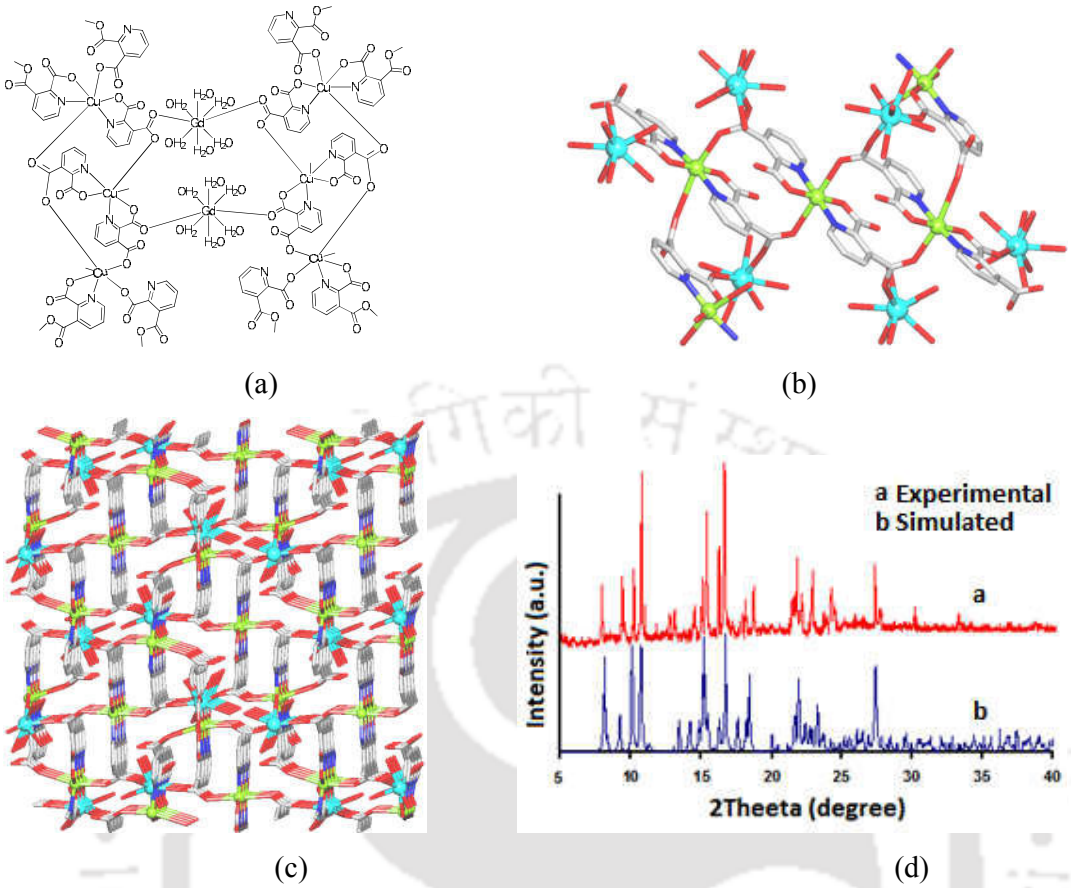

Figure 3.1.6: (a) Skeletal diagram for coordination polymer **3.1.3**. Structural fragments of **3.1.3** showing: (b) one tri-copper $[Cu_3(23pdc)_6]^{6-}$ secondary building unit interconnected by $[Gd(H_2O)_5]^{3+}$ blocks, (c) 3D metal-organic framework (view along the *a* axis). H atoms and crystallization H_2O molecules are omitted for clarity. Color codes: Cu (green), Gd (cyan), O (red), N (blue), and C (gray). (d) Powder XRD of bulk sample of coordination polymer **3.1.3**.

Whereas gadolonium ions are eight-coordinate and each exhibit a distorted square anti-prismatic geometry. This is clear that eight coordination of gadolinium ion makes three dimensional networks by providing three of the sites to oxygen of the bridging carboxylate linking copper and gadolinium ions. The coordination polymer being characterized by single crystal structure, it was also characterized by other spectroscopic tools. It shows characteristic N-H stretching at 3320cm^{-1}, and O-H stretching at 3191cm^{-1}, and carboxylate frequencies appear at 1636cm^{-1} and 1542cm^{-1}.

Since this is a synthetic approach for multi metallic system, the bulk purity is very essential. Hence the powder-XRD of the coordination polymer **3.1.3** was determined and indexed with the help of simulated spectra generated from crystallographic information file (Figure 3.1.6d) and it is found that each peak is assignable at located at super imposable position with respect to a simulated spectra. Hence the phase purity suggests that the isolated compound is in single phase with high purity. It may be noted that there are large numbers of multi-nuclear pyridinedicarboxylate complexes,[9] however, there has no study that attempts synthesizing by using characterized complexes that can systematically transform in stages to different building blocks. Apart from structural diversity of compounds **3.2.1-3.2.3**, a notable feature of the present bottom up approach consists of rather high yield of these derivatives.

3.1.3 ESR study on 2.1.13 and 3.1.1-3.1.3

In general the ESR spectra of copper(II) ions are dependent on the ligand environment.[10] Structural features of different geometries shows characteristic ESR signature representative of a particular geometry.[11] The environments around copper ions were investigated by recording respective ESR spectra [Figure 3.1.7(a-d)]. The spectra of the solid samples of the copper complexes at room temperature show characteristic intense signals and the g-values are listed in Table 3.1.2. As expected the coordination environment of copper in complex **2.1.1** and **3.1.1** are similar they show a strong absorption without resolved hyperfine structure, characteristic of square pyramidal geometry.[12] In crystal structures of these two complexes such geometries around copper ions were found in which four equatorial bond distances are 1.935Å-1.986Å and axial bond distances are 2.296Å-2.387Å.

On the other hand the complex **3.1.3** showed both $g_{\|}$ and $g_{\perp}$ showing strong Jahn-Teller distortion. This is infact true in the complex where four equatorial bond lying in xy plane are 1.937Å-1.986Å and the two Cu-O bond lengths along z-axis are 2.387Å. This clearly shows an elongation of bonds along z-axis showing Jahn-Teller effect. The g_{av} values were calculated by using $g_{av} = 1/3[g_{\|} + 2g_{\perp}]$ and the spin-orbit coupling (χ)[13] constants were determined by using $g_{av} = 2(1–2\chi/10Dq)$. The spin-orbit coupling constants are lower than those for a free copper(II) ion (-832cm^{-1})in compounds **2.1.13**, what also supports a covalent character of the copper-ligand bonds.

Table 3.1.2: The room temperature X-band ESR parameters for compounds **2.1.13** and **3.1.1-3.1.3**.

Compound	$g_{\parallel}$	$g_{\perp}$	g_{av}	10Dq	χ cm^{-1}
2.1.13	1.96	2.30	2.15	16025	-849.3
3.1.1	1.95	2.35	2.21	15723	-786.2
3.1.2	1.93	2.55	2.34	16000	-1440.0
3.1.3	2.01	2.51	2.40	15974	-1597.4
3.1.2[#]	1.99	2.18	2.12	–	–

#solution in water

On the other hand such values are higher in the case of **3.1.2** and **3.1.3**, suggesting more ionic character of the metal-ligand bonds. X-band ESR spectra of an aqueous solution of copper(II) coordination polymer **3.1.2** spectra with $g_{\parallel}$ = 1.99 and $g_{\perp}$ = 2.18 at room temperature (300 K). Since the parent compound was sensitive to pH in forming dinuclear complex the stability of the coordination polymer **3.1.2** was checked by recording ESR spectra at three different pH values namely at pH= 4, 7 and 9, by adding buffer solution to adjust the respective pH. The spectra are shown in Figure 3.1.7(d) revealed identical spectra in each case, thus showing that the coordination network of coordination polymer **3.1.2** is stable at different pH.

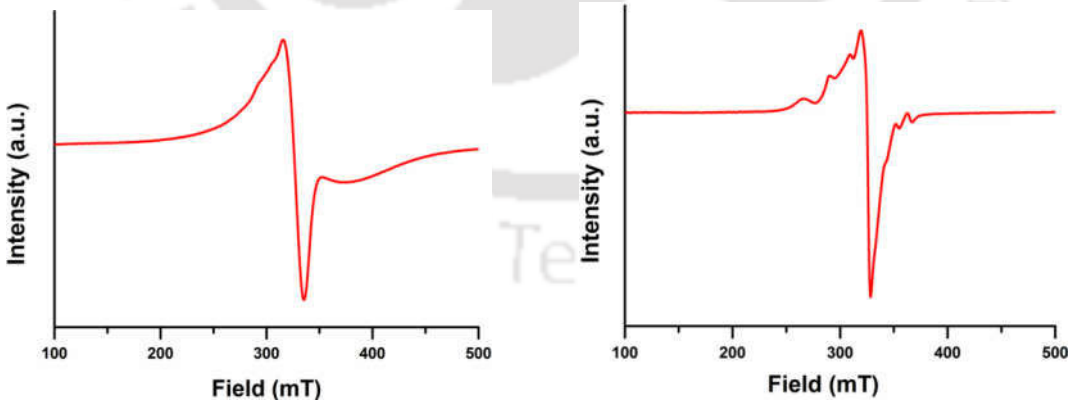

(a) (b)

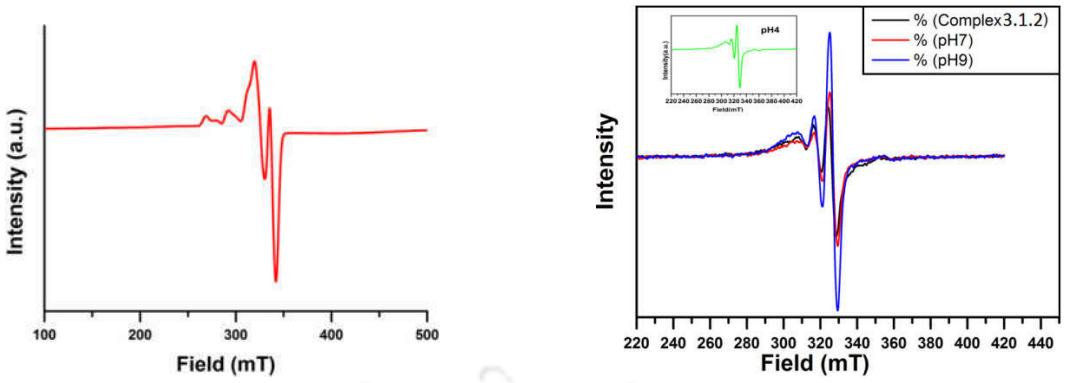

(c) (d)

Figure 3.1.7: ESR spectra of solid samples of (a) **3.1.1** (b) **3.1.2** (c) **3.1.3** and (d) ESR spectra of aqueous solution of complex **3.1.2** at three different pHs.

3.1.4 Thermogravimetry and preparation of metal oxides

Thermal decompositions of coordination polymers **3.2.2** and **3.2.3** are investigated. These are studied as utility of using these heterometallic coordination polymers for the synthesis of nano-dimensional mixed metal oxides. Mixed metal oxides are widely used in the field of catalysis.[14] Mixed metal oxides also finds applications in degradation of hazardous aromatic compounds.[15] Thermogravimetry of the compound shown in Figure 3.1.8a is for dinuclear complex **3.1.1**, which shows degradation to copper oxide at 400°C.

Both the cooordination polymers **3.1.2** and **3.1.3** have shown weight loss below 200ºC due to the loss of water molecules present in each case [Figure 3.18(b and c)], Both these coordination polymers decompose in the temperature range of 300ºC-400ºC to form mixed metal oxides. In each case the metal oxide formation took place less 350°C which is very interesting as they provide a simple route though which the metal oxide at relatively low tempearture could be prepared.

Encouraged by such results both the complexes were independently heated at 400ºC for an hour in a furnace by taking them in silica crucible and found that each yielded corresponding metal oxides. From powder-diifraction pattern it is found that complex **3.1.2** gave a mixture of cupric oxide and zinc oxide (Appendix Figure 3A1), whereas complex **3.1.3** gave a mixture of copper and gadolinium oxide without losing their integrity at this temperature range.

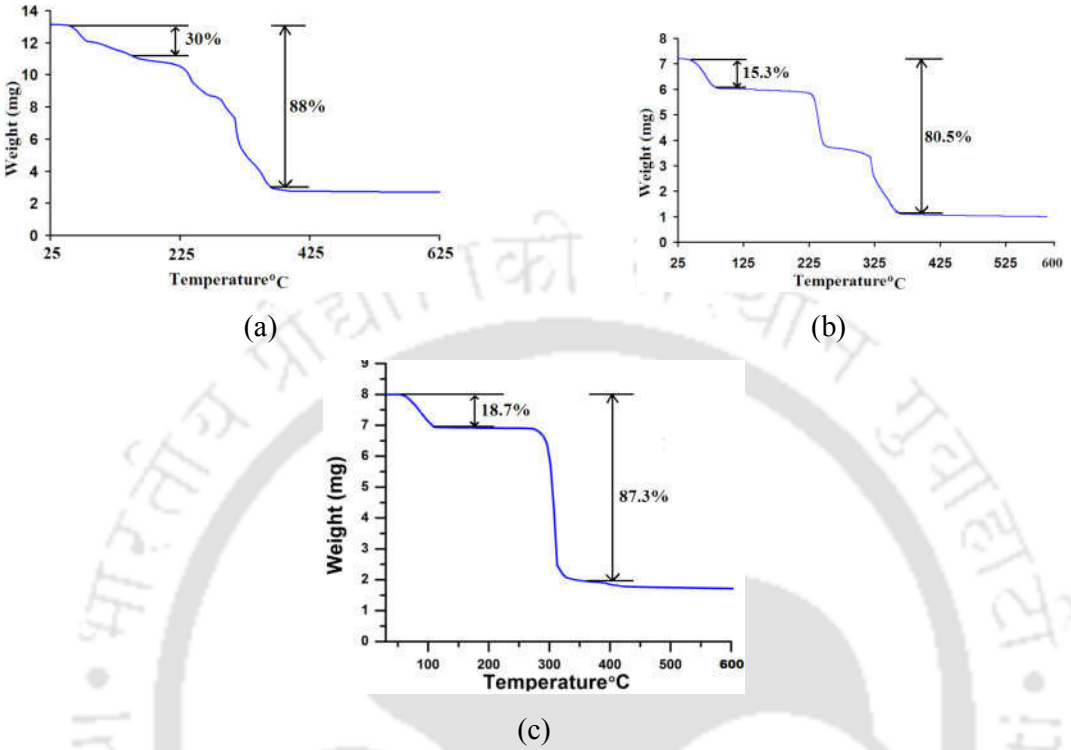

Figure 3.1.8: Thermograph of compounds (a) **3.1.1**, (b) **3.1.2** and (c) **3.1.3** (heating rate: 5°C per minute, N_2 atmosphere).

PXRD patterns of the resulting sample (Figure 3.1.9a) shows peaks for both the components. Conventional PXRD patterns for Gd_2O_3 and CuO are given in the Figure 3.1.9a for comparison, Hence such method has definite advantage over mechanical mixing which requires extra afford to make homogeneous mixture of metaloxides at precise amounts. Particle sizes of the mixed copper-gadolinum oxide was analysed by Transmission electron microscope showing that nano-dimensional particles of oxides were formed [Figure 3.1.9(b)]. The sizes of the particles varied from 20-50 nm.

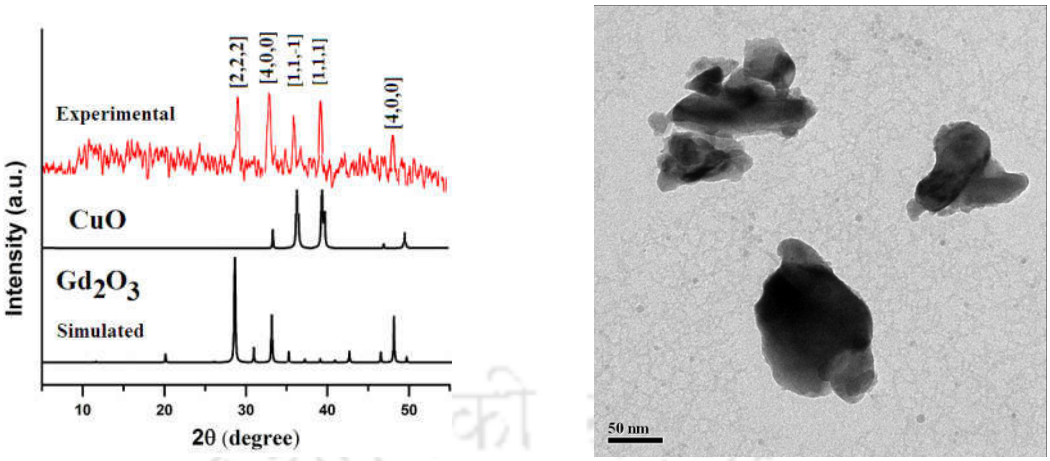

(a) (b)

Figure 3.1.9: (a) PXRD pattern of the sample derived upon the decomposition of **3.1.3** at 450ºC (top); simulated PXRD patterns for Gd_2O_3 (bottom) and CuO (middle). (b) Transmission electron micrograph of the particles obtained from thermal decomposition of **3.1.3**.

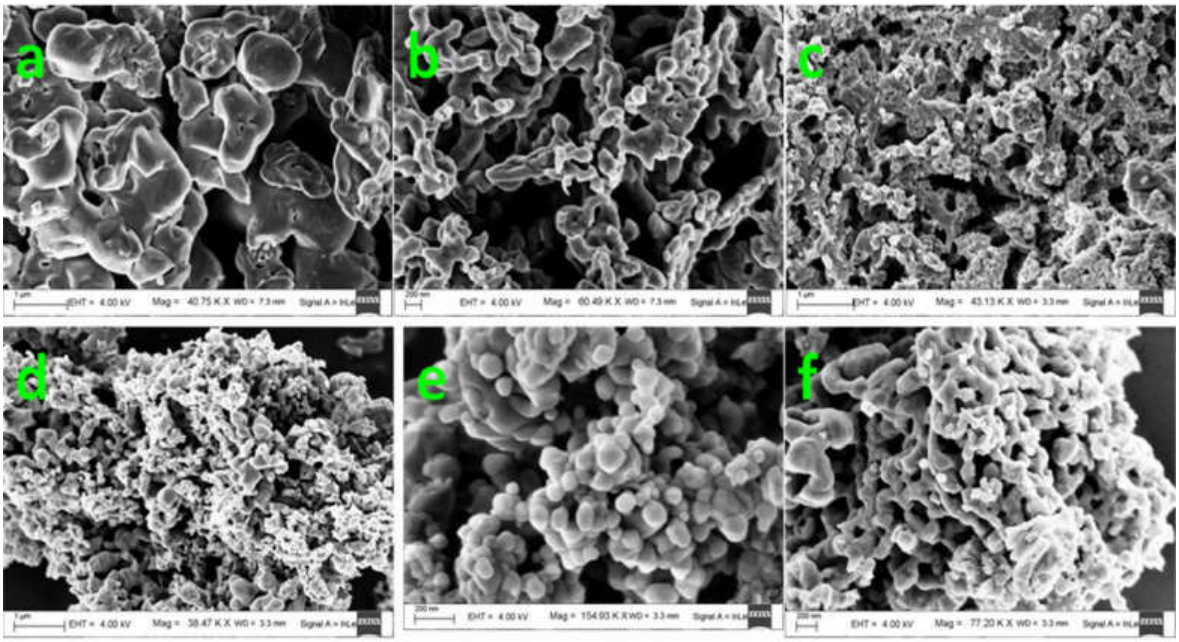

Figure 3.1.10: FESEM images: (a) and (b) copper oxide (from **2.1.13** and **3.1.1**), (c) and (d) mixed metal oxide Cu/Zn from **3.1.2**, (e) and (f) mixed metal oxide Cu/Gd from **3.1.3.**

Field-emission scanning electron microscope (FESEM) images of copper oxides obtained from decomposition of the mononuclear complex **2.1.13** and dinuclear complex **3.1.1** were also recorded. Each image shows an different morphologies of nano-dimensional particles [Figures 3.1.10 (a and b)]. FESEM of the mixed oxides prepared from thermal decompositions of **3.1.2** and **3.1.3** are analysed and images are given in Figure 3.1.10. In these cases also nano-dimensional particles are observed. From these results it is clear that the heterometallic Cu/Zn and Cu/Gd coordination polymers **3.1.2** and **3.1.3** provides a means to prepare homogeneous mixtures of nano-dimensional metal oxides, representing advantages over conventional mechanical mixing methods.

3.1.5 Summary

Careful selection of precursor have enabled to carryout synthesis of dinuclear copper complexes from mononuclear copper complexes having same set of cations and ligands. The mononuclear complex was further used for bottom up synthesis of hetero-metallic coordination polymers. Thermal decomposition of dinuclear copper complexes prove means to prepare copper oxide at relatively low temperature, on the other hand the thermal decompositions of hetero-metallic complex have yielded mixed metal oxides in homogeneous manner. Advantage of such methodology for preparation of mixed metal oxide will facilitate formation of mixture of oxides in desirable composition distributed in a homogeneous manner.

Part B

Self-assemblies of copper(II) 2,3-pyridinedicarboxylate complexes and intercalation of nucleobases

3.2.1 Background

Self-assemblies and metal-organic frameworks[15] having bio-molecules as one or more component in them would provide a relationship between materials and living sciences. Molecular recognition of bio-molecules and development of useful coordination polymers that are degradable to biocompatible byproducts have definite interest to chemists. DNA binding to metal ion is very common, and large amount of literature on DNA cleavage by metal ions are available.[16] Cytidine is a commonly used carbohydrate-containing nucleotide is a suitable substrate for study on metal-nucleotide interactions.[17] It forms various metal complexes which form interesting self-assemblies.[18] Copper(II) cytidine complex is known to bind carbon dioxide (Figure 3.2.1) to form multinuclear copper complex.[19]

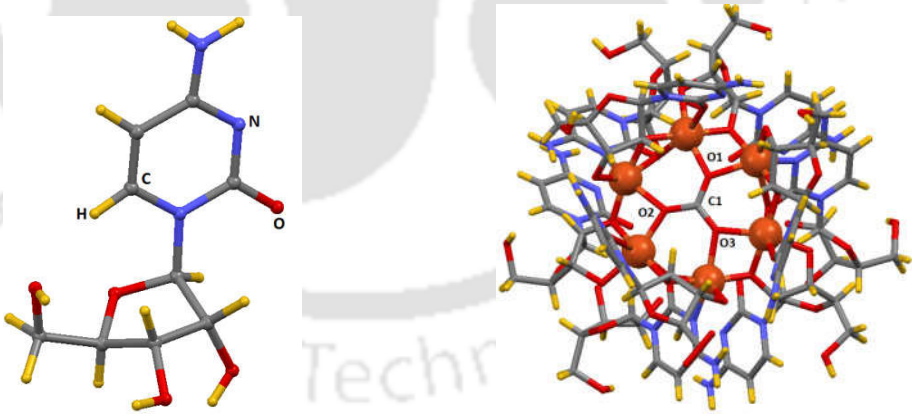

(a) (b)

Figure 3.2.1: (a) Cytidine, (b) Cu(I)multinuclear cytidine complex.

Direct coordination of cytidine to copper ions are very stable and have less scope for ligand exchange. However, any anionic complex assembly generated embedding cytosinium cation outside the primary coordination sphere will have special interest as to will provide easy access to cationic species due to presence of large hydrophobic carbohydrate part in it. In earlier part of this thesis extensive discussion on self-assemblies of anionic frames having organo-ammonium cations are discussed. Such discussions also have suggested use of organo-cations from biologically relevant molecules such as nucleobases. Use of nucleobases in self-assembling has been of interest as depending on the anionic counterpart various types of self-assemblies from each nucleobase can be achieved.[20] In this part of the thesis characterization of a cytidinium copper(II) 2,3-pyridinedicarboxylate complex and it's a cation exchange ability is discussed.

It is important to note that nucleobases undergo self-association either in neutral or protonated form through intermolecular hydrogen bonds. It would be interesting to study the self-assembly processes of these nucleobases in the interstices of relatively bulky copper(II) 2,3-pyridinedicarboxylate complex anion or similar dicarboxylate complexes.

3.2.2 Cytosiniumcopper(II) 2,3-pyridinedicarboxylate

Among the nucleobases cytosine is protonated easily and forms cytosinium cation. Cytosinium cation[21] undergoes self-assemebly and various types of homomeric assemblies such as dimeric, trimeric, tetrameric or infinite assemblies[22] are formed. Several such assemblies are stabilized by supramolecular assemblies. Some of such assemblies are listed in Figure 3.2.2. For example, monomeric form can be stabilized by trimesic acid and pyromellitic acid [23], dimer by adipic acid acid and trimer by citric acid[24], tetramer by Mn(II) 2,6-pyridinedicarboxylate[25] and infinite chain of protonated cytosine by phthalic acid[26]. Analogous to other amines addition of cytosine to a solution of copper(II) acetate with pyridinedicarboxylic acid resulted in formation of cytosinium copper(II) 2,3-pyridinedicarboxylate coordination polymer (**3.2.1**).The anionic part of **3.2.1** is comprised of dimeric copper(II) pyridinedicarboxylate repeated units to make a polymeric chain of anionic part (Figure 3.2.3a). The cations are held by electrostatic interaction and posseses strong hydrogen bonded network.

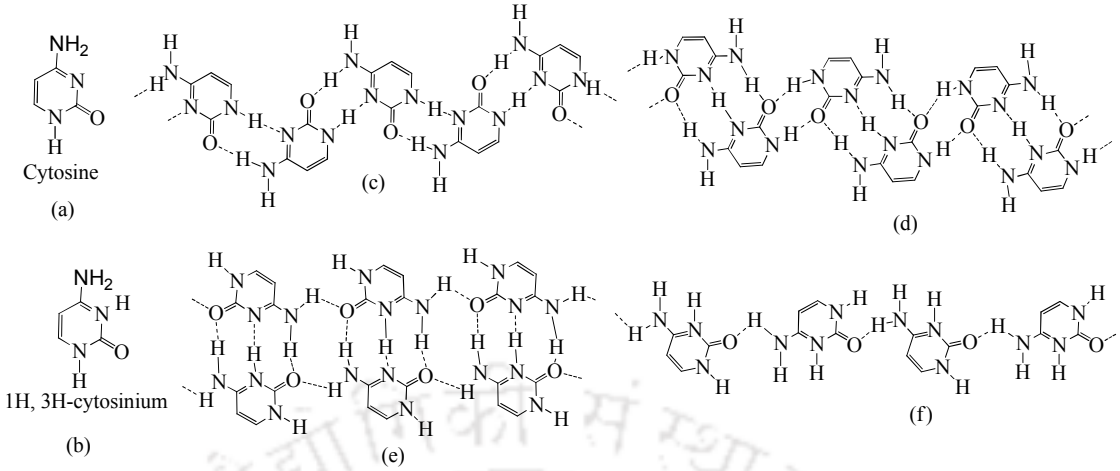

Figure 3.2.2: (a) Neutral cytosine, (b) Protonated cytosine (c) neutral cytosine, (d-e) cytosine-cytosinium, (f) cytosinium assembly.

Cytosine forms single tautomer in the form of 1H,3H-cytosinium cation. The hydrogen bonded assembly of the compound is shown in Figure 3.2.3b. Despite the single protonated form, its special geometry allows it to form discrete cation. The hydrogen bonds of water molecules contribute to the layers is shown in Figure 3.2.3(c). The coordination polymer has a layer-like structure of anionic parts and they encapsulate the cations. Separation between anionic layers is 14.1Å (Figure 3.2.5a).

Cytidinium copper(II) 2,3-pyridinedicarboxylate coordination polymer is not an exception as it was synthesized in a similar procedure as that of the other analogous organo-cation containing copper(II) 2,3-pyridinedicarboxylate complexes described in second part of chapter 2. The coordination polymer **3.2.2** has polymeric anionic part composed of infinite dinuclear repeat units, charge on each dinuclear part is balanced by two cytidinium cations. The complex **3.2.1** has similarity in structure, only difference arises from the sugar unit of the cytodinium cation. Cytosinium cations interact with the 3-carboxylate group of the polymer through Watson-Crick face of the nucleobase. Hydroxy groups of sugar molecules are involved in hydrogen bond formation to provide a tight-packed structure as illustrated in Figure 3.2.4a. To adopt charge assisted strong hydrogen bonds involving $^{+}$N-H of cytidine and oxygen atoms of carboxylate, a larger interlayer separation of the anionic layer. Inter anionic layer separation along *b* axis is ~15.9Å (Figure 3.2.5b).

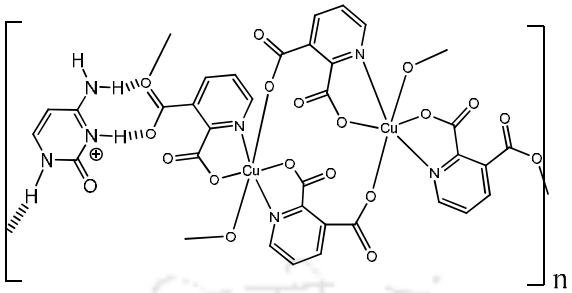

3.2.1

(a)

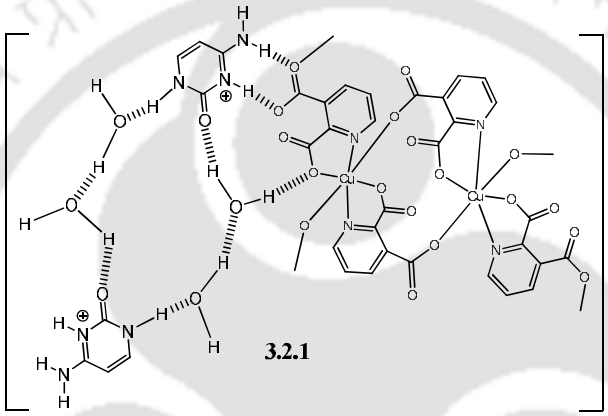

3.2.1

(b)

Figure 3.2.3:(a) Hydrogen bonds between cations and anions in assembly of the coordination polymer**3.2.1**, (c) Contribution of water molecules to hydrogen bonds in the self-assembly.

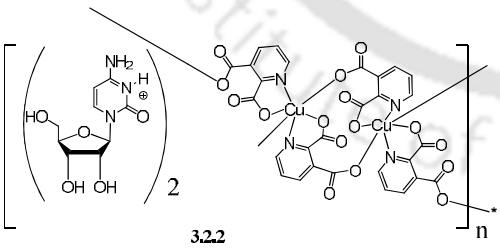

3.2.2

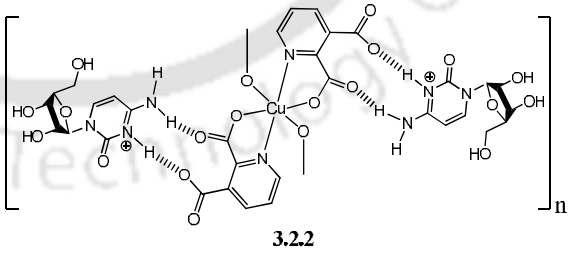

3.2.2

(a) (b)

Figure 3.2.4: (a) Copper(II) 2,3-pyridinedicarboxylate possessing cations of nucleobases. (b) Hydrogen bonds between cations and polymeric anion in self-assembly of coordination polymer **3.2.2.**

For comparison purpose the interlayer separation in analogous coordination polymer **3.2.1,** which has cytosinium cations is shown in Figure 3.2.5a. Hydrogen bond parameters of some prominent hydrogen bonds in the assembly are are tabulated in Table 3.2.1.

It is easily seen that the sugar unit present in the case of coordination polymer **3.2.2** makes increases the separation by about 1.8Å. This is large as that of twice that of O-H bond distance. Thus, the effect is due to the sugar molecule but the increase in separation is small that of a distance separation that would have been caused by a water molecule. In fact the alignment of the sugar molecules in the lattice makes it clear that it is the orientations of the cations to make tight packed structure makes the difference. Protonated cytosinium assemblies have been intercalated in layer-like structure of other metal complexes, such as oxalates and metal 2,6-pyridinedicarboxylate through similar weak interactions.[16]

Table 3.2.1: Hydrogen bond parameters in the self-assembly of complex **3.2.2**

Bond (symmetry)	dD-H(Å)	dH···A(Å)	dD···A(Å)	<D-H···A(°)
O(16)-H(16)···O(18) [1+x, y, z]	0.82	2.06	2.826(9)	156
N(3)-H(3B)···O(3) [x,y, z]	0.86	2.03	2.839(11)	157
O(13)-H(13A)···O(11) [-1+x,y, z]	0.82	1.95	2.759(9)	169
O(12)-H(12A)···O(6) [1+x, y, z]	0.82	1.98	2.775(10)	162
O(11) -H(11A)···O(7) [x,y, z]	0.82	1.94	2.754(10)	173
N(6) -H(6A)···O(8) [x, 1+y, -1+z]	0.86	2.02	2.879(10)	176
N(7) -H(7N)···O(7) [x, 1+y, -1+z]	0.92	1.88	2.788(10)	171
N(6) -H(6B)···O(6) [1-x, 1-y, -z]	0.89	1.98	2.847(6)	163

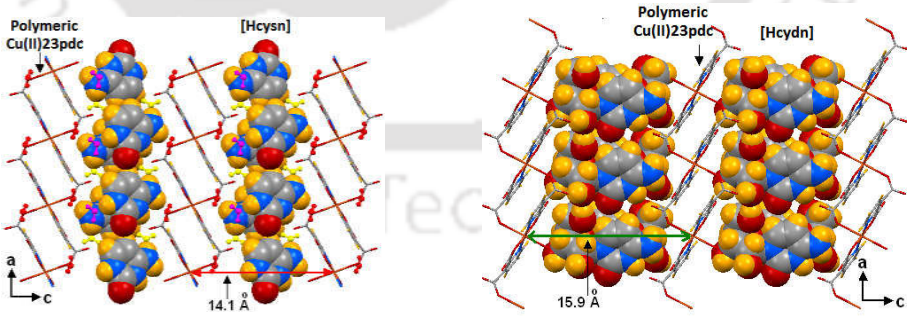

(a) (b)

Figure 3.2.5: Inter anionic layer separation caused by cytosinium cations in packing arrangement of (a) **3.2.1**, (b) **3.2.2**.

3.2.2 Spectroscopic and thermochemical study on complex 3.2.1 and 3.2.2

The coordination polymer **3.2.1** and **3.2.2** exhibit strong and broad IR-absorption bands in the range of 3527-3412cm^{-1} which are attributed to the *v*(OH) vibrations of water of crystallization. Absorption bands appearing in the range of 3304-2637cm^{-1} are related to *v*(-N^{+}-H) vibrations of protonated nitrogenous bases.

Stretching frequencies of the -COO^{-}groups of copper(II) 2,3-pyridinedicarboxylate complex anion appeared in the range of 1656-1615cm^{-1} and 1596-1582cm^{-1} for asymmetric (ν_{as}) and symmetric (ν_{s}) vibrations respectively. Visible spectra, of the coordination polymer **3.2.1** and **3.2.2** showed absorption at 772nm and 519nm due to d-d transition.

Thermogravimetric analysis (TGA) reveals that the loss of water molecules for the coordination polymer **3.2.1** tally with the number of water molecules observed in the structural unit.[27] In coordination polymer **3.2.2** is devoid of a water of crystallization, it may be due to hydroxyl group of glucose part also interacts with the carboxylate group of complex anion as a donor.

X-ray powder diffraction patterns have been recorded to check the bulk purity of the complexes and compared with those simulated from the single-crystal structures (Figure 3.2.6). The measured PXRD patterns of the compounds are in good agreement with the patterns simulated from the respective single crystal data, confirming the homogeneity of the bulk samples.

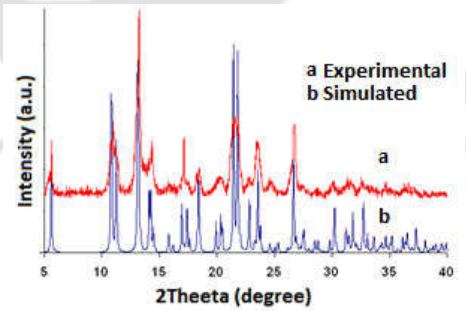

Figure 3.2.6: Powder XRD patterns of the coordination polymers**3.2.2**

Further, complex **3.2.2** underwent exchange of its cations with (i) alkali/alkaline earth metal ions, such as Na^{+}, Mg^{2+}, Ca^{2+}, (ii) transition metal ions such as Mn^{2+}/Co^{2+}, and (iii)

the exchange of larger organic cation by smaller one such as replacement of $[Hcydn]^+$ by $[Hcysn]^+$/$[1H,9H\text{-}ade]^+$.

The cation exchange reactions are shown in Scheme 3.2.1. Exchange of the cytidinium cations by metal ions resulted in polymeric complexes in which organic cations layer is replaced by a layer of aquated metal cations.

Exchange of cytidinium cations by Na^+, Mg^{2+} or Ca^{2+} ions resulted in the respective polymeric complexes namely $\{[Na_2(H_2O)_6(\mu\text{-}H_2O)_2][Cu(23pdc)_2]\}_n$**(3.2.3)**, $\{[Mg(H_2O)_6][Cu(23pdc)_2]2H_2O\}_n$**(3.2.4)** or $\{[Ca(H_2O)_5][Cu(23pdc)_2]\cdot H_2O\}_n$**(3.2.5)**. Replacement by Mn^{2+}, Co^{2+} or Mg^{2+} ions led to isostructural complexes $\{[M(H_2O)_6][Cu(23pdc)_2]\cdot 2H_2O\}_n$ [where M = Mg^{2+} (**3.2.4**), Co^{2+}**(3.2.6)**, Mn^{2+}**(3.2.7)**. The products obtained from exchange reactions were characterized in each case by determining powder XRD patterns of the products and comparing them with the reported or the data presented in this study. All the structures of the complexes listed in Scheme **3.2.2** were determined by single X-ray crystallography except structure of complexes **3.2.3** and **3.2.7** were reported earlier.[28]

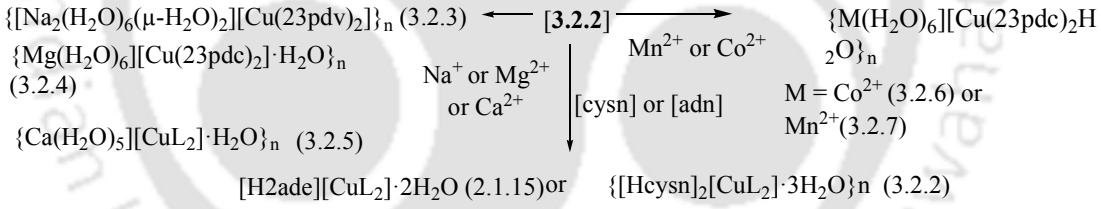

Scheme 3.2.1: Cation exchange reactions.

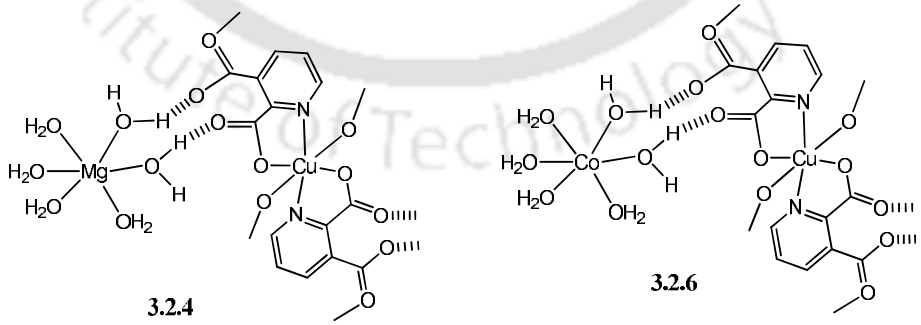

(a) (b)

Figure 3.2.7: (a) Hydrogen bonding of complexes $\{[Mg(H_2O)_6][Cu(23pdc)_2].2H_2O\}_n$ **(3.2.4)**, (b) $\{[Co(H_2O)_6][Cu(23pdc)_2].2H_2O\}_n$**(3.2.6)**.

The Na^{+} and Ca^{2+} ions are held by dative bond with carbonyl group of carboxylate ligand attached to copper ions. Thus, the coordinated carboxylate anions act as bridges in these complexes. Whereas in the iso-structural complexes **3.2.4**, **3.2.7**and **3.2.6** which contains Mg^{2+}, Mn^{2+}or Co^{2+}ions respectively, posseses discrete cationic and anionic units.

Key feature of these complexes is the carry forward of the lamellar property of the parent complex. Irrespective of metal ions used for exchange the polymeric $\{[Cu(23pdc)_2]^{2-}\}_n$ layers are consistently retained. But in the case of organic cations it depends on the cation used, for example adenine segregated the chain to form mono-nuclear units, however reverse exchange was also possible by using excess of cytidine to the corresponding cytosine complex. We have also tested the metal exchange properties with other organo-cations and cation exchange is found to be a general phenomenon.

3.2.3 Summary

A coordination polymer stabilizing cytidinium cation is established. Ability of exchanging cytidinium cations by (i) alkali/alkaline earth metal ions, such as Na^{+}, Mg^{2+}, Ca^{2+}; (ii) transition metal ions such as Mn^{2+}/Co^{2+}, and (iii) the exchange of larger organic cation by smaller one such as replacement of $[Hcydn]^{+}$ by $[Hcysn]^{+}$/$[1H,9H\text{-}ade]^{+}$ are shown to be result of the possibility to modulate the layered structures by different cations and the ability of different amines to exchange protons to serve as complementing hydrogen bonding unit to different anionic units.

3.3 Experimental Section:

Detailed synthetic methodologies are given below. Analytical data as well as spectroscopic data are also listed along with the each complex. Details of the instruments, crystallographic table are given in Appendix.

3.3.1 Synthesis and characterization of homo-and heterometallic complexes

3.3.1.1: (Hdapt)[Cu(H23pdc)(23pdc)(H_2O)]·H_2O **(2.1.13)** The complex was prepared by the similar procedure as given in chapter 1.

3.3.1.2: $(Hdapt)_4[Cu_2(23pdc)_4]\cdot 10H_2O$ **(3.1.1):** To a solution of **2.1.13** (0.309 g, 0.5 mmol) dissolved in methanol/water mixture (1:1, 30 mL), pyridine was added (5 mmol, 0.4 mL) for maintaining pH 8.0, the obtained solution was refluxed for 2 h and filtered. Slow evaporation of the filtrate led to the formation of X-ray quality crystals after 4-5 days. Isolated yield: ~68%. IR (KBr, cm^{-1}): 3472 (bs), 3379 (bs), 2932 (w), 1628 (s), 1584 (s), 1433 (w), 1387 (w), 1366 (s), 1269 (m), 1152 (w), 1115 (m), 1022 (m), 879 (w), 832 (w), 698 (m), 605 (m). UV-Vis (solid state): λ_{max} = 636 nm. ESR (solid state): g = 2.051. TGA: 50-200°C (-5H_2O and - dapt; exptl. wt. loss 32.5%, calcd.30.0%), 225-380°C (formation of CuO, exptl. wt. loss 89.1%, calcd. 88.0%).

3.3.1.2: $\{[Zn(H_2O)_4Cu(23pdc)_2]\cdot 3H_2O)\}_n$ **(3.1.2):** To a solution of **2.1.13** (0.309 g, 0.50 mmol) dissolved in methanol/water mixture (1:1, 30 mL), zinc(II) acetate dihydrate (0.072 g, 0.25 mmol) was added, resulting in the formation of a blue precipitate. To the resulting reaction mixture 4-5 drops of pyridine were added to make a homogenous solution. It was then refluxed for 2 h and filtered. Slow evaporation of the filtrate led to formation of X-ray quality crystals after 4-5 days.Isolated yield: ~73%. IR (KBr, cm^{-1}): 3421 (bs), 2922 (w), 1635 (s), 1589 (m), 1392 (m), 1272 (w), 1157 (w), 1115 (m), 1023 (m), 832 (w), 778 (w), 694 (m). UV-Vis (solid state): λ_{max} = 625 nm. ESR (solid state): g = 2.092. TGA: 50-90°C (-3H_2O; exptl. wt. loss 14.5%, calcd.15.3%), 225-365°C (formation of CuO/ZnO; exptl. wt. loss 79.2%, calcd. 80.5%).

3.3.1.2: $\{[Gd(H_2O)_5Cu_{1.5}(23pdc)_3]\cdot 5H_2O\}_n$ **(3.1.3):** A procedure similar to that of **3.1.2** was adopted for the synthesis of **3.1.3**, but gadolinium(III) acetate tetrahydrate (0.066 g, 0.20 mmol) was used instead of zinc acetate dihydrate. Isolated yield: ~62%. IR (KBr, cm^{-1}): 3320 (bs), 3191 (bs), 1636 (s), 1542 (s), 1452 (w), 1396 (m), 1360 (w), 1256 (w), 1157 (w), 1114 (w), 1021 (w), 778 (w), 707 (m). UV-Vis (solid state): λ_{max} = 626 nm. ESR (solid state): g = 2.064. TGA: 60-125°C (-10H_2O, exptl. wt. loss 16.1%, calcd. 18.7%), 225-365 °C (loss of ligands, exptal. wt. loss 81.3%).

3.3.2 Synthesis and characterization of copper(II) 2,3-pyrdinedicarboxylates

3.3.2.1: $\{[1H,3H\text{-cydn}]_2[Cu(23pdc)L_2]\cdot 6H_2O\}_n$ **(3.2.1):** It was reported earlier from our laboratory[27]

3.3.2.2: $\{(H_2cydn)_2[Cu(23pdc)_2]\}_n$ **(3.2.2):** To a solution of 2,3-pyridinedicarboxylic acid (0.167 g,1.0 mmol) dissolved in methanol (20 mL), copper(II) acetate monohydrate (0.10 g, 0.5 mmol) was added. The resulting blue solution led to the formation of a precipitate. The mixture was stirred and cytidine (0.243 g, 1 mmol) was added. This led to a homogeneous solution, which was left overnight at room temperature. This resulted in the formation of blue precipitates, which were collected by filtration and dissolved in water or a water/pyridine mixture. Slow evaporation of the solution led to suitable X-ray quality crystals after 3-4 days. Isolated yield: ~70%. IR (KBr, cm^{-1}): 3414 (s), 3075 (w), 2940 (w), 1740 (s), 1686 (s), 1637 (w), 1587 (m), 1382 (m), 1352 (m), 1272 (m), 1237 (w0, 1116 (s), 1088(m), 865 (w), 838 (m), 819 (m), 701 (m), 648 (w), 607 (w), 577 (w), 473 (w). Elemental analysis calcd for $C_{32}H_{34}CuN_8O_{18}$, C, 43.53; H, 3.85; N, 12.70 %.Found C, 43.51; H, 3.79; N, 12.68 %. Vis. (solid state) λ_{max}: 519.0 nm. g = 2.063

The cation-exchange experiments were performed by dissolving **3.2.2** (0.1 mmol) in water (5 mL). The metal chloride (0.2 mmol) organic amine (0.2 mmol) was then added to the solution. The solutions were stirred for 1 h and left for crystallization, which resulted in cation-exchanged products.

3.3.2.3: $\{Mg(H_2O)_6][Cu(23pdc)_2]\cdot 2H_2O\}_n$ **(3.2.4):** Isolated yield: ~70%. IR (KBr, cm^{-1}): 3397 (bs), 2457 (w), 1630 (s), 1593 (w), 1396 (w), 1366 (m), 1278 (w), 1120 (m), 998 (w), 976 (w).

3.3.2.4: $\{Co(H_2O)_6][Cu(23pdc)_2]\cdot 2H_2O\}_n$ **(3.2.6):** Isolated yield: ~69%. IR (KBr, cm^{-1}): 3482 (w), 3334 (w), 2921 (w), 2625 (w), 2456 (w), 1629 (m), 1590 (s), 1571 (s), 1435 (w), 1396 (s), 1366 (s), 1278 (m), 1152 (m), 1119 (s), 998 (w), 833 (m), 721 (w).

References:

1 (a) J. J. Hou, R. Zhang, Y. L. Qin, X. M. Zhang, *Cryst. Growth and Des.*, 2013, **13**, 1618-1625; (b) J. P. Zhao, Q. Yang, S. D. Han, J. Han, R. Zhao, B. W. Hu, X. H. Bu, *Dalton Trans.* 2013, **42**, 8201-8204.

2 (a) A. Cheansirisomboon, C. Pakawatchai, S. Youngme, *Dalton Trans.*, 2012, **41**, 10698-10706; (b) S. J. Liu, L. Xue, T. L. Hu, X. H. Bu, *Dalton Trans*., **2012**, **41**, 6813-6819.

3 (a) E. Gazit, *Chem. Soc. Rev*., 2007, **36**, 1263-1269; (b) E. Busseron, Y. Ruff, E. Moulin, N. Giuseppone, *Nanoscale*, 2013, **5**, 7098-7140.

4 (a) V. Berl, I. Huc, R. G. Khoury, M. J. Krische and J. M. Lehn, *Nature*, 2000, **407**, 720-723; (b) O. Ramstrom, T. Bunyapaiboonsri, S. Lohmann and J. M. Lehn, *Biochim. Biophys. Acta*, 2002, **1572**, 178-186.

5 P. Debroy, M. Banerjee, M. Prasad, S. P. Moulik, S. Roy, *Org. Lett*., 2005, **7**, 403-406.

6 C. S. Purohit, S. Verma, *J. Am. Chem. Soc*., 2006, **128**, 400-401.

7 F. H. Isikgora, C. R. Becer, *Polym. Chem*., 2015, **6**, 4497-4559.

8 J. K. Maclaren, C. Janiak, *Inorg. Chim. Acta*, 2012, **389**, 183-190.

9 S. H. Yan, X. J. Zheng, L. C. Li, D. Q. Yuanc, L. P. Jin, *Dalton Trans*., 2011, **40**, 1758-1767.

10 J. Jezierska, *Polyhedron*, 1987, **6**, 1669-1672.

11 G. Arena, R. P. Bonomo, A. Contino, C. Sgarlata, G. Spotoa, G. Tabbi, *Dalton Trans*., 2004, 3205-3211.

12 M. Massacesi, G. Ponticelli, V.G. Krishnan, *J. Mol. Struct*., 1980, **69**, 165-181.

13 J. Hathway, D.E. Billing, *Coord. Chem. Rev*., 1970, **5**, 143-207.

14 M. B. Gawande, R. K. Padey, R. V. Jayaramm, *Catal. Sci. Technol.*, 2012, **2**, 1113-1125.

15 (a) K. M. Stewart, L. W. McLaughlin, *J. Am. Chem. Soc*., 2004, **126**, 2050-2057; (b) S. Sikova, S. J. Rowan, *Chem. Soc. Rev*., 2005, **34**, 9-21.

16 J. E. Deweese, F. P. Guengerich, A. B. BurgiN, N. Osheroff, *Biochemistry*, 2009, **48**, 8940-8947.

17 S. Mansy, J. P. Frick , R. S. Tobias, *Biochim Biophys Acta*, 1975, **378**, 319-332.

18 N. Marino, D. Armentano, T. F. Mastropietro, M. Julve, F. Lloret, G. D. Munno, *Cryst. Growth and Des*., 2010, **10**, 1757-1761.

19 D. Armentano, N. Marino, T. F. Mastropietro, J. M. Lillo, J. Cano, M. Julve, F. Lloret, G. D. Munno, *Inorg. Chem*., 2008, **47**, 10229-10231.

20 J. P. G. Teran, O. Castillo, A. Luque, U. G. Couceiro, G. Beobide, P. Roman, *Cryst. Growth Des*., 2007, **7**, 2594.

21 N. B. Pavlovic, A. S. Bire, *J. Phys. Chem. A*, 2010, **114**, 10664-10675.

22 (a) F. H. Allen, *Acta Crystallogr*., 2002, **B58**, 380-388; (b) J.P. García-Teran, O. Castillo, A. Luque, U. García-Couceiro, G. Beobide, P. Román, *Cryst. Growth Des*., 2007, **7**, 2594-2600.

23 R. Thomas, G. U. Kulkarni, *J. Mol. Struct*., 2008, **873**, 160-167.

24 B Das, J. B. Baruah, *J. Mol. Struct*., 2011, **1001**, 134-138.

25 B Das, J. B. Baruah, *Cryst. Growth Des*., 2010, **10**, 3242-3249.

26 S. R. Perumalla, E. Suresh, V. R. Pedirredi, *Angew. Chem., Int. Ed. Engl*., 2005, **44**, 7752-7757.

27 B. Das, A. K. Boudalis, J. B. Baruah, *Inorg. Chem. Commun*., 2010, **13**, 1244-1248.

28 B. O. Patrick, C. L. Stevens, A. Storr, R. C. Thomson, *Polyhedron*, 2003, **22**, 3025-3035.

Chapter 4

Molecular recognition by assemblies of anionic and cationic complexes

4.1 Background

Self-assemblies of supramolecular cationic or anionic complexes guided by charge-assisted hydrogen bonds are highly stable in nature.[1] They have advantages to provide better flexibility than conventional metal-organic frameworks.[2] There are large numbers of literature available on ion and molecular recognition by metal-organic framework, whereas the recognition by supramolecular inorganic assemblies are limited.[3] Such frameworks may be varied on the basis of charge on metal containing part and can be described as anionic,[4] cationic[5] and neutral[6] frameworks, their supramolecular assemblies serve as templates in molecular recognition. The molecular recognition by these templates are based on weak interactions such π-stacking[7], C-H···π interactions[8], anion-π and cation-π interactions.[9] Design of π-stacking templates to hold planar aromatic compounds is of great interest to modulate different spaces between π-stacks to accommodate different guest molecules.[10] Selectivity in a guest binding process is generally studied through isolation of host-guest complexes, signal transduction and by determining binding constant or other related thermodynamic parameters. Spectroscopic signal transductions due to difference in binding abilities of substrates are generally utilized for detection of particular analyte. Fluorescence spectroscopic technique is one of the most sensitive techniques, but requires a fluorophore attached to the signal generating unit. Fluorescent macromolecules such as conjugated polymers[11], metal-organic frameworks[15], organic-inorganic hybrid materials[12], dendrimers[13], have been utilized as host for aromatic guests. Medium size molecules[14], as well as small inorganic molecules[15] have also attracted attention for such a purpose. From the literature it is clear that molecules having π-stacking ability play a key role to recognize specific nitro-aromatic compound.[16] A metal ion and chelating ligands having planar aromatic part, such as 2,6-pyridinedicarboxylate, 2,2′-bipyridine, 1,10-phenanthroline would have different ways to arrange planar components within their self-assemblies.

Complexes synthesized by π-decorating ligands, due to stacking arrangement of ligands would hold organic molecules in aromatic π-stacks. For this purposes four different types of complexes shown in Figure 4.1(a-d) are chosen. Choices are based on documented abilities of these classes of complexes to form layer-like structures. On the other hand, the chosen examples are representation to convey the impact of changes in coordination number and increasing nuclearity of metal ion in such complexes to provide more spaces for guest inclusions. With such a background, supramolecular templates shown in Figure 4.1(a-d) are chosen to study self-assemblies and molecular recognition of aromatic compounds are discussed in this chapter.

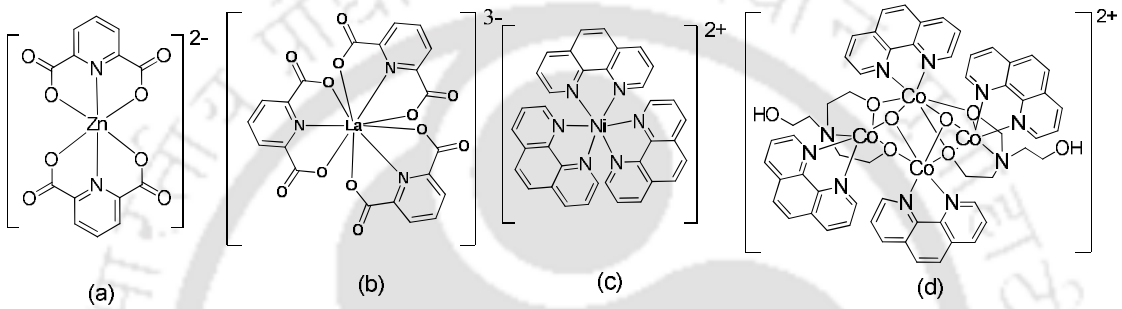

Figure 4.1: Different metal templates used for study of self-assemblies for guest inclusions.

Molecular recognition abilities of these templates in particular their self-assemblies are discussed separately under individual sub-heading. Recognition of nitroaromatic compounds is an important topic of research grown very fast because of toxic and hazardous nature of aromatic compounds.[17] Thus the molecular recognition of such compounds is a great challenge in the field of supramolecular chemistry.[18]

Part A

Molecular recognition by Zinc(II) 2,6-pyridinedicarboxylate

4.1.1 Background

As mentioned in introductory chapter bis-2,6-pyridinedicarboxylates complexes adopts layer-like structure and it has been shown that nuclearity in such complexes can be varied by changing the cations.[19a] The anionic part of such complexes commonly self-assemble to adopt layers of structures as illustrated in Figure 4.1.1(a) where the aromatic part of the 2,6-pyridinedicarboxylates are in one parallel position over each other in one crystallographic direction making an one dimension layer. There are large examples on zinc(II) 2,6-pyridinedicarboxylates whose structures are established.[19b] In such structures utility of stacking of aromatic cationic part has not been explored.

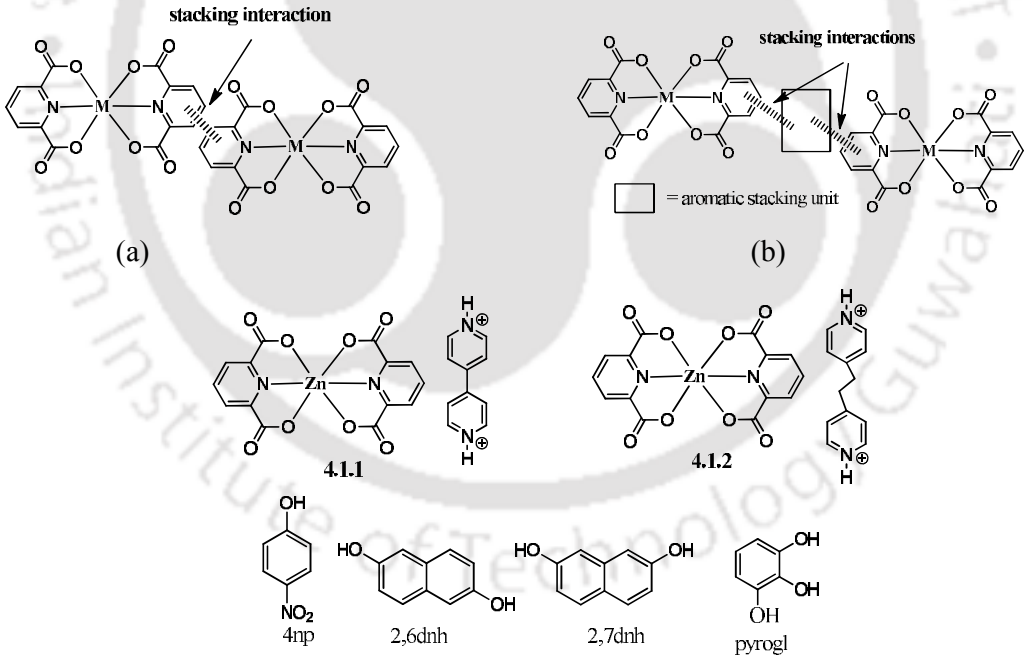

Figure 4.1.1: (a) and (b) are two ways to π-stack forming layer-like structure in metal 2,6-pyridinedicarboxylates. **4.1.1** and **4.1.2** are hosts and rests are guest molecules.

This is interesting as in the case of such a part taking part to alter the layers of zinc(II) 2,6-pyridinedicarboxylate anions, then they would control the overall packing pattern and in turn change the ability of such a system to recognize guest molecules. With such an approach the zinc(II) 2,6-pyridinedicarboxylate complexes having 4,4´-bipyridinium and 1,3-bis(4-pyridinium)propane dications are studied. Guest binding abilities of two complexes with different hydroxyaromatic compounds listed in Figure 4.1 are investigated.

4.1.2 Synthesis of complexes

Complexes $[H_2tmbpy][Zn(26pdc)_2]\cdot 5H_2O$ (**4.1.1**) and $[H_2bpy][Zn(26pdc)_2]\cdot 6H_2O$ (**4.1.2**) were synthesised to understand the any structural difference caused by 4,4´-bipyridinium and 1,3-bis(4-pyridine)propane dications abbreviated as H_2bpy and H_2tmbpy respectively. The flexible part with in the latter cation would allow a suitable packing pattern to guide the arrangements of zinc(II) 2,6-pyridinedicarboxylates in solid state. Both the complexes has characteristic N-H signals in IR spectra, namely complex **4.1.1** has such a stretching at 3443cm^{-1}, whereas the complex **4.1.2** shows such a stretching at 3415cm^{-1}.

Thermal stability of these two structurally related complexes **4.1.1** and **4.1.2** were determined from the thermal decomposition in the range of 30ºC-600ºC which are shown in Figure 4.1.2. As usual both the complexes have similar profiles but with different temperature at which the weight loss of the cations takes place. Both complexes lose amine part from the cation at about 250°C and in second step they get converted to zinc oxide. The final residues were analyzed by independently heating the complexes in crucible and comparing with PXRD pattern of zinc oxide. Zinc oxide formation temperature in the case of complex **4.1.1** is 425ºC whereas it is 380ºC for other complex. Structures of the two complexes have wide differences in the distance of separation between the π-stacking of two pyridine rings of two neighboring anions. Interactions between the two anions and with cations in two complexes are shown independently in Figure 4.1.3 (a) and (b). Complex **4.1.1** has a layer-like structure where there is a distance of ~3.49Å between the pyridine rings of parallel pyridinedicarboxylate moieties from two independent anions. This distance is reasonable for π-interaction.[20]

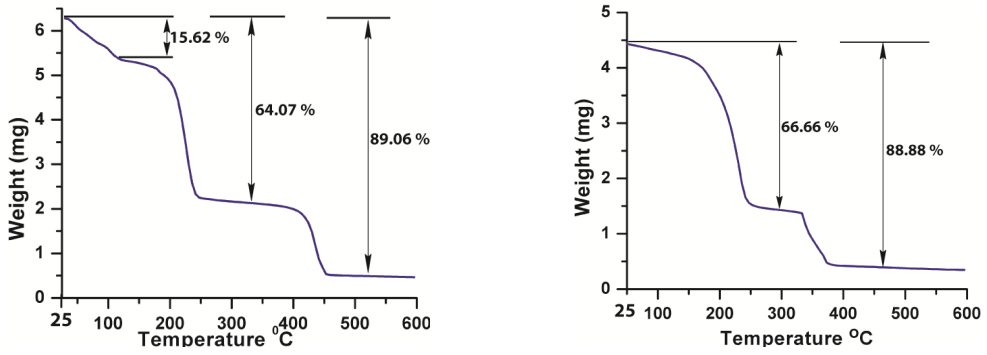

(a) (b)

Figure 4.1.2: Thermograms of complexes **4.1.1** and **4.1.2** (heating rate 5°C/min)

On the other hand, complex **4.1.2** (Figure 4.1.1b) has a π-separation ~4.2Å between the pyridine rings of $[Zn(26pdc)_2]^{2-}$ which is much larger relative to the distance observed in case of complex **4.1.1**. Despite, both having suitable geometry for π-interactions, complex **4.1.2** should be easy to disrupt for intercalation. It is known that highly π-stacking cations (e.g., quinolinium cations) tend to disrupt the π-stacking of anions and inhibit the formation of conventional layer-like structures of 2,6-pyridinedicarboxylate anions.[21]

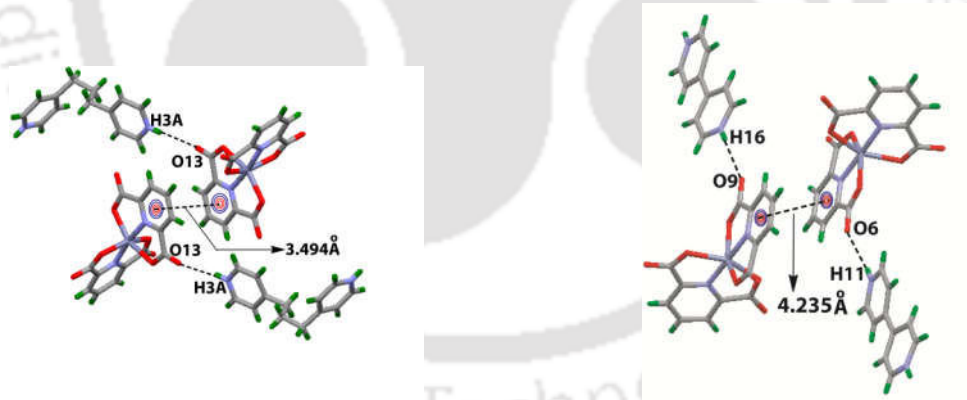

(a) (b)

Figure 4.1.3: Self-assemblies of complexes (a) **4.1.1** and (b) **4.1.2** showing some prominent supramolecular interactions.

On the other hand, the presence of planar π-ligands such as 1,10-phenanthroline or 2,2′-bipyridine provides multiple ways of π-stacking in a 2,6-pyridinedicarboxylate complex.[22]

Based on these results it can be suggested that the cations have definite role to organize the π-stacking patterns between the anions in this class of complexes. Structures of these two complexes show that in the projection of the two +N-H bonds of each case are different hence the directional nature of hydrogen bonds makes the orientation of the anions different in each case. With this background the interactions of these complexes with 4-nitrophenol are investigated.

4.1.3 Inclusion complex with 4-nitrophenol

Among the two complexes, **4.1.1** and **4.1.2,** the latter complex recognizes 4-nitrophenol. When a solution of complex **4.1.2** with 4-nitrophenol was allowed to crystallize, it yielded crystalline products of a new complex **4.1.3**. Whereas, a similar solution of complex **4.1.1** with 4-nitrophenol does not form any adduct. Crystallization of a solution of **4.1.1** and 4-nitrophenol yielded respective parent compounds. Selective interactions of complex **4.1.2** with 4-nitrophenol is established through solution study also. Addition of an aqueous solution of 4-nitrophenol to an aqueous solution of complex **4.1.2** leads to a steady growth of an absorption peak at 432nm in the UV-vis spectrum (Figure 4.1.4a). This absorption peak occurs at 36nm higher wavelength than the absorption peak of 4-nitrophenol which occurs at 396nm. On the other hand, no shift in position of absorption was observed in a similar experiment carried out between 4-nitrophenol with complex **4.1.1**.

The identity of the complex **4.1.3** was ascertained by ^{1}H-NMR, IR spectroscopy and determination of crystal structure. It shows a sharp IR stretching at 1496 cm^{-1}, which is absent in the parent complex. Complex **4.1.3** has signals from the two sets of aromatic proton signals for C-H hydrogen atoms at 6.73ppm and 7.92ppm from $[H_2bpy]^{2+}$, 7.40 and 8.56ppm due to 4-nitrophenol and at 8.21ppm and 7.70ppm from 2,6-pyridinedicarboxylate. ^{1}H-HOMOCOSY two dimensional ^{1}HNMR spectra of the complex establishes the desired correlation of the proton signals. Correlation observed between the signals of protons assigned as a and d, b and f, c and e, shown in the ^{1}H-HOMOCOSY spectra (Figure 4.1.3b) confirms the identifications of peaks from the complex. An independent experiment was carried out to see if an independent interaction between 4-nitrophenol with 4,4′-bipyridine is possible.

^{1}HNMR experiments were carried out by recording ^{1}HNMR spectra of 4-nitrophenol and 4,4′-bipyridine and an equimolar mixture of 4-nitrophenol with 4,4′-bipyridine (Figure 4.1.4c).

Comparison of these spectra have revealed that the signals of 4-nitrophenol as well as 4,4′-bipyridine are shielded and OH peak of 4-nitrophenol is affected upon mixing with 4,4′-bipyridine. This suggests charge-transfer interaction as well as proton exchange in solution. Thus, an initial interaction of 4-nitrophenol with 4,4′-bipyridine is possible.

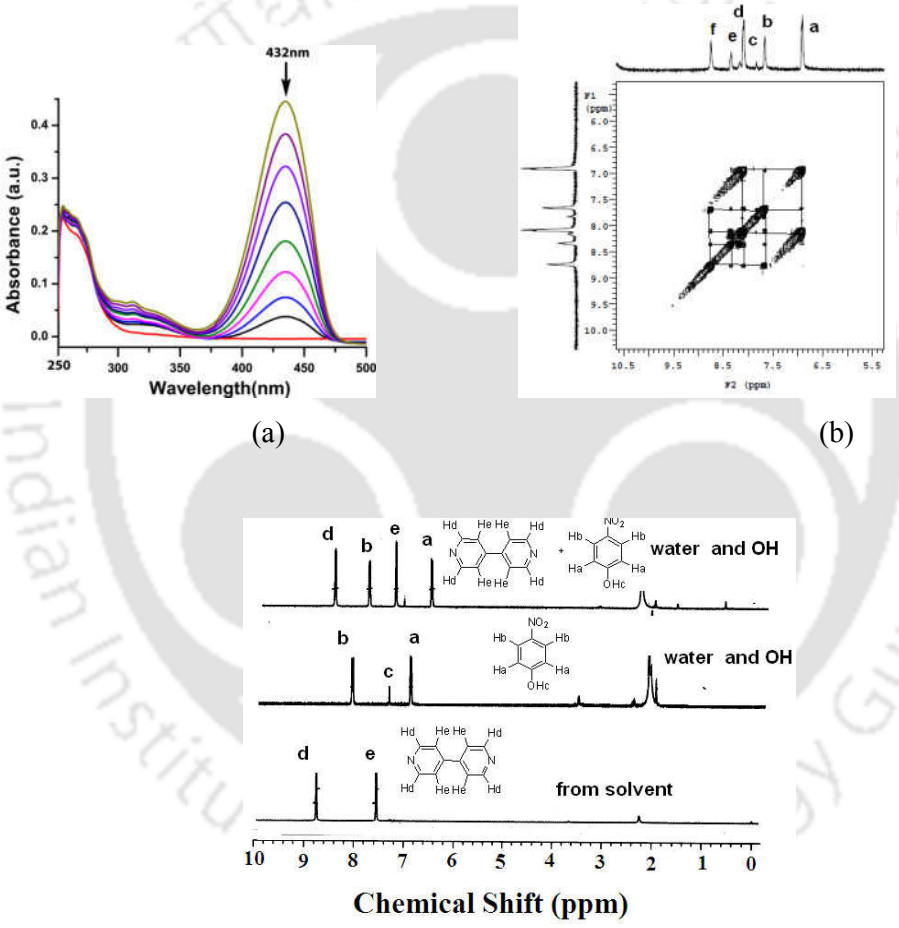

Figure 4.1.4: (a) Changes in UV-vis spectra of a methanol solution of complex **4.1.2** upon addition of 4-nitrophenol at 432nm. (b)^{1}H-HOMOCOSY spectra (5.5-10 ppm region) of complex **4.1.3.** (c) ^{1}HNMR spectra of 4,4′-bipyridine, 4-nitrophenol, mixture of 4,4′-bipyridine and 4-nitrophenol.

Structure of complex **$[H_2bpy][Zn(pdc)_2]\cdot 3.5(4np)\cdot 2H_2O$** **(4.1.3)** has 4-nitrophenol molecules placed in between π-stacks of anions (Figure 4.1.5). Since it was not possible to get crystalline product of such inclusion complex with **4.1.1**, and solution study also suggested no interactions, it is likely that cations plays the major role helping to intercalate 4-nitrophenols in complex **4.1.3**.

Thus, $[H_2bpy]^{2+}$cation plays a role in the selective recognition of 4-nitrophenol by **4.1.2**. Inclusion complex **4.1.3** has 3.5 molecules of 4-nitrophenol with respect to per zinc(II) 2,6-pyridinedicarboxylate anion. Interaction of 4-nitrophenol with complex anion occurs through π-stacking. 4-Nitrophenol molecules are sandwiched between pyridine rings of two independent anions. Distance of separation between parallel aromatic rings of host and guest is 3.79Å. This distance is much shorter than the π-π distance 4.2Å observed between two neighboring aromatic rings in parent complex. There is charge-assisted hydrogen bonds between +N-H bond with nitro group of 4-nitrophenol. These interactions coupled with weak C-H···O interactions help to generate a tight packed structure. The complex also decomposes to zinc oxide at about 430°C as shown in Figure 4.1.5 (b).

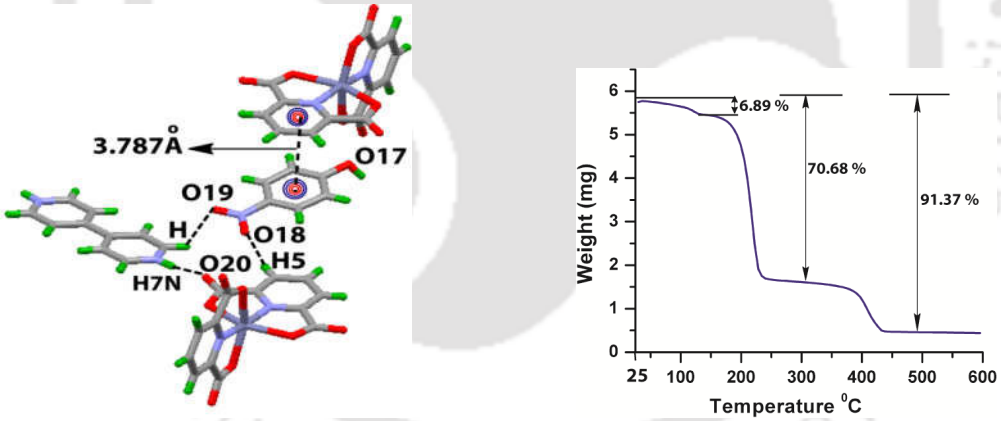

(a) (b)

Figure 4.1.5: (a) Self-assembly of **4.1.3** showing π-stacking between aroamtic rings of 2,6-pyridinedicarboxylate and 4-nitrophenol, (b) Thermogram of complex **4.1.3.**

Molecular recognition of hydroxyaromatic guests by hydrogen bonds and π-π interactions is common.[23] Single aromatic surface in hydrogen-bond receptor molecules improves significantly the complexation ability of a guest by assisting in π-stacking interactions.[24] Some host molecules can accommodate neutral aromatic guests between two aromatic surfaces.[25] Hydroxyaromatic compounds can also act as guests of crown

ethers.[26] In earlier studies, 4-nitrophenol and several dihydroxy aromatic compounds could be recognized on the basis their different binding abilities to organogels.[27] Molecularly imprinted polymers[28] and nanoparticles containing polymers[29] are used to recognize or detect 4-nitrophenol which is a high impact pollutant.

In this regard complex **4.1.2** can be made easily from readily available commercial ligands and forms isolable well characterized single solid product, which generates definite interest, due to demonstrated examples of metallo-organic frameworks[30] which selectively reduces 4-nitrophenol guest.

4.1.4 Inclusion complexes with dihydroxynaphthalenes

Cocrystallisation of **4.1.1** and **4.1.2** with various positional isomers of dihydroxynaphthalene was investigated. Among them, inclusion complexes of 2,7-dihydroxynaphthalene (2,7dhn) was possible crystallize with both these complexes. Such crystallization yielded inclusion complexes $[H_2tmbpy][Zn(26pdc)_2]\cdot 4(2,7dhn)\cdot 3H_2O$ (**4.1.4**) and $[H_2bpy][Zn(26pdc)_2]\cdot 2(2,7dhn)\cdot 5H_2O$ (**4.1.5**). While in the case of 2,6-dihydroxynaphthalene (2,6dhn) it yielded inclusion complex $[H_2tmbpy][Zn(26pdc)_2]\cdot 2(2,6dhn)\cdot 9H_2O$ (**4.1.6**) upon crystallization of a solution having 2,6-dihydroxynaphthalene with complex **4.1.1**. All these products were isolated as crystalline solids in good yields and fully characterized by IR and ^{1}HNMR spectroscopy, elemental analysis and single crystal X-ray diffraction.

^{1}HNMR signals of the complex **4.1.4** as shown in Figure 4.1.6 are observed in shifted positions from the corresponding 2,7-dihydroxynaphthalene and 1,3-bis(4-pyridine)propane. Methylene groups of 1,3-bis(4-pyridine)propane appears at 2.8-3.0ppm and at 1.9-2.2ppm as two mutiplets but these signals appears at 2.2-2.0ppm and at 1.5ppm respectively.

The signal of protons of OH groups of 2,7dhn appearing at 8.4ppm shifts to 8.6ppm in the inclusion complex from the parent compound appearing at 8.4ppm. Signals from OH protons as well as the signal from water present in solvent are very broad showing a fast exchange of the exchangeable protons. The aromatic signals from the three components appear in the region 6.4-8.4ppm and are assigned in the Figure 4.1.6. On the other hand, spectra of equimolar amounts of 1,3-bis(4-pyridine)propane, 2,7-dihydroxynaphthalene show that exchangeable protons of napthalenediol in each case are shifted to low field and the two methylene signals of the 1,3-bis(4-pyridine)propane are shielded.

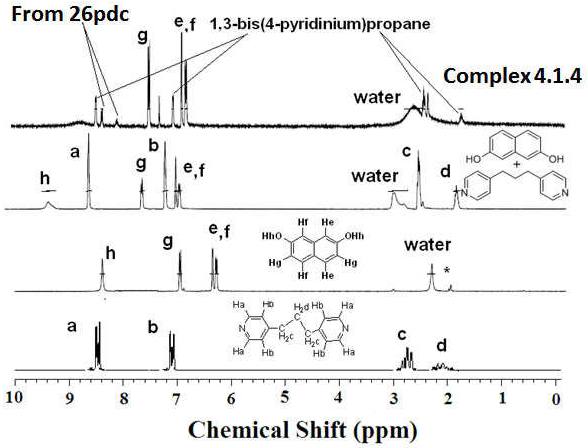

Figure 4.1.6: ^{1}HNMR spectra (DMSO-d_6) of 1,3-bis(4-pyridine)propane, 2,7-dihydroxy-naphthalene, mixture of 1,3-bis(4-pyridine)propane and 1,3-bis(4-pyridine)propane, and complex **4.1.4**.

There are also significant changes in the aromatic region showing significant interactions between the two rings. These indicated that the naphthalenediol interact with the bipyridine derivative and shifts have similar trend to the shift observed in the complex with respect to chemical shifts of parent components. Hence spectral patterns observed in the parent Zinc(II) 2,6-pyridinedicarboxylate in solution support the formation of inclusion compound by the π-stacking of the aromatic units, as well as *via* the interactions of the cations with **27dhn**. The results also support stability of the inclusion complex in solution. In fact, π-stacking in metal complexes[32] and hydrogen bond interactions[33]in phenol-pyridine systems are established. Stoddart and co-workers[34] have demonstrated the utility of bipyridinium functionalized cyclophane scaffolds as π-deficient blocks for the preparation of innumerable interlocked supramolecules, but the host-guest formation ability of bipyridine or bipyridinium cations with 2,7-dihydroxynaphthalene are not strong enough to form isolable host-guest complexes.[34] Advantage of present study is the crystallization and isolation of the inclusion complex.

In complex **4.1.4**, dihydroxynaphthalene and bipyridinium cations have stacking interactions among themselves and they remain in between the layers formed by anions. The bipyridinium cations interact with two adjacent layers of anions through -$NH^{+}\cdots$OOC-interactions. Guest molecules hydrogen bonds with anions and there is π-stacking between guest molecules and organic cations (Figure 4.1.7).

The π-π separations are in the range of 3.497Å- 3.519Å. The anions build a one-dimensional layer along crystallographic *b* axis.

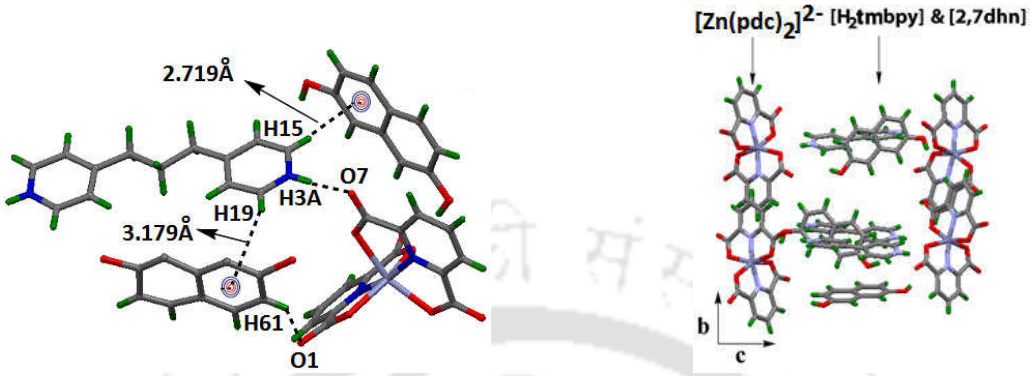

(a) (b)

Figure 4.1.7: (a) Interactions between cations, anions, and guest molecules in crystal structures of complex **4.1.4**. (b) Packing diagram showing zinc dipicolinate layer motifs in the structures of complex **4.1.4**.

Inclusion complex $[H_2bpy][Zn(26pdc)_2]\cdot 2(2,7dhn)\cdot 5H_2O$ **(4.1.5)** was obtained by crystallisation of a solution of complex **4.1.2** with **27dhn**. This complex was also characterized by conventional spectroscopic tools and by determining crystal structure. Dihydroxynaphthalene molecules and cations have their aromatic rings stacked over each other to have charge transfer interactions. The centroid to centroid distance between naphthalenediol ring and bipyridinium cation ring is 3.541Å (Figure 4.1.7). There is also weak C-H···π interactions between a C-H next to the N+H group interacting with a ring of dihydroxynapthalene providing additional strength to the tight packed structure. They are held by templates formed by two anions bridged by one 4,4'-bipyrdiunium dications.

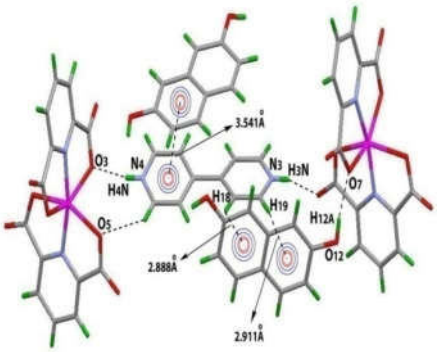

Figure 4.1.8: Interactions between cations, anions, and guest molecules of complex **4.1.5**.

Anions are positioned in layer-like arrangements among a crystallographic direction through -$NH^{+}\cdots$OOC- and holds neutral guest molecules in between the layers.

Hence, anionic layer-like arrangements holds both cations and the neutral guest molecules as shown in Figure 4.1.8.There are strong charge-assisted interactions between $[\mathbf{H_2bpy}]^{2+}$ with **27dhn**, which force an anionic part to adopt conventional π-stacks to accommodate cations together with guest molecules. These complexes have multiple components, hence each component may interact independently with each other. To check such possibilities ^{1}HNMR spectra of complex **4.1.2** in DMSO-d_6 with or without 2,7-dihydroxynapthalene was recorded by maintaining different ratios of host and guest. ^{1}HNMR spectra obtained in independent cases from solutions having molar ratios of complex **4.1.2** and 2,7-dihydroxynaphthalene in 1:0.5 and 1:1 molar are shown in Figure 4.1.8. Comparison of the spectra showed that the signals of **27dhn** were shifted up-field due to interactions with complex **4.1.2** with respect to the signals of the free compound. The signals of hydroxy proton of the 2,7-dihydroxynaphthalene are influenced to a greater extent as they broaden and appear at 9.6 ppm. Signals of protons from $[H_2bpy]^{2+}$ and 2,6-pyridinedicarboxylate parts are shifted downfield with respect to the original peaks of the complex **4.1.2** (Figure 4.1.9), suggesting interactions between these components in the complex. Each proton is assigned in the respective figures. It may be noted that due to acid-base properties of the **27dhn** and **bpy** they interact with each other, and the chemical shifts of a mixture of 2,7-dihydroxynaphthalene and 4,4'-bipyridine in DMSO-d_6 differ from the individual counterpart. These observations suggest that **4.1.2** provide strong interactions to hold the guest molecules and upon crystallization corresponding inclusion complex was isolated.

Complexation induced ^{1}HNMR shifts were previously observed on interactions of different phenolic guest molecules such as 2,7-dihydroxynaphthalene with diphenylglycoluril.[35] Such observations help to establish selective binding of guest molecules. In the present example we find that ^{1}HNMR signals are clear indicator on formation of complex **4.1.4** and **4.1.5** in solution, which in turn are also isolated in solid state and characterized.

While attempting crystallisation of solution of 2,6-dihydroxynaphthalene (**26dhn**) with complex **4.1.1** or with **4.1.2**, it was found that only complex **4.1.1** yield crystalline inclusion complex $[H_2tmbpy][Zn(26pdc)_2]\cdot 2(2,6dhn)\cdot 9H_2O$ (**4.1.6**), whereas complex **4.1.2** fail to yield crystalline inclusion complex but gave back crystals of parent complex and 2,6-dihydroxynaphthalene. The structure of the complex is shown in the Figure 4.1.10.

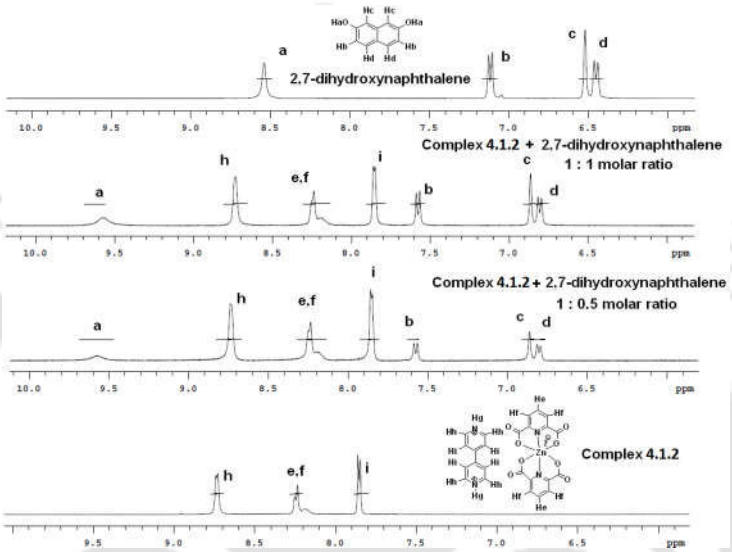

Figure 4.1.9: ^{1}HNMR (DMSO-d_6) spectra of complex **4.1.2**, 2,7-dihydroxynaphthalene and **4.1.2** with different amounts of **27dhn**.

There is strong π-π stacking between one ring of 2,6-dihydroxynaphthalene with one pyridinium ring which is reflected in the centroid to centroid distance is 3.584Å. One of pyridine ring associated in π-interaction is sandwiched by two rings of two independent molecule of 2,6-dihydroxynaphthalene diol. It may be noted that complex **4.1.4** and complex are derived from similar components other than having two different positional isomers of dihydroxynaphthalene units. Thus, the directional hydrogen bonds are guided by these counterparts.

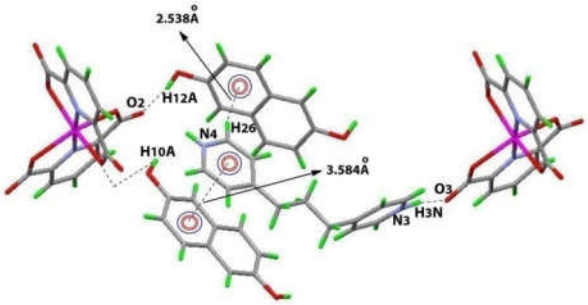

Figure 4.1.10: Self-assembly of complex **4.1.6**

This complex also showed ^{1}HNMR signals from all the three components and the broadening of the signals labile hydrogen atoms are shifted from the signals of parent counterparts showing clearly their participation in hydrogen bond in solution. The IR-spectra of the complex has strong absorption at 3407 cm^{-1} due to +N-H stretching.

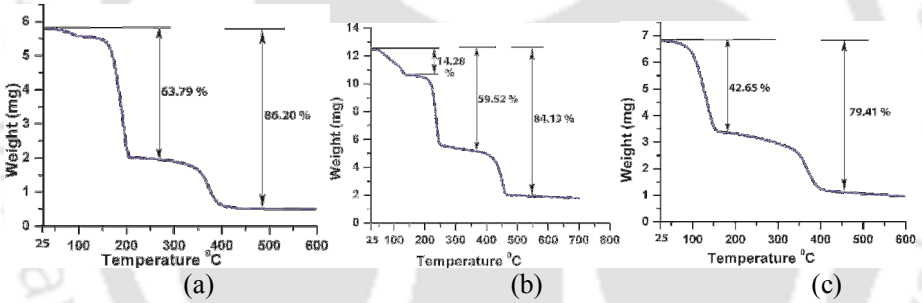

(a) (b) (c)

Figure 4.1.11: Thermograms of complexes (a) **4.1.4**, **(b) 4.1.5** and **(c) 4.1.6.**

Thermal stability of the three complexes **4.14-4.1.6** are compared in Figure 4.1.11. It is observed that each complex has similar thermal decomposition sequence yielding zinc oxide. The zinc oxide formed at 400°C, 460°C and 400°C respectively.

Two inclusion complexes **4.1.4** and **4.1.6** have similar final decomposition temperature despite of having two independent position isomers as host molecules. Whereas, complex **4.1.5** which has different cation than the complex **4.1.3,** it decomposes at slightly higher temperature. This suggests that ion-assisted hydrogen bonds make a difference in thermal stability and that of final decomposition temperature.

4.1.5 Inclusion complex with trihydroxyaromatic

Among trihydroxybenzene phloroglucinol and pyrogallol (pyrogl), latter yielded a zinc complex $[H_2bpy][Zn(26pdc)_2]\cdot 2(pyrogl)\cdot 6H_2O$ (**4.1.7**) upon interaction with complex **4.1.2**. In contrast, similar crystallization of **4.1.1** with pyrogallol did not result in the formation of crystalline inclusion complex, in such case crystalline starting materials were obtained. As in the other cases 4,4′-bipyridine interacts with pyrogallol which is clear in the ^{1}HNMR spectra of a solution containing both the counterparts. The two signals arising from A_2B_2 pattern of bipyridine, splits up to two indepent sets, this is due to non-equivalence of the environment due to interaction with pyrogallol. Aromatic signals of the pyrogallol are shielded upon interaction with bipyridine (Figure 4.1.12).

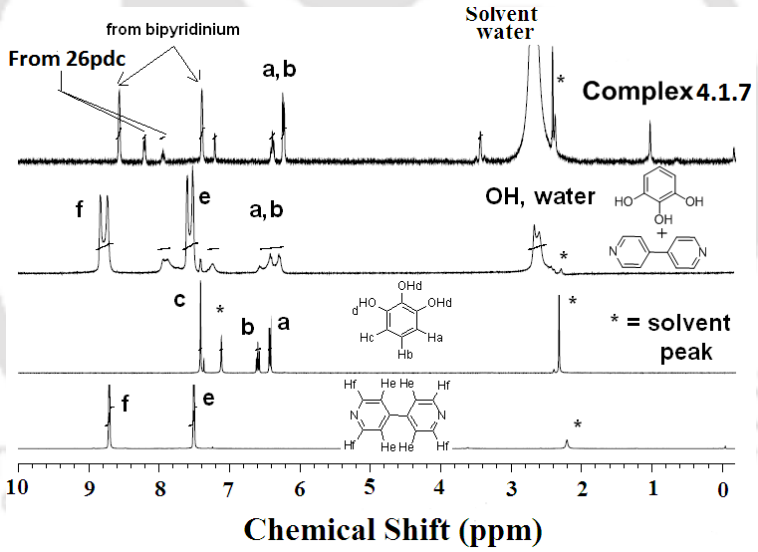

Figure 4.1.12: ^{1}HNMR spectra (DMSO-d_6) of 4,4′-bipyridine, pyrogallol, mixture of 4,4′-bipyridine and pyrogallol and complex **4.1.7**.

In the complex **4.1.7** proton signals of pyrogallol C-H bonds are further shielded so is the aromatic signals of bipyridinium cations, showing strong interactions between the bipyridinium cations. In this case also anions form layer-like arrangements and hold cations and guest molecules. Charge assisted hydrogen bonds and π-stacking are dominant interactions that stabilize packing patterns (Figure 4.1.13).

Packing is comprised of infinite hydrogen-bonded chains of guest and cation with anionic unit. Due to electrostatic nature donor-acceptor distances of hydrogen bonds between 4,4′-bipyridyl nitrogen and carboxylate oxygen atoms are relatively short, falls in the range 1.738Å -1.763Å. Pyragallol included complex **4.1.7** has six water molecules of crystallization; these water molecules can be removed by heating upto 150°C, but heating beyond such a temperature it loses the pyrrogallol, cations and ligands in two steps to finally form zinc oxide at 460°C.

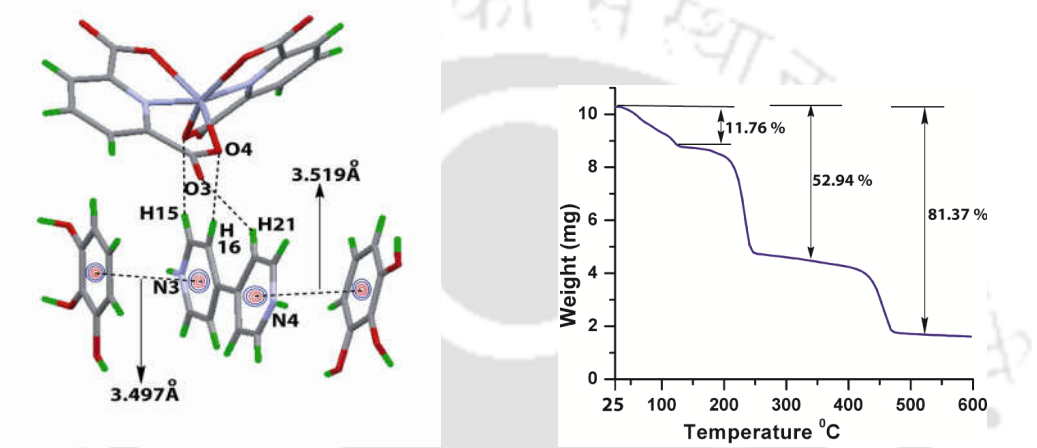

Figure 4.1.13: (a) Interactions between host and guest in complex **4.1.7**. (b) Thermogram of complex **4.1.7.**

4.1.6 Summary

From a series of inclusion complexes of hydroxyaromatics with two zinc(II)-2,6-pyridinedicarboxylate have shown that extensive π-stacking arrangements in each inclusion complex. Guest inclusion is largely influenced by the cations such as $[H_2bpy]^{2+}$ or $[H_2tmbpy]^{2+}$ cations. Based on the ability to replace stacks between 2,6-pyridinedicarboxylates groups a modular approach to recognize 4-nitrophenol has been achieved.

We have also established that the supramolecular interactions between the parent parts with different hydroxyaromatic guest molecules exist in solution and such interactions between the cations and hydroxyaromatics are reflected in solid state packing patterns of inclusion complexes. Due to directional hydrogen bonds which are assisted by charge assisted interactions, the packing patterns differ and help in preference in getting crystalline compounds in selective cases.

Part B

Lanthanum(III) tris(2,6-pyridinedicarboxylate) complex in inclusion of aromatic guests

4.2.1 Background

Supramolecular assemblies of inorganic complexes[36] provide scope secondary coordination sphere which are analogous to inorganic biological sites.[37] Mimicking such secondary sphere generated through inorganic templates for recognizing guests[38] such as polyaromatic compounds are important. Polyaromatic hydrocarbons are pollutant and their selective removal at low concentration is important.[39] Self-assemblies of 2,6-pyridinedicarboxylate (abbreviated here as **26pdc**) complexes provide information on (a) multi-component crystals, (b) complexes having different nuclearities, (c) stabilization of organic self-assemblies and (d) thermal degradation. Lanthanum-26pdc coordination polymer is a structurally characterised polymer,[40] molecular recognition property by it has not been explored. This could be due to poor solubility of this polymer, hence we sought for alternative soluble complexes for molecular recognition. Lanthanum ion is relatively large size than commonly used metal ions hence should have higher coordination number to serve as better template. With such background of lanthanide complexes[41], we studied a nona-coordinate lanthanum complex anion shown in Figure 4.2.1 for molecular recognition of aromatic nitro compounds and dihydroxynpthalenes.

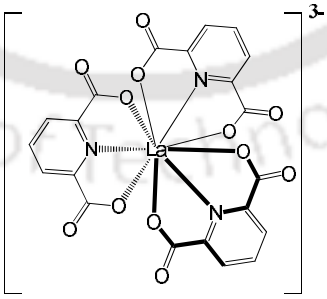

Figure 4.2.1: Complex anion $[(26pdc)_3La]^{3-}$.

4.2.2 Mononuclear and dinuclear lanthanum 2,6-pyridinedicarboxylate complex

Upon mixing lanthanum nitrate hexahydrate with 2,6-pyridinedicarboxylic acid and 4,4'-bipyridine a mononuclear lanthanum complex $(H_2bpy)_3[La(26pdc)_3]_2.15H_2O$ (**4.2.1**) is formed (Scheme 4.2.1). Complex is comprised of three chelating **26pdc**, and has nona-coordinated environment around lanthanum which is illustrated in Figure 4.2.1(a). Each complex anion shares charges from one and half 4,4´-bipyridinium cations. Anions of mono-nuclear complex in its packing pattern occur as pairs, they are located next to each other and are stacked as shown in Figure 4.2.2(b). Anions of the complex are flanked by bipyridinium cations. 4,4´-Bipyridinium cations adopt two independent types of geometries; one set is planar and other is puckered. Puckered structures of cations are due to C-C rotation occurred as a part of packing requirement so as to form strong electro-statistically guided hydrogen bonds between +N-H bond of cation with oxygen atom of the carboxylate of neighboring anion. In self-assemblies of inorganic complexes π-stacks have special status and many complexes have packing guided by such interactions.[42] One pyridine ring of the puckered 4,4'-bipyridinium cation of the complex **1** lies parallel to aromatic plane of **26pdc**. Centriod to centroid distance between rings forming such a stack is 3.83Å, suggesting presence of π -interactions. When same reaction that was used in synthesis of complex **4.2.1** was carried out at 70°C, it yielded a dinuclear complex $(H_2bpy)[La_2(26pdc)_4(H_2O)_4].3H_2O$ (**4.2.1**). Two different coordination modes are found in carboxylate groups of **26pdc** coordinating to lanthanum to form the complex **4.2.2**. Hence, **26pdc** ligands present in this dinuclear complex utilize, one set of **26pdc** as tridentate and other set as pentadentate. Pentadentate **26pdc** provides three chelating sites to a lanthanum ion and it provides two bridging chelating sites to another lanthanum ion. Cations of the dinuclear complex have π-stacking among them with distance between parallel rings is 3.61Å as shown in Figure 4.2.2(c). In this complex anions self-assemble to form channel-like structure and cations are held within the channel like structure. A coordination polymer formed from reaction of lanthanum nitrate with $26H_2pdc$ without 4,4'-bpy was reported earlier.[40] This coordination polymer is insoluble in common solvents and is not suitable to study molecular recognition properties.

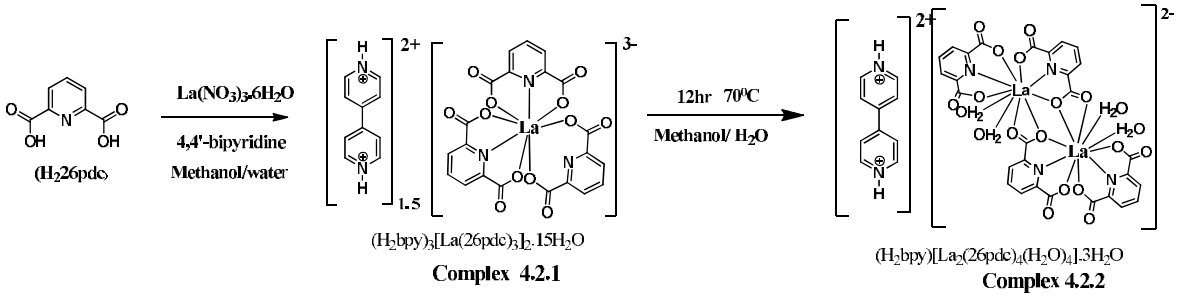

Scheme 4.2.1: Formation of mononuclear and dinuclear lanthanum complexes.

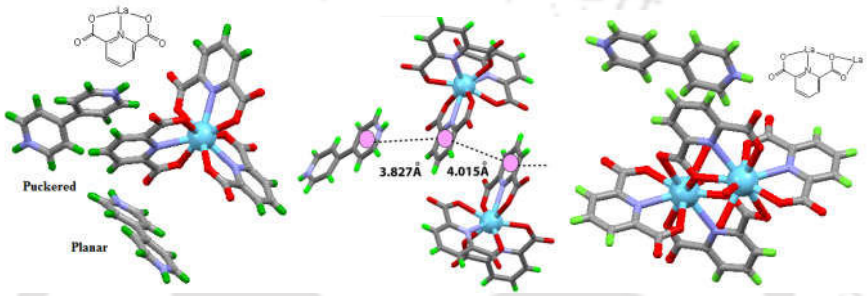

(a) (b) (c)

Figure 4.2.2: Structure of (a) Complex **4.2.1**, (b) Stacking of aromatic rings of Complex **4.2.1**, (c) Complex **4.2.2** (insets are binding modes of **26pdc**).

Thermogravimetric study shown in profiles in Figure 4.2.3(a) and Figure 4.2.3(b) for complex **4.2.1** and **4.2.2** showed that on heating at 450ºC -500ºC, both these complexes degrade to lanthanum oxide. A fresh sample of the residue of samples heated at 500ºC for 1h shows its PXRD pattern that corresponds to lanthanum oxide, but the oxide once formed in situ is highly hygroscopic. It absorbs moisture to form lanthanum hydroxide on standing, which is reflected in sample which is left in open atmosphere for an hour or so Figure 4.2.3(c). Generally lanthanum oxide is highly hygroscopic and is well known to form lanthanum hydroxide under ambient conditions.[43] Complex **4.2.1** has ^{1}HNMR has characteristic A_2B_2 pattern of bipyridinium cation showing signals at 8.54ppm and 8.29ppm (Figure 4.2.1). Three hydrogen atoms of each **26pdc** ligand appear as broad unresolved peaks centering at 8.45ppm, whereas the +N-H peak appeared at 9.18ppm.

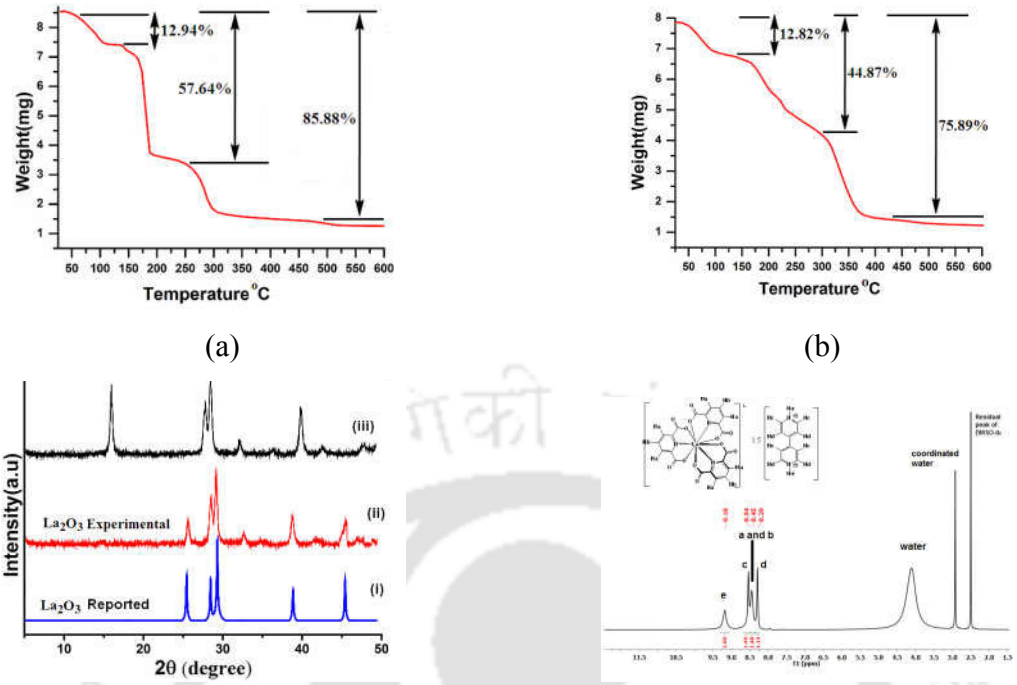

Figure 4.2.3: Thermograms of complex (a) **4.2.1** and (b) **4.2.2**. (c) Powder XRD of (i) La_2O_3 reported in literature, (ii) residue of complex **4.2.1** after heating at 500ºC showing formation of La_2O_3, (iii) La_2O_3 sample exposed to ~80% humidity for 2 hr. (d) ^{1}H-NMR spectra (600MHz, DMSO-d_6) of complex **4.2.1.**

4.2.3 Guest inclusion by complex 4.2.1

Water soluble hosts for host-guest complexes of phenolic compounds[44] is important to identify receptors for detection and separation of organic pollutant. Complex **4.2.1** and **4.2.2** are soluble in water and they have aromatic parts hinged lanthanum which should be suitable to form host-guest complexes with aromatic compounds in aqueous medium. On the other hand, these complexes are derived from 2,6-pyridinedicarboxylic acid which has medicinal value.[45] Solution of complex **4.2.1** and various dihydroxyaromatic compounds in methanol upon crystallization resulted crystalline complexes.

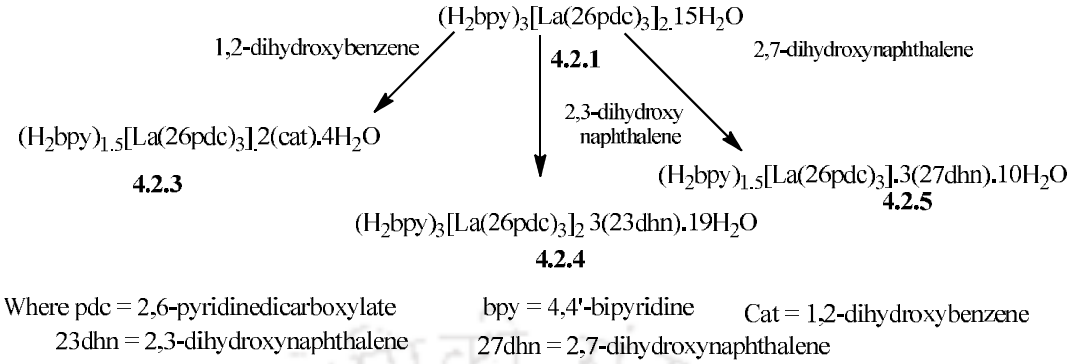

Scheme 4.2.2: Formation of host-guest complexes.

Accordingly, complex **4.2.1** reacted with 1,2-dihydroxybenzene, 2,3-dihydroxynaphthalene, 2,7-dihydroxynaphthalene to form inclusion complexes $(H_2bpy)_{1.5}[La(26pdc)_3].2(cat).4H_2O$(**4.2.3**),$(H_2bpy)_3[La(26pdc)_3]_2.3(23dhn).19H_2O$(**4.2.4**) $(H_2bpy)_{1.5}[La(26pdc)_3].3(27dhn).10H_2O$ (**4.2.5**) (Scheme 4.2.2) were obtained. These inclusion complexes have good solubility in solvents, thus ^{1}HNMR spectra of each complex was measured.

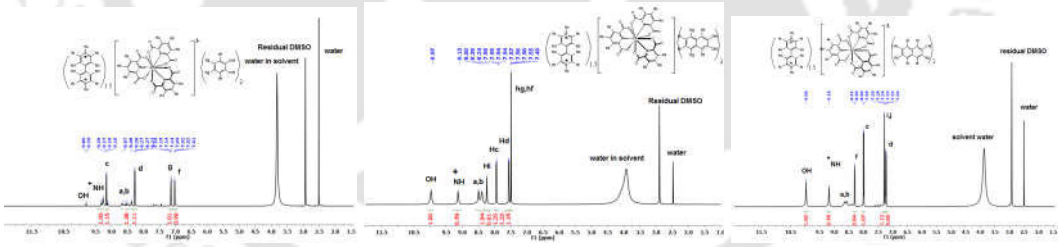

(a) (b) (c)

Figure 4.2.4: ^{1}H-NMR spectra (600MHz, DMSO-d_6) of complex (a) **4.2.3**, (b) **4.2.4**, (c) **4.2.5**.

Each of these complex has shown A_2B_2 pattern of peaks that are characteristic of 4,4´-bipyridinium cation, but their positions varied from complex to complex (Figure 4.2.4). The corresponding host parts signals are assigned in the figure suggests that there not significant changes in the aromatic signals but the OH and +NH signals are drastically affected.

Possible interaction of lanthanide complex **4.2.1** was checked by titrating it with 1,2-dihydroxybenzene in a solution in DMSO-d_6. From the ^{1}HNMR titration it was found that only the proton exchange sharpening of the +N-H peak took place as illustrated in Figure 4.2.5.

There was no significant shift in the ring protons of the 1,2-dihydroxybenzene which are observed as A_2B_2 pattern at 7.14ppm and 7.01ppm. This titration study shows that the hydrogen bond scheme involving labile hydrogen atoms of 1,2-dihydroxybenzene changes so as that of 4,4'-bipyridinium cation upon change of concentration of titrant, thus supporting host-guest interactions through formation of hydrogen bond involving +N-H which has electrostatic contribution to form strong hydrogen bonds.

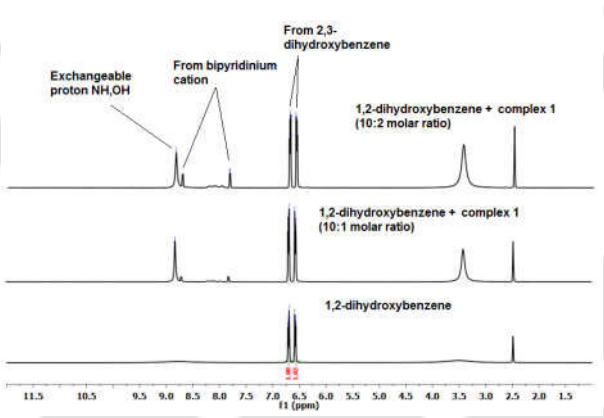

Figure 4.2.5: ^{1}H-NMR (600MHz, DMSO-d_6) of 1,2-dihydroxybenzene with different amounts of complex **4.2.1**

The crystal structures have shown that in the case of complex 1,2-dihydroxybenzene hydrogen bonds with one +N-H of 4,4'-bipyridinium cation and other +N-H is anchored to a carboxy group **26pdc** of complex anion (Figure 4.2.6a) are formed. This provides a planar organic template of cation and anion holding the host, such templates are held parallel on top of one another so that opposite ends bear tris-(26pdc)lanthanum anion.

Templates formed by anions with cations to hold 2,3- or 2,7-naphthalenediols are similar but different from the host template for 1,2-dihydroxybenzene. Two tris-(26pdc)lanthanum anions are bridged with a 4,4'-bipyridinium cation by hydrogen bonds to hold naphthalenediol guest molecules. These results suggest of cationic helps in formation of suitable template in each case to bind hydroxyaromatics (Figures 4.2.6b and Figure 4.2.6c). This is one reason for present molecular recognition by complex **4.2.1**.

In last part it has been shown that Zinc-26pdc complex having 4,4'-bipyridinium dications retain stacking interactions among anions which helps to recognize 4-nitrophenol. Packing patterns of complexes **4.2.4** and **4.2.5** show that tris(26pdc)lanthanum anions occur as interacting π-stacked pairs, having a similarity to packing found in complex **4.2.1**. Whereas, complex **4.2.3-4.2.5** lacks stacking interactions among anions, but stacking between aromatic rings of cation with cation, anion with guest takes place as illustrated in Figure 4.2.6.

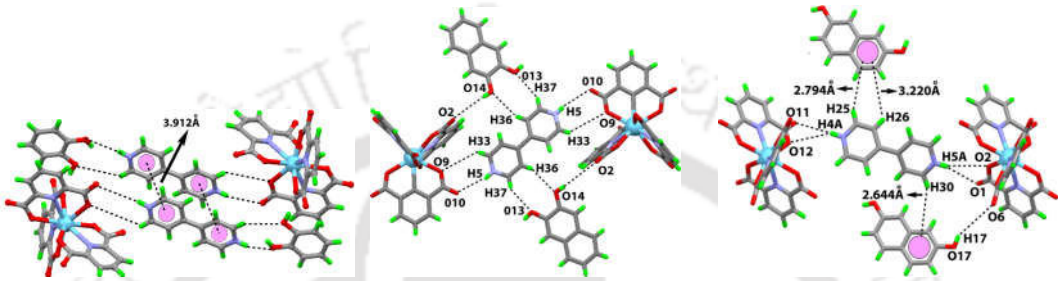

(a) (b) (c)

Figure 4.2.6: Hydrogen-bonds among host and guest molecules in (a) Complex **4.2.3**, (b) Complex **4.2.4**, (c) Complex **4.2.5** (water of crystallization molecules are omitted for clarity).

Solid samples of complex **4.2.1** and **4.2.2** have broad emission peaks at 475nm but guest included complex **4.2.3-4.2.5** are non-fluorescent (Figure 4.2.7). When we measured solid state emission spectra of earlier reported coordination polymer of lanthanum 2,6-pyridinedicarboxylate also showed emission at 475nm upon excitation at 350nm. Thus, cations do not influence the fluorescence emission of these three complexes. Such emission observed from solid sample is attributed to a ligand to metal charge transfer.

Quenching of fluorescence emission of the complexes **4.2.3-4.2.5** are not surprising due to extensive π-stacking observed in these complexes and π-stacking generally known to cause quenching of fluorescence emission.[46]

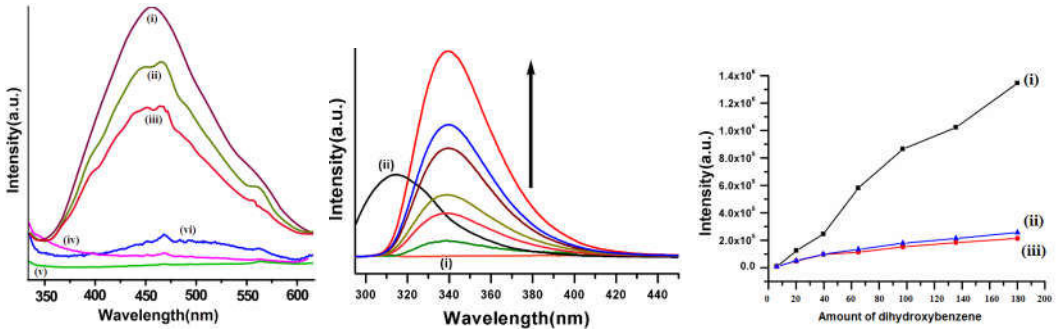

(a) (b) (c)

Figure 4.2.7: (a) Fluorescence emission of solid sample of (i) lanthanum 2,6-pyridinedicarboxylate coordination polymer, (ii-vi) complex **4.2.1** to complex **4.2.5**. (b) Fluorescence emission of a solution 1,2-dihydroxybenzene when added to a solution of complex **4.2.1** (i)complex **4.2.1** alone in water (10^{-5} M, 3 ml), (ii) of 1,2-dihydroxybenzene alone in water and rest are on addition of 1,2-dihydroxybenzene (10^{-5} M, 20 µL in each aliquot). (c) Relative fluorescence emission intensities of dihydroxyaromatics at respective emission wavelength upon addition to a solution of complex **4.2.1** (i) 1,2-dihydroxybenzene, (ii) 1,4-dihydroxybenzene, (iii) 1,3-dihydroxybenzene. (10^{-5} M, 10 µL in each aliquot, to a solution of complex **4.2.1** in water (10^{-5} M, 3ml, λ_{ex} = 310nm).

Large differences in fluorescence emission of these complexes in solution and in solid of the complexes are observed. In solution the complex **4.2.1** and **4.2.2** are non-fluorescent. An aqueous solution of complex **4.2.1** has negligible fluorescence emission showing a very weak at 309nm (Figure 4.2.7); it does not show emission peak that was observed in solid sample. Dihydroxyaromatic compounds in water, namely 1,2-dihydroxybenzene emits at 310nm, 1,3-dihydroxybenzene emits at 320nm and 1,4-dihydroxybenzene emits at 340nm. Upon addition of solution of these three positional isomers independently to three independent solutions in water of complex **4.2.1**, intensity of emission increases. Such increase is obviously due to increase in concentration of the dihydroxy aromatic in solution but in each case characteristic shift is observed.

In the cases of 1,2-dihydroxybenzene and 1,3-dihydroxybenzene, observed shifts are towards higher wavelength, whereas such emission with 1,4-dihydroxybenzene shifts toward shorter wavelength. Addition of 2,3- and 2,7-naphthalenediol solutions to complex **4.2.1** caused no shift in position of respective wavelength of emission of diol.

Relative increase intensity of emission upon interactions of three isomeric dihydroxybenzene with complex **4.2.1** are 1,2-dihydroxybenzene >> 1,3-dihydroxybenzene ≡ 1,4-dihydroxybenzene. These results suggest that change in emission intensity of complex **4.2.1** in solution does not necessarily reflect the weak interactions seen in the complexes in solid state. Earlier, it was shown that a solution of 1,4-dihydroxybenzene shows fluorescence quenching with cobalt complexes and such changes involve excited state of 1,4-dihydroxybenzene.[47a] In the present case, lanthanum ions are embedded by **26pdc** ligands and unpaired electrons of lanthanum are concealed to cause quenching in second coordination sphere, hence small shifts and enhancement of fluorescence of dihydroxy-aromatics with complex **4.2.1** is due to hydrogen bonds of phenolic OH groups with complex anions. Synchronous fluorescence technique was earlier used for simultaneous detection of 1,2- and 1,4-dihydroxybenzene[47b], but using the lanthanum complex **4.2.1**, not only provide selectivity in detection but also able to trap 1,2-dihydroxybenzene as inclusion complex. Dinuclear complex **4.2.2** has a compact self-assembled structure having less possibility to interact with dihydroxy aromatics, its coordinated water molecules are associated with hydrogen bond inhibiting interactions with guest molecules. As a consequence of which, dinuclear lanthanum complex 4.2.**2** does not show change in fluorescence of a dihydroxyaromatics in solution, hence distinctions of complex **4.2.1** and **4.2.2** is possible. Cyclodextrin[43], pyromelleticdiimide[48] form host-guest complexes with hydroxyaromatics. Though present host-guest complex have extensive π-stacking there are certain distinguishable features among them. Firstly, in present case anionic building blocks are nona-coordinated tris chelated complex which has possibility to adopt π-stacks in all three-dimensions with respect to metal ion and comprise of aromatic cations. Hence, propensity to have interplay of anion-anion, anion-cation stacking provides varieties in present cases.

4.2.4 Summary:

In conclusion, inclusion of more than one moderate size aromatic guest molecules by nonacordinate lanthanum-pdc complex is possible due to the electrostatically guided self-assemblies. Cations are responsible to provide templates in state formed by assembling of anions and depending on guests such template vary. 1,2-Dihydroxybenzene interacts at an terminal end of cation of sub-assembly between cation and anion; whereas dihydroxynaphthalenes are held by templates formed among two anions and a 4,4′-bipyridinium cation. Solid state studies on fluorescence and solution fluorescence properties of complex **4.2.1** upon interactions with dihydroxyaromatic compounds are different. Thus this study is a clear demonstration of role of averaged out weak interaction schemes reflecting properties to the rigid orderly arrangements in solid state.

Part C

Inclusion complexes of tris-(1,10-phenanthroline)nickel(II)nitrate

4.3.1 Background

In last two part of this chapter utility of 2,6-pyridinedicarboxylate complexes have been shown with two different types of situations, one having two π-decorating ligands around the zinc as metal site and other having three ligands around lanthanum. In these two classes of examples the charges on the central metal ions were +2 and +3. To understand further on guest binding by π-decorated ligands, a simple well established cationic tris(1,10-phenathroline)nickel(II) nitrate complex **4.3.1** shown in Figure 4.3.1 chosen. This complex is stable, easy to prepare and have qualifications to assemble π-aromatics as described in earlier part of the chapter. Moreover nickel complexes with π-decorated ligands have been shown to form host-guest complexes through π-interactions.[49] Furthermore, such a complex bears fluorescence part as ligand which is an added advantage to study their interactions. A series of nitro-phenols and nitro-carboxylic acids were studied and the partner molecules from which crystal structures are obtained are listed in Figure 4.3.1.

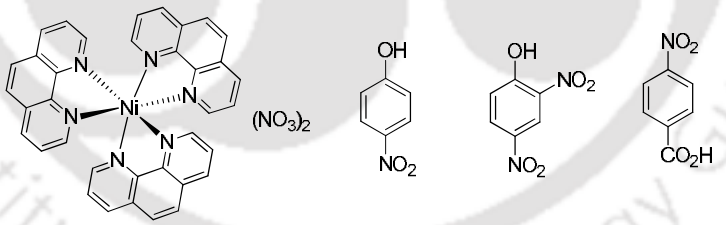

4.3.1

Figure 4.3.1: Host complex **4.3.1** and different nitroaromatic guests.

4.3.2 Synthesis of host guest complexes of 4.3.1

Tris-(1,10-phenathroline)nickel(II) complex is easily prepared by reacting 1,10-phenanthroline (**phn**) with nickel nitrate.[50] This complex when crystallized from aqueous methanol it gave crystals of complex **4.3.1** as dihydrate. Guest inclusion of several nitro aromatics such as 4-nitrophenol, 3-nitrophenol, 2,4-dinitrophenol, 2,4,6-trinitrophenol, 2-nitrobenzoic and 3-nitrobenzoic acid with **4.3.1** were studied by performing simple evaporation of respective homogeneous solution. But only three inclusion complexes namely with 4-nitrophenol, 2,4-dinitrophenol and 3-nitrobenzoic acid were obtained. The complexes were characterized by determining their crystal structure. Infra-red spectra of the complex **4.3.1,** has ionic nitrate stretching at 1338 cm^{-1}, whereas, such peak for complexes **4.3.2-4.3.4** appear in the ranges of 1340-1344 cm^{-1}. Stretching of nitro group/s of nitroaromatics of complexes **4.3.2-4.3.4** appears as sharp peak in the region of 1382-1365 cm^{-1}. Each complex has a sharp C=C stretch due to presence of 1,10-phenanthroline in the ranges of 1620-1626 cm^{-1}. In addition to these C=C stretch of aromatic ring of nitroaromatic in these complexes **4.3.2-4.3.4** appears at 1585 cm^{-1}, 1590 cm^{-1} and 1518 cm^{-1} respectively. Molar conductance values obtained from aqueous solutions of the complexes **4.3.2-4.3.4** are supportive of their 2:2 electrolytic natures.

Crystal structure of the complex $[Ni(phn)_3](NO_3)_2.Hnp.2H_2O$ (**4.3.2**) is shown in Figure 4.3.2(a). Cationic part of inclusion complex of **4.3.2** has a conventional octahedral geometry as found in $[Ni(phn)_3](NO_3)_2$ complex. 4-Nitrophenol molecules of the complex **4.3.2** are arranged as head to head orientations in its solid state packing pattern. Such pairs of 4-nitrophenol guest molecules are held over planar ring of one 1,10-phenanthroline ligand in the complex. Two 4-nitrophenol molecules appear in close vicinity in the packing, and show short O···O contact 2.468Å. This type of short contact may be attributed to the pull and push on 4-nitrophenol molecule to form π-stack and to form hydrogen bond between them. The extra strength to the self-assembly of complex **4.3.2** comes from electrostatic contributions of ions, which probably helps to compensate repulsive interactions if at all present to settle the positions of the two 4-nitrophenol neighbor molecules in the lattice. Nitrate ions are aquated and are located at two symmetry independent positions. Anions of the complex **4.3.2** form hydrogen bonded network.

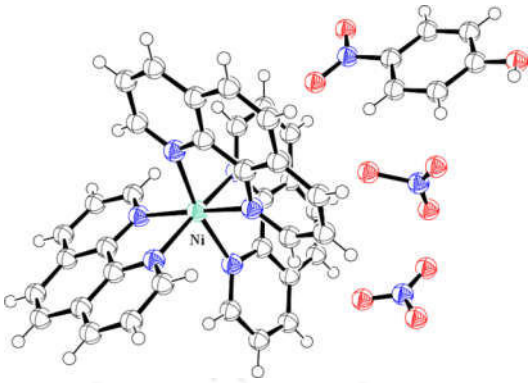

Figure 4.3.2: (a) Structure of complex **4.3.2** (ORTEP drawn with 40% thermal ellipsoids and water molecules are omitted for clarity).

Since, three 1,10-phenanthroline ligands are attached to one nickel ion in the complex, cationic component has large hydrophobic contributions to the packing pattern, which should disfavor accommodation of interstitial water molecules. But hydrogen bonded anion-water network holds the water molecules in the lattice. Examples of anion water clusters are observed in substantial numbers of 1,10-phenanthroline complexes.[51] Though their origin have not been addressed, our observations on anionic water networks holding the cations suggests that vacant hydrophobic sites in lattice enforces water molecules to coordinate to anions to stabilize within the lattice to provide a tight packed structure. Due to crystallographic disorder associated with hydrogen atoms, it was not possible to locate the hydrogen atoms on the oxygen atoms of water molecules; hence the cyclic structures of such aquated anions are not discussed.

Complexes **4.3.3** and **4.3.4** belong to a special category of complexes which posses two $[Ni(phn)_3]^{2+}$ cations in each case and these cations are neutralized by dissimilar anions distributed over cations. Four cationic charges from two complex cations is neutralized with the aid of odd numbers of two structurally dissimilar mono-negative anions. Complex **4.3.3** has three 2,4-dinitrophenolate and a nitrate which are distributed over two $[Ni(phn)_3]^{2+}$ ions. Similarly, complex **4.3.4** has two $[Ni(phn)_3]^{2+}$ ions whose charges are compensated by negative changes of one 3-nitrobenzoate and three nitrate ions. Hence, these two complexes may be considered as dimeric complexes having two symmetry independent complex cations. Both complexes have lattice water molecules contributing to the respective packing pattern. Structures of complexes **4.3.3** and **4.3.4** after omitting the lattice water molecules are drawn in Figure 4.3.3.

In complex **4.3.3**, there are two non-equivalent 2,4-dinitrophenolate. One set of anions comprising of two independent 2,4-dinitrophenolate ions show crystallographic disorder.

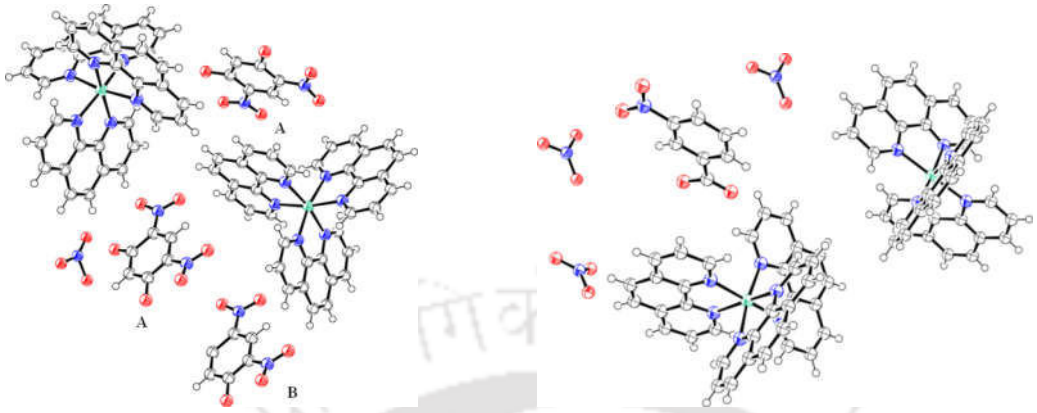

(a) (b)

Figure 4.3.3: Structure of (a) Complex **4.3.3** (A = 2,4-dinitrophenolate having two oxygen atom distributed at two crystallographically equivalent positions, B = 2,4-dinitrophenolate). (b) Complex **4.3.4** (ORTEPs are with 40% thermal ellipsoids and water molecules in each case are omitted).

Two 2,4-dinitrophenolate ions in the complex **4.3.3** have electron densities of oxygen atoms equally distributed across two crystallographic equivalent positions in the individual ring of 2,4-dinitrophenolate ion (marked as A of Figure 4.3.3 (a). In this complex the other crystallographic independent 2,4-dinitro phenolate anion marked as B in Figure 4.3.3 (a) is without crystallographic disorder.

4-Nitrophenolate ions are in almost parallel manner above a 1,10-phenanthroline ligand in complex **4.3.2**, whereas, 2,4-dinitrophenolate ions in complex **4.3.3** are held by anion-π interactions through O···π aromatic interactions of two nitro groups. Complex **4.3.4** has 3-nitrobenzoate ions parallel over 1,10-phenanthroline ligand and an oxygen atom from nitro group is involved in side-on O···π interactions with 1,10-phenanthroline ring of one ligand as illustrated in Figure 4.3.3 (b). These O···π interactions may be suggested on the basis of the perpendicular projection of the oxygen atom with an appropriate distance from the π-cloud of 1,10-phenanthroline. Generally O···π interactions fall in the range of 3.5Å,[52] and in the complex **4.3.3** and complex **4.3.4,** the O···π distances are in the ranges of 2.96Å-3.4Å.

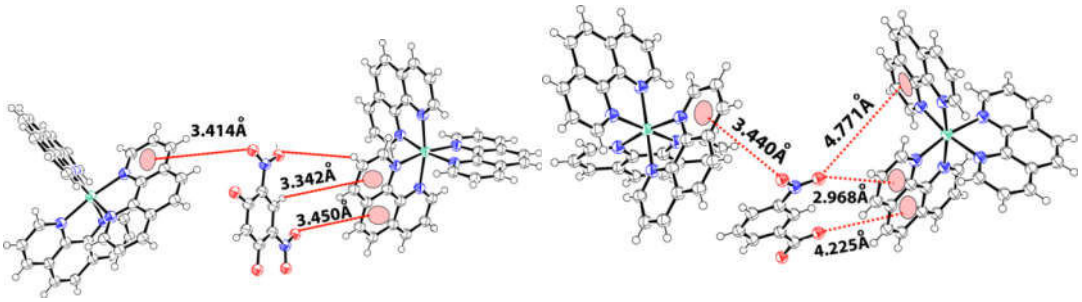

(a) (b)

Figure 4.3.4: Anion-π interactions in the complex (a) **4.3.3** and (b) **4.3.4**.

Although, some other distances beyond 3.5Å are included in Figure 4.3.3(a) and (b), such a distance greater than 3.5Å is too large to have effective interactions. Thus, those are not significant, showing that only the nitro groups participate in such interactions. There are several orientations of nitro-group to provide O···π interactions with a π-system[53] in the present case the O···π interactions are head to face interactions. The overall weak interactions in these three inclusion complexes that control the packing patterns are diagrammatically given in Figure 4.3.5. From the schematic diagrams arrived at from crystal structures show that in these complexes the O···π and C-H···π interactions are predominant so as the C-H···O interactions.

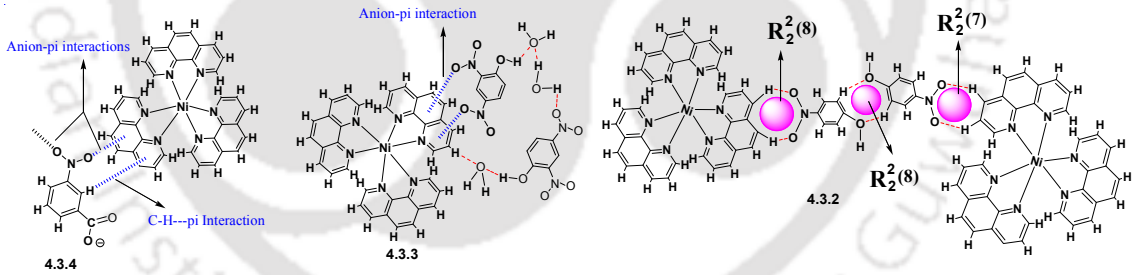

Figure 4.3.5: Schematic representation showing some prominent interactions in self-assemblies of complexes **4.3.2-4.3.4.**

Solid samples of complexes **4.3.1-4.3.4** have characteristic d-d transitions[54] for $^3A_{2g} \rightarrow {}^3T_{1g}$ (P) transitions at 406nm, 396nm, 468nm and 380nm, respectively. These complexes have $^3A_{2g} \rightarrow {}^3T_{1g}(F)$ transitions at 534nm, 525nm, 543nm and 532nm respectively.

The absorptions at 788nm for complex **4.3.1**, 792nm for complex **4.3.2**, 789nm for complex **4.3.3** and 790nm for complex **4.3.4** are assigned $3A_{2g} \rightarrow 3T_{2g}$.

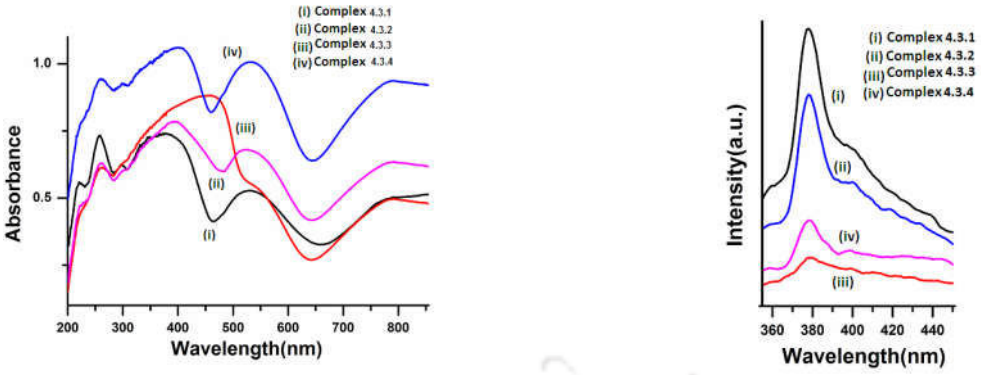

(a) (b)

Figure 4.3.6: (a) UV-Vis spectra of solid samples of complexes (i) **4.3.1** (ii) **4.3.2,** (iii) **4.3.3 and**, **(iv) 4.3.4**. (b) Fluorescence emission of solid samples of complexes upon excitation at 340nm.

Solid samples of these complexes are weakly fluorescence upon excitation at 340nm. This emission is due to π-π emission, and among them complexes **4.3.3** and **4.3.4** are quenched, where emission intensities complexes **4.3.1** and **4.3.2**.

The anion-π interactions causes fluorescence quenching,[55] O···π interactions are very prominent in the complexes **4.3.3** and **4.3.4**. This causes the fluorescence quenching in these complexes. While the complexes **4.3.1** as well as **4.3.2** do not have such interaction makes a fluorescence ON state in these two examples.

4.3.3 Study on interactions of 4.3.1 with nitroaromatics in solution

UV-visible spectral study showed interactions between nitroaromatic compounds with complex **4.3.1** in solution. For example, a solution of the complex **4.3.1** on addition of 4-nitrophenol shows a new absorption peak at 358nm. Such peak observed from a solution of 2,4-dinitrophenol and complex **4.3.1** appears at 371nm, whereas for 3-nitrobenzoic acid and complex **4.3.1** such new peak is at 307nm (Figure 4.3.6). In solution the complexes show strong absorptions due to π-π transition originating from 1,10-phenanthroline in the ranges of 313-368nm. Nitroaromatics generally interact with electron-rich π-aromatic systems; such effect quenches fluorescence of the donor fluorescent molecule.[56]On the other hand, anion bound to electron deficient aromatic compound causes visible spectral changes.[57] Fluorescence emission of the complex **4.3.1** was dependent on solvent. In the case of solvent like methanol and DMF single emission peak at 378nm was observed upon excitation at 340nm.

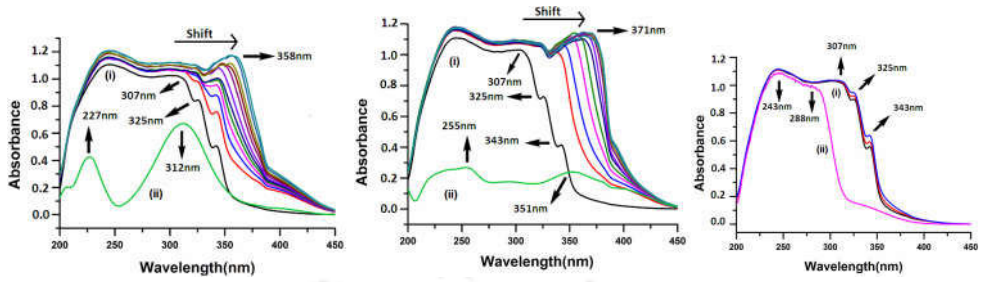

(a) (b) (c)

Figure 4.3.7: UV-Vis titration with complex **4.3.1** with (a) 4-nitrophenol, (b) 2,4-dinitrophenol, (c) 3-nitrobenzoic acid. In each case (i) complex **4.3.1**(10^{-4} M in methanol), (ii) respective nitroaromatic compound (10^{-4} M, 3 ml in methanol) and rest are upon addition of respective nitroaromatic compound to a solution of complex **4.3.1** (10^{-4} M, 20 μL in each aliquot).

Whereas the complex **4.3.1** in DMSO shows dual fluorescence emits at 378nm and 411nm. The emission peak at 411nm has vibrational features by showing the closely related peaks. Dual fluorescence arises due to exciplex formation in dimethylsulphoxide. It may be noted that phenanthrene derivatives are well known for exciplex formation in dimethylsulphoxide solution to show emission at two widely separated wavelengths, where the longer wavelength emission has broad peaks.[58]Exciplex formation in case of the phenanthroline complex is common. [59] The dual fluorescence shown by the complex in DMSO showed vibrational features in the longer wavelength peak probably due to the vibrational relation of excited state.[60] Thus, dual emission in DMSO shown by $[Ni(phn)_3](NO_3)_2$ is not an exception and so as the single emission in other solvents.

DMSO solvent being highly polar segregates the π-stacking among the $[Ni(phn)_3]^{2+}$ cations and hence in addition to the fluorescence emission of conventional π-stacked system, there is new excimer emission at longer wavelength. Irrespective of dual or single emission shown by complex **4.3.1** in different solvents the intensity of emission gets quenched upon addition of nitroaromatic compounds. 4-Nitrophenol, 2,4-dinitrophenol, 3-nitrobenzoic acid of which we obtained crystal structures of nickel complexes having nitroaromatic as component were interacted in solution to see the fluorescence changes.

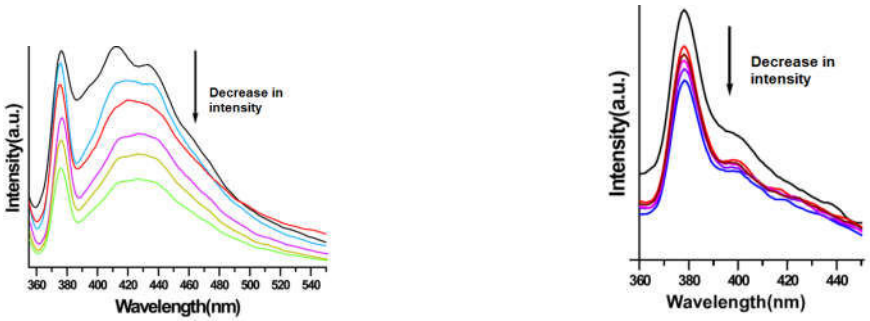

(a) (b)

Figure 4.3.8: Changes in fluorescence spectra of (a) complex **4.3.1** in DMF (10^{-5} M in 3 ml) and rest are upon addition of 4-nitrophenol to the solution (20 μL, 10^{-5} M in each aliquot). (b) An identical experiment in methanol.

In different solvents similar quenching were observed but extent of change caused by each nitroaromatic had difference. The plots of emission intensity against amount of nitroaromatics in three different solvents, methanol, DMF or DMSO are shown in Fig. 4.3.7(a).Association constants of the nitroaromatic compounds were determined by isothermal calorimetry titration using single binding site model (Figure 4.3.8). Among the three nitroaromatic compounds studied the affinity of 2,4-dinitrophenol to interact with complex **4.3.1** is highest. Association constants of 4-nitrophenol, 2,4-dinitrophenol, 3-nitrobenzoic acid with the complex **4.3.1** were found to be 514 M^{-1}, 924 M^{-1}, 1040 M^{-1} respectively. Number of nitroaromatic molecules interacting in solution with per $[Ni(phn)_3](NO_3)_2$ molecule are dependent on substrates. For example, there are approximately four 2,4-dinitrophenol molecules interact with one molecule of complex **4.3.1**, whereas two molecules of 4-nitrophenol or 3-nitrobenzoic acid can interact independently with one molecule of $[Ni(phn)_3](NO_3)_2$. These clearly indicate that the compositions found out by determining structures are different from the one in solution. This is also obvious as the binding constant determined in solution donot refer to the inclusion complex but provides the type of association between complex **4.3.1** and nitroaromatics. On the other hand solution study has revealed that the enthalpy changes are in the ranges of 1.43 Kcal/mole to 3.14 Kcal/mole which corresponds to energy associated with weak interactions such as anion-π interactions (< 5 Kcal/mole)[61] These energies are close to weak interactions that are like anion-π interactions which are observed in crystal structures. Hence, one may safely suggest the role of such interactions in quenching of fluorescence.

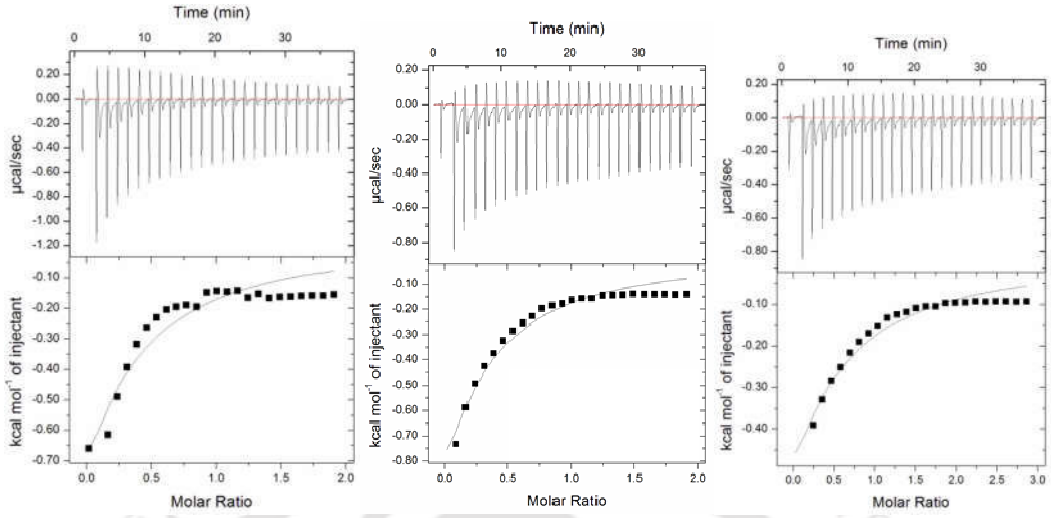

Figure 4.3.9: Isothermal calorimetric titration of complex **4.3.1** with (a) 4-nitrophenol, (b) 2,4-dinitrophenol; (c) 3-nitrobenzoic acid.

Table 4.3.1: Thermodynamic parameters determined by Isothermal Titration Calorimetry

Complex	Titrant	K_a (M^{-1})	ΔH(Kcal/ mol)	ΔS (cal/mol/deg)	Number of nitroaromatic binding to per nickel complex
$[Ni(phn)_3](NO_3)_2$	2,4-dinitrophenol	1024	2.272	75.2	0.253
$[Ni(phn)_3](NO_3)_2$	4-nitrobenzoic acid	924	1.430	47.2	0.502
$[Ni(phn)_3](NO_3)_2$	4-Nitrophenol	514	3.138	10.2	0.447

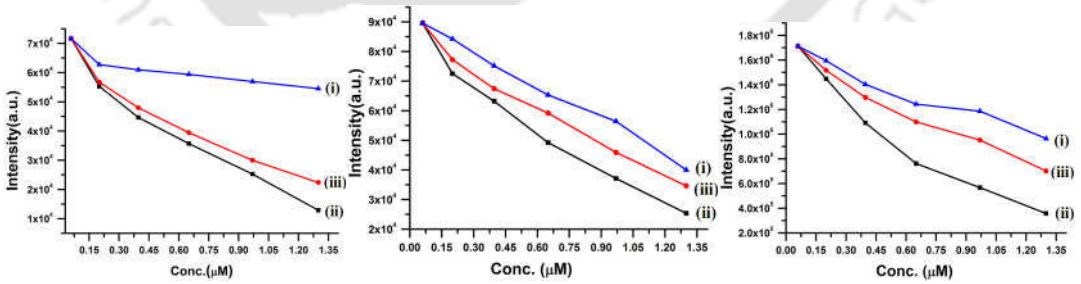

Figure 4.3.10: Plots of changes in fluorescence intensity of complex **4.3.1** in (a) methanol (b) DMSO and (c) DMF against concentration of (i) 4-nitrophenol, (ii) 2,4-dinitrophenol, (iii) 3-nitrobenzoic acid (complex **4.3.1** 10^{-5}M in each case).

The contributions of anion-π interactions as revealed in the crystal structures of **4.3.3** and **4.3.4** are similar. These data differentiate anion-π interactions of 3-nitrobenzoic acid and 2,4-dinitrophenol from π-stacking interactions of 4-nitrophenol in forming an inclusion complex of **4.3.1** with 4-nitrophenol impact is much higher than the one caused by-π-stacking in **4.3.1**. In solutions these are reflected in the relative slopes of the decrease in the fluorescence intensities of complex **4.3.1** on independent titrations. The changes in fluorescence intensity of the complex upon interactions with different nitrophenols in three different solution respectively in methanol, dimethylsulphoxide and dimethyformamide are shown in Figure 4.3.9, suggests a similar trend in quenching in individual quenching effect. One point is clear from these is the relative quenching by the 2,4-dinitrophenol and 3-nitrobenzoic acid remained high in each solvent.

Structurally complex **4.3.2** is more ordered, in which nitrophenol is a guest, and formation of this complex in solution also shows the least entropy change, on the other hand complexes obtained from reactions of 2,4-dinitrophenol or 3-nitrobenzoic acid with complex **4.3.1**, were mixed anionic complexes and have less orderly distribution of identical anions around per cationic species; which is also reflected in solution by showing higher entropy values in comparison to the 4-nitrophenol interacting with $[Ni(phn)_3](NO_3)_2$.

4.3.4 Summary

Anion-π interactions of aromatic nitro-compounds taking place between oxygen of nitro group on aromatics and π-cloud of 1,10-phenanthroline ligand of $[Ni(phn)_3]^{2+}$ in specific complexes are shown. Ability of $[Ni(phn)_3]^{2+}$ complexes to discriminate nitroaromatic compounds by specific changes in fluorescence emissions due to O···π interactions has been established. It also provided examples of unevenly distributed anions among cations in mixed anionic complexes. Nickel-phenanthroline provides templates to form inclusion complexes with nitroaromatics and data are supportive of the fact that there is an added value of O···π interactions in the case 2,4-dinitrophenol and 3-nitrobenzoic acid in showing fluorescence quenching. Additional contribution from O···π interactions present in these two examples has made them to have similar association constants as compared to 4-nitrophenol and values are larger than the association constant of 4-nitrophenol with complex **4.3.1** that lacks O···π interactions.

Part D

Tetranuclear Cobalt Complexes for Inclusion of Nitrophenols

4.4.1 Background

In the last three parts mono-nuclear complexes have been focused. Similar argument for π-decorated polynuclear complexes holds good, and use of polynuclear complexes will have certain advantages. It will provide a bigger template and it may be possible to work at nano-dimension where properties are much different from bulk materials. With such an objective we choose to study a series of cobalt complex that can be easily prepared and have interesting properties. The representative tetranuclear complex shown in Figure 4.4.1 is a mixed-valent oxido bridged cobalt complex and analogous complexes are known in literature.[62] These complexes are soluble and have wide range applications as magnetic materials[63] and in catalysis.[64] In this study such complexes with 2,2'-bipyridine and 1,10-phenanthroline were chosen as a decorating ligand for inclusion of aromatic guest molecules.

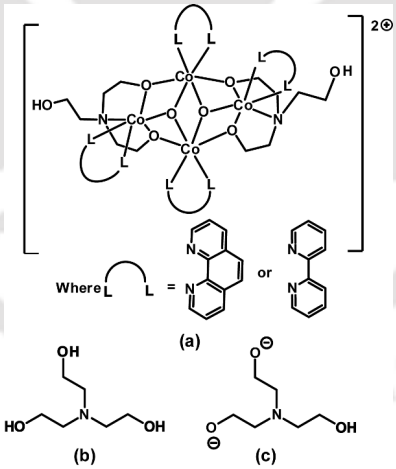

Figure 4.4.1: (a) Oxido-bridged tetranuclear cobalt complex cation possesing $Htea^{2-}$ and bis-chelating ligands. Structure of (b) H_3tea, (c) $Htea^{2-}$.

4.4.2 Synthesis of mixed valent oxido-bridged Cobalt (+2, +3) complexes

Tetranuclear mixed valent complex having cobalt at +2, +3 oxidation states, namely $[(\mu_2\text{-Htea})_2(phn)_2Co_2(\mu_3\text{-O})_2Co_2(phn)_2]Cl_2.5H_2O$ (**4.4.1**) was formed from reaction of cobalt chloride with 1,10-phenanthroline (**phn**) and triethanolamine (**H_3tea**). In an earlier report it was shown that similar reaction of cobalt nitrate yielded hydroxide-bridged mixed-valent tetranuclear cobalt complex.[65] Thus, a change of anion makes a difference in the composition of such complexes. On the other hand when a similar reaction was carried out by changing the decorating ligand from 1,10-phenanthroline to 2,2'-bipyridine a drastic difference in composition was observed. In this case a reaction performed using 2,2'-bipyridine in lieu of 1,10-phenanthroline, a double salt $[(\mu_2\text{-Htea})_2(bpy)_2Co_2(\mu_3\text{-O})_2Co_2(bpy)_2]Cl_2.[Co(H_2O)_6]\ Cl_2.5H_2O$ (**4.4.2**) was formed.

The tetranuclear complexes$[(\mu_2\text{-Htea})_2(phn)_2Co_2(\mu_3\text{-O})_2Co_2(phn)_2]Cl_2.5H_2O$ (**4.4.1**) and $[(\mu_2\text{-Htea})_2(bpy)_2Co_2(\mu_3\text{-O})_2Co_2(bpy)_2]Cl_2.[Co(H_2O)_6]Cl_2.5H_2O$ (**4.4.2**) both were characterized by determing their structures. Both has a defect dicubane tetranuclear cobalt complex cation analogous to earlier reported related mixed valent cobalt complexes with slight variations of ligands.[66] In both the complexes tetranuclear cationic parts are similar (Figure 4.4.2) and has four cobalt sites chelated by 1,10-phenanthroline or 2,2´-bipyridine ligands respecively.

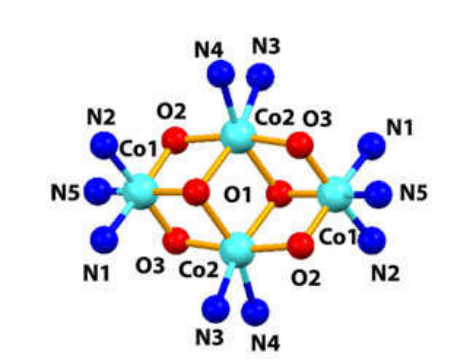

Figure 4.4.2: Environment in tetranuclear cobalt core in complex **4.3.1** and **4.3.2**.

Cores of these two complexes have very close similarity hence are discussed together. In both the complexes **4.4.1** and **4.4.2** have $Htea^{2-}$ ions bridging three cobalt ions through two oxygen atoms. Thus, two arms among three flexible arms of $Htea^{2-}$ were used in coordination, leaving one ethylhydroxy group free as shown in Figure 4.4.2.

There are two dissimilar environments for distorted octahedral cobalt ions. Among them, two environmentally similar cobalt ions have three nitrogen atoms and three oxygen atoms coordinating, while the other two environmentally equivalent cobalt ions have four oxygen atoms and two ligating nitrogen atoms. Cobalt-ligand bond lengths in N3O3 environment were different from cobalt-ligand distance of the ones in N2O4 environment. Co-O and Co-N bond lengths in complex **4.4.1** at N3O3 environment which were in ranges from 1.87Å(2) to 1.97(2)Å and 1.95(2)Å to 2.00(2)Å respectively. Similar Co-O and Co-N bond lengths at N2O4 environment were in the range between 2.04(2) Å to 2.16(2)Å and 2.12(2)Å to 2.15(2)Å respectively. These bond lengths suit the cobalt centers to have +3 or +2 oxidation states respectively.[67] Accordingly cobalt ions in N2O4 environment are at +2 oxidation state whereas rest are at N3O3 environment are at +3 oxidation state.

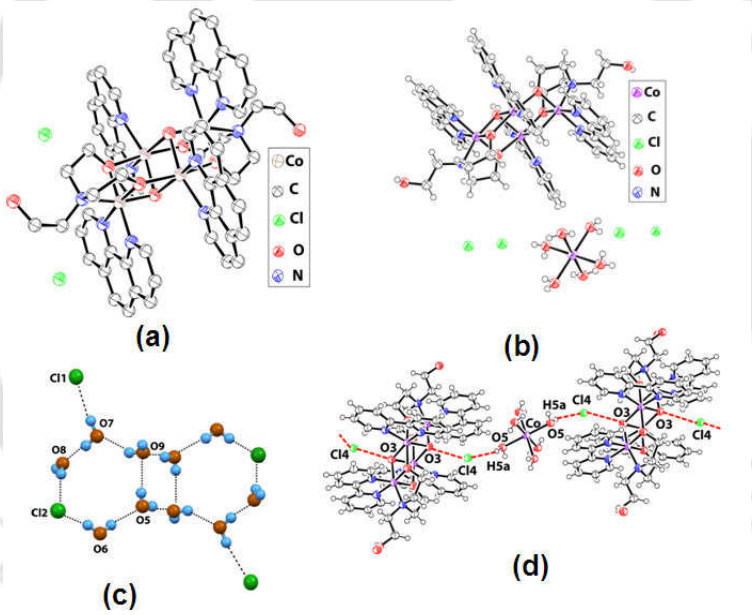

Figure 4.4.3: (a) Structure of complex **4.4.1** (ORTEP drawn with 50% thermal elipsoids). (b) complex **4.4.2** and (c) Chloride assisted water cluster in complex **4.4.1**. (d) Assembling of tetranuclear complex cations by $[Co(H_2O)_6]Cl_2$ in complex **4.4.2**.

There are five water molecules of crystallization which anchored chloride ions by hydrogen bonds generating cyclic hexameric sub-assemblies connected by tetramers as shown in Figure 4.4.3c. Chloride water clusters embedded in hydrophobic pockets of inorganic molecules are routinely observed.[68]

Complex **4.4.1** had hydrophobic pockets in packing pattern created by organic ligands, which were occupied by lattice water. Among two chloride ions of the complex **4.4.1**, one chloride ion was part of cyclic hydrogen bonded assembly formed with water, whereas other chloride ion was outside the hydrogen bonded cyclic assembly shown in Figure 4.4.3(c). Cyclic assemblies are held to ethylhydroxy groups by hydrogen bond. On the other hand, complex **4.4.2** shown in Figure 4.4.3(b) has an extra $[Co(H_2O)_6]Cl_2$ complex molecule cocrystallised. Hence the difference in the packing pattern arises due to the fact that complex **4.3.1** has packing pattern guided by chloride ions whereas in the case of **4.3.2** it is by another neutral complex along with chloride ions. Tetranuclear cations in these two complexes have comparable end to end distances, which are ~1.69nm and ~1.62nm respectively. Hence these cationic units are nano-dimensional.

4.4.3 Inclusion complexes of 4.3.1 with nitroaromatics

After having structural understanding on these nano-dimensional cationic complexes with two different ligands having π-stacking ability, their reactions independently with positional isomers of nitrophenols are studied. It is found that among several reactions using nitrophenols success in crystallizing inclusion complex were with 4-nitrophenol and 2,4-dinitrophenol. In the case of 4-nitrophenol, it reacted with complex **4.4.1**, forming $[(\mu_2\text{-Htea})_2(phn)_2Co_2(\mu_3\text{-}O)_2Co_2(phn)_2]Cl.np.2Hnp.H_2O$ (**4.4.3**), whereas a similar reaction with 2,4-dinitrophenol gave $[(\mu_2\text{-Htea})_2(phn)_2Co_2(\mu_3\text{-}O)_2Co_2(phn)_2]Cl.dnp.3H_2O$ (**4.4.4**).

In complex **4.4.3** three molecules of 4-nitrophenol are included per complex of **4.3.1**. Among them, one 4-nitrophenol molecule formed 4-nitrophenolate and replaced a chloride ion and the other two 4-nitrophenol molecules remained as neutral guest. Formation of this complex did not affect the cationic part, but major reorganization took place among anions. Structure of the complex is shown in Figure 4.4.4(a). Chloride ion formed hydrogen bonds with ethylhydroxy group.

It showed Cl···π interactions (3.53Å) involving 1,10-phenanthroline as given in Figure 4.4.4(b). Cl···π interactions[69] are encountered in organic and inorganic complexes.[70] Such interactions are favourable when confinement of an anion within a π-cloud[71] is done or an anion is brought to close proximity of a π-cloud by supporting interactions.[72]

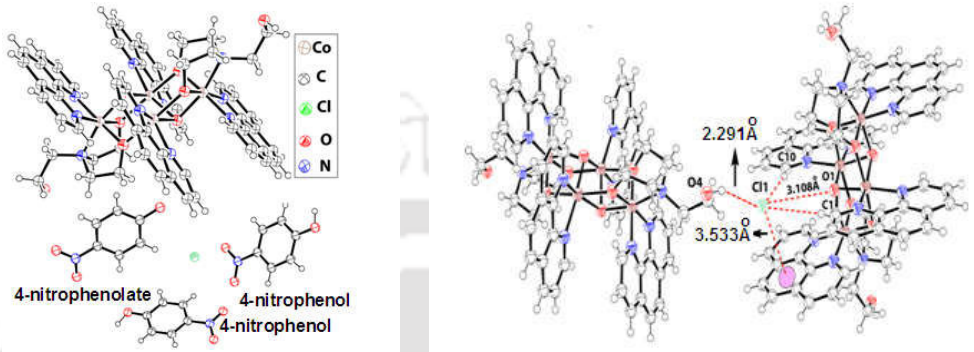

Figure 4.4.4: (a) Structure of complex **4.4.3** and (b) Cl···π interactions in complex **4.4.3**.

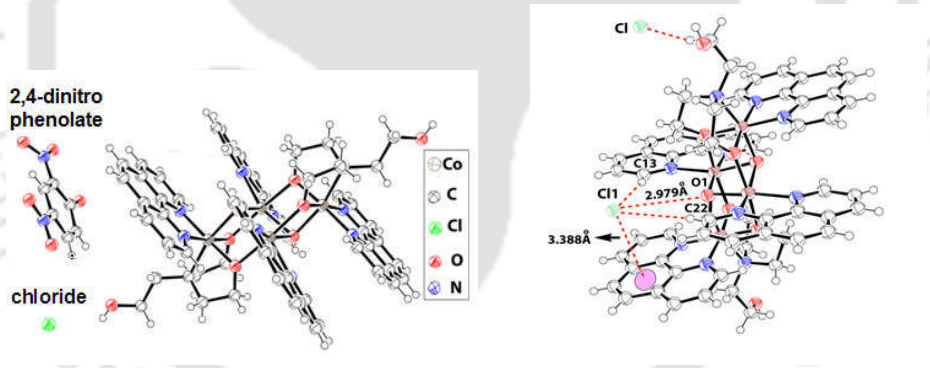

Figure 4.4.5: (a) Structure of complex **4.4.4** and (b) Cl···π interaction in complex **4.4.4** (Cl1 and Cl have half occupancies; ORTEP diagrams are drawn with 50% thermal ellipsoids).

In the present case we observed that oxide and chloride ions are in close proximity to have very weak O4···Cl3 interactions as shown in Figure 4.4.3(b). Cl···O interactions[73] in organic compounds is an important interaction; but observed distances between the Cl3...O4 are much larger in present cases. Hence, such interactions arise as a consequence of packing requirement.

We also independently performed reactions of 2-nitrophenol and 3-nitrophenol with complex **4.4.1** but we could not obtain crystals from such reactions. But a reaction of complex **4.4.1** with an equivalent amount of 2,4-dinitrophenol resulted in crystallization of complex $[(\mu_2\text{-Htea})_2(phn)_2Co_2(\mu_3\text{-}O)_2Co_2(phn)_2]Cl.dnp.3H_2O$ (**4.4.4**).

In this crystallization process cationic part of the parent compound remained as it is, whereas a chloride ion was replaced by a 2,4-dinitrophenolate. Structure of the complex **4.4.4** is shown in Figure 4.4.5 (a). The complex has chloride ions distributed over two crystallographically equivalent positions marked as Cl and Cl1 in Figure 4.4.5(b), each had half occupancies. Complex showed Cl···π interactions with rings of 1,10-phenanthroline. It has a chloride ion equally distributed between two crystallographically equivalent positions. Uptake of nitroaromatics in these complexes varied from substrates, for example, in case of 4-nitrophenol uptake was three molecules per complex dication, whereas for 2,4-dinitrophenol uptake was one molecule per complex.

Three positional isomers of nitrophenol when were independently reacted with complex **4.4.2**, only crystalline complex from reaction of 3-nitrophenol (Equation 4.4.1) was obtained. Product was a inclusion complex $[(\mu_2\text{-Htea})_2(bpy)_2Co_2(\mu_3\text{-}O)_2Co_2(bpy)_2]Cl.(3np).(3Hnp).H_2O$ (**4.4.5**) (where 3-nitrophenol = 3Hnp). This inclusion complex was formed by replacement of a chloride ion by 3-nitrophenolate and it had also a neutral 3-nitrophenol molecule. This product also lacked mononuclear cobalt complex that was present in complex **4.4.2**.

$[(\mu_2\text{-Htea})_2(bpy)_2Co_2(\mu_3\text{-}O)_2Co_2(bpy)_2]Cl_2.[Co(H_2O)_6]Cl_2.5H_2O + 2(3Hnp)$

$\rightarrow [(\mu_2\text{-Htea})_2(bpy)_2Co_2(\mu_3\text{-}O)_2Co_2(bpy)_2]Cl.(3np).(3Hnp).H_2O + HCl + Co(H_2O)_6Cl_2 + 4H_2O$

Where 3Hnp = 3-nitrophenol

Equation 4.4.1

Structure of complex **4.4.5** is shown in Figure 4.4.5 (a). Complex has regular oxido bridged tetranuclear cobalt cation. It has two hanging flexible CH_2CH_2OH arms which hold the 3-nitrophenol by forming O4-H···O8 hydrogen bond. 2,2'-Bipyridine is involved in C-H···Cl interactions with two C-H bonds of 2,2'-bipyridine ring to hold the chloride-

ion in a close vicinity of an oxygen atom of oxido bridging cobalt sites. The distance of O1···Cl1 is 2.979Å.This distance is conducive for such an interaction.[69] In complex **4.4.5**, 3-nitrophenolate anion form hydrogen bonds to ethylhydroxy group.

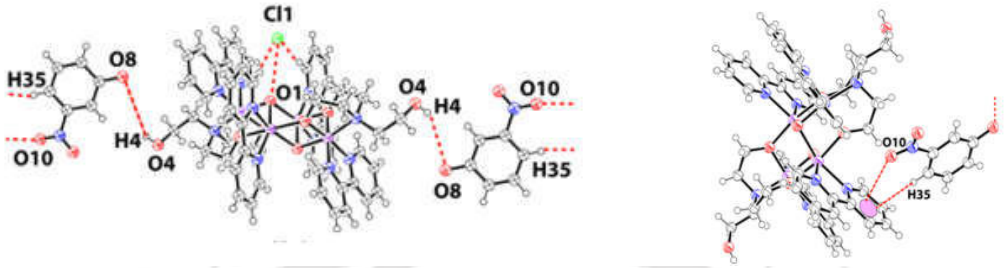

(a) (b)

Figure 4.4.6: (a) Structure of complex **4.4.2**. (b) Hydrogen bond between nitrophenolate and ethylhydroxy group**.** (c) O···π interactions in complex **4.4.5**.

There is also O···π interactions between nitro group and the 2,2'-bipyridine ring as shown in Figure 4.4.5. The O10···π ($d_{O\cdots\pi}$ = 355.3Å) and C-H35···π ($d_{C\text{-}H\cdots\pi}$ = 3.227Å) interactions as illustrated in Figure 4.4.3 facilitates 3-nitrophenolate tightly in the self-assembly of the complex.

$[(\mu_2\text{-Htea})_2(bpy)_2Co_2(\mu_3\text{-}O)_2Co_2(bpy)_2]Cl_2.[Co(H_2O)_6]Cl_2.5H_2O + M(OCOCH_3)_2$

$\rightarrow [(\mu_2\text{-Htea})_2(bpy)_2Co_2(\mu_3\text{-}O)_2Co_2(bpy)_2][MCl_4].H_2O + [Co(H_2O)_6](OCOCH_3)_2 + 4H_2O$

{Where M = Zn (**4.4.6**), Cd (**4.4.7**)} **Equation 4.4.2**

Since complex **4.4.2** holds a neutral cobalt complex as a guest, exchange of this guest metal complex may or may not be possible while forming a complex through cation exchange. It is found that complex **4.4.2** underwent cation exchange reaction with zinc or cadmium acetate (Equation 4.4.2). In such reaction, zinc acetate or cadmium acetate abstracted chloride ions to form $[MCl_4]^{2-}$(M = Zn or Cd) anion.

Thus, cation exchange complexes have tetranuclear cobalt cation whose charge is neutralized by $[MCl_4]^{2-}$. Each $[MCl_4]^{2-}$ anion had distorted tetrahedral geometry. The structure of the two complexes are shown in Figures 4.4.4(a) and Figure 4.4.4(b).Tetrahedral $[ZnCl_4]^{2-}$ had Zn-Cl bond distances were in the range 2.24(2)Å - 2.32(2)Å, whereas Cd-Cl bond distances of $[CdCl_4]^{2-}$ were in range of 2.43(3)Å-2.50(3)Å.

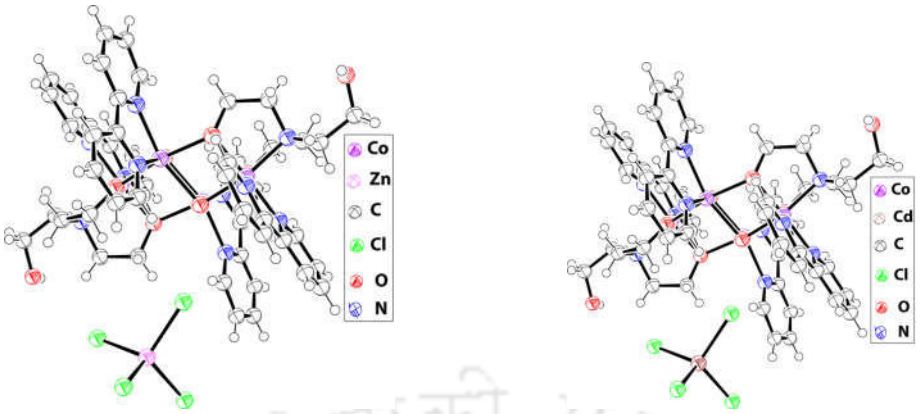

(a) (b)

Figure 4.4.7: Structure of (a) complex **4.4.6** and (b) Complex **4.4.7** (ORTEP drawn with 50% thermal ellipsoids).

Having established series of tetranuclear complexes metal ligand bond parameters are compared to see a possible impact of the decorating ligands and the anionic part on the core. The metal-bond parameters are listed in Table 4.4.1. Two different sets of metal-ligand bond parameters distinguishing cobalt sites are observed for similar Co-O or Co-N bonds. Shorter bond-lengths are for two cobalt ions at +3 oxidation state and longer are for cobalt ions at +2 oxidation state. Comparison suggests there is not significant change in the shape of the internal tetranuclear core. This is suggestive of the fact that the decorating ligands are responsible in being selective to bind different types of partner molecules making difference in packing patterns.

Table 4.4.1 Cobalt-ligand bond distances (Å) in tetranuclear cation in complexes **4.4.1-4.4.7**.

Co-L Bond	Complex 4.4.1	Complex 4.4.2	Complex 4.4.3	Complex 4.4.4	Complex 4.4.5	Complex 4.4.6	Complex 4.4.7
Co1-O1	2.13(1)	2.18(2)	2.14(4)	2.14(5)	2.15(3)	2.16(3)	2.17(5)
Co1-O2	2.04(2)	2.02(2)	2.02(3)	2.05(7)	2.05(2)	2.03(3)	2.04(5)
Co1-O3	2.06(2)	2.07(2)	2.05(3)	2.06(7)	2.05(3)	2.03(3)	2.04(5)
Co1-N1	2.15(2)	2.13(3)	2.12(4)	2.12(7)	2.14(5)	2.11(4)	2.12(6)
Co1-N2	2.13(2)	2.13(3)	2.14(5)	2.14(6)	2.13(5)	2.10(5)	2.09(6)
Co2-N5	2.00(2)	1.99(3)	2.00(5)	1.99(8)	2.01(3)	2.00(4)	2.00(6)
Co2-O1	1.94(2)	1.93(2)	1.93(3)	1.95(6)	1.93(2)	1.94(3)	1.94(4)
Co2-O2	1.87(2)	1.88(2)	1.86(3)	1.89(5)	1.86(3)	1.86(3)	1.85(5)
Co2-O3	1.87(2)	1.87(2)	1.87(3)	1.87(5)	1.87(4)	1.87(3)	1.87(5)
Co2-N3	1.95(2)	1.95(3)	1.96(5)	1.95(7)	1.95(4)	1.95(5)	1.95(6)
Co2-N4	1.97 (2)	1.95 (3)	1.96(4)	1.96(6)	1.95(5)	1.95(5)	1.93(6)

4.4.4 Solution study

Interactions of complexes **4.4.1** and **4.4.2** in solution with selected aromatic nitrophenols were studied by UV-visible spectroscopy. 4-Nitrophenol or 2,4-dinitrophenol did not cause significant change of UV-visible spectra of complex **4.4.1** (Figure 4.4.7).The apparent changes are due to the increase in concentration of the parent compound due to which increase in absorption at the original peak of individual compounds are observed. UV-absorbance of complex **4.4.2** present at 205nm, 230nm and 305nm were increased upon addition of 2-nitrophenol and original peaks of 2-nitrophenol at 278 and 351nm were not observed. These are shown in Figure 4.4.8(a) and (b). Similar trend was observed upon addition of 3-nitrophenol to a solution of complex **4.4.2**.

Upon interactions of 4-nitrophenol with complex **4.4.2**, intensity of the peak at 320nm is increased with a slight shift towards higher wavelength as shown in Figure 4.4.8(c). Solution of complex **4.4.1** as well as complex **4.4.2** are weakly fluorescent, both emit at 309nm ($\lambda_{ex,}$ 270nm). Observed emissions are ligand centric, as emissions of these complexes were at similar positions to that of ligand. Addition of nitrophenols consistently decreased fluorescence emission of solutions of complex **4.4.1** and **4.4.2**, Extent of changes caused by nitrophenols are shown in plot given in Figure 4.4.9. Changes caused in each case is different and selective to metal complexes.

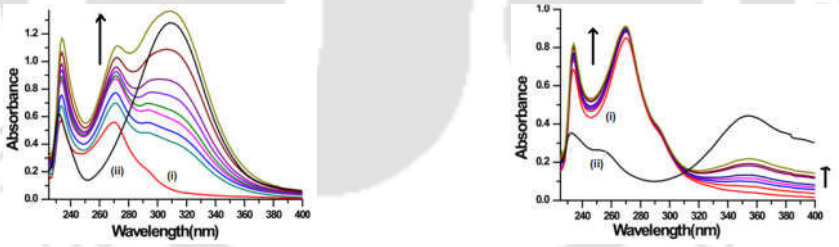

(a) (b)

Figure 4.4.8: UV-Vis spectra of complex **4.4.1** upon addition of a) 4Hnp and (b) 2,4-dinitrophenol. In each case respective (i) nitro aromatic (10^{-4} M in 3 ml) and spectra of complex **4.4.1**(10^{-4} M in 3 ml) upon addition of respective nitro aromatic at similar concentration, rest are upon addition of respective solution of 4-nitrophenol (in 20 µL aliquot).

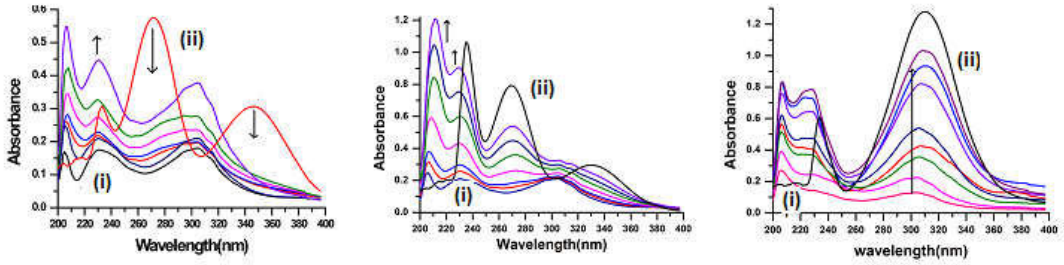

(a) (b) (c)

Figure 4.4.9: UV-Vis spectra of complex **4.4.2** upon addition of (a) 2Hnp (10^{-4} M in 3 ml); (b) 3Hnp and (c) 4Hnp. In each case curve (i) corresponds to complex **4.4.2** (10^{-4} M) whereas (ii) corresponds to individual nitrophenol at similar concentration; rest are upon addition of respective solution of nitrophenol (in 20 µL aliquot).

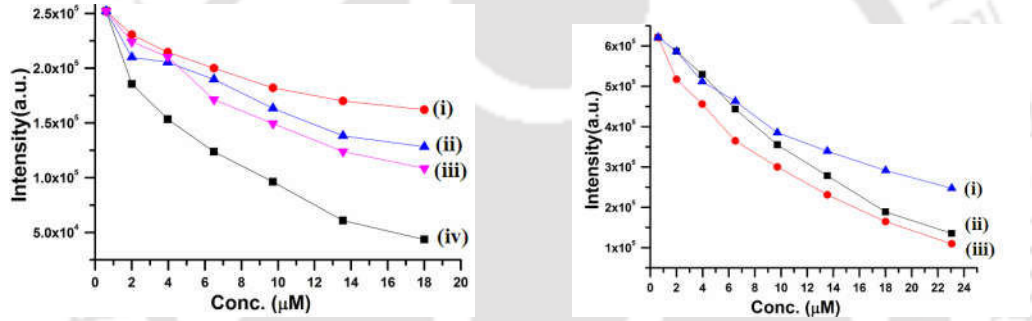

(a) (b)

Figure 4.4.10: Changes in fluorescence intensities (a) of complex **4.4.1**with increase in concentrations of (i) 2,4-dinitrophenol, (ii) 2-nitrophenol, (iii)3-nitrophenol, (iv) 4-nitrophenol and (b) of complex **4.4.2** with increase in concentrations of (i) 4-nitrophenol, (ii) 2-nitrophenol, (iii) 3-nitrophenol (in each case 3ml of 10^{-5}M complex in methanol)

Quantum yields of emission at 309nm of complex **4.4.1**, upon addition of equivalent amounts of nitrophenols are listed in Table 4.4.2. 2-Nitrophenol caused least quenching to fluorescence of both the complexes among the nitro phenols that are studied, whereas **4.4.3** or 4-nitrophenols did not show uniform trend. 3-Nitrophenol was found to be a good quencher for both complexes. 3-Nitrophenol cannot adopt a quinone form through resonance; whereas quinone like structure is possible in other two isomers.

Quinone type structure of 2- or 4-nitrophenol in solution prevented formation of exciplex by self-interactions between phenolic and quinonic forms. Generally, π-stacking and anion-π interactions and O···π interactions[73] cause fluorescence quenching.

Table 4.2.2: Quantum yields of complex **4.4.1** and **4.42** with or without nitrophenols[#]

Substrate	Quantum yield
Complex **4.4.1**	0.020
Complex **4.4.1** with 2-nitrophenol	0.012
Complex **4.4.1** with 3-nitrophenol	0.010
Complex **4.4.1** with 4-nitrophenol	0.009
Complex**4.4.1**with2,4dinitrophenol	0.014
Complex **4.4.2**	0.064
Complex **4.4.2** with 2-nitrophenol	0.050
Complex **4.4.2**with 3-nitrophenol	0.010
Complex **4.4.2** with 4-nitrophenol	0.045

(λ_{ex}, 270 nm, methanol, quinine sulphate as reference)

4.4.5 Solid state fluorescence emission

Solid samples were very poorly fluorescent, yet they could be compared to know about effects of nitrophenols. Nitrophenol/ate containing complexes had lower fluorescence than respective parent complex **4.4.1** or **4.4.2**. The fluorescence emission spectra solid samples of the complexes are shown in Figure 4.4.10.

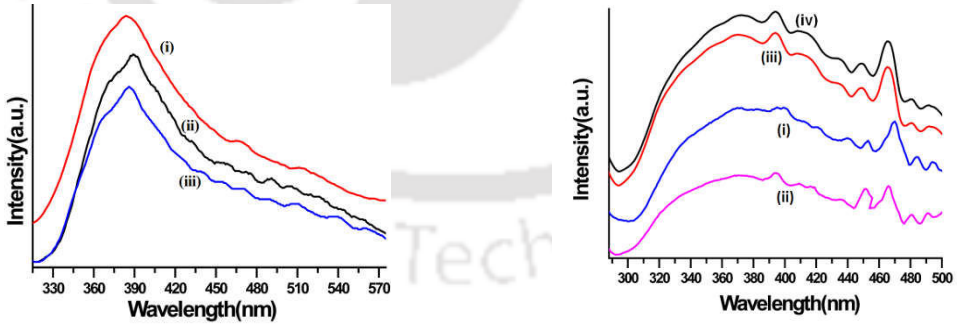

(a) (b)

Figure 4.4.11 : (a) Solid state fluorescence spectra (excitation at 280nm) of (i) Complex **4.4.1**, (ii) Complex **4.4.3**, (iii) Complex **4.4.4**. (b) Solid state fluorescence spectra (excitation at 265nm) of (i) Complex **4.4.2**, (ii) Complex **4.4.5**, (iii) Complex **4.4.6**, (iv) complex **4.4.7**.

Among complexes **4.4.3** and **4.4.4**, complex **4.4.4** had lower fluorescence intensity. The difference between these two complexes in solid state was that complex **4.4.4** had O···π interactions of nitro group. This interaction causes quenching of fluorescence.[74] Whereas, complex **4.4.5** had lower emission than complex **4.4.2** but complex **4.4.6** and **4.4.7** were higher than complex **4.4.2** as given in Figure 4.4.10 (b).

These can be easily explained through C-H···π interactions in **4.4.5,** which reduce intensity of emissions, whereas bigger anion in these complexes helped to keep cations of tetranuclear complex apart thereby causing enhancement of fluorescence. In solid state complex **4.4.1** and **4.4.2** are comparable in terms of acting as templates to hold planar molecules.

In solid state O···π interactions are present, but rigidity of the structure permits limited faces of such templates to interact with nitrophenols, as a result of this a set of fluorophores away from nitrophenols in lattice could not interact with them. But in solution nitrophenol molecules have liberty to interact with fluorophore in uniform manner to cause effective quenching; which is the reason to show differences in quenching effect in solid and solution.

4.4.6 Summary

Bis-chelating hetero-aromatic nitrogen ligands decided overall compositions of mixed valent tetranuclear oxido-bridged complexes. Exchange of neutral metal complex present ina double salt helped to accommodate tetrahedral anionic species. Interplay of weak interactions of nitrophenols with fluorophores attached to nano-dimensional cationic templates quench fluorescence. Fluorescence emission quenching by nitrophenols in solid state and solution complement each other but with much differences in magnitude of quenching.

4.5 Experimental Section

Detailed synthetic methodologies are given below. Analytical data as well as spectroscopic data are also listed along with the each complex. Details of the instruments, crystallographic table are given in Appendix.

4.5.1 Synthesis and characterization of zinc(II) 2,6-pyrdinedicarboxylates

$[H_2tmbpy][Zn(26pdc)_2]\cdot 5H_2O$ **(4.1.1)** and $[H_2bpy][Zn26pdc)_2]\cdot 6H_2O$ **(4.1.2)**: To an aqueous solution (20 ml) of 2,6-pyridinedicarboxylic acid (0.167 g, 1 mmol), an aqueous solution of zinc(II)acetate dihydrate (0.109 g, 0.5 mmol) was added and stirred for half an hour. A white precipitate was obtained. The pH of the solution was measured and found to be ~5. The solid obtained from this reaction was further reacted with a heterocyclic compound (0.5 mmol in 20 ml methanol), namely 1,3-bis(4-pyridine)propane for **4.1.1** or 4,4'-bipyridine for **4.1.2**, in independent experiments to obtain a homogeneous solution in each case. The solutions, on standing at room temperature, resulted in the formation of crystals of **4.1.1** and **4.1.2** after 3-4 days.

4.5.1.1: $[H_2tmbpy][Zn(26pdc)_2]\cdot 5H_2O$ **(4.1.1):** Isolated yield: ~70%. IR (KBr, cm^{-1}): 3443 (br), 3086 (w), 1629 (s), 1490 (w), 1431 (w), 1375 (s), 1277 (m), 1184 (w), 1076 (w), 980 (w), 909 (w), 818 (m). ^{1}H-NMR (400 MHz, $CDCl_3$): δ (ppm) 8.49 (m, 4H), 8.40 (d, J = 8Hz, 4H), 8.15 (t, *J* = 8 Hz, 2H), 7.12 (m, 4H), 3.50 (broad, D_2O-exchangeable protons), 2.68 (m, 4H), 2.02 (m, 2H).

4.5.1.2: $[H_2bpy][Zn(26pdc)_2]\cdot 6H_2O$ **(4.1.2):** Isolated yield: ~72%. IR (KBr, cm^{-1}): 3415 (br), 3074 (w), 2924 (w), 1634 (s), 1502 (m), 1427 (w), 1375 (s), 1276 (m), 1189 (m), 1078 (m), 1034 (m), 913 (m), 793 (m), 677 (m). ^{1}H-NMR (400 MHz, $CDCl_3$, ppm): 8.75 (d, *J* = 8 Hz, 4H), 8.39 (d, *J* = 8 Hz, 4H), 8.15 (t, *J* = 8 Hz, 2H), 7.59 (d, *J* = 6Hz, 4H), 3.50 (broad, D_2O-exchangeable protons).

4.5.1.3: $[H_2bpy][Zn(26pdc)_2]\cdot 3.5(4np)\cdot 2H_2O$ **(4.1.3):** An aqueous solution of **4.1.2** (1 mmol, 5 ml) was mixed with an aqueous solution of 4-nitrophenol (0.14g, 1 mmol, 5 ml) and the obtained mixture was left to slowly evaporate in air, giving colorless crystals of **3** in 10 days. Isolated yield: ~68%. IR (KBr, cm^{-1}): 3408 (br), 3096 (w), 2957 (w), 1633 (s), 1583 (s), 1496 (s), 1435 (w), 1384 (m), 1337 (s), 1286 (s), 1245 (m), 1108 (s), 1075 (m), 1032 (w), 993 (m), 852 (s), 812 (s), 776(w). ^{1}H-NMR (400 MHz, $CDCl_3$, ppm):

8.56 (d, *J* = 8 Hz,4H), 7.92 (d, *J* = 8 Hz, 2H), 7.70 (m, 2H), 7.40 (m, 2H), 6.73 (d, *J* = 8 Hz, 4H), 3.00 (broad, D_2O-exchangeable protons).

4.5.1.4: $[H_2tmbpy][Zn(26pdc)_2]\cdot 4(2,7dhn)\cdot 3H_2O$ **(4.1.4):** An aqueous solution of complex **4.1.1** (1 mmol, 5 ml) was mixed with an aqueous solution of 2,7-dihydroxynapthalene (0.30 g, 2 mmol, 5 ml) and the obtained mixture was left to slowly evaporate in air, leading to the formation of colorless crystals of **4.1.4.** Isolated yield: ~41%.IR (KBr, cm^{-1}): 3406 (bs), 3086 (w), 2918 (w), 1632 (s), 1500 (w), 1459 (w), 1424 (m), 1281 (m), 1254 (w), 1209 (s), 1151 (m), 1075 (w) 950 (w), 912 (w), 869 (w), 803 (s), 725(w).^{1}H-NMR (400 MHz, $CDCl_3$, ppm): 8.36 (d, *J* = 8.4 Hz, 4H), 8.26 (d, *J* = 8 Hz, 4H), 8.05 (t, J = 8Hz, 2H), 7.42 (d, *J* = 8.2 Hz,4H), 6.99 (d, *J* = 4.4 Hz, 4H), 6.83 (s, 4H), 6.76 (d, *J* = 6 Hz,4H), 3.0 (broad, broad exchangeable protons), 2.53 (t, *J* = 7 Hz, 4H), 1.86 (m, *J* = 7.2 Hz, 2H).

4.5.1.5: $[H_2bpy][Zn(26pdc)_2]\cdot 2(2,7dhn)\cdot 5H_2O$ **(4.1.5):** An aqueous solution of complex **4.1.2** (1 mmol, 5 ml) was mixed with an aqueous solution of 2,7-dihydroxynaphthalene (0.30 g, 2 mmol, 5 ml) and the obtained mixture was left undisturbed to slowly evaporate in air. Reddish, block-shaped crystals of complex **4.1.5** were obtained in ten days.

Isolated yield:~74%. IR (KBr, cm^{-1}): 3507 (br), 3101 (w), 2965 (w), 1632 (s), 1512 (m), 1481 (w), 1390 (s), 1312 (m), 1275 (m), 1212 (m), 1153 (w), 1076 (m), 1029 (w), 978 (w), 916 (w), 875 (w), 840 (w), 802 (s), 765 (w). ^{1}H-NMR (400 MHz, $CDCl_3$, ppm): 8.60 (d, *J* = 8 Hz, 4H), 8.25 (d, *J* = 8 Hz, 4H), 7.42 (t, *J* = 8 Hz, 2H), 6.81 (s, 4H), 6.75 (s, 2H), 6.73 (m, 4H), 2.8 (broad, exchangeable protons).

4.5.1.6: $[H_2tmbpy][Zn(26pdc)_2]\cdot 2(2,6dhn)\cdot 8H_2O$ **(4.1.6):** An aqueous solution of **4.1.1** (1 mmol, 5 ml) was mixed with an aqueous solution of 2,6-dihydroxynaphthalene (0.30 g, 2 mmol, 5 ml) and the obtained mixture was left undisturbed to slowly evaporate in air. Reddish, block-shaped crystals of **4.1.7** were obtained in ten days. Isolated yield: ~69%. IR (KBr, cm^{-1}): 3407 (bs), 3040 (w), 1630 (s), 1593 (s), 1508(w), 1432 (m), 1374 (s), 1280 (w), 1257 (w), 1229 (s), 1147 (w), 1118 (w), 1077 (m), 1038 (w), 937 (w), 913 (w), 859 (s), 797 (w), 772 (m), 729 (m), 681 (w).^{1}H-NMR (400 MHz, $CDCl_3$, ppm): 8.34 (d, *J* = 8 Hz, 4H), 8.23 (d, *J* = 8 Hz, 4H), 7.98 (t, *J* = 8 Hz, 2H), 7.34 (d, *J* = 8 Hz, 4H), 6.96 (d, *J* = 8 Hz, 4H), 6.91 (s, 4H), 6.89 (m, 4H), 2.5 (t, *J* = 8 Hz, 4H), 1.84 (m, *J* = 7.6 Hz, 2H).

4.5.1.7: $[H_2bpy][Zn(26pdc)_2]\cdot 2(pyrogl)\cdot 6H_2O$ **(4.1.7):** An aqueous solution of **4.1.2** (1 mmol, 5 ml) was mixed with an aqueous solution of pyrogallol (0.25 g, 2 mmol, 5 ml)

and the obtained mixture was left undisturbed to slowly evaporate in air. Colorless, block-shaped crystals of **4.1.7** were obtained in ten days. Isolated yield: ~68%. IR (KBr, cm^{-1}): 3351 (bs), 2913 (w), 2675 (w), 1627 (s), 1609 (s), 1466 (m), 1431 (w), 1431 (s), 1391 (s), 1287 (m), 1220 (w), 1184 (w), 1073 (s), 986 (w), 918 (w), 820 (w), 772 (m), 730 (w). ^{1}H-NMR (400 MHz, $CDCl_3$, ppm) 8.65 (m, 4H), 8.30 (d, *J* = 7.2 Hz, 4H), 8.05 (t, J = 8Hz, 2H), 7.48 (m, 4H), 6.5 (t, *J*= 7 Hz, 2H), 6.34 (d, *J* = 8 Hz, 4H), 2.60 (broad, D_2O-exchangeable protons).

4.5.2 Synthesis and characterization of lanthanum(III) 2,6-pyrdinedicarboxylates

4.5.2.1: $(H_2bpy)_3[La(26pdc)_3]_2.15H_2O$ **(4.2.1)** To a solution of 2,6-pyridinedicarboxylic acid (0.250g, 1.5 mmol, 10ml) in methanol a solution of lanthanum nitrate hexahydrate (0.216 g , 0.5 mmol, 10 ml water) was added and stirred for half an hour.

A white precipitate was formed, this precipitate was dissolved by adding 20 ml water and 4,4'-bipyridine (0.351 g, 2.25 mmol) was added to make a homogeneous solution. This solution on standing at room temperature yielded crystals (0.71g) of complex after 4 days. Isolated yield: ~70% (based on lanthanum). Elemental analysis calcd for $C_{72}H_{88}La_2N_{12}O_{39}$: C, 42.74; H, 4.38; N, 8.31; found, C, 42.91, H, 4.00; N, 8.34. IR (KBr, cm^{-1}): 3414 (bs), 3092 (w), 3056 (w), 1773 (w), 1734 (m), 1677 (s), 1624 (s), 1590 (s), 1489 (m), 1441(m), 1384 (s), 1266 (m), 1202 (m), 1070 (m), 1015(w), 977 (m), 918(w), 858 (w), 756 (m), 699 (m). ^{1}HNMR (600MHz, DMSO-d_6): 9.18 (bs, 3H, NH-proton), 8.54 (bs, 6H, CH-peak of bipyridinium), 8.45 (bs, 9H, CH of pyridine), 8.29 (bs, 6H, CH-peak of bipyridinium).

4.5.2.2: $(H_2bpy)[La_2(26pdc)_4(H_2O)_4].3H_2O$ **(4.2.2):** When a methanol solution with identical substrates as that was used for preparation of complex **4.2.1** was refluxed for 12 hs, after that allowed to slowly evaporate the solvent by keeping it standing at room temperature yielded 0.323g crystalline complex $(H_2bpy)[La_2(26pdc)_4(H_2O)_4].3H_2O$ (**4.2.2**). Isolated yield: ~50%. Elemental analysis calcd for $C_{38}H_{36}La_2N_6O_{27}$: C, 35.48; H, 2.82; N, 6.53; found, C, 35.87; H, 3.03; N, 6.60. IR (KBr, cm^{-1}): 3379 (bs), 1619 (s), 1493 (w), 1434 (m), 1387 (m), 1270 (m), 1187 (m), 1075 (m), 1013 (m), 917 (m), 823 (m), 775(m), 732 (s).

4.5.2.3: Preparation of inclusion complexes

Slow evaporation of respective solution of complex **4.2.1** (2.2 g, 1mmol) in 20 ml methanol with dihydroxyaromatic (1mmol), namely 1,2-dihydroxybenzene, 2,3-dihydroxynaphthalene or 2,7-dihydroxynaphthalene yielded crystalline guest included complex in each case.

4.5.2.4: $(H_2bpy)_{1.5}[La(26pdc)_3].2(cat).4H_2O$ **(4.2.3):** Isolated yield: ~63%. IR (KBr, cm^{-1}): 3441(bs), 1626 (s), 1518 (w), 1468 (w), 1430 (w), 1383 (s), 1271(m), 1191 (w), 1074 (w), 1007 (w), 919 (w), 849 (w), 812 (m), 724 (m). Elemental analysis calcd for $C_{54}H_{88}LaN_7O_{20}$: C, 50.11; H, 6.85, N, 7.58; found, C, 51.64; H, 4.01, N, 7.81. ^{1}HNMR (600MHz, DMSO-d_6): 9.26 (bs, 3H, NH-proton), 9.17 (bs, 6H, CH-peak of bipyridinium), 8.67-8.38 (m, 9H, CH of pyridine), 8.28 (m, 6H, CH-peak of bipyridinium), 7.14 (m, 4H, CH of 1,2-dihydroxybenzene), 7.01(m, 4H, CH of 1,2-dihydroxybenzene).

4.5.2.5: $(H_2bpy)_3[La(26pdc)_3]_2.3(23dhn).19H_2O$ **(4.2.4):** Isolated yield of crystalline product: ~65%. Elemental analysis calcd for $C_{102}H_{107}La_2N_{12}O_{49}$: C, 47.80, H, 4.21, N, 6.56 ; found, C, 48.41, H, 4.76; N, 6.67. IR (KBr, cm^{-1}): 3416 (bs), 1628(s), 1384 (s), 1259 (m), 864 (m), 796 (w), 748 (m). ^{1}HNMR (600MHz, DMSO-d_6): 9.97 (s, 4H, from OH). 9.13 (bs, 3H, NH-proton), 9.17 (bs, 6H, CH-peak of bipyridinium), 8.50 (s, 3H, CH of pyridine), 8.24 (s, 6H, CH of pyridine), 7.95 (s, 3H, CH of naphthalenediol), 7.57(s, 6H, CH of pyridine), 7.49 (m, 6H, CH of naphthalenediol).

4.5.2.6: $(H_2bpy)_{1.5}[La(26pdc)_3].3(27dhn).10H_2O$ **(4.2.5):** Isolated yield: ~62%. Elemental analysis calcd for $C_{66}H_{86}LaN_6O_{28}$: C, 51.13, H, 4.59, N, 5.42; found, C, 51.81; H, 4.35; N, 5.49. IR (KBr, cm^{-1}) : 3412 (bs), 1632 (s), 1519 (w), 1486 (w), 1431 (w), 1383 (s), 1274 (w), 1241(w), 1208 (m), 1152 (m), 1075 (m), 1014 (w), 919 (w), 839 (m), 803 (m), 765 (w). ^{1}HNMR (600MHz, DMSO-d_6): 9.96 (s, 4H, from OH). 9.18 (bs, 3H, NH-proton), 8.71-8.50 (m, 9H, CH of pyridine), 8.31(bs, 6H, CH-peak of bipyridinium) 8.00 (m, 6H, CH of naphthalenediol), 7.24 (s, 12H, CH of naphthalenediol), 7.22 (s, 6H, CH of bipyridinium).

4.5.3 Synthesis and characterization of nickel(II)1,10-phenanthroline complexes

4.5.3.1: $[Ni(Phn)_3](NO_3)_2.2H_2O$ **(4.3.1):** Complex **4.3.1** was synthesized by following a similar procedure that was reported earlier[50] by crystallizing the complex **4.3.1** from aqueous methanol. Guest inclusion and ligand exchange reactions were carried out by

adding respective solution of nitro-compound to a solution of $[Ni(Phn)_3](NO_3)_2{\cdot}2H_2O$ in methanol. Crystals of individual complex were obtained after standing the respective solution at ambient conditions for 5-6 days.

4.5.3.2: $[Ni(phn)_3](NO_3)_2.(Hnp).2H_2O$ **(4.3.2):** Isolated yield: ~25%. IR (KBr, cm^{-1}): 3229 (bs), 1626(m), 1585 (s), 1517 (s), 1422 (m), 1385 (s), 1340 (w), 1219 (w), 1140 (m), 1102 (m), 1032 (w), 997 (w), 848 (s), 777(m), 725 (s), 643(w). Vis (methanol): λ_{max}= 358nm ($\varepsilon = 1.2\ 1 \times 10^4\ M^{-1}\ cm^{-1}$). Molar conductance: 230 $cm^2\ mol^{-1}$.

4.5.3.3: $[Ni(phn)_3]_2(NO_3)(Hdnp)_3.11H_2O$ **(4.3.3):** Isolated yield: ~22%. IR (KBr, cm^{-1}): 3405 (bs), 3054 (w), 2964 (w), 1623 (m), 1590(m), 1516(m), 1423(m), 1382(s), 1260(w), 1223(w), 1137(w), 1089(w), 1020(w), 847(m), 804(w), 724 (m), 640(w), 615(w). Vis (methanol): λ_{max} = 371nm ($\varepsilon = 1.09 \times 10^4\ M^{-1}\ cm^{-1}$). Molar conductance: 226 $cm^2\ mol^{-1}$.

4.5.3.4: $[Ni(phn)_3]_2(NO_3)_3.(nba).11H_2O$ **(4.3.4):** Isolated yield: ~27%. IR (KBr, cm^{-1}): 3385 (bs), 3045 (w), 1626 (s), 1518 (s), 1424 (m), 1383 (s), 1344 (w), 1222(w), 1145 (w), 1102(w), 848(m), 780(w), 724 (m), 642 (w). Vis (methanol): λ_{max} = 307nm ($\varepsilon = 1.06 \times 10^4\ M^{-1}\ cm^{-1}$). Molar conductance: 235 $cm^2\ mol^{-1}$.

4.5.3.5: Microcalorimetry Titration

Isothermal Titration Calorimetric experiments were performed by ITC 200 Micro calorimeter**.** Separate solutions of complex and nitroaromatic compounds were prepared in methanol. Nitro compounds were kept in syringe with 10 mM while cationic complex was in sample cell with 1mM concentration. ITC analysis was performed at 27 °C with 25 injections keeping the time interval 90 seconds. Stirring was done at 350 rpm. Final isotherm in each case was analyzed by origin 8.5 software. After subtractions of control, the final fitting was obtained in single binding site model.

4.5.4 Synthesis and characterization of cobalt(II/III)tetranuclear complexes

4.5.4.1: Synthesis of $[(\mu_2\text{-Htea})_2(phn)_2Co_2(\mu_3\text{-O})_2Co_2(phn)_2]Cl_2.5H_2O$ **(4.4.1):** A solution of 1,10-phenanthroline (0.180g, 1mmol), cobalt(II) chloride hexahydrate (0.237g, 1mmol), triethanolamine (0.130ml, 1mmol) was prepared in 25 ml methanol. The solution was refluxed for 3 hrs. On cooling the solution yielded dark pink crystals. Isolated yield: ~83%. Anal.Calcd for $C_{60}H_{68}Cl_2Co_4N_{10}O_{13}$ (%), C, 49.00, H, 4.75; Found: C, 49.63, H, 4.22. IR (KBr, cm^{-1}): 3357 (bs), 2934 (w), 1629 (s), 1516 (s), 1428 (s), 1227 (w), 1140 (w), 1094 (m), 1018 (m), 942 (m), 847 (s), 775 (w), 722 (s), 658 (w), 613 (w).

Molar conductance (methanol): 245 cm^2 mol^{-1}. UV-visible: λ_{max}= 233nm (methanol, ε = 5600 M^{-1} cm^{-1}), 270nm (ε = 5500 M^{-1} cm^{-1}), 546nm (ε = 154 M^{-1} cm^{-1}).

4.5.4.2: $[(\mu_2\text{-Htea})_2(bpy)_2Co2(\mu_3\text{-}O)_2Co_2(bpy)_2]Cl_2.[Co(H_2O)_6]Cl_2.5H_2O$ **(4.4.2)**: A solution of 2,2' bipyridine (0.156g, 1mmol), cobalt(II) chloride hexahydrate (0.0.355g, 1.5mmol), triethanolamine (0.130ml, 1 mmol)in 25 ml methanol was refluxed for 3 hrs. On cooling the solution to room temperature yielded crystals of complex **4.4.2**. Isolated yield: ~75%.Anal.calcd. for $C_{52}H_{76}N_{10}O_{17}Cl_4Co_5$ (%): C 40.26, H 4.90, N 9.03; Found C 40.30, H 4.96, N 9.41. IR (KBr, cm^{-1}) : 3443 (bs), 1629 (s), 1526 (s), 1440 (s), 1382 (w), 1346 (w), 1082 (s), 1021(s), 916 (w), 802 (w). UV-visible: λ_{max}= 205nm (methanol, ε = 2502 M^{-1} cm^{-1}), 230nm (ε = 2106 M^{-1} cm^{-1}), 305nm (ε = 2121 M^{-1} cm^{-1}), 555nm (ε = 177 M^{-1} cm^{-1}).

4.5.4.3 Inclusion complexes of 4.4.1

Complex **4.4.3** and complex **4.4.4** were prepared in a similar procedure as that of complex **4.4.1** and for complex **4.4.3**, 4-nitrophenol (0.139 g, 1 mmol) and for complex **4.4.4**, 2,4-dintrophenol (0.184 g, 1 mmol) were taken as additional reactants. These two reactions were invariant of concentration of nitrophenol used in these reactions.

4.5.4.4:$[(\mu_2\text{-Htea})_2(phn)_2Co_2(\mu_3\text{-}O)_2Co_2(phn)_2]Cl.(2np).(2Hnp).H_2O$ **(4.4.3):** Isolated yield: ~25%. Anal.Calcd for $C_{78}H_{74}ClCo_4N_{13}O_{18}$ (%), C, 53.44, H, 4.25; Found: C, 53.63, H, 4.22. Found: C, 52.63, H, 4.22. IR (KBr, cm^{-1}): 3355 (bs), 3151 (w), 2933 (w), 2902 (w), 1626 (s), 1583 (s), 1515 (s), 1490 (w), 1457 (w), 1427 (s), 1333 (m), 1290 (m), 1249 (w), 1140 (w), 1096 (s), 1027 (m), 944 (w), 847 (s), 776 (w), 723 (s), 603 (w). Molar conductance (methanol): 232 cm^2 mol^{-1}. UV-visible: λ_{max}= 234nm (methanol, ε = 9867 M^{-1} cm^{-1}), 307nm (ε = 10875 M^{-1} cm^{-1}), 543nm (ε = 179 M^{-1} cm^{-1}).

$[(\mu_2\text{-Htea})_2(phn)_2Co_2(\mu_3\text{-}O)_2Co_2(phn)_2]Cl.dnp.3H_2O$ **(4.4.4):** Isolated yield: ~30%. Anal.Calcd for $C_{66}H_{62}ClCo_4N_{12}O_{15}$ (%), C, 51.55, H, 4.07; Found: C, 51.59, H, 4.12. IR (KBr, cm^{-1}): 3379 (bs), 3156 (w), 2934 (w), 2898 (w), 2836 (w), 1623 (s), 1596 (s), 1556 (w), 1519 (m), 1487 (w), 1427 (m), 1314 (s), 1255 (m), 1089 (w), 1024 (s), 917 (m), 848 (m), 723 (m), 610 (m). Molar conductance (methanol): 237 cm^2 mol^{-1}. UV-visible: λ_{max}= 233nm (methanol, ε = 7735 M^{-1} cm^{-1}), 270nm (ε = 8904 M^{-1} cm^{-1}), 544nm (ε = 191 M^{-1} cm^{-1}).

4.5.4.5: Inclusion complexes and cation exchange of complex 4.4.2

Complex **4.4.5** was prepared in a similar procedure as that of complex **4.4.2** but in this case 3-nitrophenol (0.139g 1mmol) was taken as additional reactant. This reaction led to crystals after two on keeping the reaction mixture at room temperature.

Complexes **4.4.6** and **4.4.7** were prepared by reaction of equimolar amount of complex **4.4.2** with Zn(II)acetate dihydrate or cadmium acetate in methanol, respectively by adopting a similar procedure to that of complex **4.4.5**, on standing for 4-5 days crystals of respective compounds were obtained.

4.5.4.6: $[(\mu_2\text{-Htea})_2(bpy)_2Co_2(\mu_3\text{-O})_2Co_2(bpy)_2]Cl.3np.3Hnp.H_2O$ **(4.4.5):** Isolated yield: ~65%. IR (KBr, cm^{-1}): 3380 (bs), 1596 (s), 1499 (m), 1444 (m), 1341(s), 1286 (m), 1245 (w), 1163 (w), 1106 (m), 1029 (w), 954 (w), 851(m). UV-visible: λ_{max}= 208nm (methanol, ε = 5989 M^{-1} cm^{-1}), 230nm (ε = 4359 M^{-1} cm^{-1}), 272nm (ε = 2625 M^{-1} cm^{-1}), 553nm (ε = 214 M^{-1} cm^{-1}).

4.5.4.7: $[(\mu_2\text{-Htea})_2(bpy)_2Co_2(\mu_3\text{-O})_2Co_2(bpy)_2]ZnCl_4.H_2O$ **(4.4.6):** Isolated yield: ~62%. IR (KBr, cm^{-1}): 3380 (bs), 3070 (w), 1637 (w), 1603(s), 1562 (w), 1441(s), 1301(m), 1246 (m), 1157 (m), 1092 (s), 1021(m), 944 (w), 923 (w), 771(w). UV-visible: λ_{max}= 207nm (methanol, ε = 4110 M^{-1} cm^{-1}), 229nm (ε = 2801 M^{-1} cm^{-1}), 296nm (ε = 3046 M^{-1} cm^{-1}), 306 nm(ε = 3301 M^{-1} cm^{-1}), 552nm(ε = 225 M^{-1} cm^{-1}).

4.5.4.8: $[(\mu_2\text{-Htea})_2(bpy)_2Co2(\mu_3\text{-O})_2Co_2(bpy)_2]CdCl_4.H_2O$ **(4.4.7):** Isolated yield: ~60%. IR (KBr, cm^{-1}): 3378 (bs), 2926 (w), 1637 (m), 1602 (s), 1562 (m), 1440 (s), 1404 (w), 1300 (w), 1247 (w), 1158 (w), 1092 (s), 1021 (m), 920 (m), 777 (m). UV-visible: λ_{max}= 207nm (methanol, ε = 4772 M^{-1} cm^{-1}), 230nm (ε = 2495 M^{-1} cm^{-1}), 295nm (ε = 2583 M^{-1} cm^{-1}), 305 nm (ε = 2658 M^{-1} cm^{-1}), 554 nm (ε = 162 M^{-1} cm^{-1}).

References:

1 (a) K. T. Holman, A. M. Pivovar, J. A. Swift, M. D. Ward, *Acc. Chem. Res*., 2001, **34**, 107-118; (b) M. D. Ward, *Chem. Commun*., 2005, 5838-5842.

2 G. R. Newkome, B. D. Woosle, E. He, C. N. Moorefield, R, Guther, G. R. Baker, G. H. Escamilla, J. Merrill, H. Luftmann, *Chem. Commun*., 1996, 2737-2738.

3 H. Li, X. Feng, Y. Guo, D. Chen, R. Li, X. Ren, X. Jiang, Y. Dong, B. Wang, *Sci. Rep*., 2014, **4**. 4366.

4 (a) J. W. Cai, *Cryst. Growth Des*., 2012, **12**, 2684-2690; (b) X. Y. Wang and S. C. Sevov, *Chem. Mater*., 2007, **19**, 4906-4912.

5 J. P. G. Teran, O. Castillo, U. G. Couceiro, G. Beobide, P. Roman, *Inorg. Chem*., 2007, **46**, 3593-3602.

6 B. Manna, A. V. Desai, S. K. Ghosh, *Dalton Trans*., 2016, **45**, 4060-4072.

7 H. W. Roesky, M. Andruh, *Coord. Chem. Rev*., 2003, **236**, 91-119.

8 G. Aragay, D. Hernandez , B. Verdejo, E. C. E. Adan, M. Martinez, P. Ballester, Molecules, 2015, **20**, 16672-16686.

9 (a)Y. Xue, A. V. Davis, G. Balakrishnan, J. P. Stasser, B. M. Staehlin, P. Focia, T. G Spiro, J. E P. Hahn, Thomas V, O, Halloran, *Nat. Chem. Biol*., 2008, **4**, 107-109; (b) B. L. Schottel, H. T. Chifotides, K. D. Dunbar, *Chem. Soc. Rev*., 2008, **37**, 68-83.

10 A. S. Singh, S. S. Sun, *RSC Adv*., 2012, **2**, 9502-9510.

11 S. Yamaguchi, T.M. Swager, *J. Am. Chem. Soc*., 2001, **123**, 12087-12088.

12 J. Liu, S. Yang, F. Li, L. Dong, J. Liu, X. Wang, Q. Pu, *J. Mater. Chem. A*, 2015, **3** 10069-10076.

13 J. Geng, P. Liu, B. Liu, G. Guan, Z. Zhang, M. Y. Han, *Chem. Eur. J*., 2010, **16**, 3720-3727.

17 V. Balzani, P. Ceroni, A. Juris, M. Venturi, S. Campagna, F. Puntoriero, S. Serroni, *Coord. Chem. Rev*., 2001, **219**, 545-572.

14 S. Xu, H. Lu, *Chem. Commun*., 2015, **51**, 3200-3203.

15 M. Kandpal, A.K. Bandela, V.K. Hinge, V.R. Rao, C.P. Rao, *ACS Appl. Mater. Interfaces*, 2013, **5**, 13448-13456.

16 S. S. Nagarkar,A. V. Desai , P. Samanta, S. K. Ghosh, *Dalton Trans*., 2015, **44**, 15175-15180.

17 H. Sohn, M. J. Sailor, D. Magde, W.C. Trogler, *J. Am. Chem. Soc*., 2003, **125**, 3821-3830.

18 J. M. Lehn, *Angen. Chem. Int. Ed. Engl*., 1990, **29**, 1304-1319.

19 (a) B. Das, J. B. Baruah, *Inorg. Chim. Acta*, 2010, **363**, 1479-1487; (b) J. C. MacDonald, P. C. Dorrestein, M. M. Pilley, M. M. Foote, J. L. Lundburg, R. W. Henning, A. J. Schutlz, J. L. Manson, *J. Am. Chem. Soc*., 2000, **122**, 11692-11694.

20 J. M. Harrowfield, N. Lugan, G. H. Shahverdizadeh, A. A. Soudi, P. Thuery, Eur. *J. Inorg. Chem*., 2006, 389-396.

21 B. Das, D. C. Crans, J. B. Baruah, *Inorg. Chim.Acta*, 2013, **408**, 204-208.

22 K. T. Holman, M. D. Ward, *Angew. Chem. Int. Ed.,* 2000, **39**, 1653-1656.

23 (a) H.J. Kim, D. Moon, M. S. Lah, J. I. Honga, *Tetrahedron Lett*., 2003, **44**, 1887-1890; (b) R. E. Sheridan, H. W. Whitlock, Jr., *J. Am. Chem. Soc*., 1988, **110,** 4071-4073.

24 (a) R. R. Jr. *Angew. Chem. Int. Ed.,*1990, **29,** 245-255; (b) S. Goswami, A. D. Hamilton, D. J. van Engen, *J. Am. Chem. Soc*.,1989, **111**, 3425-3426.

25 (a) S. C. Zimmerman, W. Wu, *J. Am. Chem. Soc*., 1989, **111**, 8054-8055; (b) S. C. Zimmerman, C. M. V. Zyl, *J. Am. Chem. Soc*., 1987, **109,** 7894-7896.

26 R. Kusaka, Y. Inokuchi, T. Haino, T. Ebata, *J. Phys. Chem. Lett.*, 2012, **3**, 1414-1420.

27 B. Escuder, J. F. Miravet, J. A. Saez, *Org. Biomol. Chem*., 2008, **8**, 4378-4383.

28 W. Guan, J. Pan, X. Wang, W. Hu, L. Xu, X. Zou, C. Li, *J. Separation Sci*., 2011, **34**, 1244-1252.

29 G. Xu, L. Yang, M. Zhong, C. Li, X. Lu, X. Kan, *Microchim. Acta*, 2013, **180**, 1461-1469.

30 C. Rosler, R. A. Fischer, *CrystEngComm*., 2015, **17**, 199-217.

31 (a) B. M. Holligan, J. C. Jeffery, M. D. Ward, *J. Chem. Soc. Dalton Trans*., 1992, 3337-3344; (b) J. Rubin, G. S. Panson, *J. Phys. Chem*., 1965, **69**, 3089-3091.

32 D. B. Amabilino, J. F. Stoddart, *Chem. Rev*., 1995, **95**, 2725-2828.

33 L. Fang, M. A. Olson, D. Benitez, E. Tkatchouk, W. A. Goddard, J. F. Stoddart, *Chem. Soc. Rev*., 2010, **39**, 17-29.

34 M. D. Garcia, C. Alvarino, E. M. L. Vidal, T. Rama, C. Peinador, J. M. Quintela, *Inorg. Chim. Acta*, 2014, **417**, 27-37.

35 R. P. Sijbesma A. P. M. Kentgens, E. T. G. Lutz, J. H. van der Maas, R. J. M. Nolte, *J. Am. Chem. Soc*., 1993, **115**, 8999-9005.

36 (a) J. M. Lehn, *Angew. Chem. Int. Ed. Eng*., 1990, **29**, 1304-1319; (b) F. Zeng, S.C. Zimmerman, *Chem. Re*v., 1997, **97,** 1681-1712; (c) T. R. Cook,Y. R. Zheng, P. J. Stang, *Chem. Rev*., 2013, **113,** 734-777; (d) W. Y. Sun, M. Yoshizawa, T. Kusukawa, M. Fujita, Curr. Opin. *Chem. Biol*., 2002, **6,** 757-764; (e) D. L. Reger, J. J. Horger, M. D. Smith, G .J. Long, *Chem. Commun*., 2009, 6219-6221; (f) D. L. Reger, A. Leitner, P. J. Pellichia, M. D. Smith, *Inorg. Chem*., 2014 ,**53**, 9932-9945.

37 (a) R. L. Shook ,A. S. Borovik, *Inorg. Chem*., 2010, **49,** 3646-3660; (b) S. A. Cook, A.S. Borovik, *Acc. Chem. Res*., 2015, **48**, 2407-2414.

38 J. W. Cai, *Cryst. Growth Des*., 2012, **12**, 2684-2690; (b). X. Y. Wang, S. C. Sevov, *Cryst. Growth Des*., 2008, **8**, 1265-1270; (c) A. P. Cote, G. K. H. Shimizu, *Chem.Eur. J.*, 2003, **9**, 5361-5370; (d) S. A. Dalrymple, G. K. H. Shimizu, *J. Am. Chem. Soc*., 2007, **129**, 12114-12116; (e) J. P. Garcia-Teran, O. Castillo, U. Garcia-Couceiro, G. Beobide, P. Roman, *Inorg. Chem*., 2007, **46**, 3593-602; (f) C. G. Simon, M. G. Borras, L. Gomez, I. G. Bosch, S. Osuna, M. Swart, J. M. Luis, C. Rovira, M. Almeida, I. Imaz, D. Maspoch, M. Costas and X. Ribas, *Chem. Eur. J*., 2013, **19,**1445-1456.

39 T. Kamegawa, H. Seto, S. Matsuura, H. Yamashita, *ACS Appl. Mater. Interfaces*, 2012, **4**, 6635-6639.

40 N. Okabe, H. N. Okabe, H. Kyoyama, *ActaCrystallogr*., 2002, **E58**, m226-227.

41 (a)Y. Cui, B. Chen, G. Qian, *Coord. Chem. Rev*., 2014, **76-86**, 273-274; (b) R. Das, R. Sarma, J. B. Baruah, *Synthesis and Reactivity in Inorganic, Metal-Organic and Nano-Metal Chem*., 2011, **41**, 165-172; (c) S. Maji, K. S. Viswanathan, *J. Luminiscence*., 2009, **129**, 1242-1248; (d) H. Xiao, M. Chen, C. Mei, H. Yin, X. Zhang, X. Cao, *Spectrochim. Acta.*, 2011, **84A**, 238-242; (e). C. Tao, K. Du, Q. Yin, J. Zhu, H. Yan, F. Zhu, L. Zhang, *RSC Adv*., 2015, **5**, 58936-58942.

42 H. W. Roesky, M. Andruh, *Coord. Chem. Rev*., 2003, **236**, 91-119.

43 M. Ghiasi, A. Malekzadeh, Superlattices *Microstruct*., 2015, **77**, 295-304.

44 V. Blanco, M Chas, D. Abella, C. Platas-Iglesias, C. Peinador, J. M. Quintella, *Org. Letters*., *2008,***10**, 409-412.

45 (a) K. Odashima, A. Itai, Y. Litaka, K. Koga, *J. Am. Chem. Soc*., 1980, **102**, 2504-2505;

(b) M. Anibarro, K. Gessler, I. Uson, G. M. Sheldrick, W. Saeger, *Carbohydr. Res*., 2001, **333**, 251-256; (c). L. Yang, D. C. Crans, S. M. Miller, L. A. Cour, O. P. Anderson, P. M. Kaszynski, M. E. Godzala, D. L. Austin, G. R. Wilsky, *Inorg. Chem*., 2002, **41**, 4859-4671.

46 (a) M. Mascal, A. Armstrong, M. D. Bartberger, *J. Am. Chem. Soc*., 2002, **124,** 6274-6276; (b) Y. S. Rosokha, S. V. Lindermna, S. V. Rosokha, J. K. Kochi, *Angew. Chem. Int. Ed*., 2004, **43**, 4650-4652.

47 (a) J. Feitelson, N. Shaklay, *J. Phys. Chem*., 1967, **71**, 2582-2586; (b) M. F. Pistonesi, M. S. Di Nezio, M. E. Centurion, M. E. Palomeque, A. G. Lista, B. S. F. Band, *Talanta*, 2006, **69**, 1265-1268.

48 (a) N. Barooah, J. B. Baruah, *J. Mol. Struct*., 2008, **872**, 205-211; (b) N. Barooah, R. J. Sarma, J. B. Baruah, *CrystEngComm*., 2006, **8**, 608-615; (c) N. Barooah, R. J. Sarma, J. B. Baruah, *Crystal Growth Des*., 2003, **3**, 639-641.

49 J. Marek, P. Kovel, Z. Travnicek, *Polish J. Chem*., 1995, **69**, 591-596.

50. M. Tabatabaee, N. Zaji, M. Parvez, *Acta Crystallogr*., 2011, **67E**, m794-m795.

51 (a). B. Das, J. B.Baruah, *J. Mol. Struct*., 2013, **1034**, 144-151; (b) X. H. Duo, L. J. Feng, Z. G. Lianag, *Sci. China Chem*., 2010, **53**, 2539-2546; (c) E. Melnic, E. B. Coropceanu, O. V. Kulikova, A. V. Siminel, D. Anderson, H. J. R. Jacquez, A. E. Masunov, M. S. Fonari, V. Ch. Kravtsov, *J. Phys. Chem. C*, 2014, **118**, 30087-30100.

52 (a). B. P. Hay, R. Custelcean, *Cryst. Growth Des*., 2009**, 9**, 2539-2545; (b). B. L. Schottel, H. T. Chifotides, K. R. Dunbar, *Chem. Soc. Rev*., 2008, **37**, 68-83; (c) P. Khakhlary, J. B. Baruah, *J. Chem. Sci*., 2015, **127**, 95-102.

53 D. X. Wang, M. X. Wang, *J. Am. Chem. Soc*., 2013, **135**, 892-897.

54 F. A. Cotton, G. Wilkinson, C. A. Murillo, M. Bochmann, Advanced Inorganic Chemistry, Sixth edition, John Wiley & Sons, New York, 1999.

55 J. K. Nath, J. B. Baruah, *New J. Chem*., 2013, **37**, 1509-1519.

56 (a) N. Venkatramaiah, A. D. G. Firmino, F. A. Almeida Paz, J. P. C. Tome, *Chem. Commun*., 2014, **50**, 9683-9686; (b) L. Basabe-Desmonts, D. N. Reinhoudt, M. Crego-Calama, *Chem. Soc. Rev*., 2007, **36**, 993-1017.

57 (a) M. Mascal, A. Armstrong, M. D. Bartberger, *J. Am. Chem. Soc*., 2002, **124**, 6274-6276.; (b) Y. S. Rosokha, S. V. Lindermna, S. V. Rosokha, J. K. Kochi, Angew. *Chem. Int. Ed*., 2004, **43**, 4650-4652.

58 F. D. Lewis, B. E. Cohen, *J. Phys. Chem*., 1994, **98**, 10591-10597.

59 P. Alreja, N. Kaur, *RSC Adv*., 2016, **6**, 23169-23217.

60 D. V. Scaltrito, D. W. Thompson, J. A. O'Callaghan, G. J. Meyer, *Coord. Chem. Rev*., 2000, **208**, 243-266.

61 (a) E. Melnic, E. B. Coropceanu, O. V. Kulikova, A. V. Siminel, D. Anderson, H. J. R. Jacquez, A. E. Masunov, M. S. Fonari, V. Ch. Kravtsov, *J. Phys. Chem. C*, 2014, **118**, 30087-30100; (b). B. P. Hay, R. Custelcean, *Cryst. Growth Des*., 2009, **9**, 2539-2545; (c). B. L. Schottel, H. T. Chifotides, K. R. Dunbar, *Chem. Soc. Rev*., 2008, **37**, 68-83.

62 (a) S. R. Hosseinian, V. Tangoulis, M. Menelaou, C. P. Raptopoulou, V. D. Psycharis, *Dalton Trans*., 2013, **42**, 5355-5366; (b) A. I. Nguyen, R. G. Hadt, E. I. Solomon, T. D. Tilley, *Chem. Sci*., 2014, **5**, 2874-2878; (c) H. Sakiyama, A. K. Powell, *Dalton Trans*., 2014, **43**, 14542-14545; (e) V. Tangoulis, M. Skarlis, C. P. Raptopoulou, C. D. Samara, *Eur. J. Inorg. Chem.*, 2014, **16**, 2678-2686.

63 (a) H. Sakiyama, A. K. Powell, *Dalton Trans.,* 2014, **43**, 14542-14545; (b) V. Tangoulis, M. Skarlis, C. P. Raptopoulou, C. D. Samara, *Eur. J. Inorg. Chem.*, 2014, **16**, 2678-2686.

64 (a) R. Chakrabarty, P. Sarmah, B. Saha, S. Chakravorty, B. K. Das, *Inorg. Chem*., 2009, **48**, 6371-6379; (b) A. I. Nguyen, R. G. Hadt, E. I. Solomon, T. D. Tilley, *Chem. Sci*., 2014, **5**, 2874-2878.

65 S. R. Hosseinian, V. Tangoulis, M. Menelaou, C. P. Raptopoulou, V. Psycharis, C. D. Samara, *Dalton Trans*., 2013, **42**, 5355-5366.

66 Z. A. Siddiqi, A. Siddique, M. Shahid, M. Khalid, P. K. Sharma, Anjuli, M. Ahmad, S. Kumar, Y. Lan, A. K. Powell, *Dalton Trans*., 2013, **42**, 9513-9522.

67 R. Chakrabarty, P. Sarmah, B. Saha, S. Chakravorty, B. K. Das, *Inorg. Chem*., 2009, **48**, 6371-6379.

68 T. Nakajima, K. Seto, A. Scheurer, B. Kure, T. Kajiwara, T. Tanase, M. Mikuriya, H. Sakiyama, *Eur. J. Inorg. Chem*., 2014, 5021-5033.

69 R. Destro, E. Sartirana, L. Loconte, R. Soave, P. Colombo, C. Destro, L. L. Presti, *Cryst. Growth Des*., 2013, **13**, 4571-4582.

70 (a) R. Custelcean, M. G. Gorbunova, *J. Am. Chem. Soc*., 2005, **127**, 16362-16363; (b) D. L. Reger, R. F. Semeniuc, C. Pettinari, F. L. Giles, M. D. Smith, *Cryst. Growth. Des*., 2006, **6**, 1068-1070; (c) J. R. Butchard, O. J. Curnow, D. J. Garrett, R. G. A. R. Maclagan, *Angew. Chem. Int. Ed*., 2006, **45**, 7550-7553; (d) V. Gorteau, G. Bollot, J. Mareda, A. P. velasco, S. Matile, *J. Am. Chem. Soc*., 2006, **128**, 14788-14789; (e) S. Q. Bai, G. Y. H. Quek, L. L. Koh, T. S. A. Hor, *CrystEngComm*., 2010, **12**, 226-233; (f) R. R. Fernandes, A. M. Kirillov, M. Fatima, C. G. da Silva, Z. Ma, J. A. L. da Silva, J. J. R. F. da Silva, A. J. L. Pombeiro, *Cryst. Growth Des.,* 2008, **8**, 782-785.

71 (a) A. S. Gaballa, C. Wagner, S. M. Teleb, E. M. Nour, M. A. F. Elmosallamy, G. N. Kaluderovic, H. Schmidt, D. Steinborn, *J. Mol. Struct*., 2008, **876**, 301-307; (b) S. M. M. Sony, M. N. Ponnuswamy, *Cryst. Growth Des*., 2006, **6**, 736-742.

72 T. Z. Huyskens, M. Lily, D. Sutradhar, A. K. Chandra, *J. Phys. Chem. A*, 2013, **117**, 8010-8016.

73 K. Shankar, J. B. Baruah, *Inorg. Chim. Acta*, 2016, **453**, 135-141.

74 (a) M. Mascal, A. Armstrong, M. D. Bartberger, *J. Am. Chem. Soc*., 2002, **124**, 6274-6276; (b) Y. S. Rosokha, S. V. Lindermna, S. V. Rosokha, J. K. Kochi, *Angew. Chem. Int. Ed*., 2004, **43**, 4650-4652.

Chapter 5

Self-assembly of Copper(II) bis-ethylenediamine carboxylate complexes and fluorescence modulations in copper(II) bis-ethylenediamine 2,2′-biquinoline-4,4′-dicarboxylate

5.1 Background

In continuation with earlier chapters in which the four different types of templates were chosen, there are Influence of the size, shape and functionality of an organic anion in interlayer separations of layered hybrid structures is a need of the hour to utilize them as advance material.[1] Advent of interesting frameworks from ethylenediamine complexes[2] provides a scope to relook at ethylenediamine based metal complexes. Furthermore, existing literature suggests that nitrobenzoate complex of copper ethylenediamine complex adopts layered structure.[3] This was an interesting point to generate interest to choose carboxylate as anions to guide layered structures of copper complexes of ethylenediamine which is a classical chelating ligand. The copper(II)ethylenediamine complexes,[4] have versatility and could be a source of different building blocks for supramolecular assemblies as illustrated in Figure 5.1.

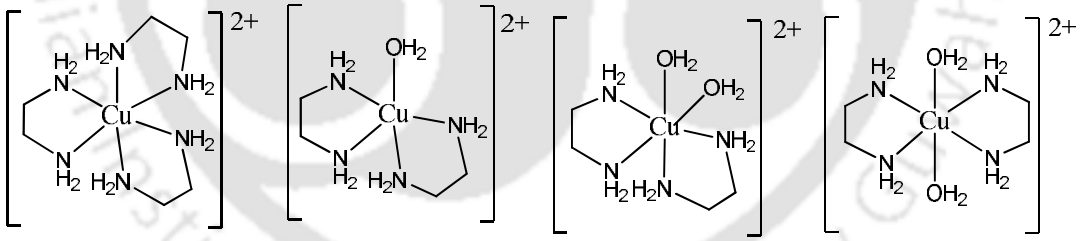

Figure 5.1: Different copper ethylenediamine complex cations.

To understand self-assembling properties and scopes of anion exchange, and to understand interlayer separations in solid state and modulation of fluorescence properties of anions in solution of copper(II) ethylenediamine complexes a study based on structural and thermochemical and fluorescence properties are presented in this chapter.

5.2 Synthesis and characterisation of copper(II) bis-ethylenediamine carboxylates

Reactions of ethylenediamine with copper(II) acetate followed by treatment with different aromatic carboxylic acids yielded copper complexes illustrated in Scheme 5.1. In the present case two types of complex cations which are either $[Cu(en)_2(H_2O)_2]^{2+}$ or the $[Cu(en)_2(H_2O)]^{2+}$ were found in the complexes listed in Scheme 5.1.

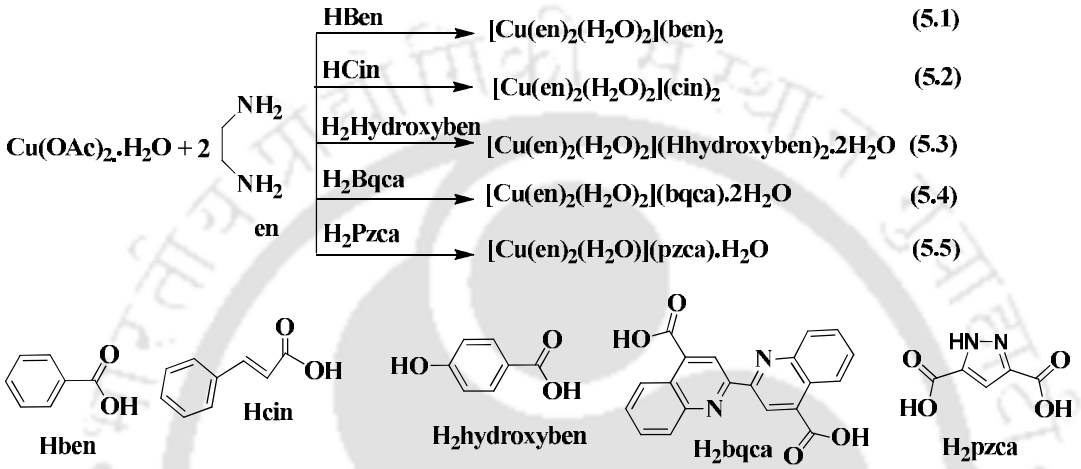

Scheme 5.1: Synthesis of copper(II) bis-ethylenediamine complexes.

These complexes were characterized by various spectroscopic techniques. Polycrystalline samples of the complexes **5.1-5.5** showed ESR spectra corresponding to tetragonal distortion[5] and from the observed $g_{\perp}$ and $g_{\parallel}$ the g_{av} values were determined. Each complex showed single visible absorption characteristic of d-d transition of d^9-electronic configuration of copper(II) ion, based on the respective absorption maximum the 10Dq values of the complexes were determined.[6] These values were used to calculate the spin-orbit coupling, which are listed in Table 5.1.

Crystal structures of the complexes **5.1-5.5** were determined by single X-ray diffraction. On the other hand, powder X-ray diffraction (XRD) patterns of each bulk samples after complete evaporation of solvent were taken and their phase purities were ascertained.

The experimental powder XRD pattern of each complex was compared with the respective powder XRD pattern generated from the XRD data obtained through single crystal structure which shows a good agreement to have the respective complex in the crude precipitate (Appendix 5A1).

Table 5.1: ESR parameters of the complexes

Complex	g_{av}	10Dq (cm^{-1})	χ (cm^{-1})
5.1	2.10	17825	-445
5.2	2.08	18018	-360
5.3	2.07	17331	-303
5.4	2.08	17452	-349
5.5	2.02	17605	-88

But the powder XRD pattern of freshly recrystallised bulk sample showed presence of single component. Hence, these complexes are very advantageous in terms of their easy preparation procedure and purification by simple crystallization technique. A representative powder XRD pattern of the freshly crystallized samples of the complex **5.4** is shown in Figure 5.2 showing the phase purity of the bulk crystalline product.

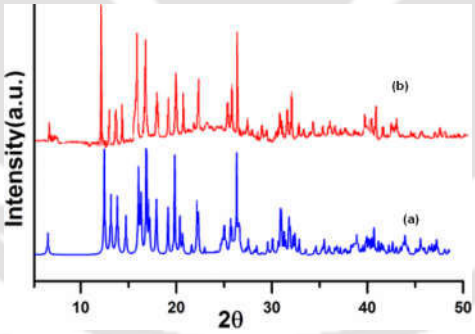

Figure 5.2: Powder X-ray diffraction pattern of complex **5.4**. (a) Computer generated from the CIF file of single crystal diffraction data and (b) is the experimentally determined pattern from bulk sample.

The complexes are thermally less stable and water molecules are lost on heating in the range of 100ºC-225ºC. Finally complexes degrade to form copper oxide at a temperature range 350ºC-550ºC.

This was confirmed by comparing a PXRD of the end product after combustion with PXRD of standard sample and the corresponding weight loss in respective thermo grams are given as (Appendix Figure 5A2) tallies with the calculated weight loss to obtain from the decomposition of the respective complex.

It may be noted that the nano-size copper oxide particles are formed by thermal decompositions of metal-organic frameworks.[7] In an earlier study[8] it was shown that bis-ethylenediamine copper(II) acetate dihydrate decomposes to copper oxide at >360°C. Cinnamate and pyrazoledicaroxylate complexes have decomposition temperatures at 325°C and 350°C respectively, which are mild and lower than reported acetate complex, showing promise in getting a method for synthesis of copper oxide under mild conditions with these systems. Complex **5.4** undergoes exchange of its anion on reaction with different carboxylic acid such as benzoic acid, cinnamic acid, hydroxybenzoic acid and pyrazole-3,5-dicarboxylic acid to form respective carboxylate complexes. These all complexes obtained through anion exchange were confirmed by comparing their spectroscopic features with the one synthesized from reaction scheme shown in Scheme 5.1.

5.3 Structures of copper(II) bis-ethylenediamine carboxylates

Complexes **5.1-5.4** have common $[Cu(en)_2(H_2O)_2]^{2+}$ cation but have different carboxylate ions. Cationic part in each case adopts distorted octahedral geometry around copper ion with four nitrogen atoms occupying the four corner of an equatorial plane, whereas the axial positions are occupied by two water molecules. The complex **5.1** has average Cu-N bond lengths in the range of 2.008Å-2.021Å and has Cu-O bond lengths 2.590Å and 2.618Å. Comparing these values with the reported Cu-O distances[9a] in copper complexes, the Cu-O bond containing axis is assigned as the Jahn-Teller axis. Cations of complex **5.1** are hydrogen bonded with benzoate (Figure 5.3a). In addition to these interactions, there are intermolecular N-H···O interactions between the NH_2 group with benzoate.

Hydrogen bonds of the benzoates with coordinated water molecules have puckering feature to form criss-cross geometry. Complex **5.2 (**Figure 5.3b) has also a similar structure to the complex **5.1**.

Self-assembly of the complex **5.3** has wide difference from the one observed for complex **5.1** and complex **5.2**. Self-assembly is assisted by water of crystallization and the hydroxy group of the 4-hydroxybenzoate (Figure 5.3c). Two hydroxybenzoate ions are hydrogen bonded in different ways to cations. One 4-hydroxybenzoate is associated with the coordinated water molecule, whereas other is associated with the water of crystallization.

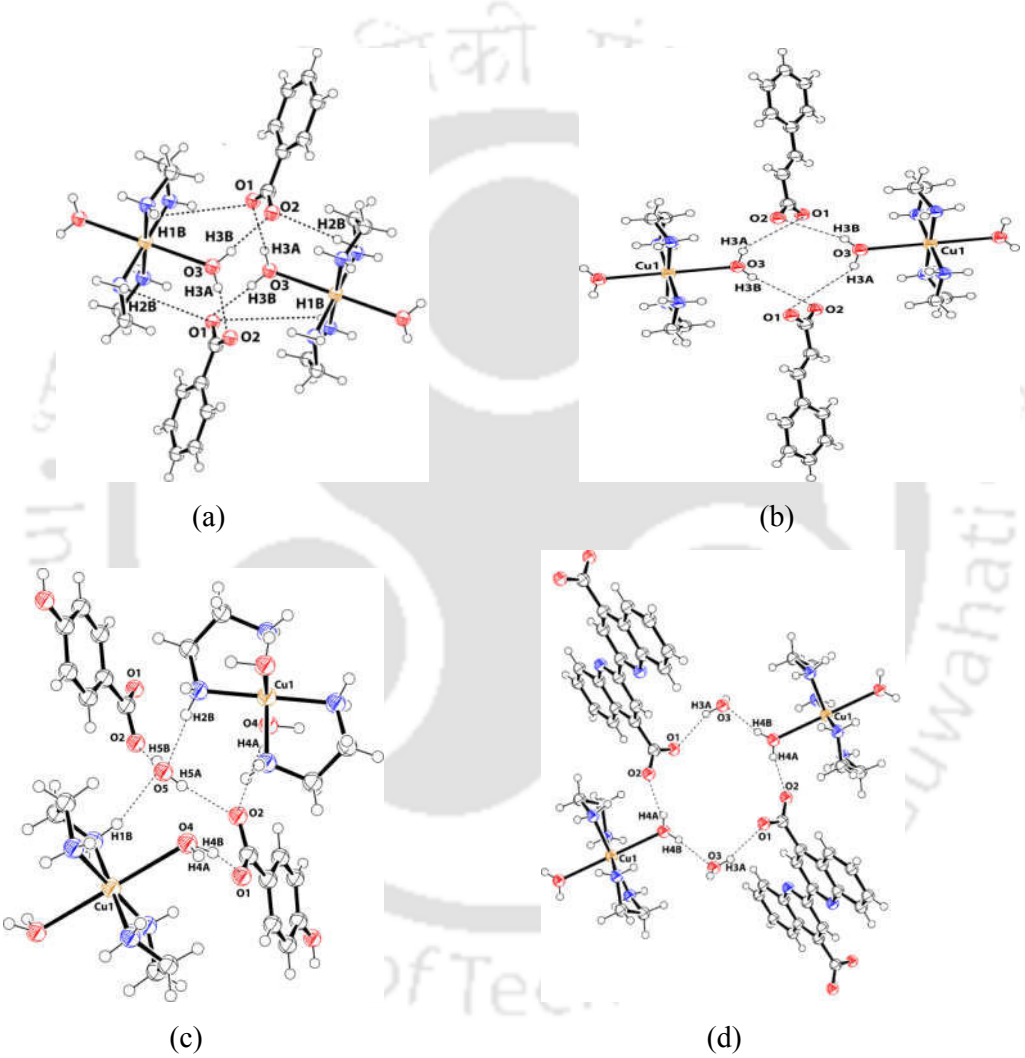

Figure 5.3: Self-assemblies of (a) complex **5.1**, (b) complex **5.2**, (c) complex **5.3**, (d) complex **5.4**. (ORTEP with 50% thermal ellipsoids).

In complex **5.4**, there is one biquinoline dicarboxylate ion per divalent cationic unit. These dianions are held by strong hydrogen bonds (Figure 5.3d).

It has a water of crystallization molecule which contributes to the overall packing pattern by forming hydrogen bonds with dicarboxylates. Structure and composition of the complex **5.5** is different from other four carboxylate complexes, it possesses a penta-coordinated dication $[Cu(en)_2(H_2O)]^{2+}$. Cationic part complex has square pyramidal geometry around copper ion and has one pyrazole dicarboxylate.

This complex has hydrogen bonds between the pyrazole N-H and oxygen atom of carboxylate make dimeric assemblies without direct participation of the coordinated water molecules (Figure 5.4).

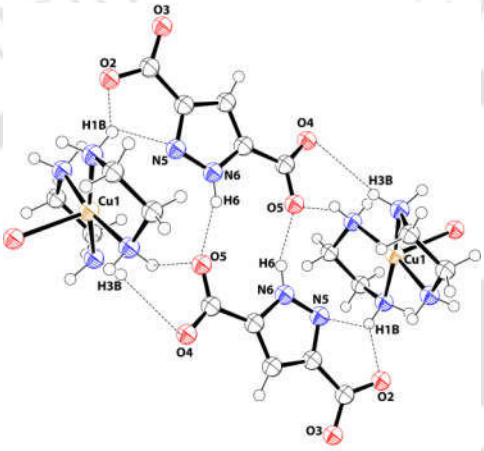

Figure 5.4: Self-assembly of complex **5.5**.

5.4 Layer-like structures in copper(II) bis-ethylenediamine carboxylates

Each complex has arrangements of cations and anions as separate layers. Directions of extension of layers in terms of crystallographic directions are independent of each other. These cationic layer-like self-assemblies are guided by anions. Hence the packing patterns of such layer-like packing are shown in Figure 5.5. The distances between two nearest neighbouring copper ions in the adjustment layers in the packing pattern of these complexes **5.1-5.5** are 6.21Å, 6.37Å, 7.20Å, 6.84Å and 6.67Å respectively.

Layered structures of anionic carboxylates are well established.[9b] In such cases organo-cations can control the interlayer separation. The present set of complexes possessing layered structures are soluble in common solvent such as methanol, water etc provides large scope to explore their transformations from one to another by anion exchange.

Accordingly the layered structures could be modified by treating with appropriate carboxylic acid. For example, the complex **5.4** could be converted to complex **5.1** on treatment with benzoic acid, whereas the complex **5.4** could be converted quantitatively to complex **5.2** or **5.3** by independently treating with cinnamic acid or 4-hydroxybenzoic acid. This provides wide perspective to study them as modifiable layered structures.

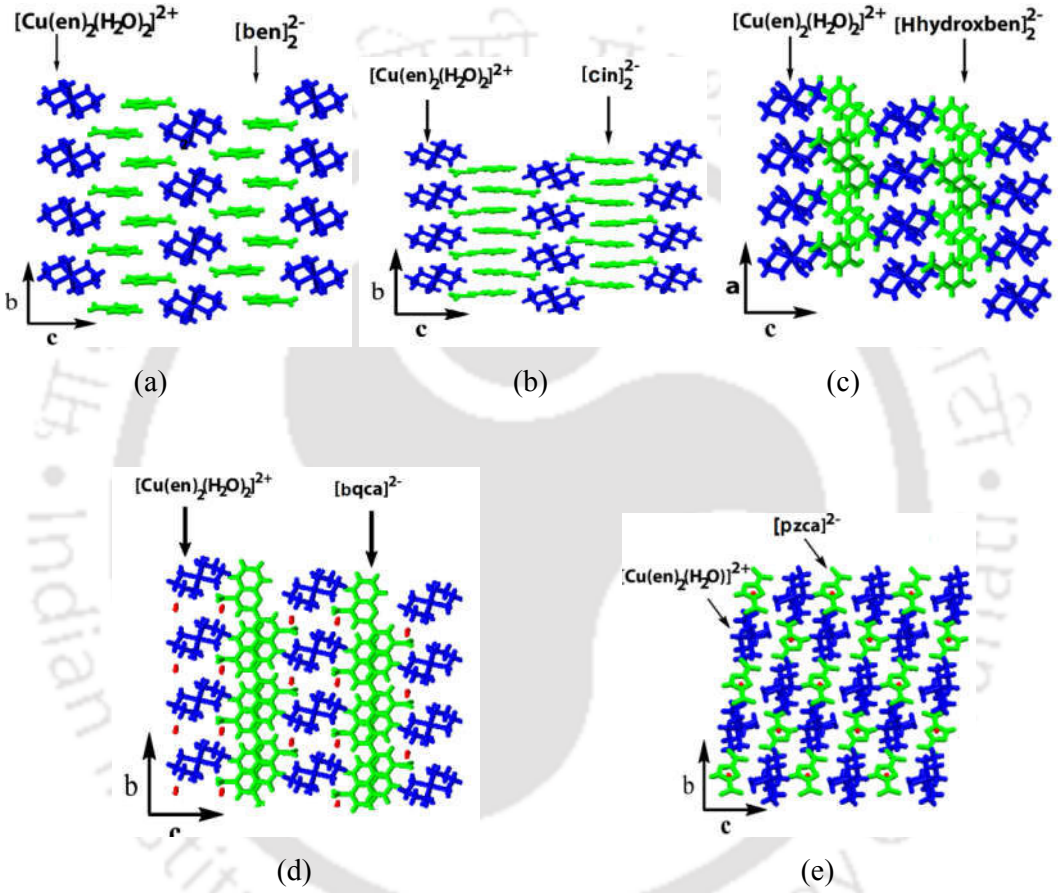

Figure 5.5: Layer-like arrangements of ions in packing patterns of complexes (a-e) **5.1-5.5**.

Anionic layers held by rigid dication[10] such as 4,4'-bipyridinium generates different porous scaffolds to encapsulate guest molecules, whereas cationic assemblies.[11] Bis-ethylenediamine copper(II)hexacyanochromate[12] adopts porous 3D-polymeric structure.

5.5 Sub-assemblies formed by hydrogen bonds in the complexes

Dicarboxylic acids are precursor for various copper complexes which shows interesting properties.[13]Among two dicarboxylic acid complex of diquinolinedicarboxylate complex **5.4** is an example of a complex having porous packing pattern, whereas tight packed non-porous structures were observed in pyrazoledicarboxylate so are the cases with **5.1-5.3.** Robust hydrogen bonded sub-assemblies have been developed from the assemblies of non-covalently linked carboxylic acids[14] Different hydrogen bond motifs has clear implications on the surface area of porous structures.[15]

Thus, analysis of hydrogen bonded motif in layered structures not only make their packing pattern clear but also help to reason out stabilities. Self-assembling processes in hydrogen bonded covalent synthesis are guided by Ettter's rules and hence can be easy to describe such systems by graph-set notations[16] which needs definite attention. These complexes serves as examples of different types of cyclic hydrogen bonded sub-assemblies.[17]

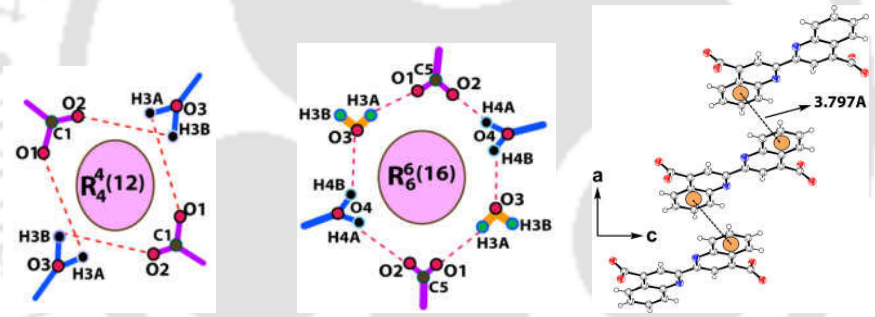

(a) (b) (c)

Figure 5.6: Hydrogen bonded sub-assemblies found in self-assemblies of copper complexes (a) **5.1** and **5.2**, (b) **5.4**, (c) π-Stacking among quinoline rings in crystal lattice of the complex **5.4**.

There are puckered $R^4_4(12)$ cyclic type hydrogen bonded sub-assemblies in the complexes **5.1-5.2** illustrated in Figure 5.6(a) $R^4_4(12)$ hydrogen bonded sub-assemblies are come across in various organic systems but the puckered geometry is common.[17]

Table 5.2: Hydrogen-bond parameters of sub-assemblies in lattice of complex **5.4**

D-H···A	$d_{D-H(Å)}$	$d_{H\cdots A(Å)}$	$d_{D\cdots A(Å)}$	∠D-H···A(°)
O(4)-H(4A)···O(2) 1-x,-y,1-z]	0.81	2.04	2.828(4)	163
O(4)-H(4B)···O(3) [x,-1+y,z]	0.84	2.00	2.824(2)	167
O(3)-H(3A)···O(1) [x,y,z]	0.79	2.09	2.855(2)	161
O(3)-H(2B)···O(2) [-1+x,y,z]	0.79	2.05	2.818(2)	163

Complex **5.3** has two cyclic motifs holding the carboxylate ions, cationic complex and water molecules. Solid state self-assembly of the complex **5.4** predominantly has hydrogen bonds (Figure 5.6b) and face to face π-interactions between quinoline rings (Figure 5.6c). Presence of an easily rotatable C_{ipso}-C_{ipso} bond in anion, it adopts anti-orientation in the complex.

With in the solid state self-assembly of the complex, two molecules of complex **5.4** form cyclic sub-assemblies by hydrogen bonding between two coordinated water molecules, two anions and two cations (Figure 5.6b). Such cyclic sub-assembly has $R_6^6(16)$ graph set notation.[18] Each sub-assembly has O3-H···O1, O4-H···O3 and O4-H···O2 hydrogen bonds, whose bond parameters are listed in Table 5.2. Bond parameters listed in Table 5.2 are suggestive of hydrogen bonds with moderate strength.[19] Generally, hydrogen bonded cyclic sub-assemblies are useful constituent of supramolecular materials having interesting properties.[20] On the other hand, the complex **5.5** forms dimeric hydrogen bonded self-assembly of anions. This results in $R^2_2(10)$ motif involving two N6-H···O5 interactions (Figure 5.4). Thus, this series of complexes constitute varieties of hydrogen bonded motifs that are of interest in crystal engineering and supramolecular chemists.

In practice large cyclic sub-assemblies within a non-covalent self-assembly present in layered structures generate porous scaffolds.[21] The complex **5.4** is not an exception, due to presence of large size $R_6^6(16)$ sub-assemblies it is porous. It may be noted that robust non-covalently linked sub-assemblies in crystal lattice make less stable packing but in this particular case assembly is guided by hydrogen bonds with electrostatic interactions, hence is stable at room temperature.

But sub-assemblies break down on heating to 120°C by losing water molecules. This is confirmed by thermogravimetry where there is a loss of 8.71% weight when heated from 37°C to 120°C (Figure 5.7a) is observed. This weight loss corresponds to loss of three water molecules per complex.

Theoretical weight loss for three water molecules is 9.32%. Difference is attributed to hygroscopic nature of the complex. Loss of water molecules is attributed from IR spectra of a sample of complex **5.4** heated at 120°C. IR spectra of complex **5.4** recorded at 32°C and that of a freshely heated sample of complex **5.4** at 120°C, and also IR spectra of a sample of complex **5.4** which was kept in atmosphere of 75% humidity at 32°C after heat treatment are compared in Figure 5.7 (c).

Complex **5.4** has a broad OH-stretching frequency at 3413 cm^{-1}, which diminished on heating, so as sharp peaks appearing at 1648 cm^{-1} and at 1604 cm^{-1}. Regions of the IR spectra showing spectral changes are marked by including those regions in boxes in Figure 5.7(c). However, original IR spectrum of the complex is recovered when heat treated sample is left in a humid atmosphere of about 73% humidity.

This suggests that dehydration changes structure of complex **5.4** but original packing could be regenerated upon absorption of humidity. Proof for reversible hydration and dehydration of the complex **5.4** was also revealed in powder XRD pattern of the sample under different conditions.

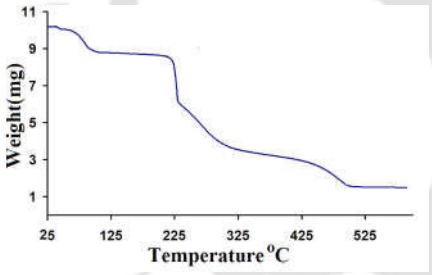

(a)

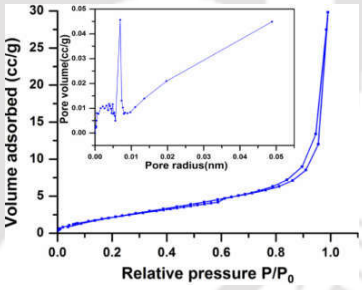

(b)

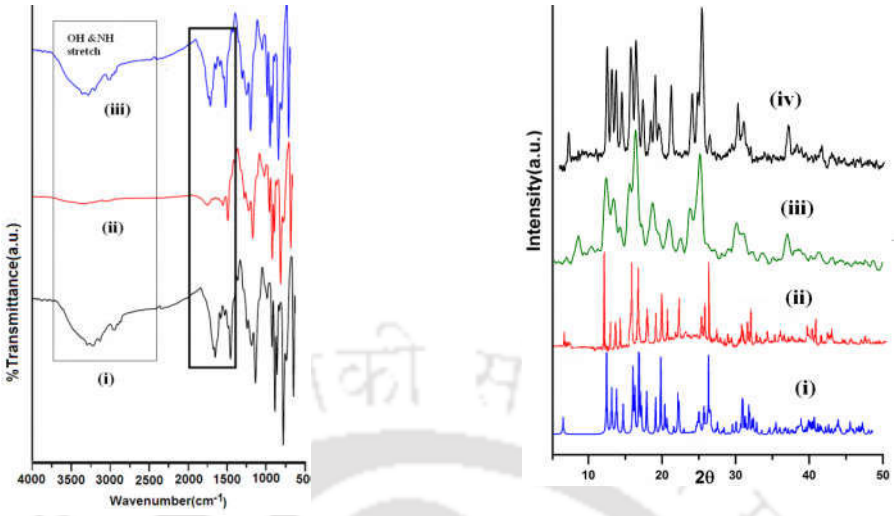

(c) (d)

Figure 5.7: (a) Thermogram of the complex **5.4** (heating rate 10ºC per minute). (b) Nitrogen adsorption isotherm for complex **5.4** at 77 K and pore size distribution (inset). Surface area = 15.092 m²/g. (c) FTIR of (i) complex **5.4**, (ii) complex **5.4** heated at 120°C for 2 hrs; (iii) Heat treated sample kept at humid condition (75% humidity) for 2 hrs. (d) Powder X-ray diffraction patterns of complex **5.4** (i) computer generated from crystallographic information file and (ii) experimental pattern from bulk sample of complex **5.4**, (iii) complex **5.4** heated at 120°C for 2 hrs, (iv) Heat treated sample of complex **5.4** after keeping at 75% humidity condition for 2 hrs.

Powder XRD pattern of bulk sample of complex **5.4** shown in Figure 5.7(d) tallies with corresponding theoretically generated powder XRD pattern from crystallographic information file [Figure 5.7d (i)]. On the other hand, powder XRD pattern of a freshly heated sample at 120°C was different from hydrated sample, it suggests dehydration of complex **5.4** on heating. Powder XRD pattern of a heat treated sample after standing for 2 hrs at 75% humid condition gave a powder XRD pattern which was super-imposable with the powder XRD pattern of the original sample [Figure 5.7d (iv)]. These results clearly indicate that control heating results in formation of a dehydrated complex which reabsorbs moisture to form original complex. Anions present in the lattice are arranged such that a portion of the quinoline rings of two nearest neighbouring anions are parallel. Centroid to centroid distances between portions of parallel rings is 3.797Å. This distance is suitable to have π-interactions between these rings.[22]

Porous nature of the complex was also reflected in the surface area of the complex determined by nitrogen gas absorption isotherm.

The isotherm is shown in Figure 5.7(b) which resembles type II of IUPAC recommended isotherm.[23]From this isotherm surface area was found as15.092 m^2/g. This low surface area value is suggestive of the fact that during sample preparation the complex was decomposed; which indeed tallies with findings observed through IR and XRD studies. Thermogram of complex **5.4** is shown in Figure 5.7(a) where 83.40% weight loss on heating to 500°C corresponds to copper oxide, theoretically calculated weight loss 84.53% for such decomposition. Copper oxide formation was confirmed by comparing powder XRD with authentic copper oxide sample. Copper oxide particles with different morphologies were 25nm-50nm sizes as measured by FESEM as illustrated in Figure 5.8 (a) and TEM in Figure 5.8(b)

Thus this complexes are good precursors for nano-size copper oxide particles where substrates are mononuclear complexes in contrast to metal-organic frameworks.[22]

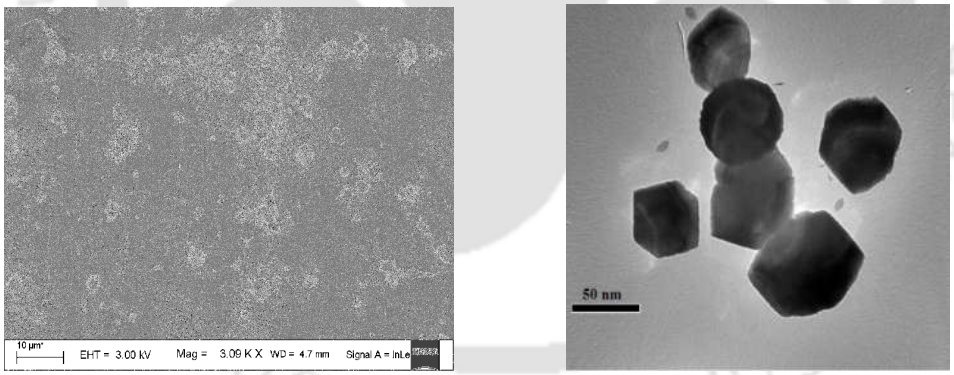

Figure 5.8: (a) FESEM and (b) TEM images of the copper oxide obtained by heating complex **5.4** at 500°C.

5.6 Modulation of fluorescence of copper diquinolinedicarboxylate complex 5.4

Modulation of fluorescence emission of a fluorescent compound is of fundamental importance.[24] Interactions of a metal ion with a fluorescent receptor changes original fluorescence emission.[25] The paramagnetic metal ions such as Cu^{2+} ions are often used to quench fluorescence of receptors,[26] but limited examples on fluorescence enhancement of a receptor by interactions with Cu^{2+} ions are also available.[27]

Self-assemblies formed by weak interactions such as π-stacking.[28] As discuss in chapter four that anion-π interactions[29] contribute to changes in fluorescence emissions of a compound. π-Stacking[30] largely influence fluorescence behaviour of a compound[31] and face to face π-interactions of aromatic compounds are well known to cause fluorescence quenching.[32] A small change in electronic and steric factor can change self-assembly of π-stacked molecules or ions to affect fluorescence properties.[33] On the other hand, fluorescence emissions of many polyaromatic receptors are guided by solvents [34] molecules affecting fluorescence emission are also reflected in fluorescence properties of solvates in solid state.[35] Study of weak interactions in self-assemblies helps to establish effect of conformations and guided by interplay of weak interactions.[36] The energy of face to face π-stacking interactions is of the extent of 15.5 kJ mol^{-1}.[37] Such interactions among ligands in inorganic complexes influence packing patterns and coordination geometry.[38]

On the other hand difference in degree of self-association among molecules of a compound, may cause difference in respective fluorescence emission in solid or in solution.[39] Thus, construction of new schemes to modulate fluorescence properties through interplay of weak interactions is essential. In order to study modulation of fluorescence of a fluorescent nitrogen containing dicarboxylic acid (Figure 5.9) namely, 2,2'-biquinoline-4,4'-dicarboxylic acid abbreviated as **H_2bqca** by interplay of supramolecular effects.

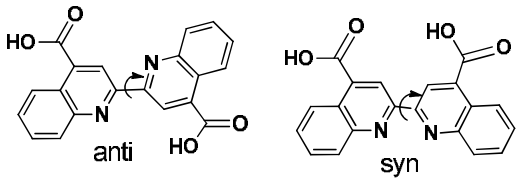

Figure 5.9: Two conformers of 2,2'-biquinoline-4,4'-dicarboxylic acid (**H_2bqca***)*

Choice of this compound is due to following reasons: (a) Anion from this compound **H_2bqca** is big in size, hence a non-covalent assembly constructed by such anions may be easily dismantled, (b) A big anion will be reluctant to coordinate to a metal ion,- (c) **H_2bqca** being a flexible molecule will have possibility to adopt different orientations by rotation around C_{ipso}-C_{ipso} bond as illustrated in Figure 5.9, (d) There is existing literature on coordination ability of the **H_2bqca** for chelation and to form coordination polymers[40] and (e) Most importantly **H_2bqca** is likely to π-stack as a characteristic feature associated with quinoline based compounds.[41] It is also well known fact that **H_2bqca** is commonly used to detect Cu^+ ions[42] and sugar, such detections are based on redox and fluorescence properties.[43] Besides these, **H_2bqca** chelates to Cu^{2+} ions.[44] It also forms framework structures with interesting properties[45] having applications in material science[46] and supramolecular chemistry.[47] **H_2bqca** has active hydrogen atoms, hence may show excited state proton transfer observed in structurally related systems.[48] With these backgrounds, we have carried out a concerted study on stability of hydrogen bonded sub-assemblies within solid state self-assembly of a copper complex and also studied interplay of weak interactions associated with **H_2bqca** to modulate fluorescence emissions and the importance of cationic complexes to modulate fluorescence properties. A methanol solution of **H_2bqca** showed fluorescence emission at 396nm upon excitation at 320nm. Fluorescence emission spectra of the ligand were dependent on solvents (Figure 5.10). Wavelengths of emission in different solvents and respective quantum yield are listed in Table 5.3. Quantum yield in methanol solvent was highest among all the solvents. The trend in change in quantum yields in different solvents did not have a linear correlation with polarity index.[49] Hence it may be suggested that the interactions of solvent molecules with excited state of the fluorophore causing a proton transfer may be shifting the emission wavelength and guide intensity of emissions.

Methanol enhances fluorescence emission intensity of polyaromatic compounds[50] and excited state proton transfer[51] by protic solvents of solvatoemissive hydroxyquinoline derivatives.[48] Hence from structural similarities between these structures a similar process operates in the present case too.

Table 5.3: Fluorescence emission and quantum yield of **H_2bqca** in different solvents.

Solvent	Emission wavelength (nm)	Quantum yield
Methanol	396	0.61
Ethanol	389	0.23
DMF	400	0.10
Water	392	0.06
DMSO	379	0.05

By virtue of paramagnetic copper(II) ion present in complex **5.4**, it is expected to be non-fluorescent. But we found interesting fluorescence properties associated with complex **5.4**. It was highly fluorescent in methanol [Figure 5.10a (iv)]. However, we also found the same complex non-fluorescent in solid state. If paramagnetic effect alone would have affected fluorescence, it would have generated non-fluorescent state in both the cases. We observed that **H_2bqca** in solid state show fluorescence emission at 399nm on excitation at 310nm. A solid sample of complex **5.4** showed very weak rather negligible emission at 474nm [Figure 5.10b(ii)]. Since powder XRD study revealed inter-conversion of hydrated to anhydrous form of complex **5.4** and vice versa, same effect should translate to fluorescence properties in solid state. Thus, fluorescence emission spectra of a sample of complex **5.4** heated at 120°C for half an hour was recorded.

Anhydrous complex formed by heating showed fluorescence emission at 499nm has intensity comparable to the emission intensity of **H2bqca** in solid state. Shift in emission wavelength of solid samples towards higher side of the complex with respect to ligand **H_2bqca** suggested to an exciplex emission. Emission at 499nm of heat treated sample of the complex was broad and vibration features were observed [Figure 5.10b (iii)]. This clearly indicates that upon heating alignment of π-systems changed facilitating changes in emission.

On the other hand, fluorescence emission of the heat treated sample was decreased with time on keeping in 75% humid environment at 32°C. Spectral changes were noted by recording spectra at five minutes time intervals, which are shown in Figure 5.10b(iii)-(x).

These changes showed that complex **5.4** recovered original hydrated form and reached a fluorescence quenched state. Such observations are important for academic purpose to understand interplay of weak interactions and imply utilities for modulation of fluorescence in solid state. Existing literature suggests that **H2bqca** generates intense fluorescence on interaction with diamagnetic Cu^{+} ions.[46] In such a case coordination of neutral **H2bqca** took place through nitrogen atoms[46] forming a cationic complex of Cu^{+}. But in complex **5.4** oxidation state of copper is +2 and **bqca** anions are outside coordination sphere. Quenching effect of the copper ions is absent in the complex **5.4** in solution suggests no impact of paramagnetic Cu^{2+} ions in the complex **5.4** to influence fluorescence.

On the other hand, in solid state anions of the complex **5.4** have π-stacking interactions between fluorophoric **bqca** anions. Whereas in solution solvent molecules can segregate the π-stacking interactions.[52] Packing pattern of the complex **5.4** suggests that fluorophores are away from the paramagnetic Cu^{2+} ions due to chelation by ethylenediamine. Thus, there is no direct contact of the copper ions with anions. On the other hand, a methanol solution of complex **5.4** showed higher fluorescence intensity than corresponding equimolar solution of **H_2bqca** [Figure 5.10a (iv)] in methanol. This difference of fluorescence from parent carboxylic acid is attributed to deprotonated species of **H_2bqca** in the complex. This is due anions conjugated to aromatic group to show higher intensity of fluorescence than the parent acid due to higher delocalisation.[53]

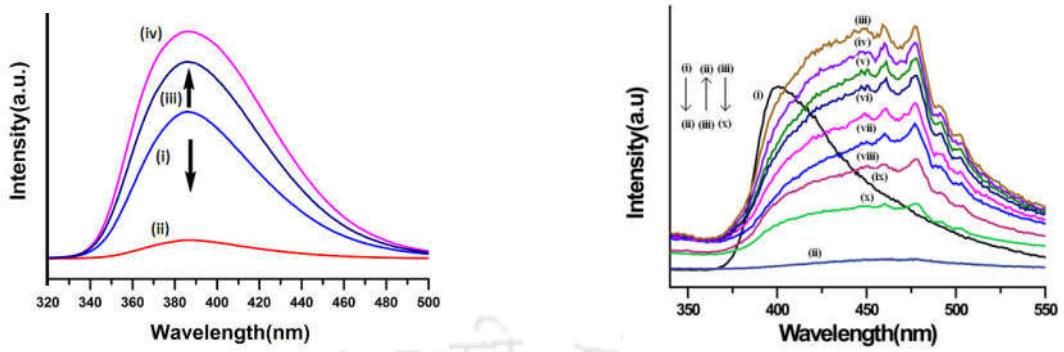

(a) (b)

Figure 5.10: (a) Fluorescence emission of a methanol solution of (i) **H_2bqca** (10^{-5} M, 3 ml) (ii) solution of **H_2bqca** and copper(II)acetate solution (equimolar 10^{-5} M, 3 ml) (iii) Addition of equimolar amount of ethylenediamine to the solution containing **H_2bqca** and copper(II)acetate (equimolar 10^{-5} M, 3 ml) (iv) complex **5.4** in methanol (10^{-5} M, 3 ml; λ_{ex} 320 nm). (b) Solid state fluorescence spectra of the (i) **H_2bqca**, (ii) complex **5.4**, (iii) Complex **5.4** heated at 120°C for half an hour, (iv-x) Heat treated complex in 75% humidity after every five minutes time interval; (λ_{ex} = 310 nm).

Control experiments were carried out to understand competitive effect of chelation of ethylenediamine to Cu^{2+} ions. It was found that fluorescence emission of methanol solution of **H_2bqca** was quenched by addition of a solution of Cu^{2+} ions [Figure 5.10a (i) and (ii)]. Whereas, addition of a solution of ethylenediamine to a solution containing **H_2bqca** with Cu^{2+} ions, fluorescence emission intensity was recovered and accordingly increased with the concentration of ethylenediamine. In such a case observed fluorescence emission had higher intensity than that of a solution of **H_2bqca** {Figure 5.10(a)(i)-(iii)} in methanol. Thus, fluorescence quenching caused by Cu^{2+} ions could be recovered by chelating effect of ethylenediamine with Cu^{2+} ions. Upon chelation the **H_2bqca** is no longer in direct contact with Cu^{2+} ions, which causes the increase in fluorescence emission. Thus the entire process can be explained on the basis of Scheme 5.2. When a solution of $[Cu(en)_2(H_2O)_2](OAc)_2$ was added to a methanol solution of **H_2bqca** fluorescence emission was increased (Figure 5.11a).

This observation is in contrast to effect of copper(II)acetate solution added to **H_2bqca** (Figure 5.11b) solution where quenching of fluorescence took place.

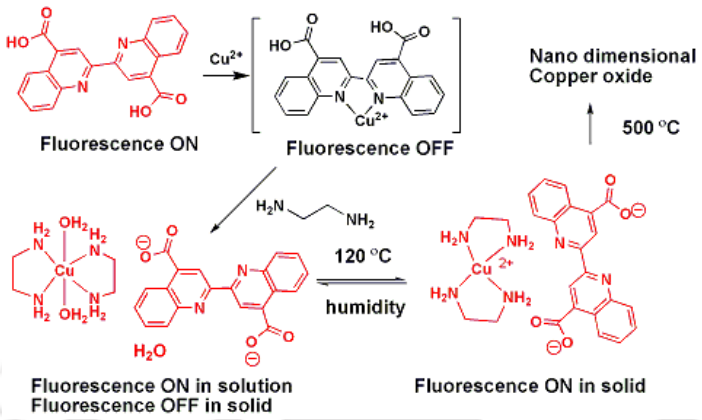

Scheme 5.2: Modulation of fluorescence of **H_2bqca** and thermal decomposition of complex **5.4**.

This shows that ON and OFF fluorescence can be easily caused by utilizing interplay of chelate effect of ethylenediamine with coordination effect of **H_2bqca**. Increase in emission by adding solution of complex $[Cu(en)_2(H_2O)_2](OAc)_2$ to **H_2bqca** solution is due to formation of complex $[Cu(en)_2(H_2O)_2](bqca).H_2O$, confirmed by isolation of this complex.

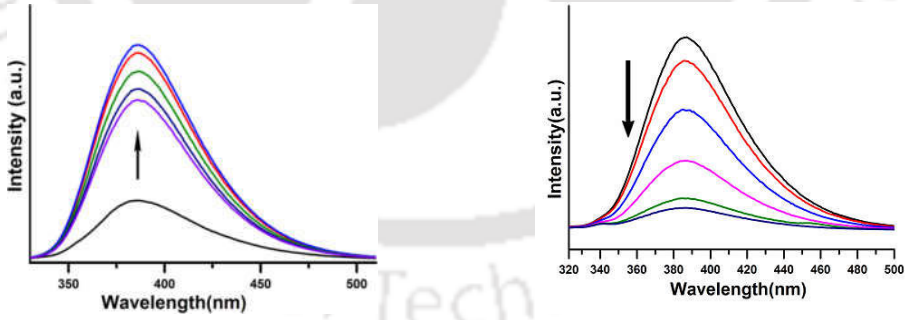

(a) (b)

Figure 5.11: (a) Increase in fluorescence emission of methanol solution of **H_2bqca** (10^{-5} M in 3 ml; λ_{ex} = 320 nm) on addition of $[Cu(en)_2(H_2O)_2](OAc)_2$ (10^{-5} M, 20 µL in each aliquot). (b) Quenching of fluorescence of a solution of **H_2bqca** (10^{-5} M in 3 ml; λ_{ex} = 320 nm) on addition of copper(II)acetate (10^{-5} M, 20 µL in each aliquot).

On the other hand, anions of copper salts did not contribute to quenching of fluorescence. Quenching of fluorescence emission of solution of **H_2bqca** was also observed by adding copper(II) sulphate or copper(II) nitrate in an identical fashion as that of copper(II) acetate. A similar trend of ON and OFF fluorescence sequence was observed in solvents such as ethanol, water and dimethylsulphoxide as shown in Figures 5.12(a)-(c).

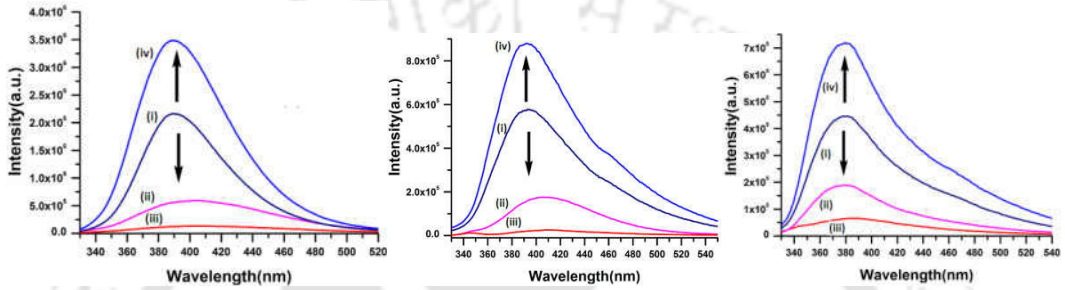

(a) (b) (c)

Figure 5.12: Fluorescence emission of (a) an ethanol solution of (i) **H_2bqca** ((10^{-5} M, 3 ml) (ii) solution of **H_2bqca** and copper(II) acetate solution (equimolar 10^{-5} M, 3 ml) (iii) Addition of copper(II) acetate in excess to the solution containing **H_2bqca** and copper(II) acetate (equimolar 10^{-5} M, 3 ml) (iv) Addition of equimolar amount of ethylenediamine to the solution containing **H_2bqca** and copper(II) acetate (equimolar 10^{-5} M, 3 ml).(b) and (c) are identical experiments in (b) water (c) DMSO respectively.

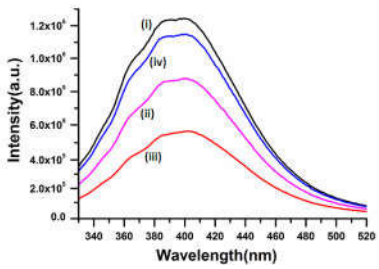

Figure 5.13: Fluorescence emission of a solution in DMF of (i) **H_2bqca** (10^{-5} M, 3 ml) (ii) solution of **H_2bqca** and copper(II)acetate solution (equimolar 10^{-5} M, 3 ml) (iii) Addition of copper(II) acetate in excess to the solution containing **H_2bqca** and copper(II)

acetate (equimolar 10^{-5} M, 3 ml). (iv) Addition of excess amount of ethylenediamine to the solution containing **H_2bqca** and copper(II) acetate (10^{-5} M, 3 ml).

This shows that without any difficulty the modulation is achieved in aqueous solution, thus it provides scope to study fluorescence changes of **H2bqca**, in aqueous medium. On the other hand, a solution of **H2bqca** in dimethylfomamide showed quenching of fluorescence on addition of copper(II) acetate. When ethylenediamine was added to this particular solution, fluorescence emission could be partially recovered (Figure 5.13) which can be considered as an exceptional case. This was attributed to coordinating ability of DMF molecules to copper ions inhibiting chelation of ethylenediamine. This establishes that the ligating ability of a solvent and its competition with chelation by ethylenediamine plays a crucial role to cause OFF and ON sequence.

However, addition of ethylenediamine to a methanol solution containing **H2bqca** and copper(II) acetate showed single exponential with life-time 2.066 ns. This suggests that addition of ethylenediamine enforces to retrace original fluorescence emission path by releasing **bqca** from the coordination sphere by chelating itself to copper ions. Hence, life-time measurements have added support to the Scheme 5.2.

5.7 Summary

Layer-like structures of copper(II) bis-ethylenediamine complex having various aromatic carboxylic acids are established. Anion exchanges in these layer-like structures are possible. π-Stacking interactions among fluorophoric anions and chelating effect of ethylenediamine of complex **5.4** have influenced fluorescence emissions. Modulation of fluorescence emission intensities of **H2bqca** by copper ions is achieved in solid state by dehydration and rehydration. Whereas in solution, chelating effect of ethylendiamine does this trick. Masking direct contact of fluorophores with paramagnetic ions in aqueous medium or related solvents clearly delineate scopes to develop new systems based on interplay of weak interactions.

5.8 Experimental section

Detailed synthetic methodologies are given below. Analytical data as well as spectroscopic data are also listed along with the each complex. Details of the instruments, crystallographic table are given in Appendix.

5.8.1 Synthesis of copper(II) bis-ethylenediamine complexes

5.8.1.1: $[Cu(en)_2(H_2O)_2]bqca.2H_2O$ **(5.4)**: To a solution of ethylenediamine (0.07 ml, 1 mmol) in methanol (20 ml) a solution of copper(II)acetate monohydrate (0.09 gm, 0.5 mmol) was added and stirred for 1 hr. at room temperature. A blue solution was formed, to this solution 0.5 mmol of **H_2bqca** was added and stirred for 30 minutes so as to obtain a homogenous solution. The reaction mixture was kept at room temperature for crystallization, after 6-7 days crystals were obtained and collected by filtration. Isolated yield: ~78%. Elemental anal calcd. for $C_{24}H_{32}O_7N_6Cu$, C, 49.69; H, 5.56; N, 14.49; found 48.71; H, 5.79; N, 14.14. IR (KBr, cm^{-1}): 3413 (bs), 3307 (m), 3240 (w), 2955 (w), 2919 (w), 1648 (s), 1604 (s), 1552 (s), 1419 (m), 1379 (s), 1201 (w), 1041 (s), 882 (w), 768 (m), 664 (m), 594 (w), 536 (w). Vis (methanol): λ_{max} = 573 nm (ε = 50 M^{-1} cm^{-1}). X-band ESR (solid state) g_{av} = 2.08. Molar conductance: 258 cm^2 mol^{-1}. Thermogravimetry (> 500°C, exptal weight loss 83.40%; whereas theoretical loss to obtain CuO is 84.53%)

5.8.1.2: Ligand exchange reactions on 5.4

The complex **5.4** (1 mmol) was dissolved in 10 ml methanol, to which respective carboxylic acid (2 mmol) namely benzoic acid or 4-hydroxy benzoic acid, cinnamic acid or 1 mmol of pyrazole-3, 5-dicarboxylic acid was added and mixed thoroughly and left for crystallization. After 2-3 days green crystals were obtained in each case.

5.8.1.3: $[Cu(en)_2(H_2O)_2](ben)_2$ **(5.1):** Isolated yield: ~87%. IR (KBr, cm^{-1}): 3312 (w), 3215 (w), 3128 (w), 2961 (w), 1652 (m), 1595 (m), 1550 (s), 1388 (s), 1276 (w), 1163 (w), 1107 (w), 1042 (s), 977 (m), 931 (w), 837 (m), 706 (s), 680 (w). Elemental anal calcd. for $C_{18}H_{30}O_6N_4Cu$, C, 46.79; H, 6.55; N, 12.13; found 46.75; H, 6.59; N, 12.44. Vis (methanol): λ_{max} = 561 nm (ε = 53 M^{-1} cm^{-1}). X-band ESR (solid state) g_{av} = 2.10. Molar conductance (methanol): 270 cm^2 mol^{-1}. Thermogravimetry (> 420°C exptal weight loss 84.90%, whereas theoretical loss to obtain CuO is 84.77%)

5.8.1.4: $[Cu(en)_2(H_2O)_2](cin)_2$ **(5.2):** Isolated yield: ~78%. IR (KBr, cm^{-1}): 3443 (bs), 3306 (m), 3215 (m), 3132 (m), 1639 (m), 1559 (s), 1492 (m), 1448 (m), 1406 (s), 1278 (w), 1237 (w), 1163 (w), 1105 (w), 1143 (s), 969 (m), 876 (w), 770 (m), 710 (w), 688 (m). Elemental anal calcd. for $C_{22}H_{34}CuN_4O_6$, C, 51.40; H, 6.67; N, 10.90; found 51.38; H, 9.75; N, 10.98. Vis (methanol): λ_{max} = 555 nm ((ε = 22 M^{-1} cm^{-1}). X-band ESR (solid state) g_{av} = 2.08). Molar conductance: 220 cm^2 mol^{-1}. Thermogravimetry (> 320°C exptal weight loss 85.36%; whereas theoretical loss to obtain CuO is 84.52%)

5.8.1.5: $[Cu(en)_2(H_2O)_2](Hhydroxyben)_2.H_2O$ **(5.3):** Isolated yield: ~76%. IR (KBr, cm^1): 3505 (bs), 3325 (w), 3279 (w), 3158 (w), 1604 (s), 1527 (s), 1502 (m), 1384 (s), 1277 (m), 1237 (m),1169 (m), 1105 (w), 1046 (s), 861 (m), 797 (m), 759 (m), 759 (m). Vis (methanol) : λ_{max} = 577 nm (ε = 37 M^{-1} cm^{-1}). X-band ESR (solid state) g_{av} = 2.07. Molar conductance: 234 cm^2 mol^{-1}. Thermogravimetry (> 500°C exptal weight loss 85.60% ; whereas theoretical loss to obtain CuO is 85.00%).

5.1.8.6: $[Cu(en)_2(H_2O)](pzca).H_2O$ **(5.5):** Isolated yield: ~81%. IR (KBr, cm^{-1}): 3377 (bs), 1647 (s), 1484 (m), 1382 (s), 1350 (m), 1325 (m), 1179 (w), 1104 (w), 1042 (s), 992 (w), 824 (m), 520 (w). UV-Vis: λ_{max} = 568 nm (ε = 48 M^{-1} cm^{-1}). X-band ESR (solid state) g_{av} = 2.02. Molar conductance: 198 cm^2 mol^{-1}.

5.8.1.7: $[Cu(en)_2(H_2O)_2](OAc)_2$ was prepared by reported procedure.[57]

5.8.2: Life time decay study

Life-time of fluorescence emission of (Appendix 5A) **H2bqca** showed single exponential decay with life-time 1.983 ns. Whereas a solution of copper(II)acetate and **H2bqca** had two life-times 0.326 ns and 2.018 ns respectively with 60:40 probability ratio. This shows that majority of excited molecules of **H2bqca** decay through a path having shorter life-time. Thus, quenching in methanol by copper ions is caused by change in the path of emission. However, addition of ethylenediamine to a methanol solution containing **H2bqca** and copper(II)acetate showed single exponential with life-time 2.066 ns.

This suggests that addition of ethylenediamine enforces to retrace original fluorescence emission path by releasing **bqca** from the coordination sphere by chelating itself to copper ions. Hence, life-time measurements have added support to the Scheme 5.2.

References:

1 C. Sanchez, B. Julian, P. Belleville, M. Popal, *J. Mater. Chem*., 2005, **15**, 3559-3592.

2 (a) X. Y. Wang, S. C. Sevov, *Cryst. Growth Des*., 2008, **8**, 1265-1270; (b) X. Y. Wang, S. C. Sevov, *Chem. Mater*., 2007, **19**, 4906-4912.

3 W. T. A. Harrison, A. M. Z. Slawin, R. P. Sharma, B. Sharma, S. Bhama, *Acta Crystallogr*., 2007, **E63**, m178-m180.

4 (a) A. B. P. Lever, E. Mantovani, *Inorg. Chem*., 1971, **10**, 817-826; (b) F. D. Dwyer, I. K. Reid, F. L. Garvan, *J. Am. Chem. Soc*., 1961, **83**, 1285-1287; (c) A. Yuan, J. Zou, B. Li, Z. Zha, C. Duan, Y. Liu, Z. Xu, S. Keizer, *Chem. Commun.*, 2000, 1297-1298; (d) Y. Inada, K. Ozutsumi, S. Funahashi, S. Soyama, T. Kawasima, M. Tanaka, *Inorg. Chem.*, 1993, **32**, 3010-3014.

5 D. Kevelson, R. J. Niedman, *Chem. Phys*., 1961, **35**, 149-155.

6 (a) B. J. Hathway, D. E. Billing, *Coord. Chem. Rev*., 1970, **5**, 143-207; (b) D. Kevelson, R. J. Niedman, *Chem. Phys*., 1961, **35**, 149-155.

7 (a) N. N. Sheno, A. Morsali, *Int. J. Nanosci. Nanotechnol*., 2012, **8**, 99-104; (b) K. Shankar, A. M. Kirillov, J. B. Baruah, *Polyhedron*, 2015, **102**, 521-529.

8 V. Zeleak, Z. Vargova, K. Gyoryova, E. Veernikova, V. Balek, *J. Thermal Anal. Calorimetry*, 2005, **82**, 747-754.

9 (a) I. M. Procter, B. J. Hathaway, P. Nicholls, *J. Chem. Soc*., 1968, 1678-1684; (b) A. M. Beatty, B. A. Helfrich, G. A. Hogan, B. A. Reed, *Cryst Growth Des*., 2006, **6**, 122-126.

10 J. Prakash, S. C. Sevov, *Inorg. Chem*., 2011, **50**, 12739-12746.

11 X. Y. Wang, S. C. Sevov, *Cryst. Growth Des*., 2008, **8**, 1265-1270.

12 A. Yuan, J. Zou, B. Li, Z. Zha, C. Duan, Y. Liu, Z. Xu, S. Keizer, *Chem. Commun.*, 2000, 1297-1298.

13 Y. Gong, M. M. Zhang, J. B. Qin, J. Li, J. P. Menga, J. H. Lin, *Dalton Trans*., 2014, **43**, 8454-8460.

14 M. Sugahara, K. Sada, M. Miyata, *Chem. Commun.*, 1999, 293-294.

15 E, Pidcock , W. D. S. Motherwell, *Crystal Growth Des*., 2005, **5**, 2322-2330.

16 (a) M. C. Etter, *Acc. Chem. Res*., 1999, **23**, 120-126; (b) M. C. Etter, J. C. McDonald, J. Bernstein, *Acta Crystallogr.*, 1990, **B46**, 256-262.

17 F. H. Allen, W. D. S. Motherwell, P. R. Raithby, G. P. Shields, R. Taylor, *New J. Chem*., 1999, **23**, 25-34.

18 M. C. Etter, *Acc. Chem. Res*., 1999, **23**, 120-12619; (b) T. Steiner, *Angew. Chem. Int. Ed. Eng*., 2002, **41**, 49-76.

20 E. Melnic, E. D. Coropceanu, O. V. Kulikova, A. V. Siminel, D. Anderson, H. J. R. Jacquez, A. E. Masunov, M. A. Fonari, V. Ch. Kravtsov, *J. Phys. Chem. C*, 2014, **118**, 30087-30100.

21 I. Hisaki, S. Nakagawa, N. Ikenaka, Y. Imamura, M. Katouda, M. Tashiro, H. Tsuchida, T. Ogoshi, H. Sato, N. Tohnai, M. Miyata, *J. Am. Chem. Soc.*, 2016, **32**, 138,6617-6628.

22 C. R. Martinez, B. L. Iverson, *Chem. Sci*., 2012, **3**, 2191-2201.

23 K. S. W. Sing, D. H. Everett, R. A. W. Haul, L. Moscou, R. A. Pierotti, J. Rouquerrol, T. Siemieniewska, *Pure and Appl. Chem.*, 1985, **57**, 603-619.

24 A. P. D. Silva, H. Q. N. Gunaratne, T. Gunnnlaugsson, A. J. M. Huxley, C. P. McCoy, J. T. Rademacher, T. E. Rice, *Chem. Rev*., 1997, **97**, 1515-1566.

25 M. Formica, V. Fusi, L. Giorgi, M. Micheloni, *Coord. Chem. Rev*., 2012, **256**, 170-192.

26 F. Gouanve, T. Schuster, E. Allard, R. M. Renault, C. Larpent, *Adv. Func. Mater*., 2007, **17**, 2746-2756.

27 (a) L. Huang, J. Su, D. Zhong, H. Wang, R. Liu, L. Yu, Q. Zhu, S. Liu, *RSC Adv*., 2013, **3**, 13286-13292; (b) G. M. Pechtl, *Proc Natl. Acad. Sci. USA*, 1974, **71**, 4684-4687.

28 X. F. Fu, Y. F. Yue, R. Guo, L. L. Li, W. Sun, C. J. Fang, C. H. Xu, C. H. Yan, *CrystEngComm*., 2009, **11**, 2268-2271.

29 (a) P. A. Gale, C. Caltagirone, *Chem. Soc. Rev.*, 2015, **44**, 4212-4227; (b) D. X. Wang, M. X. Wang, *J. Am. Chem. Soc*., 2013, **135**, 892-897.

30 C. R. Martinez, B. L. Iverson, *Chem. Sci*., 2012, **3**, 2191-2201.

31 J. D. Wuest, *Nature Chem*,. 2012, **4**, 74-75.

32 P. Ganesan, A. K. Chandiran, P. Gao, R. Rajalingam, M. Gratzel, M. K. Nazeeruddin, *ChemPhysChem*., 2015, **16**, 1035-1041.

33 Z. J. Donhauser, B. A. Mantooth, K. F. Kelly, L. A. Bumm, J. D. Monnell, J. J. Stapleton, D. W. P. Jr, A. M. Rawlett, D. L. Allara, J. M. Tour, P. S. Weiss, *Science*, 2001, **292**, 2303-2307.

34 H. Cao, V. Chang, R. Hernandez, M. D. Heagy, *J. Org. Chem.*, 2005, **70**, 4929-4934.

35 X. F. Fu, Y. F. Yue, R. Guo, L. L. Li, W. Sun, C. J. Fang, C. H. Xu, C. H. Yan, *CrystEngComm*, 2009, **11**, 2268-2271.

36 F. C. Spano, *Annu. Rev. Phys. Chem*., 2006, **57**, 217-243.

37 P. Ganesan, A. K. Chandiran, P. Gao, R. Rajalingam, M. Gratzel, M. K. Nazeeruddin, *ChemPhysChem,* 2015, **16**, 1035-1041.

38 D. E. Wu, X. L. Lu, M. Xia, *New J. Chem.*, 2015, **39**, 6465-6473.

39 K. A. Will, H. J. M. Ramirez, G. Merino, D. Mattia, G. Oskam, M. D. Jones, S. E. Lewis, P. J. Cameron*, RSC Adv*., 2013, **3**, 23361-23369.

40 S. Waffenschmidt, L. Jaenicke, *Anal. Biochem*., 1987, **165**, 337-340.

41 A. Tarai, J. B. Baruah, *Cryst. Growth Des*., 2016, **16**, 126-135.

42 J. Xie, *Zeist. Anorg. Allgem. Chem*., 2009, **635**, 384-388.

43 J. R. Weiser, N. G. Ricapito, A. Yueh, E. L. Weiser, D. Putnam, *Anal. Biochem*., 2012, **430**, 116-122.

44 Y. N. Zhang, J. Q. Liu, T. Wang, G. L. Wen, G. P. Yang, Y. Y. Wang, Q. Z. Shi, *J. Mol. Struct*., 2008, **878**, 116-123.

45 J. Ye, P. Zhang, K. Ye, H. Zhang, S. Jiang, L. Ye, G. Yang, Y. Wang, *J. Solid State Chem*., 2005, **179**, 438-439.

46 J. R. Weiser, N. G. Ricapito, A. Yueh, E. L. Weiser, D. Putnam, *Anal. Biochem*., 2012, **430**, 116-122.

47 Y. Liu, Y. Song, Y. Chen, X. Q. Li, F. Ding, R. Q. Zhong, *Chem. Eur. J*., 2004, **10**, 3685- 3696.

48 B. Kang, K. C. Ko, S. Y. Park, D. J. Jang, J. Y. Lee, *Phys. Chem. Chem. Phys*., 2011, **13**, 6332-6339.

49 A. R. Katritzky, D. C. Fara, H. Yang, K. Tamm, T. Tamm, M. Karelson, *Chem. Rev*., 2004, **104**, 175-198.

50. X. F. Fu, Y. F. Yue, R. Guo, L. L. Li, W. Sun, C. J. Fang, C. H. Xu, C. H. Yan, *CrystEngComm*., 2009, **11**, 2268-2271.

51 K. C. Wu, Y. M, Cheng, Y. S. Lin, Y. S. Yeh, S. C. Pu, Y. H. Hu, J. K. Yu, P. T. Che, *Chem. Phys. Letters*, 2004, **384**, 203-209.

51 B. Kang, K. C. Ko, S. Y. Park, D. J. Jang, J. Y. Lee *Phys. Chem. Chem. Phys*., 2011, **13**, 6332-6339.

52 P. A. Gale, C. Caltagirone, *Chem. Soc. Rev.*, 2015, **44**, 4212-4227.

53 Y. Liu, Y. Song, H. Wang, H. Y. Zhang, T. Wada, Y. Inoue, *J. Org. Chem*., 2003, **68**, 3687-3690.

Conclusion

In this thesis the self-assemblies of various complex anions and cations are utilized to generate supramolecular architectures that have layer-like structures. A systematic study was carried out to intercalate organo-cations in anionic framework and aromatic anions in cationic framework. Layer-like structures of pyridinedicarboxylate of bivalent and trivalent metal ions having extensive π-π interactions are analyzed. Formation of mononuclear, dinuclear, trinuclear and coordination polymers of two different positional isomers of pyridinedicarboxylates have revealed that layer like-structures and inter-layer separations in these copper(II)pyridinedicarboxylates complexes are dependent on cations. Careful selection of precursors have enabled to carryout synthesis of dinuclear or higher nuclear complexes from mononuclear copper complexes having same set of cations and ligands. The organo-cations can be interchanged, so as the nuclearity of the complexes can be changed upon changes of cations. Organo-cations held in layer-like structures through interplay of weak interactions decides the interlayer separations and such separations are more affected by the complementarity of these interactions rather than the obvious effects arising from size of the cations. Another important finding is thermal degradation of these complexes at relatively low temperature to form metal oxides. Thermal decomposition of dinuclear copper(II) complexes prove means to prepare copper oxide at relatively low temperature, on the other hand the thermal decompositions of hetero-metallic complex have yielded mixed metal oxides in homogeneous manner. It has been shown that carefully chosen mononuclear pyridnedicarboxylate complex can be used for further used for bottom up synthesis of hetero-metallic coordination polymers. Advantage of such complexes was taken in preparation of mixed metal oxide in desirable compositions distributed in a homogeneous manner. Mixed metal complexes prepared from the understanding on building of higher nuclearity complexes have provided a means to prepare mixed metal oxides, which is difficult to maintain the ratios in appropriate manner. Success in making nano-dimensional mixed oxide of copper with other metal ions is highlight of the work.

Cationic counterpart guiding packing patterns to selectively recognize neutral molecule for multicomponent systems are revealed and shown that the cations and anions along with guest molecules self-assemble to make different secondary coordination spheres by controlling the stacking patterns. In such assemblies cationic part has important role. Besides the stacking effects electrostatically guided hydrogen bonds are responsible to tightly hold guest molecules. Pyridinedicarboxylate ligands with trivalent lanthanum cations have provided a bigger template and helped to understand molecular recognition properties and the template that have been formed by self-assembling processes were identified. It is also shown that guest inclusion of neutral molecules is largely influenced by the cations such as 4,4′-bipyridinium or cation of 1,3-bis(4-pyridine)propane. Based on the ability to replace stacks between 2,6-pyridinedicarboxylates groups a modular approach to recognize 4-nitrophenol has been established. Self-assemblies of tetranuclear cobalt complex with π-decorated ligands have been utilized to show molecular recognition of nitro-aromatic compounds.

The other interesting finding of this thesis was to intercalation of toxic and hazardous nitro-aromatic compounds in metal cationic framework. Due to extensive stacking interactions among the 1,10-phenanthroline molecule or derivative complexes the intercalated complexes do not form layered structures, whereas the complexes synthesized by copper(II) bis-ethylenedaimmine with various aromatic carboxylic acids forms well-defined layer-like structures. Carboxylate anion exchanges in these layer-like structures are demonstrated. π-Stacking interactions among fluorophoric anions and chelating effect of ethylenediamine of complex containing 2,2'-biquinoline-4,4'-dicarboxylic(**H2bqca)** have influenced fluorescence emissions. Modulation of fluorescence emission intensities of **H2bqca** by copper ions is achieved in solid state by dehydration and rehydration. Whereas in solution, chelating effect of ethylendiamine does this trick. Masking direct contact of fluorophores with paramagnetic ions in aqueous medium or related solvents clearly delineate scopes to develop new systems based on interplay of weak interactions.

In a nutshell this thesis has provided basis by delineating the scopes to utilize inorganic layer-like structures formed by π-decorated ligands in generating new assemblies, new material properties and in molecular recognition.

Appendix

Details of the analytical equipment

X-Ray Crystallography

The X-ray crystallographic data were collected at 296 K with Mo Kα radiation (λ = 0.71073 Å) using a Bruker Nonius SMART CCD diffractometer equipped with a fine focus 3.0 KW sealed tube. The SMART software (v 2.1.4) was used for data collection and also for indexing the reflections and determining the unit cell parameters; the collected data were integrated using SAINT software. The structures were solved by direct methods and refined by full-matrix least-square calculations using SHELXTL software. All the non-H atoms were refined in the anisotropic approximation against F^2 of all reflections. All the H atoms were refined in isotropic approximation and treated as 'riding' in calculated positions. The locations of the H atoms of the protonated organic molecules were justified by difference Fourier synthesis map. The H-atoms attached to water molecules were located in the difference Fourier synthesis maps, and refined with isotropic displacement coefficients. The hydrogen atoms attached to water molecules could not be located in few occasions. It was also necessary to apply restrains to optimize the distances of some hydrogen atoms of water molecules. The CIF of all the compounds characterized by single crystal X-ray structure are included in the soft copy.

Powder X-ray diffraction pattern were collected on a Bruker D2 Phaser desktop diffractometer with Cu Kα radiation (λ = 1.5418Å) equipped with an integrated PC and scintillation counter detector and DIFFRACT. SUITE software. Diffraction patterns were collected over a 2θ range of 5-40º at a step scan rate of 0.02º.

FTIR, UV-Visible, NMR and Mass spectroscopy

The FT-IR spectra were recorded with a Perkin Elmer Spectrum One spectrophotometer in the spectral region 4000-400 cm^{-1} using KBr pellets. UV-visible absorption spectra were recorded using Perkin-Elmer Lambda 750 spectrophotometer equipped with double cell compartment. All the chemicals and solvents used were as obtained from the standard suppliers such as Sigma Aldrich, E. Merck, Ranbaxy etc. The solvents for optical spectroscopy were of HPLC grade (Aldrich or Merck) and used as such. The ^{1}HNMR spectra were recorded in a Varian 400 MHz Mercury Plus spectrometer. The chemical shifts in the NMR spectra recorded in D_2O are all given in ppm. ESI-MS spectra were recorded on a Agilent Q TOF 6520 high resolution mass spectrometer.

Thermal studies, elemental analyses, magnetic moment and conductivity measurement

Thermal analyses (TG / DTA) were performed on both Mettler Toledo TGA/SDTA 851^{e} and Waters SDT Q 600 thermal analyzer with a heating rate of 7ºC/min under nitrogen environment. Elemental analyses were performed with a Perkin-Elmer PE 2400 II CHNS micro analytical analyzer. Molar conductance measurements of the complexes were calculated using Elico conductivity meter, model CM 180 and room temperature magnetic moments were measured using a Sherwood scientific magnetic susceptibility balance.

Table 1A: Crystallographic parameters of all complexes

Complex	**2.1.1**	**2.1.2**	**2.1.3**
Formula	$C_{20}H_{30}CuN_4O_{10}$	$C_{16}H_{24}CuN_4O_{12}$	$C_{22}H_{36}CuN_4O_{12}$
formula weight	550.00	527.93	612.09
crystal system	Monoclinic	Triclinic	Triclinic
Space group	$P2_1/c$	*P-1*	*P-1*
a (Å)	11.3777(15)	6.1845(3)	6.20730(10)
b (Å)	6.2596(9)	8.1568(4)	9.9639(2)
c (Å)	20.920(2)	10.9703(5)	11.8651(3)
α (deg)	90.00	70.148(3)	68.9490(10)
β (deg)	121.649(8)	82.111(3)	80.5640(10)
γ (deg)	90.00	83.340(3)	88.0400(10)
V (Å^3)	1268.3(3)	514.16(4)	675.36(2)
Z	2	1	1
$\rho_{calc.}$ (g cm^{-3})	1.401	1.705	1.505
μ (mm^{-1})	0.918	1.137	0.877
F(000)	544	273	321
reflns collected	8683	7380	9081
reflns unique	2064	2518	2309
Ranges (h, k, l)	-13≤ h ≤ 13 -7 ≤ k ≤7 -23 ≤ l ≤ 23	-8≤ h ≤ 8 -10 ≤ k ≤10 -14 ≤ l ≤ 14	-7≤ h ≤ 7 -11 ≤ k ≤11 -13 ≤ l ≤ 13
Complete-ness to 2θ	97.9	96.9	97.0
GOF (F^2)	1.061	1.014	1.058
$R_1[I \geq 2\sigma(I)]$	0.0673	0.0298	0.0496
wR_2 $[I \geq 2\sigma(I)]$	0.1791	0.0834	0.1112
R_1 (all data)	0.1019	0.0340	0.0521
wR_2 (all data)	0.2037	0.0851	0.1117
Largest diff peak/hole	1.102 / -0.387	0.359 / -0.481	1.011 / -1.016

Complex	**2.1.4**	**2.1.5**	**2.2.1**
Formula	**$C_{20}H_{24}CuN_4O_{14}$**	**$C_{19}H_{17}CuN_3O_{13}$**	**$C_{20}H_{32}CuN_4O_{14}$**
formula weight	607.97	558.90	616.04
crystal system	Triclinic	Monoclinic	Triclinic
Space group	*P-1*	*C2/c*	*P-1*
a (Å)	9.0345(4)	21.6963(13)	9.0129(15)
b (Å)	13.3334(6)	14.8361(13)	12.6761(17)
c (Å)	13.4916(6)	6.8547(5)	13.0543(12)
α (deg)	65.122(2)	90.00	113.147(11)
β (deg)	75.461(2)	102.763(7)	90.103(11)
γ (deg)	70.519(2)	90.00	105.573(13)
V (Å^3)	1378.29(11)	2151.9(3)	1311.3(3)
Z	2	4	2
$\rho_{calc.}$(g cm^{-3})	1.465	1.725	1.560
μ (mm^{-1})	0.865	1.095	0.910
F(000)	626	1140	642
reflns collected	18297	10197	8200
reflns unique	4696	1898	4592
Ranges (h, k, l)	-10≤ h ≤ 10 -15 ≤ k ≤15 -16 ≤ l ≤ 16	-25≤ h ≤ 25 -17 ≤ k ≤17 -8 ≤ l ≤ 8	-10≤ h ≤ 10 -13 ≤ k ≤15 -15 ≤ l ≤ 15
Complete-ness to 2θ	97.0	99.8	99.7
GOF (F^2)	1.040	1.180	1.058
$R_1[I \geq 2\sigma(I)]$	0.0509	0.0563	0.0687
wR_2 $[I \geq 2\sigma(I)]$	0.1507	0.1735	0.1635
R_1 (all data)	0.0573	0.0674	0.1014
wR_2 (all data)	0.1574	0.1859	0.2020
Largest diff peak/hole	0.972 / -0.977	0.784 / -0.610	0.094 / -0.800

Complex	**2.2.2**	**2.2.3**	**2.2.4**
Formula	$C_{50}H_{74}Cu_3N_{12}O_{36}$	$C_{20}H_{34}CuN_4O_{13}$	$C_{28}H_{44}CuN_6O_{16}$
formula weight	1609.83	602.05	784.23
crystal system	Triclinic	Triclinic	Monoclinic
Space group	*P-1*	*P-1*	*P21/a*
a (Å)	7.3979(5)	8.6201(7)	14.0765(7)
b (Å)	14.4130(8)	13.1040(7)	9.4805(3)
c (Å)	15.7932(9)	13.3617(13)	15.3959(6)
α (deg)	75.612(5)	107.296(7)	90.00
β (deg)	82.510(5)	108.463(8)	116.278(5)
γ (deg)	78.590(5)	97.992(6)	90.00
V (Å^3)	1593.06(16)	1320.79(18)	1842.29(13)
Z	1	2	2
ρ_{calc} (g·cm^{-3})	1.678	1.514	1.414
μ (mm^{-1})	1.103	0.898	0.670
F(000)	833	630	822
reflns collected	10820	8992	6878
reflns unique	5598	4660	3251
Ranges (h, k, l)	-8≤ h ≤ 8 -16 ≤ k ≤17 -10 ≤ l ≤ 18	-10≤ h ≤ 9 -15 ≤ k ≤15 -15 ≤ l ≤ 11	-16≤ h ≤ 16 -18 ≤ k ≤10 -11 ≤ l ≤ 16
Complete-ness to 2θ	99.9	99.9	99.9
GOF (F^2)	0.985	0.831	0.955
$R_1[I \geq 2\sigma(I)]$	0.0504	0.0597	0.0505
wR_2 $[I \geq 2\sigma(I)]$	0.1097	0.1620	0.1402
R_1 (all data)	0.0726	0.0917	0.0505
wR_2 (all data)	0.1281	0.2132	0.1402
Largest diff peak/hole	0.081 / -0.628	0.079 / -0.457	0.061 / -0.271

Complex	**2.2.5**	**2.2.6**	**2.2.7**
Formula	$C_{16}H_{28}Cu\ N_4O_{14}$	$C_{32}H_{24}CuN_6O_{12}$	$C_{19}H_{26}CuN_4O_{10}$

formula weight	563.96	748.11	533.98
crystal system	Triclinic	Triclinic	Triclinic
Space group	*P-1*	*P-1*	*P-1*
a (Å)	7.1562(13)	6.6726(4)	7.3437(2)
b (Å)	7.2456(13)	10.7950(10)	10.6541(2)
c (Å)	11.618(2)	12.0764(10)	15.0967(3)
α (deg)	82.299(10)	65.544(9)	73.9280(10)
β (deg)	89.056(10)	79.053(6)	89.5720(10)
γ (deg)	70.660(10)	77.697(6)	79.7710(10)
V (Å^3)	563.03(17)	768.56(11)	1115.88(4)
Z	1	1	2
$\rho_{calc.}$(g·cm^{-3})	1.663	1.616	1.589
μ (mm^{-1})	1.051	0.790	1.043
F(000)	293	383	554
reflns collected	3290	4952	13499
reflns unique	1830	2699	3602
Ranges (h, k, l)	-7≤ h ≤ 8 -8 ≤ k ≤8 -13 ≤ l ≤ 13	-7≤ h ≤ 7 -11 ≤ k ≤12 -12 ≤ l ≤ 14	-8≤ h ≤ 8 -12 ≤ k ≤12 -17 ≤ l ≤ 17
Complete-ness to 2θ	97.2	999	96.5
GOF (F^2)	1.045	0.922	1.021
$R_1[I \geq 2\sigma(I)]$	0.0430	0.0628	0.0281
wR_2 $[I \geq 2\sigma(I)]$	0.1214	0.1779	0.0712
R_1 (all data)	0.0480	0.0780	0.0323
wR_2 (all data)	0.1244	0.1964	0.0776
Largest diff peak/hole	0.076 / -0.499	0.105 / -0.835	0.056 / -0.270

Complex	**2.2.8**	**3.1.1**	**3.1.2**
Formula	**$C_{66}H_{84}Cu_3N_{12}O_{40}$**	**$C_{32}H_{26}CuN_{12}O_{13}$**	**$C_6H_{13}CuNO_9Zn$**
formula weight	1876.07	850.18	372.08
crystal system	Triclinic	Triclinic	Monoclinic

Space group	*P-1*	*P-1*	*C2/c*
a (Å)	11.0057(4)	9.5980(3)	21.2665(12)
b (Å)	14.0625(6)	10.9279(4)	7.0608(4)
c (Å)	14.8817(6)	18.2028(6)	16.3185(9)
α (deg)	104.224(2)	103.362(2)	90.00
β (deg)	104.901(2)	93.001(2)	118.676(3)
γ (deg)	95.615(2)	92.072(2)	90.00
V (Å^3)	2125.40(15)	1852.70(11)	2149.8(2)
Z	1	1	4
$\rho_{calc.}$(g cm^{-3})	1.466	1.524	1.150
μ (mm^{-1})	0.842	0.336	2.127
F(000)	971	870	748
reflns collected	22258	25351	11494
reflns unique	6879	6521	1945
Ranges (h, k, l)	-12≤ h ≤ 12 -16 ≤ k ≤16 -17 ≤ l ≤ 17	-11≤ h ≤ 11 -13 ≤ k ≤ 12 -21 ≤ l ≤ 21	-25 ≤ h ≤ 21 -8 ≤ k ≤ 8 -18 ≤ l ≤ 19
Complete-ness to 2θ	97.3	97.3	99.7
GOF (F^2)	0.954	1.029	1.107
$R_1[I \geq 2\sigma(I)]$	0.0450	0.0490	0.0472
wR_2 $[I \geq 2\sigma(I)]$	0.1162	0.1442	0.1491
R_1 (all data)	0.0647	0.0658	0.0570
wR_2 (all data)	0.1277	0.1571	0.1590
Largest diff peak/hole	0.065 / -0.380	0.061/-0.420	0.114/-0.945

Complex	**3.1.3**	**3.2.2**	**3.2.4**
Formula	**$C_{21}H_{31}Cu_2GdN_3O_{22}$**	**$C_{32}H_{34}CuN_8O_{18}$**	**$C_{14}H_{22}CuMgN_2O_{16}$**
formula weight	961.82	882.21	562.19
crystal system	Monoclinic	Triclinic	Triclinic
Space group	*$P2_1/n$*	*P1*	*P-1*
a (Å)	11.7915(5)	6.7564(8)	6.9758(8)

b (Å)	13.1431(5)	8.3947(11)	7.5074(9)
c (Å)	19.6019(8)	15.916(3)	11.3187(13)
α (deg)	90.00	79.240(12)	85.179(7)
β (deg)	96.196(2)	89.650(11)	72.204(7)
γ (deg)	90.00	81.465(10)	66.030(7)
V (Å^3)	3020.1(2)	876.8(2)	515.18(10)
Z	2	1	1
$\rho_{calc.}$(g·cm^{-3})	1.058	1.671	1.812
μ (mm^{-1})	1.834	0.720	1.180
F(000)	952	455	289
reflns collected	26939	5307	5593
reflns unique	4407	4242	1629
Ranges (h, k, l)	-14 ≤ h ≤ 14 -14 ≤ k ≤ 14 -22 ≤ l ≤ 23	-8 ≤ h ≤ 7 -9 ≤ k ≤ 9 -18 ≤ l ≤ 17	-8 ≤ h ≤ 7 -8 ≤ k ≤ 8 -12 ≤ l ≤ 13
Complete-ness to 2θ	95.3	99.9	95.3
GOF (F^2)	1.174	0.957	1.082
$R_1[I \geq 2\sigma(I)]$	0.0406	0.0609	0.0378
wR_2 $[I \geq 2\sigma(I)]$	0.1155	0.1425	0.1009
R_1 (all data)	0.0513	0.0834	0.0447
wR_2 (all data)	0.1260	0.1680	0.1060
Largest diff peak/hole	0.132 /-0.843	0.448/ -0.410	0.078/ -0.628

Complex	**3.2.5**	**3.2.6**	**4.1.1**
Formula	**$C_{14}H_{18}CaCuN_2O_{14}$**	**$C_{14}H_{22}CoCuN_2O_{16}$**	**$C_{27}H_{32}N_4O_{13}Zn$**
formula weight	541.92	596.81	685.94
crystal system	Monoclinic	Triclinic	Triclinic
Space group	*$P2_1$*	*P-1*	*P -1*
a (Å)	6.66210(10)	7.0078(4)	9.4470(2)
b (Å)	20.4492(4)	7.5881(5)	11.2899(3)
c (Å)	7.58000(10)	11.3217(6)	14.6544(4)

α (deg)	90.00	85.343(4)	99.037(2)
β (deg)	104.4700(10)	72.348(3)	101.948(2)
γ (deg)	90.00	65.866(3)	94.145(2)
V (Å^3)	999.90(3)	522.92(5)	1501.22(7)
Z	2	1	2
ρ_{calc} (g cm^{-3})	1.800	1.895	1.517
μ (mm^{-1})	1.427	1.898	0.891
F(000)	554	304	712
reflns collected	9998	4756	10210
reflns unique	3172	1675	5157
Ranges (h, k, l)	-7 ≤ h ≤ 7 -23 ≤ k ≤ 23 -8 ≤ l ≤ 8	-8 ≤ h ≤ 8 -8 ≤ k ≤ 8 -13 ≤ l ≤ 13	-11 ≤ h ≤ 9 -13 ≤ k ≤ 12 -6 ≤ l ≤ 17
Complete-ness to 2θ	95.0	96.2	97.4
GOF (F^2)	1.042	0.0383	0.905
$R_1[I \geq 2\sigma(I)]$	0.0240	0.1337	0.0372
wR_2 $[I \geq 2\sigma(I)]$	0.0625	0.0409	0.1214
R_1 (all data)	0.0243	0.1369	0.0448
wR_2 (all data)	0.0627	1.078	0.1372
Largest diff peak/hole	0.048 / -0.266	0.093/ -1.010	0.055 / -0.349

Complex	**4.1.2**	**4.1.7**	**4.1.5**
Formula	**$C_{24}H_{20}N_4O_{14}Zn$**	**$C_{36}H_{40}N_4O_{20}Zn$**	**$C_{67}H_{60}N_4O_{19}Zn$**
formula weight	653.81	914.09	1290.56
crystal system	Monoclinic	Monoclinic	triclinic
Space group	*P 21/n*	*P -1*	*P -1*
a (Å)	15.5716(6)	10.6100(7)	9.8461(8)
b (Å)	18.7124(7)	12.0306(9)	17.2949(14)
c (Å)	20.0292(7)	15.6789(11)	19.0502(14)
α (deg)	90.00	90.00	69.645(4)

β (deg)	101.267(2)	98.640(4)	82.611(4)
γ (deg)	90.00	90.00	87.867(4)
V (Å^3)	5723.7(4)	1978.6(2)	3016.1(4)
Z	8	2	2
$\rho_{calc.}$(g cm^{-3})	1.517	1.534	1.421
μ (mm^{-1})	0.934	0.710	0.488
F(000)	2672	948	1344
reflns collected	75438	18632	53725
reflns unique	20345	7225	13311
Ranges (h, k, l)	-16 ≤ h ≤ 22 -22 ≤ k ≤ 22 -24 ≤ l ≤ 23	-12 ≤ h ≤ 12 -14 ≤ k ≤ 14 -14 ≤ l ≤ 18	-12 ≤ h ≤ 12 -22 ≤ k ≤ 22 -24 ≤ l ≤ 24
Complete-ness to 2θ	99.9	98.3	98.3
GOF (F^2)	0.991	1.054	1.254
$R_1[I \geq 2\sigma(I)]$	0.0490	0.1038	0.0914
wR_2 $[I \geq 2\sigma(I)]$	0.1246	0.2626	0.1818
R_1 (all data)	0.0749	0.1108	0.1303
wR_2 (all data)	0.1429	0.2653	0.1977
Largest diff peak/hole	0.103/ -0.717	0.141 / -0.627	0.089/ -0.816

Complex	**4.1.6**	**4.2.1**	**4.2.2**
Formula	**$C_{47}H_{54}N_4O_{20}Zn$**	**$C_{72}H_{80}La_2N_{12}O_{39}$**	**$C_{30}H_{30}O_4N_4La$**
formula weight	1060.31	2015.30	1271.87
crystal system	Monoclinic	Monoclinic	Monoclinic
Space group	*C 2/c*	*C 2/c*	*C 1 2/c 1*
a (Å)	35.4376(15)	10.2700(4)	10.4192(3)
b (Å)	14.2504(6)	30.9226(14)	22.2606(7)
c (Å)	20.2796(9)	26.8158(13)	20.4469(6)
α (deg)	90.00	90.00	90
β (deg)	105.902(2)	99.754(5)	98.615(3)
γ (deg)	90.00	90.00	90

V (Å^3)	9849.3(7)	8392.9(7)	4688.9(2)
Z	8	4	4
ρ_{calc}.(g cm^{-3})	1.430	1.595	1.8015
μ (mm^{-1})	0.582	1.105	1.898
F(000)	4432	4088	2487.6074
reflns collected	43501	17153	9646
reflns unique	8610	7385	4265
Ranges (h, k, l)	-42 ≤ h ≤ 42 -15 ≤ k ≤ 15 -25 ≤ l ≤ 23	-12 ≤ h ≤ 12 -36 ≤ k ≤ 36 -20 ≤ l ≤ 31	-13 ≤ h ≤ 13 -28 ≤ k ≤ 26 -27 ≤ l ≤ 14
Complete-ness to 2θ	99.3	99.70	97.87
GOF (F^2)	1.071	1.060	1.0602
$R_1[I \geq 2\sigma(I)]$	0.0508	0.0402	0.0367
wR_2 $[I \geq 2\sigma(I)]$	0.1535	0.1005	0.0819
R_1 (all data)	0.1848	0.0508	0.0470
wR_2 (all data)	0.1781	0.1081	0.0895
Largest diff peak/hole	0.090 / -0.487	0.840/-0.548	1.5049/-0.6592

Complex	**4.2.3**	**4.2.4**	**4.2.5**
Formula	**$C_{54}H_{50}LaN_7O_{20}$**	**$C_{101.50}H_{69}LaN_7O_{49}$**	**$C_{66}H_{66}LaN_6O_{28}$**
formula weight	1255.92	2518.50	1530.16
crystal system	Monoclinic	Monoclinic	Triclinic
Space group	*C 2/c*	*C 2/c*	*P-1*
a (Å)	19.1608(9)	32.7715(9)	11.0693(5)
b (Å)	11.5962(4)	13.6052(4)	14.9989(6)
c (Å)	26.161(2)	24.5888(5)	22.2463(10)
α (deg)	90.00	90.00	85.774(3)
β (deg)	104.486(7)	95.919(2)	87.817(4)
γ (deg)	90.00	90.00	69.061(4)
V (Å^3)	5628.0(5)	10904.8(5)	3439.9(2)
Z	4	4	2

$\rho_{calc.}$(g cm^{-3})	1.482	1.534	1.477
μ (mm^{-1})	0.841	0.874	0.711
F(000)	2560	5072	1570
reflns collected	10422	22285	26508
reflns unique	4961	10144	12071
Ranges (h, k, l)	-22 ≤ h ≤ 22 -13 ≤ k ≤ 9 -31 ≤ l ≤ 21	-25 ≤ h ≤ 39 -15 ≤ k ≤ 16 -29 ≤ l ≤ 29	-13 ≤ h ≤ 13 -17 ≤ k ≤ 17 -26 ≤ l ≤ 26
Complete-ness to 2θ	99.80	99.80	99.80
GOF (F^2)	1.094	0.885	1.083
$R_1[I \geq 2\sigma(I)]$	0.0757	0.0580	0.1157
wR_2 $[I \geq 2\sigma(I)]$	0.1869	0.1672	0.2560
R_1 (all data)	0.0917	0.0846	0.1324
wR_2 (all data)	0.1961	0.1952	0.2656
Largest diff peak/hole	1.474/-0.594	1.197/-1.088	1.080/-1.889

Complex	**4.3.2**	**4.3.3**	**4.3.4**
Formula	**$C_{42}H_{29}N_9NiO_{11}$**	**$C_{90}H_{77}N_{19}Ni_2O_{28}$**	**$C_{158}H_{146}N_{32}Ni_4O_{47}$**
formula weight	894.43	1990.13	3479.91
crystal system	Triclinic	Triclinic	Triclinic
Space group	*P-1*	*P-1*	*P-1*
a (Å)	13.0133(4)	15.1684(6)	13.0081(5)
b (Å)	13.1342(4)	15.6383(6)	16.1054(5)
c (Å)	13.1849(4)	22.1650(6)	21.1460(9)
α (deg)	80.163(2)	90.679(3)	69.532(3)
β (deg)	64.763(2)	108.239(3)	81.699(3)
γ (deg)	73.009(2)	110.754(4)	78.402(3)
V (Å^3)	1946.69(10)	4624.7(3)	4052.4(3)
Z	2	2	1
$\rho_{calc.}$(g cm^{-3})	1.503	1.429	1.426
μ (mm^{-1})	0.577	0.498	0.551

F(000)	920	2064	1764
reflns collected	27637	35254	27107
reflns unique	6628	16078	14227
Ranges (h, k, l)	-15≤ h ≤ 15 -15≤ k ≤ 14 -15≤ l ≤ 15	-14≤ h ≤ 18 -18 ≤ k ≤ 18 -26 ≤ l ≤ 26	-15≤ h ≤ 15 -19 ≤ k ≤ 18 -25 ≤ l ≤ 25
Complete-ness to 2θ	96.6	98.7	
GOF (F^2)	1.044	1.133	1.157
$R_1[I \geq 2\sigma(I)]$	0.0617	0.0786	0.0794
wR_2 $[I \geq 2\sigma(I)]$	0.1836	0.1564	0.1942
R_1 (all data)	0.0755	0.1160	0.1106
wR_2 (all data)	0.1930	0.1737	0.2092
Largest diff peak/hole	0.527/-0.653	0.802 /-0.473	0.526/-0.558

Complex	**4.4.1**	**4.4.2**	**4.4.3**
Formula	$C_{60}H_{78}Cl_4Co_4N_{10}O_{18}$	$C_{52}H_{82}Cl_8Co_5N_{10}O_{20}$	$C_{96}H_{86}Cl_2Co_4N_{16}O_{28}$
formula weight	1604.84	1745.57	2218.43
crystal system	Monoclinic	Monoclinic	Triclinic
Space group	*P 21/c*	*P 21/n*	*P-1*
a (Å)	14.5347(10)	14.2676(2)	11.5819(9)
b (Å)	17.6433(12)	14.3552(3)	12.6053(11)
c (Å)	13.3349(9)	17.4809(3)	18.6587(10)
α (deg)	90.00	90.00	94.509(6)
β (deg)	99.016(4)	90.2930(15)	98.483(6)
γ (deg)	90.00	90.00	112.670(8)
V (Å^3)	3377.4(4)	3580.30(11)	2458.5(3)
Z	2	2	1
ρ_{calc}.(g cm^{-3})	1.578	1.6191	1.498
μ (mm^{-1})	1.200	1.507	0.804
F(000)	1656	1796.6195	1140
reflns collected	32471	15209	16226

reflns unique	6204	6173	8628
Ranges (h, k, l)	-17≤ h ≤ 17 -21 ≤ k ≤ 21 -16 ≤ l ≤ 16	-13≤ h ≤ 16 -17≤ k ≤ 0 -20≤ l ≤ 12	-13≤ h ≤ 13 -14≤ k ≤ 13 -21≤ l ≤ 22
Complete-ness to 2θ	98.70	99.78	99.80
GOF (F^2)	1.012	0.9641	0.973
$R_1[I \geq 2\sigma(I)]$	0.0360	0.0435	0.0634
wR_2 $[I \geq 2\sigma(I)]$	0.0933	0.1256	0.1316
R_1 (all data)	0.0456	0.0569	0.1214
wR_2 (all data)	0.0999	0.1419	0.1834
Largest diff peak/hole	0.751 /-0.435	0.9452/-1.1095	0.761 /-0.443

Complex	**4.4.4**	**4.4.5**	**4.4.6**
Formula	**$C_{72}H_{64}Cl_2Co_4N_{14}O_{24}$**	**$C_{50}H_{50}ClCo_2N_9O_{17}$**	**$C_{52}H_{62}Cl_8Co_4N_{10}O_{10}Zn_2$**
formula weight	1783.99	1202.32	1637.18
crystal system	Triclinic	Triclinic	Monoclinic
Space group	*P-1*	*P-1*	*P 21/n*
a (Å)	11.9196(9)	12.8277(10)	14.5244(10)
b (Å)	12.6403(8)	15.4597(14)	14.5390(10)
c (Å)	13.6806(9)	15.9045(14)	15.4285(8)
α (deg)	94.512(5)	116.795(9)	90.00
β (deg)	107.345(6)	107.517(7)	90.864(6)
γ (deg)	100.584(6)	90.042(7)	90.00
V (Å^3)	1914.4(2)	2650.1(5)	3257.7(4)
Z	1	2	2
$\rho_{calc.}$(g cm^{-3})	1.547	1.5066	1.669
μ (mm^{-1})	1.006	0.757	2.108
F(000)	912	1242.3449	1656
reflns collected	12790	22567	13134
reflns unique	7080	9238	5686

Ranges (h, k, l)	-14≤ h ≤ 14 -15≤ k ≤ 15 -16≤ l ≤ 16	-16≤ h ≤ 14 -19≤ k ≤ 20 -20≤ l ≤ 21	-15≤ h ≤ 17 -17≤ k ≤ 15 -13≤ l ≤ 18
Complete-ness to 2θ	99.30	99.76	99.00
GOF (F^2)	1.172	1.0422	1.080
$R_1[I \geq 2\sigma(I)]$	0.0935	0.0728	0.0602
wR_2 $[I \geq 2\sigma(I)]$	0.1747	0.1846	0.1701
R_1 (all data)	0.1517	0.0990	0.0738
wR_2 (all data)	0.2032	0.2158	0.1868
Largest diff peak/hole	0.878/ -0.655	1.6198/-1.5631	1.385/-1.314

Complex	**4.4.7**	**5.1**	**5.2**
Formula	$C_{52}H_{57}Cd_2Cl_8Co_4N_{10}O_9$	$C_{18}H_{30}CuN_4O_6$	$C_{22}H_{34}CuN_4O_6$
formula weight	1710.20	462.01	514.08
crystal system	Monoclinic	Monoclinic	Monoclinic
Space group	*P 21/n*	*P* $2_1/n$	*P* $2_1/n$
a (Å)	14.5113(9)	6.2163(13)	6.3753(3)
b (Å)	14.6361(8)	26.982(5)	29.3283(15)
c (Å)	15.5388(9)	7.1615(18)	7.0612(4)
α (deg)	90.00	90.00	90.00
β (deg)	90.410(5)	115.307(13)	114.144(3)
γ (deg)	90.00	90.00	90.00
V (Å^3)	3300.2(3)	1085.9(4)	1204.78(11)
Z	2	2	2
ρ_{calc}.(g cm^{-3})	1.721	1.413	1.417
μ (mm^{-1})	1.997	1.046	0.951
F(000)	13266	486	542
reflns collected	13266	6021	11377
reflns unique	5760	1720	2720
Ranges	-14 ≤ h ≤ 17 -17 ≤ k ≤ 17	-5 ≤ h ≤ 7 -27 ≤ k ≤ 31 -6 ≤ l ≤ 8	-8 ≤ h ≤ 8 -36 ≤ k ≤ 38 -8 ≤ l ≤ 9

(h, k, l)	$-18 \leq l \leq 11$		
Complete-ness to 2θ	99.00	95.1	98.4
GOF (F^2)	1.108	0.888	0.851
$R_1[I \geq 2\sigma(I)]$	0.0742	0.0583	0.0370
wR_2 $[I \geq 2\sigma(I)]$	0.1813	0.1238	0.1046
R_1 (all data)	0.0992	0.1207	0.0702
wR_2 (all data)	0.2085	0.1509	0.1357
Largest diff peak/hole	1.553/-1.321	0.322 / -0.373	0.323/ -0.375

Complex	**5.3**	**5.4**	**5.5**
Formula	**$C_{18}H_{34}CuN_4O_{10}$**	**$C_{24}H_{34}CuN_6O_8$**	**$C_9H_{21}CuN_6O_6$**
formula weight	530.03	598.12	372.86
crystal system	Monoclinic	Triclinic	Triclinic
Space group	*P* $2_1/c$	*P -1*	*P -1*
a (Å)	11.9009(6)	6.8365(2)	8.486(2)
b (Å)	9.4413(4)	7.3268(2)	9.205(2)
c (Å)	10.8734(5)	13.7621(4)	10.299(2)
α (deg)	90.00	93.400(2)	95.810(11)
β (deg)	100.311(2)	100.844(2)	95.490(11)
γ (deg)	90.00	103.313(2)	106.206(11)
V ($Å^3$)	1202.00(10)	655.03(3)	762.1(3)
Z	2	1	2
$\rho_{calc.}$ ($g \cdot cm^{-3}$)	1.464	1.516	1.625
μ (mm^{-1})	0.967	0.894	1.472
F(000)	558.91	313.45	388
reflns collected	14605	9211	5536
reflns unique	2709	3351	2578
Ranges (h, k, l)	$-12 \leq h \leq 14$ $-11 \leq k \leq 12$ $-13 \leq l \leq 10$	$-9 \leq h \leq 9$ $-9 \leq k \leq 9$ $-18 \leq l \leq 18$	$-10 \leq h \leq 6$ $-10 \leq k \leq 10$ $-12 \leq l \leq 12$

Complete-ness to 2θ	98.1	99.7	96.6
GOF (F^2)	1.185	1.066	0.987
$R_1[I \geq 2\sigma(I)]$	0.0281	0.0286	0.0714
wR_2 $[I \geq 2\sigma(I)]$	0.0879	0.0873	0.1900
R_1 (all data)	0.0332	0.0309	0.0848
wR_2 (all data)	0.0913	0.0892	0.2014
Largest diff peak/hole	0.373/ -0.213	0.309 / -0.368	1.085 / -0.931

Table 2A: Hydrogen bond parameters for the complex

	Bond (symmetry)	$d_{D-H(Å)}$	$d_{H\cdots A(Å)}$	$d_{D\cdots A(Å)}$	<D-H···A(°)
2.1.2	N(2)-H(2B)···O(4) [-1+x, y, z],	0.89	1.98	2.8491(19)	165
	N(2)-H(2C)···O(5) [-1+x, y, z],	0.89	2.40	2.969(2)	122
	N(2)-H(2C)···O(6) [1-x,-y,1-z]	0.89	2.31	3.007(2)	135
	O(5)-H(5A)···O(2) [1-x,-y,1-z]	0.88	2.00	2.815(2)	154
	O(5)-H(5B)···O(3) [x,y,z]	0.86	1.98	2.798(2)	159
	O(6)-H(6A)···O(2) [x,y,z]	0.85	2.03	2.864(2)	165
2.1.3	N(2)-H(2A)···O(4) [-1+x, y, z],	0.89	2.03	2.921(4)	176
	N(2)-H(2B)···O(3) [1-x,1-y,-z]	0.89	1.99	2.850(3)	163
	O(6)-H(6B)···O(5) [x,y,z]	0.95(5)	1.96(4)	2.902(5)	171(5)
	O(5)-H(5A)···O(6 [x,y,z]	0.98(5)	1.84(5)	2.803(5)	170(5)
	O(5)-H(5B)···O(2) [1-x,1-y,-z]	0.95(3)	1.85(3)	2.796(4)	172(5)
	O(6)-H(6A)···O(6) [-x,-y,1-z]	0.94(4)	1.93(6)	2.833(6)	162(9)
2.1.4	N(3)-H(3)···O(3) [x,1+y,-1+z]	0.91	2.56	3.175(4)	126
	N(3) -H(3)···O(4) [x,1+y,-1+z]	0.91	1.78	2.686(5)	171
	N(4)-H(4A)···O(7) [1-x,1-y,1-z]	0.91	1.78	2.691(5)	172
	N(4) -H(4A)···O(8) [1-x,1-y,1-z]	0.91	2.55	3.130(4)	165
2.1.5	N(2)-H(2N)···O(2) [1/2-x,1/2+y,1/2-z]	0.97(6)	2.33(7)	3.140(8)	141(5)
	N(2)--H(2N)···O(3) [1/2-x,1/2+y,1/2-z]	0.97(6)	2.43(7)	3.085(8)	124(6)
	C(5)-H(5)···O(7) [-x,y,1/2-z]	0.93	2.56	3.40(3)	150
	N(3) -H(3A)···O(5) [x,y,z]	0.89	1.99	2.884(2)	177

	N(3) -H(3A)···O(6) [x,y,z]	0.89	2.59	3.191(2)	126
	N(3) -H(3B)...O(4) [-1/2+x,1/2-y,1/2+z]	0.89	1.97	2.849(2)	168
	N(3) -H(3C)···O(9) [1/2+x,1/2-y,-1/2+z]	0.89	1.88	2.761(3)	171
2.1.6	N(4) -H(4A)···O(4) [x,y,z]	0.89	1.98	2.760(3)	146
	N(4) -H(4B)···O(7) [-1/2+x,1/2-y,1/2+z]	0.89	1.89	2.762(3)	168
	N(4)-H(4C)···O(2) [1-x,1-y,1-z]	0.89	2.14	2.757(3)	126
	O(9 -H(9A)···O(10) [1-x,1-y,1-z]	0.76(4)	2.01(3)	2.756(3)	173(4)
	O(9)-H(9B)···O(3) [1-x,1-y,1-z]	0.67(4)	2.11(4)	2.759(3)	166(4)
	O(10)-H(10A)···O(1) [3/2-x,-1/2+y,1/2-z]	0.81(3)	2.09(3)	2.886(2)	169(3)
	O(10)-H(10B)···O(7) [x,y,z]	0.85(3)	2.01(4)	2.818(2)	160(3)
	N(3)-H(3A)···O(3) [2-x,1-y,1-z]	0.86	1.89	2.746(7)	172
	N(4)-H(4)···O(9) [x,y,z]	0.86	1.78	2.634(9)	173
	N(5)-H(5)···O(10) [1-x,1-y,1-z]	0.86	1.79	2.645(9)	170
2.1.7	N(6)-H(6)···O(7) [1-x,1-y,-z]	0.86	1.89	2.737(8)	167
	O(9)-H(9A)···O(4) [1-x,1-y,1-z]	0.92(4)	1.91(5)	2.710(8)	143(4)
	O(9)-H(9B)···O(8) [x,y,z]	0.92(5)	1.90(5)	2.728(9)	150(4)
	O(10)-H(10A)···O(4) [1-x,1-y,1-z]	0.92(5)	1.91(6)	2.728(9)	146(5)
2.1.8	N(3)-H(3N)···O(3) [x,y,z]	0.99(4)	2.48(8)	3.166(11)	126(5)
	N(3)-H(3N)···O(4) [x,y,z]	0.99(4)	1.79(4)	2.784(10)	173(8)
	N(6)-H(6A)···O(12) [1+x,y,z]	0.89	1.92	2.804(7)	170
	N(6)-H(6C)···O(4) [2-x,1-y,1-z]	0.89	1.89	2.759(7)	165
	N(5)-H(5C)···O(10) [1+x,y,z]	0.89	2.09	2.932(6)	157
2.1.9	N(5)-H(5A)···O(12) [1-x,1-y,1-z]	0.89	1.90	2.787(6)	178
	N(5)-H(5B)···O(3) [1-x,1-y,1-z]	0.89	1.85	2.731(8)	168
	N(7)-H(7A)···O(4) [2-x,1-y,1-z]	0.89	1.94	2.810(8)	164
	N(7)-H(7B)···O(15) [1+x,-1+y,z]	0.89	2.13	3.010(8)	170
	N(2)-H(2N)···O(4) [x,y,z]	0.87(2)	1.96(2)	2.718(3)	145(2)
	O(6)-H(6B)···O(7) [x,y,z]	0.81(3)	2.03(3)	2.838(5)	173(3)
	O(7)-H(7B)···O(8) [-1+x, y, z],	0.78(4)	2.00(4)	2.754(4)	162(4)
2.1.10	O(5)-H(5A)···O(3) [1+x,y,z]	0.82	1.74	2.557(2)	172
	O(8)-H(8A)···O(6) [x,y,z]	0.82(5)	1.98(5)	2.791(5)	170(5)
	O(8)-H(8B)···O(2) [1+x,y,z]	0.77(4)	2.07(4)	2.813(4)	166(4)
	O(7)-H(7A)···O(1) [x,y,z]	0.81(3)	2.02(3)	2.829(4)	174(3)
	N(7)-H(7B)···O(4) [1+x,y,z]	0.89	2.19	2.992(9)	150
	N(7)-H(7B···(2) [1+x,y,z]	0.89	2.35	2.951(8)	125
	N(7)-H(7A)···O(16) [1-x,1-y,1-z]	0.89	1.94	2.826(8)	177
	N(7)-H(7C)···O(4) [1-x,-y,1-z]	0.89	1.99	2.844(8)	161
	N(8)-H(8B)···O(12) [1-x,1-y,-z].	0.89	2.02	2.877(8)	161
	N(8)-H(8C)···O(20) [x,-1+y,z],	0.89	1.89	2.783(8)	177
2.1.11	N(6)-H(6C)···O(3) [x,y,z]	0.89	2.46	3.038(9)	123

	N(6)-H(6C)···O(4) [x,y,z]	0.89	2.18	3.030(9)	160
	N(6) -H(6B)···O(14) [x,y,z]	0.89	2.05	2.937(8)	172
	N(6)-H(6A)···O(17) [x,y,z]	0.89	2.01	2.900(9)	178
	N(5)-H(5C)···O(6) [x,y,-1+z]	0.89	1.93	2.809(9)	170
	N(5)-H(5A)···O(6) [-x,1-y,1-z]	0.89	2.01	2.834(8)	154
	N(5)-H(5B)···O(21) [-1+x, y, z],	0.89	1.90	2.787(10)	170
	N(3)-H(3A)···O(5) [x,y,z]	0.89	1.99	2.884(2)	177
	N(3)-H(3B)···O(4) [-1/2+x,1/2y,1/2+z]	0.89	1.97	2.849(2)	168
	N(3)-H(3C)···O(9) [x,y,z]	0.89	1.88	2.761(3)	171
	N(4)-H(4C)···O(2) [1-x,1-y,1-z]	0.89	2.14	2.757(3)	126
	N(4)-H(4B)···O(7) [-1/2+x,1/2-y,1/2+z]	0.89	1.89	2.762(3)	168
2.1.12	N(4)-H(4A)···O(4) [x,y,z]	0.89	1.98	2.760(3)	146
	O(9)-H(9B)···O(3) [1-x,1-y,1-z]	0.67(4)	2.11(4)	2.759(3)	166(4)
	O(9)-H(9A)···O(10) [1-x,1-y,1-z]	0.76(4)	2.01(3)	2.756(3)	173(4)
	O(10)-H(10A)···O(1) [3/2-x,-1/2+y,1/2-z]	0.81(3)	2.09(3)	2.886(2)	169(3)
	O(10)-H(10B)···O(7) [x,y,z]	0.85(3)	2.01(4)	2.818(2)	160(3)
	N(3)-H(3A)···O(17) [x,y,z]	0.90	2.32	3.178(5)	159
	N(3)-H(3B)···O(19) [x,-1+y,z]	0.90	2.27	3.147(5)	165
	N(4)-H(4A)···O(14) [-1+x,y,z]	0.89	1.97	2.851(5)	170
	N(4)-H(4B)···O(15) [1-x,1-y,1-z]	0.89	1.82	2.702(5)	172
	N(4)-H(4C)···O(24)[-1+x,y,z]	0.89	2.05	2.918(5)	166
	N(7)-H(7A)···O(1) [x,1+y,z]	0.90	2.08	2.971(5)	169
	N(7)-H(7B)···O(8) [x,y,z]	0.90	2.21	3.087(5)	163
	N(8)-H(8A)···O(18) [1-x,1-y,1-z]	0.89	1.94	2.793(5)	161
2.1.14	N(8)-H(8B)···O(6) [1-x,1-y,1-z]	0.89	1.94	2.820(5)	169
	N(8)-H(8C)···O(16) [x,y,z]	0.89	1.98	2.870(5)	173
	N(17)-H(17A)···O(23) [x,y,z]	0.89	2.15	2.986(6)	157
	N(17)-H(17B)···O(9) [1-x,-y,-z]	0.89	2.07	2.882(5)	152
	N(17)-H(17C)···O(17)[x,y,z]	0.89	2.10	2.955(5)	161
	N(18)-H(18A)···O(11) [1-x,1-y,-z]	0.89	1.87	2.742(5)	165
	N(18)-H(18B)···O(20) [1-x,1-y,-z]	0.89	1.97	2.852(6)	174
	N(18)-H(18C)···O(2) [x,1+y,z]	0.89	1.84	2.699(5)	163
	N(6)-H(6A)···N(5) [1-x,-y,1-z]	0.79(3)	2.17(3)	2.926(3)	161(3)
2.1.15	N(6)-H(6B)···O(2) [-1+x,-1+y,z]	0.80(3)	2.15(4)	2.850(3)	146(3)
	N(3)-H(3N)···O(3) [-1+x,-1+y,z]	0.87(3)	1.77(3)	2.638(3)	174(3)
	N(3)-H(3N)···O(7) [1-x, -y, -z]	0.96(5)	1.61(5)	2.564(6)	172(5)
	N(4)-H(4N)···O(3) [-x, 1-y, 1-z]	0.99(6)	1.77(6)	2.711(7)	157(6)
	O(9)-H(9OB)···O(4) [1+x, y, z]	0.94(5)	1.82(4)	2.752(6)	171(6)
	O(9)-H(9OA)···O(12) [1-x, 1-y, -z]	0.96(7)	1.87(5)	2.755(7)	153(9)

	O(10)-H(10C)···O(3) [x, y, z]	0.91(10)	1.81(10)	2.721(7)	176(9)
2.2.1	O(10)-H(10D)···O(11) [1-x, 1-y, 1-z]	1.00(9)	1.79(8)	2.751(7)	159(8)
	O(12)-H(12C)···O(10) [x, y, z]	0.96(13)	1.75(13)	2.703(9)	172(13)
	O(12)-H(12D)···O(13) [1-x, 1-y, 1-z]	0.97(3)	1.83(4)	2.772(11)	166(3)
	O(13)-H(13C)···O(14) [1-x, -y, 1-z]	0.97(11)	1.99(9)	2.775(9)	137(9)
	O(14)-H(14C)···O(2) [x, y, 1+z]	0.95(14)	1.84(13)	2.771(9)	165(8)
	N(3)-H(3A)···O(10) [-1+x,y,z]	0.89	1.92	2.811(3)	174
	N(3)-H(3B)···O(7) [-x,-y,-z]	0.89	1.88	2.761(3)	169
	N(3)-H(3C)···O(6) [x, y, z]	0.89	2.48	3.252(3)	146
	N(4)-H(4A)···O(4) [1-x,1-y,1-z]	0.89	1.91	2.797(3)	171
2.2.2	N(4)-H(4C)···O(3) [x, 1+y, z]	0.89	1.94	2.762(3)	154
	O(9)-H(9C)···O(8) [-x, -y,-z]	0.91(3)	1.89(3)	2.744(3)	157(3)
	O(9)-H(9D)···O(4) [x,1-y,-z]	0.91(3)	1.87(3)	2.757(3)	165(3)
	O(10)-H(10C)···O(6) [x, y, z]	0.94(4)	1.96(4)	2.876(3)	166(4)
	N(3)-H(3N)···O(3) [2-x, 1-y, 1-z]	0.88(6)	1.85(6)	2.726(6)	174(6)
	N(4)-H(4N)···O(7) [1+x, -1+y, 1+z]	0.94(7)	1.71(7)	2.646(6)	179(10)
	O(9)-H(8AA)···O(11) [1-x, 1-y, 1-z]	0.96(5)	2.11(7)	2.955(6)	146(9)
	O(9)-H(8AB)···O(8) [-1+x, y, z]	0.95(6)	1.76(7)	2.716(5)	175(8)
	O(10)-H(10B)···O(12) [x, y, z]	0.87(9)	2.15(8)	2.878(11)	142(9)
2.2.3	O(11)-H(9AA)···O(4) [-1+x, y, z]	0.95(6)	1.88(6)	2.812(8)	166(7)
	O(12)-H(12B)···O(13) [x, y, z]	0.96(15)	2.00(19)	2.914(10)	158(10)
	O(13)-H(13B)···O(4) [-1+x, y, z]	0.94(6)	1.86(6)	2.796(8)	172(9)
	O(13)-H(13A)···O(9) [-x, 1-y, -z]	0.96(12)	1.90(13)	2.818(8)	159(17)
	N(2)-H(2A)···O(8) [-1/2+x, 1/2-y, z]	0.89	1.99	2.868(4)	171
	N(2)-H(2B)···O(3) [-1/2+x,1/2-y, 1+z]	0.89	1.91	2.769(4)	162
	O(5)-H(5OB)···O(2) [x, y, z]	0.95(9)	2.24(9)	3.025(7)	139(8)
2.2.4	O(6)-H(6OA)···O(3) [1/2-x, 1/2+y,1-z]	0.96(4)	1.80(4)	2.752(5)	174(4)
	O(7)-H(7OA)···O(4) [x, y, -1+z]	0.93(3)	1.88(3)	2.780(5)	163(5)
	O(7)-H(7OB)···O(8) [x, y, z]	0.95(6)	1.95(6)	2.861(5)	162(5)
	O(8)-H(8OB)···O(6) [x, y, z]	0.94(6)	1.89(5)	2.820(6)	167(5)

	N(2)-H(2B)···O(4) [2-x,1-y,-z]	0.89	2.10	2.921(4)	153
	N(2)-H(2C)···O(5) [x,1+y,z]	0.89	2.05	2.877(5)	155
	N(2)-H(2A)···O(6) [x, y, z]	0.89	2.21	3.037(5)	154
2.2.5	O(6)-H(6B)···O(3) [1-x,1-y,-z]	0.94(4)	1.75(4)	2.688(5)	178(6)
	O(6)-H(6A)···O(5) [x, y, z]	0.95(5)	1.86(5)	2.807(5)	170(7)
	O(7)-H(7A)···O(2) [1-x,-y,1-z]	0.93(6)	1.95(6)	2.796(5)	150(6)
	O(7)-H(7B)···O(6) [x, y, z]	0.95(7)	1.98(6)	2.926(5)	173(7)
	N(2)-H(2N)···O(3) [2-x,-y,1-z]	0.95(4)	1.78(4)	2.722(6)	171(4)
2.2.6	N(3)-H(3A)···O(5) [x,y,-1+z]	0.96(7)	2.16(7)	3.073(7)	157(7)
	N(3)-H(3B)···O(1) [x, y, z]	0.95(9)	2.27(8)	3.119(6)	150(5)
	N(4)-H(4A)···O(13) [1-x,1-y,1-z]	0.89	1.97	2.798(4)	155
	N(4)-H(4B)···O(10) [2-x,1-y,1-z]	0.89	1.98	2.861(4)	169
	N(5)-H(5A)···O(19) [-x,1-y,-z]	0.89	2.00	2.872(4)	167
2.2.7	N(5)-H(5B)···O(12) [-x,1-y,-z]	0.89	1.98	2.843(4)	164
	N(6)-H(6A)···O(7) [x, y, z]	0.89	1.88	2.766(4)	171
	N(6)-H(6B)···O(15) [x, y, z]	0.89	1.89	2.762(4)	165
	N(4)-H(4B)···O(6) [-1+x,y,z]	0.89	2.16	2.929(5)	144
	N(4)-H(4C)···O(14) [-x,1-y,1-z]	0.89	1.88	2.761(6)	172
	N(5)-H(5A)···O(15) [x, y, z]	0.90	1.94	2.830(6)	170
2.2.8	N(5)-H(5B)···O(12) [x,-1+y,1+z]	0.90	1.81	2.691(4)	165
	N(6)-H(6A)···O(4) [1-x,1-y,1-z]	0.89	1.99	2.799(5)	151
	N(6)-H(6B)···O(4) [1-x,1-y,1-z]	0.89	1.83	2.697(6)	165
	N(6)-H(6C)···O(18) [x, y, z]	0.89	2.00	2.846(8)	159

Spectroscopic details and Thermogravimetry of complexes

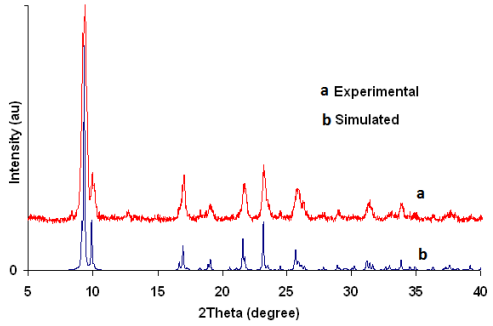

2.1.1

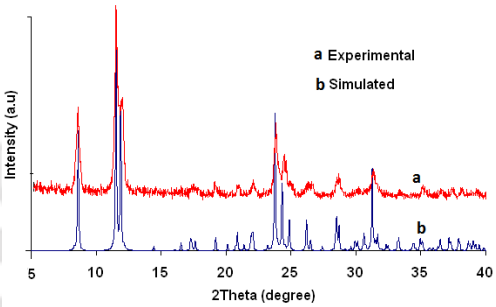

2.1.2

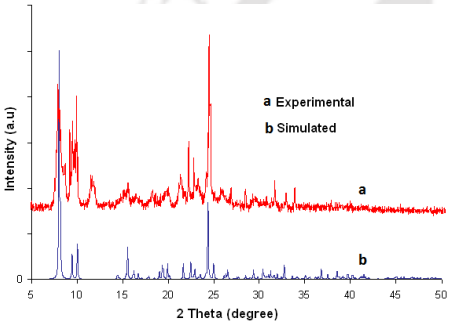

2.1.3

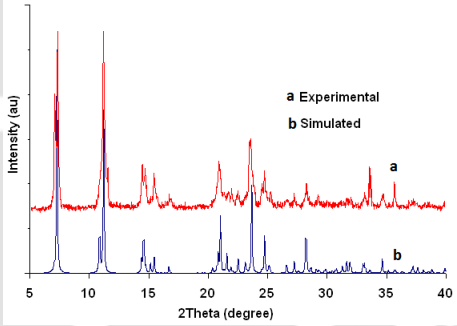

2.1.4

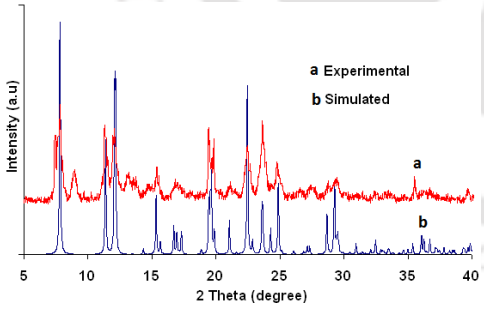

2.1.7

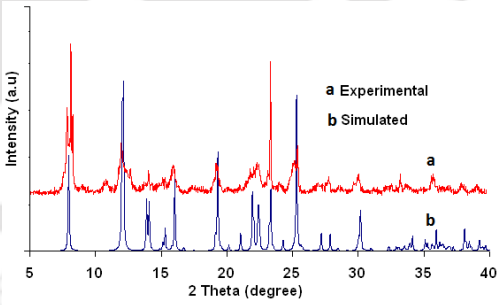

2.18

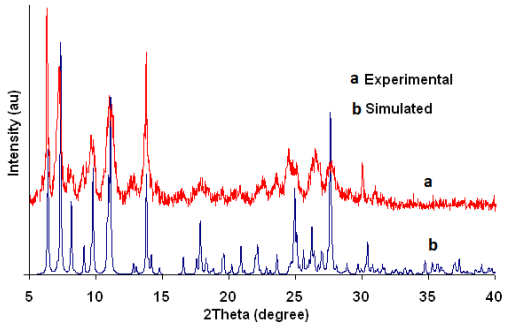

2.1.10

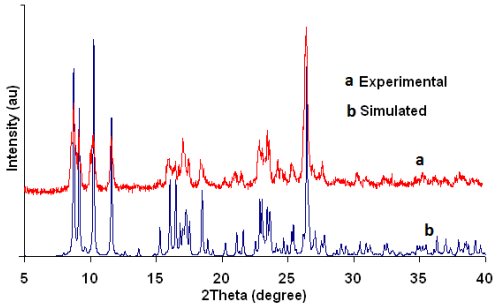

2.1.11

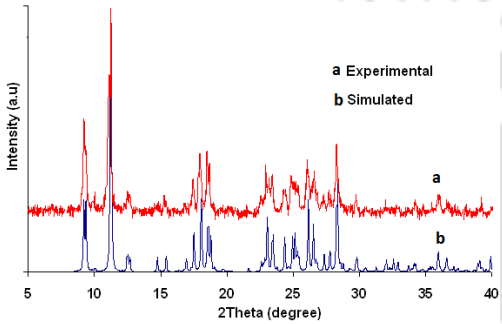

2.1.12

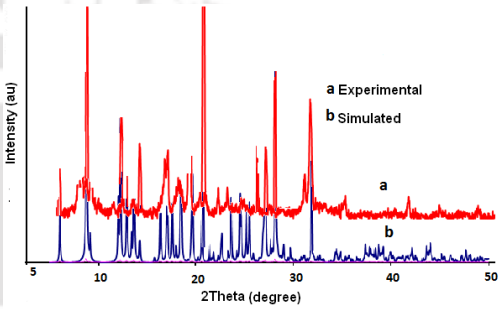

2.2.2

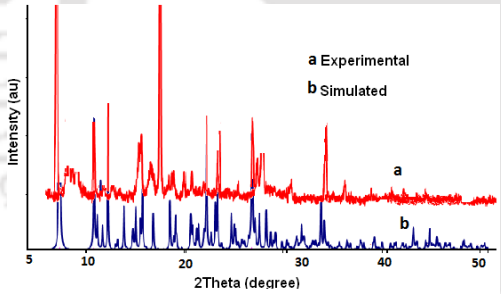

2.2.3

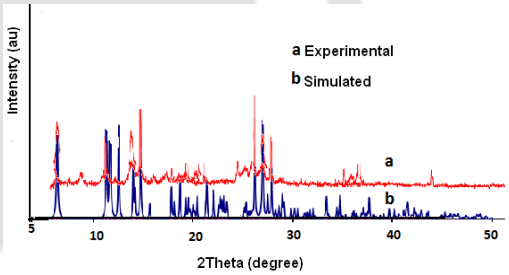

2.2.4

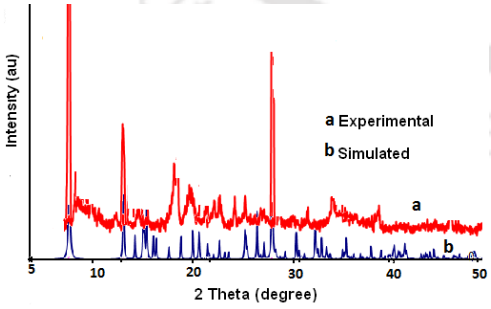

2.2.5

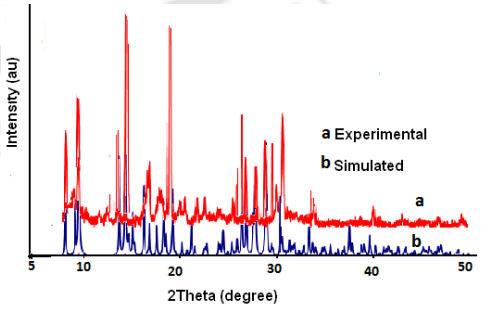

2.2.6

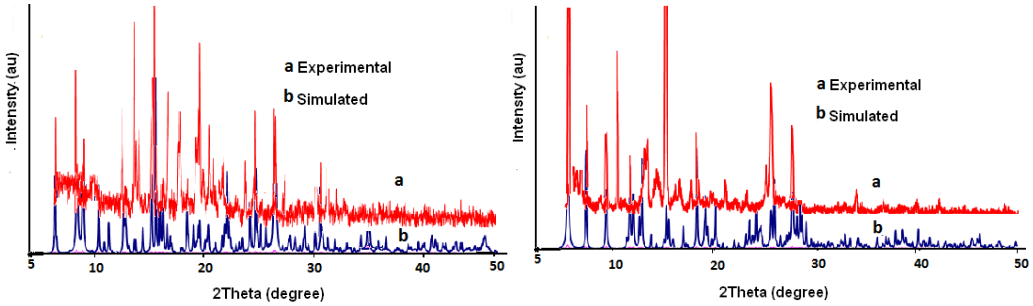

2.2.7 **2.2.8**

Figure 2A1: Powder X-ray diffraction pattern of the Copper(II)pyridinedicarboxylates.

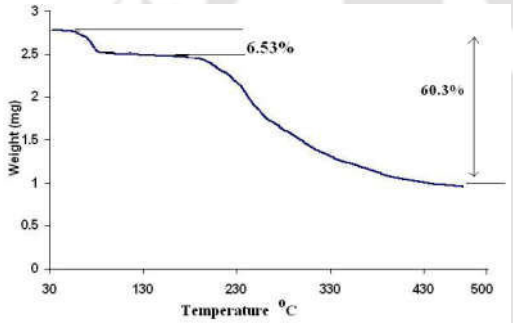

2.1.1

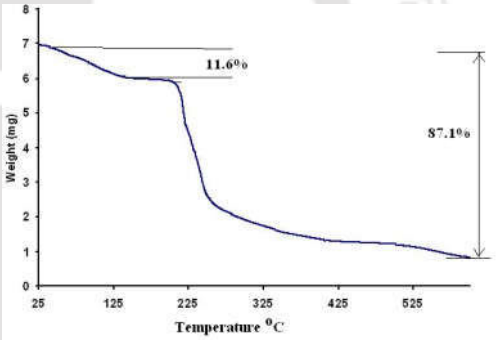

2.1.3

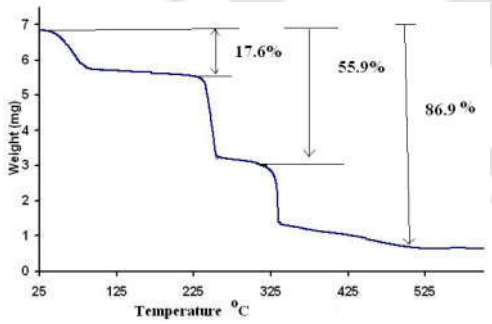

2.1.4

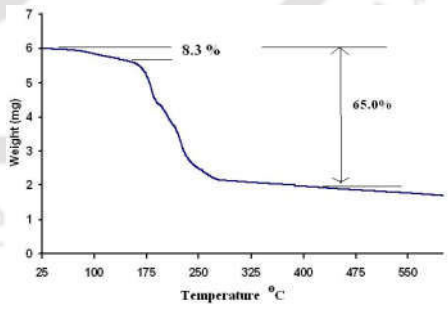

2.1.12

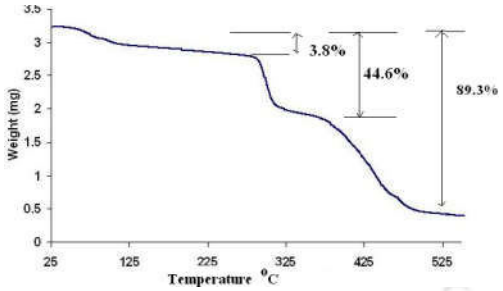

2.1.15

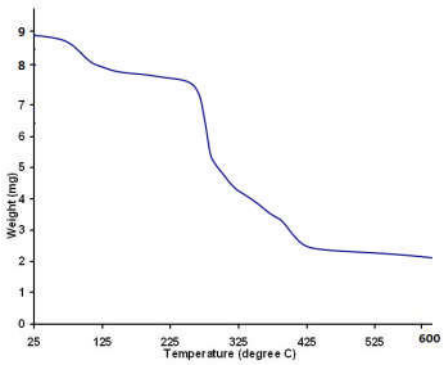

2.2.1

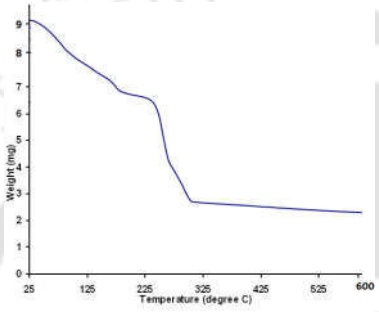

2.2.2

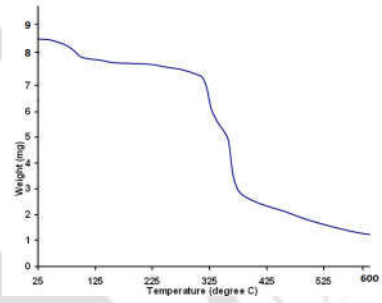

2.2.3

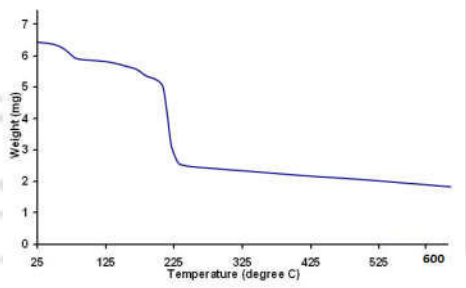

2.2.4

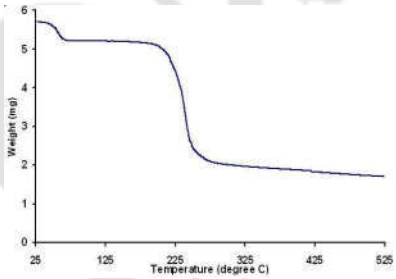

2.2.5

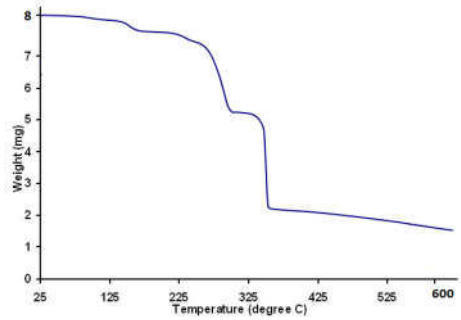

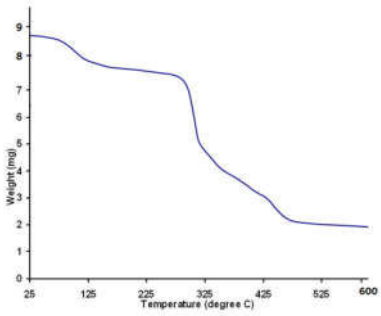

2.2.6 **2.2.7**

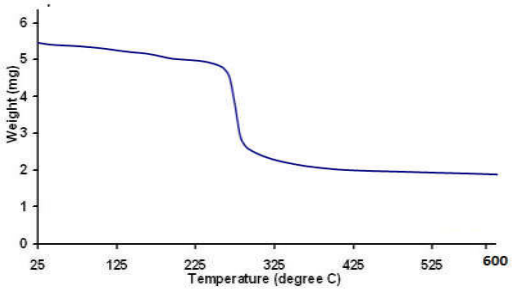

2.2.8

Figure 2A2: Thermogram of selected Copper(II) pyridinedicarboxylates.

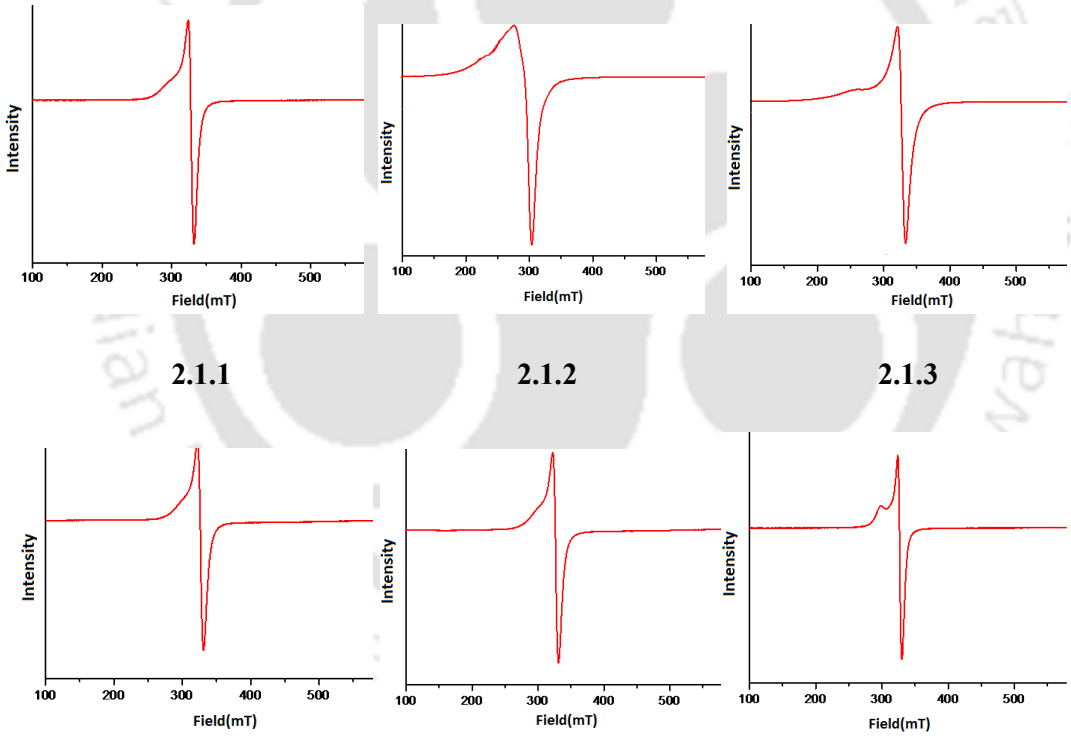

2.1.1 **2.1.2** **2.1.3**

2.1.5 **2.1.6** **2.1.7**

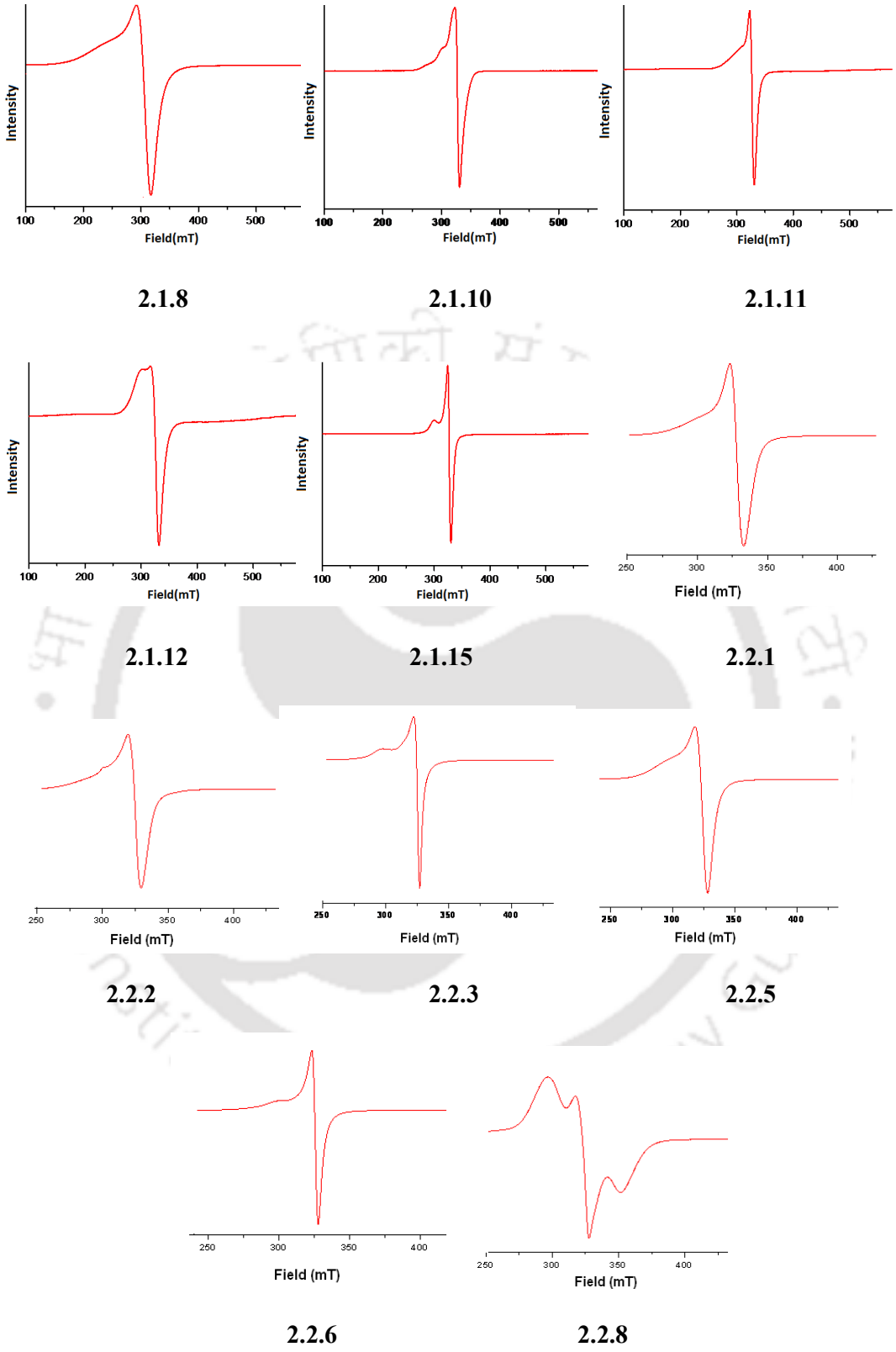

Figure 2A3: ESR Spectra of Copper(II)2,3-pyridinedicarboxylates.

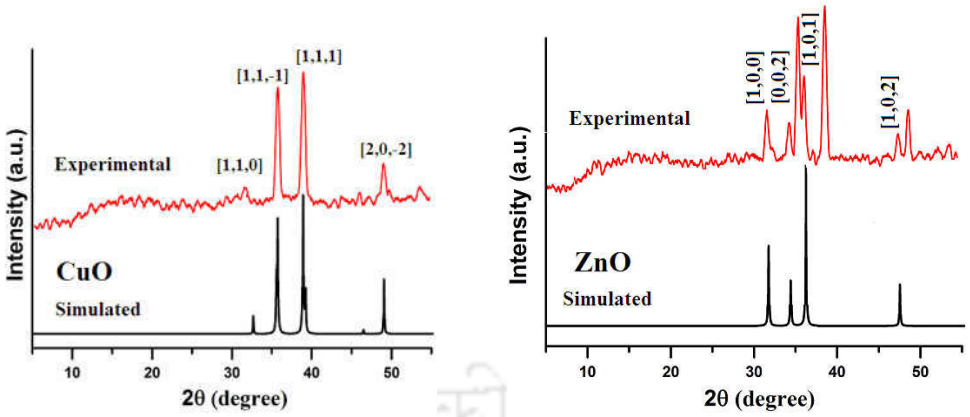

(a) (b)

Figure 3A1: (a) Top plot represents the PXRD pattern of residue of compound **3.1.1** after heating at 450°C. Bottom is the simulated PXRD pattern of copper(II) oxide, (b) Top plot represents the powder XRD pattern of residue of compound **3.1.2** after heating at 450°C. Bottom is the simulated PXRD pattern of zinc(II) oxide.

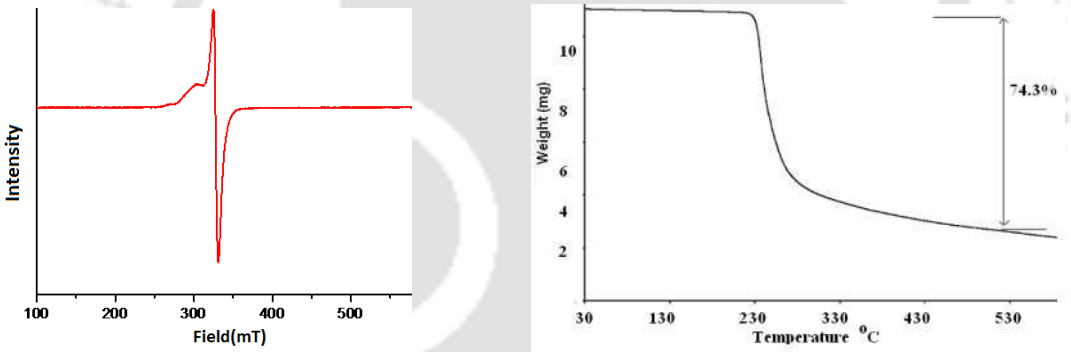

(a) (b)

Figure 3A2: ESR spectra of complex **3.2.2.** (b) Thermogram of complex **3.3.2**.

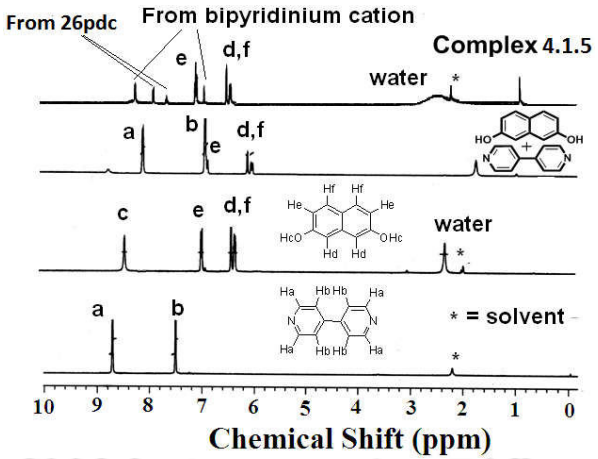

Figure 4A1: ^{1}H-NMR (DMSO-d_6) spectra of (i) 4,4′-bipyridine, (ii) 2,7-dihydroxynaphthalene, (iii) 1:1 mixture of 4,4′-bipyridine and 2,7-dihydroxynaphthalene, and (iv) complex **4.1.5**.

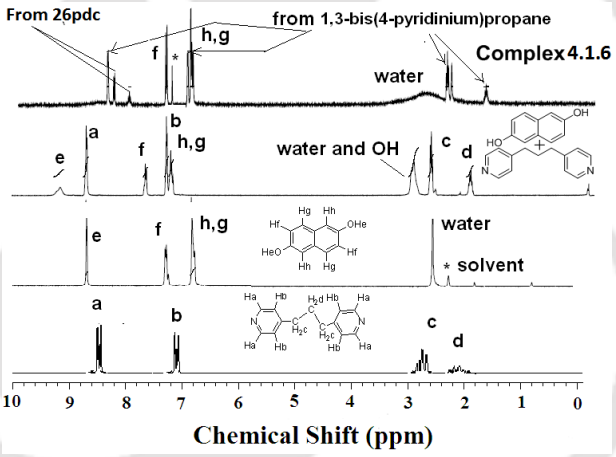

Figure 4A2: ^{1}H-NMR spectra(DMSO-d_6) of 1,3-bis(4-pyridine)propane, 2,6-dihydroxynaphthalene, mixture of 1,3-bis(4-pyridine)propane and 2,6-dihydroxynaphthalene, and complex **4.1.6**.

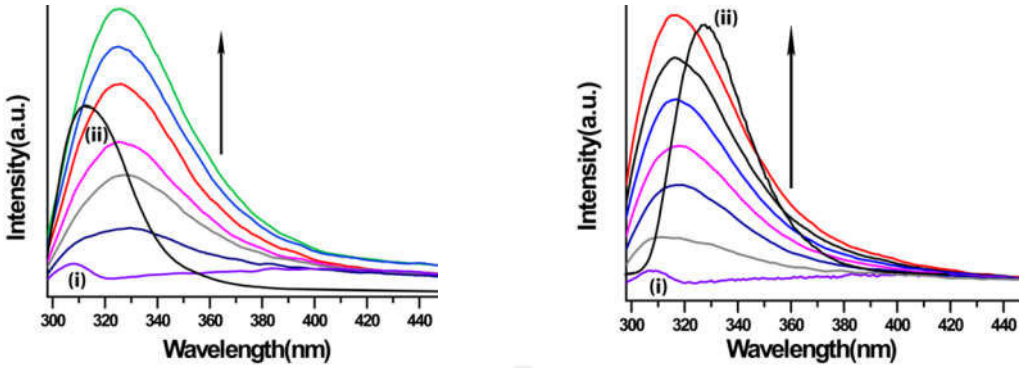

Figure 4A3: Fluorescence emission hydroxyaromatic compounds on addition to a solution of complex **1** (a) 1,3-dihydroxybenzene, (b) 1,4-dihydroxybenzene. In each case: i) complex **4.2.1** in water (10^{-5} M, 3 mL, λ_{ex} = 280 nm), (ii) Corresponding dihydroxyaromatic compound in water and rest are on addition of dihydroxyaromatic compound (10^{-5} M, 20 µL in each aliquot)

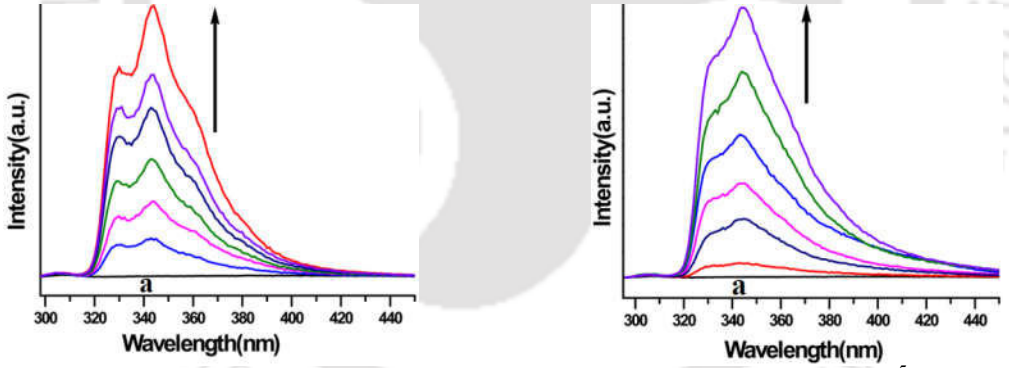

Figure 4A4: (i) Fluorescence emission of a solution of complex **4.2.1** (10^{-5} M, 3 mL) and rest are fluorescence emission on addition of 2,3-dihydroxynaphthalene (10^{-5} M, 20 µL in each aliquot complex **4.2.1** methanol solution (10^{-5} M in 3 mL; λ_{ex} = 280 nm), (ii) Fluorescence emission of a solution of complex **4.2.1** (10^{-5} M, 3 mL) and rest are changes in fluorescence emission on addition of 2,7-dihydroxynaphthalene (10^{-5} M, 20 µL in each aliquot to a solution of complex **4.2.1** in methanol (10^{-5} M in 3 mL; λ_{ex} = 280 nm).

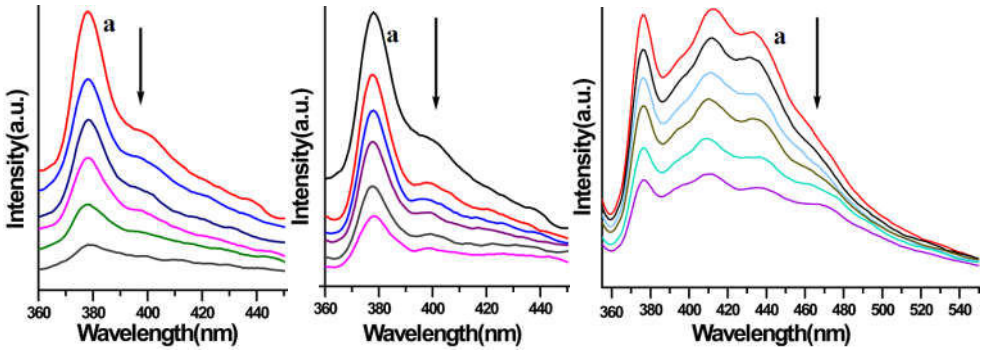

(i) (ii) (iii)

Figure 4A5: (i) Fluorescence spectra of complex **4.3.1** in methanol **(a)** (10^{-5} M in 3 mL) and rest are upon addition of 2,4-dinitrophenol to the solution (20 µL, 10^{-5} M in each aliquot) solution. (ii) Fluorescence spectra of complex **4.3.1** in methanol **(a)** (10^{-5} M in 3 mL) and rest are upon addition of 3-nitrobenzoic acid to the solution (20 µL, 10^{-5} M in each aliquot) solution. (iii) Fluorescence spectra of complex **4.3.1** in DMSO **(a)** (10^{-5} M in 3 mL) and rest are upon addition of 2,4-dinitrophenol to the solution (20 µL, 10^{-5} M in each aliquot) solution.

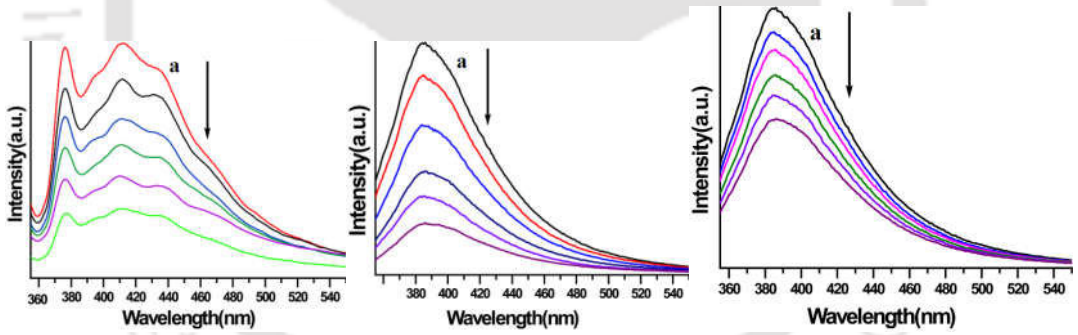

(i) (ii) (iii)

Figure 4A6: (i) Fluorescence spectra of complex **4.3.1** in DMSO **(a)** (10^{-5} M in 3 mL) and rest are upon addition of 3-nitrobenzoic acid to the solution (20 µL, 10^{-5} M in each aliquot) solution. (ii) Fluorescence spectra of complex **4.3.1** in DMF **(a)** (10^{-5} M in 3 mL) and rest are upon addition of 2,4-dinitrophenol to the solution (20 µL, 10^{-5} M in each aliquot) solution. (iii) Fluorescence spectra of complex **4.3.1** in DMF **(a)** (10^{-5} M in 3 mL) and rest are upon addition of 3-nitrobenzoic acid to the solution (20 µL, 10^{-5} M in each aliquot) solution.

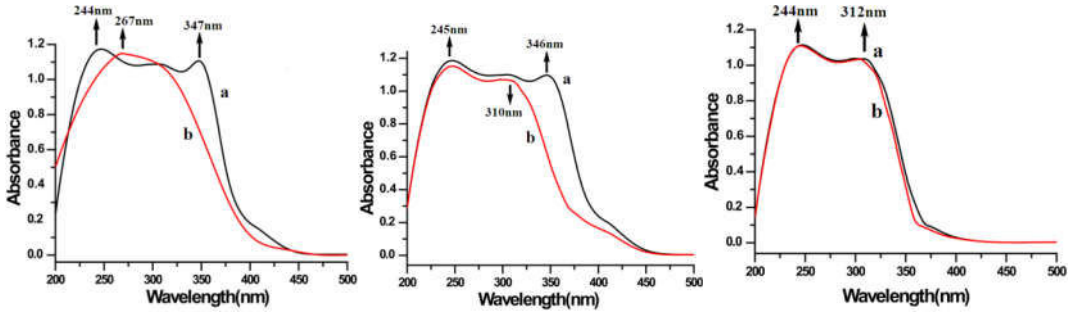

(i) (ii) (iii)

Figure 4A7: (i) UV-visible spectra of freshly prepared solution of complex **4.3.2** (a) (10^{-4} M, 3 mL in methanol), (b) complex **4.3.2** after 2 days. (ii) UV-visible spectra of freshly prepared solution of complex **4.3.3** (a) (10^{-4} M, 3 mL in methanol), (b) complex **4.3.3** after 2 days.(iii) UV-visible spectra of freshly prepared solution of complex **4.3.4** (a) (10^{-4} M, 3 mL in methanol), (b) complex **4.3.4** after 2 days.

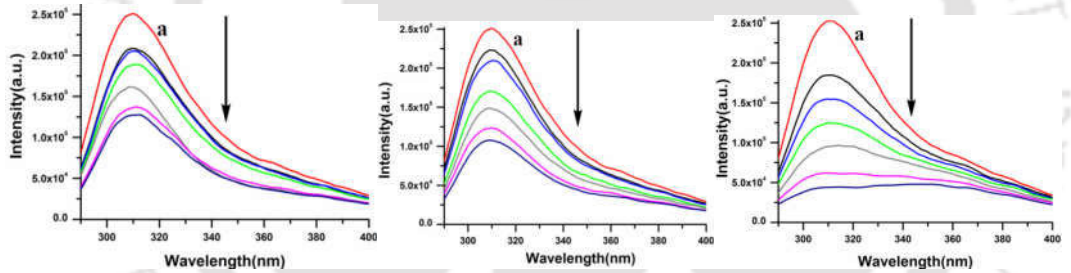

(i) (ii) (iii)

Figure 4A8: (i) Fluorescence emission of a methanol solution of **4.4.1**(10^{-5} M, 3 mL) and rest are changes in fluorescence emission of solution of **4.4.1** (10^{-5} M in 3 mL; λ_{ex} = 270 nm) on addition of 2-nitrophenol (10^{-5} M, 20 µL in each aliquot). (ii) Fluorescence emission of a solution **4.4.1** (10^{-5} M, 3 mL) and rest are changes in fluorescence emission of methanol solution of **4.4.1** (10^{-5} M in 3 mL; λ_{ex} = 270 nm) on addition of 3-nitrophenol (10^{-5} M, 20 µL in each aliquot).(iii) Fluorescence emission of a methanol solution of **4.4.1** (10^{-5} M, 3 mL) and rest are changes in fluorescence emission of solution of complex **4.4.1** (10^{-5} M in 3 mL; λ_{ex} = 270 nm) on addition of 4-nitrophenol (10^{-5} M, 20 µL in each aliquot).

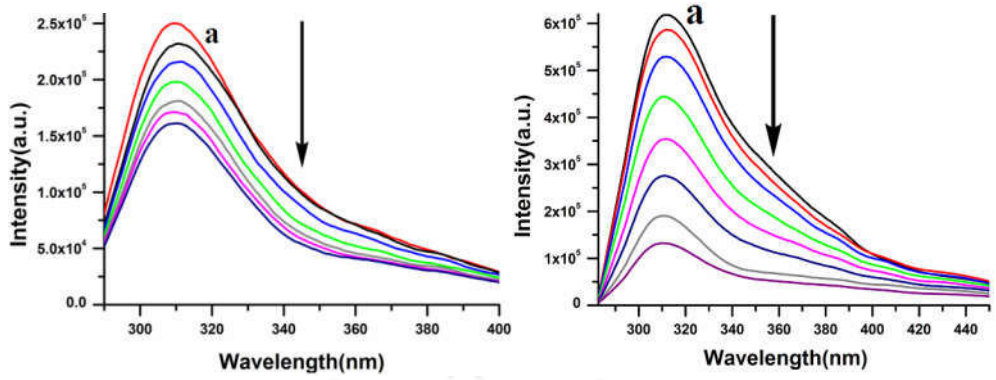

(i) (ii)

Figure 4A9: (i) Fluorescence emission of a solution of **4.4.1** (10^{-5} M, 3 mL) and rest are changes in fluorescence emission of **4.4.1** methanol solution (10^{-5} M in 3 mL; λ_{ex} = 270 nm) on addition of 2,4-dinitrophenol (10^{-5} M, 20 µL in each aliquot). (ii) Fluorescence emission (λ_{ex} = 265 nm) of a methanol solution of complex **4.4.2** (10^{-5} M, 3 mL) and rest are changes on addition of 2-nitrophenol (10^{-5} M, 20 µL in each aliquot).

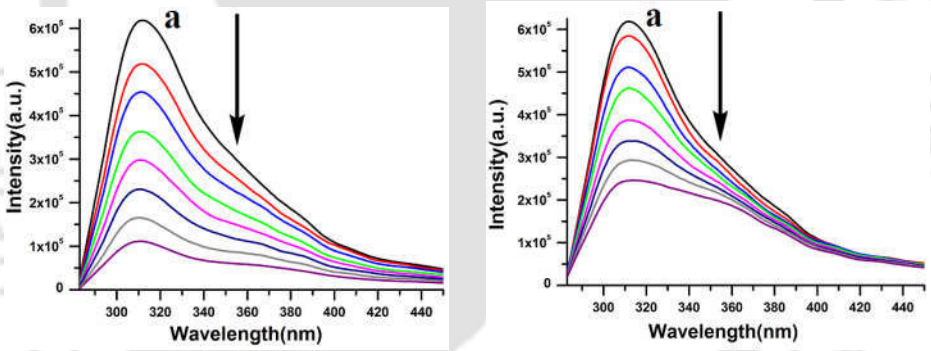

(i) (ii)

Figure 4A10: (i) Fluorescence emission (λ_{ex} = 265 nm) of a methanol solution of **4.4.2** (10^{-5} M, 3 mL) and rest are changes on addition of 3-nitrophenol (10^{-5} M, 20 µL in each aliquot). (ii) Fluorescence emission (λ_{ex} = 265 nm) of a methanol solution complex **4.4.2** (10^{-5} M, 3 mL) and rest are changes on addition of 4-nitrophenol (10^{-5} M, 20 µL in each aliquot).

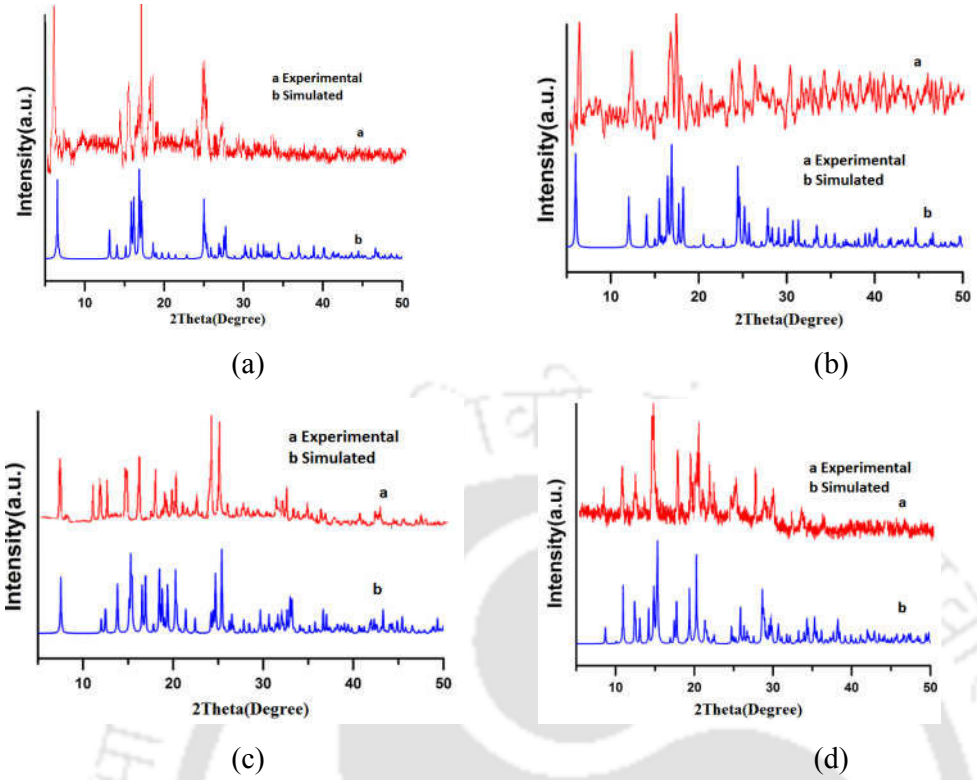

Figure 5A1: Powder X-ray diffraction pattern of complexes (a) **5.1**, (b) **5.2**, (c) **5.3**, (d) **5.5**, (In each case top is experimental and bottom is generated from crystallographic information file).

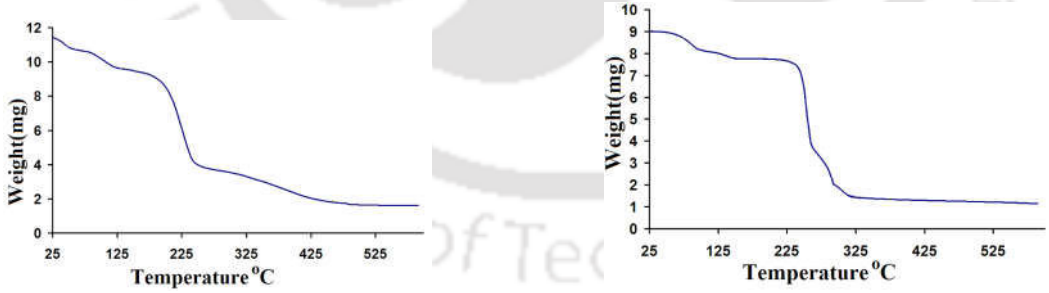

5.1 **5.2**

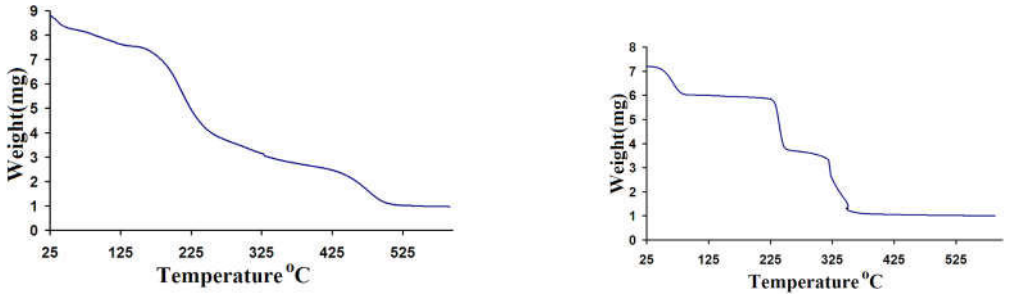

5.3 **5.5**

Figure 5A2: Thermogram of Copper(II) bis-ethylenediammine carboxylate complexes.

5A: Life time decay study

Life-time of fluorescence emission of (Figure 5A2-5A4) H2bqca showed single exponential decay with life-time 1.983 ns. Whereas a solution of copper(II) acetate and H2bqca had two life-times 0.326 ns and 2.018 ns respectively with 60 : 40 probability ratio. This shows that majority of excited molecules of H2bqca decay through a path having shorter life-time. Thus, quenching in methanol by copper ions is caused by change in the path of emission. However, addition of ethylenediamine to a methanol solution containing **H2bqca** and copper(II)acetate showed single exponential with life-time 2.066 ns. This suggests that addition of ethylenediamine enforces to retrace original fluorescence emission path by releasing bqca from the coordination sphere by chelating itself to copper ions. Hence, life-time measurements have added support to the Scheme 5.2.

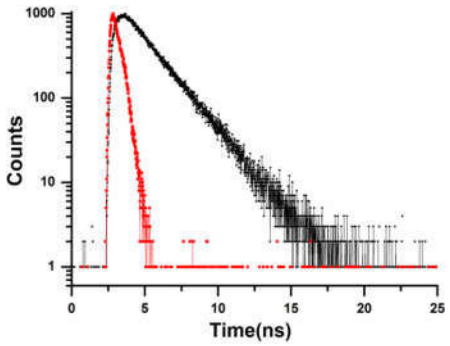

❖ **Discrete Components Analysis (Reconvolution)**

Fitting range : [301; 1800] channels
χ^2 : 0.846

Exp Num	B	err_B	f	err_f	τ (ns)	err_τ
1	0.026	5.1e-4	100.0	2.023	1.983	0.001

Background : 0.611 Background error : 0.056
Shift : -0.241 ns Shift error : 3.714
IRF Background : 0.017 fixed

Figure 5A2: Time resolved fluorescence emission of a solution of H_2bqca (10^{-5} M, 3 ml in methanol) (Red line is back ground).

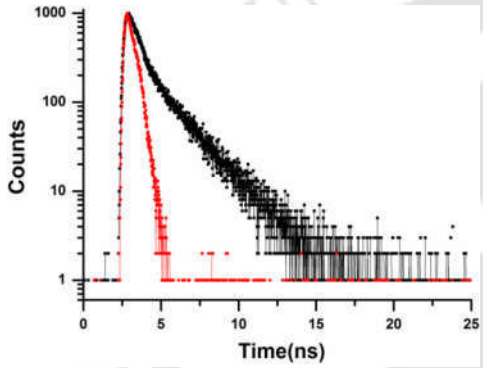

❖ **Discrete Components Analysis (Reconvolution)**

Fitting range : [280; 1800] channels
χ^2 : 0.858

Exp Num	B	err_B	f	err_f	τ (ns)	err_τ
1	0.077	0.011	60.01	40.33	0.326	0.174
2	0.008	3.1e-4	39.99	1.600	2.018	0.004

Background : 0.947 Background error : 0.056
Shift : -0.671 ns Shift error : 5.444
IRF Background : 0.017 fixed

Figure 5A3: Time resolved fluorescence emission of a solution of H_2bqca and copper(II) acetatesolution (equimolar 10^{-5} M, 3 ml in methanol) (Red line is back ground).

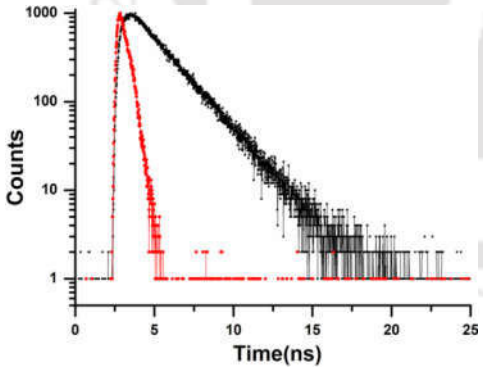

❖ **Discrete Components Analysis (Reconvolution)**

Fitting range : [312; 1800] channels
χ^2 : 0.941

Exp Num	B	err_B	f	err_f	τ (ns)	err_τ
1	0.027	0.001	100.0	4.502	2.066	0.002

Background : 0.453 Background error : 0.067
Shift : -0.330 ns Shift error : 8.151
IRF Background : 0.017 fixed

Figure 5A4: Time resolved fluorescence emission of a solution of equimolar amount of ethylenediamine to the solution containing **H_2bqca** and copper(II)acetate (equimolar 10^{-5} M, 3 ml in methanol) (Red line is back ground).

List of Publication

1. **K. Shankar**, B. Das, J. B. Baruah. Organic cations controlling the nuclearity of copper(II)2,5-pyridinedicarboxylates.
   RSC Advances, 2013, **3**, 26220-262292.

2. **K. Shankar**, B. Das, J. B. Baruah. Cation Exchange in Layered Copper(II)-Coordination Polymers.
   Eur. J. Inorg. Chem., 2013, 6147-6155.

3. **K. Shankar**, A. M. Kirillov, J. B. Baruah. A modular approach for molecular recognition by zinc dipicolinate complexes.
   Dalton Trans., 2015, **44**, 14411-14423.

4. **K. Shankar**, A. M. Kirillov, J. B. Baruah. Bottom up synthesis for homo- and heterometallic 2,3-pyridinedicarboxylate coordination compounds. *Polyhedron*, 2015, **102**, 521-529.

5. **K. Shankar**, J. B. Baruah. Modulation of Fluorescence Emissions of Copper(II) 2,2'-biquinoline-4,4'-dicarboxylates.
   Chem. Select, 2016, **1**, 3038-3044.

6. **K. Shankar**, J. B. Baruah. Tetranuclear Cobalt Complexes as Nano-Dimensional Template for Inclusion of Nitrophenols.
   Chem. Select, 2016, **1**, 5152-5158.

7. **K. Shankar**, J. B. Baruah. Mixed anionic and inclusion complexes of nickel(II) with nitroaromatics showing selectivity in oxygen-π interactions.
   Inorg. Chim. Acta, 2016, **435**, 135-141.

8. **K. Shankar**, J. B. Baruah. Inclusion of hydroxyaromatics by a lanthanum(III) 2,6-dipicolinate complex
   Polyhedron, **DOI**: 10.1016/j.poly.2017.01.053